

**MESOSCALE MODELING OF AEROSOL LEVELS IN İSTANBUL USING A
HIGH RESOLUTION MM5/CMAQ AIR QUALITY MODELING SYSTEM**

ULAŞ İM

BOĞAZİÇİ UNIVERSITY

2009

**MESOSCALE MODELING OF AEROSOL LEVELS IN İSTANBUL USING A
HIGH RESOLUTION MM5/CMAQ AIR QUALITY MODELING SYSTEM**

by

Ulaş İm

B.S. in Environmental Engineering Yıldız Technical University, 2000

M.S. in Environmental Technology, Boğaziçi University, 2003

Submitted to the Institute of Environmental Sciences in partial fulfillment of

the requirements for the degree of

Doctor

of

Philosophy

in

Environmental Technology

**Boğaziçi University
2009**

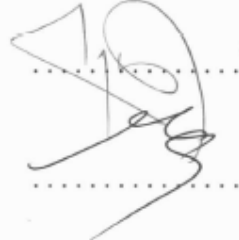
MESOSCALE MODELING OF AEROSOL LEVELS IN İSTANBUL USING A HIGH
RESOLUTION MM5/CMAQ AIR QUALITY MODELING SYSTEM

APPROVED BY:

Prof. Dr. Orhan Yenigün*
(Thesis Supervisor)



Assoc. Prof. Ali Kerem SAYSAL



Prof. Dr. Mete TAYANÇ



Assoc. Prof. Dr. Nadim COPTY



Prof. Dr. Selahattin İNCECİK

DATE OF APPROVAL 26.06.2009

ACKNOWLEDGEMENTS

I would like to express my sincere gratitude and thanks to numerous people for having helped me on this long run.

First and foremost, I would like to thank my advisor, Professor Orhan Yenigün, for helping and supporting me throughout my study and providing me the trust and the flexibility to make numerous changes and modifications on both the focus and the methodologies I have used during this research. Finally, I would like to thank him for giving me the opportunity to work at different institutes and universities to make the most out of this study. I extend my deep gratitude to him.

Secondly, I would like to express my very special thanks to Professor Selahattin İncecik from İstanbul Technical University, Department of Meteorological Engineering, for the valuable support and trust to my work, mentally by his positive energy, and technically through providing me the opportunity to access his infrastructure at his department, and academically by his valuable comments, evaluations and discussions. He did his best to enlarge my vision on this very broad field of air quality modeling in Turkey, through numerous projects he made me get involved.

I am also very grateful to Professor Mete Tayanç from Marmara University, Department of Environmental Engineering. I will always gratefully remember his support in times when I was most depressed and felt like quitting.

Very special thanks to Ass. Prof. Alper Unal and Assoc. Prof. Tayfun Kındap from İstanbul Technical University, Eurasian Institute of Earth Sciences, for their support in this work and sharing their valuable experience in air quality modeling field. I would like to thank Assoc. Prof. Tayfun Kındap for sharing his expertise on meteorological modeling. I would like to express my special thanks to Ass. Prof. Alper Unal for sparing even his weekends to accomplish this study, and for sharing his knowledge on emissions and chemistry and transport modeling.

I am grateful to Kostandinos Markakis from Aristotle University of Thessaloniki, Laboratory of Atmospheric Physics, for his valuable work and guidance in the emission modeling of this study. I would also like to thank him as a good friend and wish him success in his PhD work. I am also grateful to Dr. Anastasia Poupkou from the same laboratory for her help and guidance in chemical speciation of the emissions part. Finally, I would like to thank their professor, Dimitros Melas, for giving them the opportunity to make this collaboration possible and providing me the European emissions.

I would to express my special thanks to Professor Nikos Mihalopoulos from University of Crete, Environmental Chemistry Process Laboratory, for his academic guidance and support on aerosol chemistry. I would also like to thank Christina Theodisi for the analyses of the aerosol samples.

Very special thanks to Dr. Ümit Anteplioglu, who encouraged me to take part in air quality modeling research. I will always remember him and be aware of the great loss of the community by his recent pass. May he rest in peace ...

I would like to thank Professor Sema Topçu from İstanbul Technical University, Department of Meteorological Engineering, for her support and encouragement for my study. I am also grateful to Dr. M. Talat Odman from Georgia Institute of Technology, School of Civil and Environmental Engineering, U.S.A., for his guidance and help on the field of chemistry and transport modeling.

Most importantly, I would like to express my sincere thanks to my most beloved wife, Esra Oruç İm, for her continuous support on this work, my career and decisions. I am in debt to her for her constant patience. I am also grateful to my parents for encouraging me during my academic career and their love.

Last but not least, I would like thank all my friend and colleagues for their support and encouragement.

Finally, the financial support provided by TÜBİTAK project 105Y105, TUJJB project TUJJB-TUMEHAP-03-06 and Boğaziçi University Research Fund project 07HY101D.

ABSTRACT

İstanbul is the largest and most populated city of Turkey and one of the biggest megacities in the world that frequently experiences high air pollution levels. Statistical approaches have been widely used to study these episodes. However, air quality modeling has not been much used to understand the nature and the meteorological and chemical backgrounds of these episodes. This study aims to evaluate the aerosol levels in İstanbul by establishing a mesoscale air quality modeling system using the PSU/NCAR MM5 meteorological model and CMAQ chemistry and transport model on a high temporal and spatial resolution. A high resolution emission inventory is developed for the modeling purposes for the first time for the city of İstanbul.

The inventory covers most of the important anthropogenic source sectors including energy, residential and industrial combustion, traffic and shipping on 2 km horizontal resolution and hourly temporal resolution. The results shows that on-road traffic emissions are the main source for most of the pollutants such as CO, PM and NO_x, industrial combustion is responsible for a high portion of SO₂ emissions and solvent use and traffic are the main contributors for NMVOC emissions. However large uncertainties may be introduced due to the activity data, emission factors and temporal profiles used in the study.

The modeling study is conducted for a 5-day period from January 13 to January 17, 2008. The period included a 5-day winter episode of PM₁₀, with 24-hour averaged concentrations reaching at least twice as high as the EU legislation of 50 µgm⁻³. The results from the MM5 simulation are compared with observations from Kandilli and Finokalia (Crete) meteorological stations. Statistical measures show that the model captured the surface temperature and wind profiles successfully. On the other hand, better agreement can be achieved by optimization studies that focus on the physics option used for the parameterizations.

Finally, the results from the CMAQ model are compared with Alibeyköy and Beşiktaş air quality stations that are operated by the Greater Municipality of İstanbul on hourly bases for the total PM₁₀ levels. Additional analyses are conducted on daily bases using the data obtained from the samples collected from Boğaziçi University air quality station that include chemically speciated PM₁₀ concentrations such as sulfate, nitrate and ammonium aerosols. As stated above, PM levels in İstanbul are simulated by mesoscale air quality models before but evaluation of these levels on speciated aerosol levels are done for the first time in this study. The statistical evaluation of model results on hourly basis shows poor agreement with the observations. On the other hand, the comparison on daily basis shows good agreement with the observations for PM₁₀ levels. Additionally, comparisons for sulfate, nitrate and ammonium concentrations show good agreement, particularly for sulfate and nitrate aerosols. The spatial distribution of aerosol levels show that the highest concentrations occur where the highest emission sources are located. The differences between model results and observation may arise from numerous sources, including parameterization in meteorological modeling, emission factors, profiles and activity levels used in emission modeling and the uncertainties from measurements.

In order to understand the sensitivity of aerosol levels to different emission scenarios, Brute force analyses are conducted for the İstanbul domain. All pollutants, SO₂ only, NO_x only, NH₃ only and VOCs only are increased and reduced by 10 per cent and responses of PM₁₀, sulfate, nitrate and ammonium aerosols on the whole domain are calculated. It has been shown that sulfur and nitrogen availability, photochemical activity, as well as the flow due to meteorology influence the aerosol levels on upwind and downwind in different scales. Overall, it is clear that model evolutions should be conducted for long term simulations in order to understand the general performance characteristics of the modeling system used.

ÖZET

İstanbul, Türkiye'nin en büyük ve kalabalık şehri olmakla beraber dünyadaki en büyük mega kentlerden biridir ve sıkça yüksek hava kirliliği seviyelerine maruz kalmaktadır. Bu seviyeleri incelemek için istatistik yöntemler sıkça kullanılmıştır. Ancak, bu kirlilik seviyelerinin doğasını, yani meteorolojik ve kimyasal alt yapısını anlamamıza yardımcı olabilecek hava kalitesi modelleri çok az kullanılmıştır. Bu çalışma, İstanbul'daki aerosol seviyelerinin, yüksek zamansal ve mekansal çözünürlükte, PSU/NCAR MM5 mezo ölçek meteorolojik modeli ve CMAQ kimyasal taşınım modelinden oluşmuş olan bir model sistemi ile simule etmeyi amaçlamaktadır. Yine bu amaçla, İstanbul için ilk defa yüksek çözünürlüklü bir emisyon envanteri geliştirilmiştir.

Emisyon envanteri, 2 km mekansal çözünürlükte ve saatlik olarak enerji, evsel ve endüstriyel yanma, trafik ve gemicilik dahil olmak üzere, önemli antropojenik kaynakların önemli bir kısmını kapsamaktadır. Sonuçlar, araç trafiğinin CO, PM ve NO_x gibi çoğu kirletici için, sanayinin SO₂ için, trafik ve çözücü kullanımının ise NMVOC' ler için en önemli kaynak olduğunu göstermektedir. Ancak, kullanılan aktivite verisi, emisyon faktörleri ve zamansal profillerden kaynaklanan önemli belirsizliklerin mevcut olduğu unutulmamalıdır.

Modelleme çalışması, 13-17 Ocak 2008 tarihlerini kapsayan 5 günlük bir dönem için yapılmıştır. Bu aralık, PM₁₀ için 24 saatlik Avrupa Birliği standardı olan 50 µgm⁻³ değerini aşan 5 günlük bir episode kapsamaktadır. MM5 meteorolojik modelinin sonuçları, Kandilli ve Finokalia (Girit) meteoroloji istasyonu verileri ile karşılaştırılmıştır. İstatistik analizler, modelin yüzey sıcaklık ve rüzgar profillerini başarılı bir şekilde simule ettiğini göstermektedir. Diğer bir yandan, model parametirizasyonu, farklı fizik seçenekleri test edilerek geliştirilebilir ve daha iyi sonuçlar elde edilebilir.

CMAQ tarafından hesaplanan PM₁₀ konsantrasyonları, saatlik olarak İstanbul Büyükşehir Belediyesi tarafından işletilen Alibeyköy ve Beşiktaş hava kalitesi istasyonu verileri ile karşılaştırılmıştır. Ek olarak, Boğaziçi Üniversitesi hava kalitesi istasyonunda

günlük olarak toplanan PM_{10} ve sülfat, nitrat ve amonyum aerosol seviyeleri için de karşılaştırmalar yapılmıştır. Yukarıda da belirtildiği gibi İstanbul' daki PM_{10} seviyeleri, mezo ölçek modeller yardımıyla araştırılmıştır. Ancak, ilk defa bu çalışmada, İstanbul' daki aerosol kimyasal bileşen seviyeleri bir model sistemi vasıtası ile incelenmeye çalışılmıştır. Saatlik bazda yürütülen istatistik değerlendirme çalışmaları, gözlem verileri ile uyumluluğun düşük olduğunu göstermektedir. Diğer yandan, 24 saatlik ortalamalar için yapılan istatistik analizler, modelin PM_{10} konsantrasyonlarını kabul edilebilir ölçülerde simule edebildiğini göstermektedir. Aynı şekilde, sülfat, nitrat ve amonyum aerosolları için yapılan analizler, özellikle sülfat ve nitrat için modelin iyi çalıştığını göstermektedir. Aerosol konsantrasyonlarının mekansal dağılımı incelendiğinde, en yüksek konsantrasyonların emisyonların yüksek olduğu yerlerde meydana geldiği görülmektedir. Model ile gözlemler arasındaki farklar, meteorolojik modellemede kullanılan parametrisasyonlar, emisyon modellemesinde kullanılan emisyon faktörleri, profiller ve aktiviteler ile ölçümlerden kaynaklanan belirsizlikler gibi birçok hata kaynağından meydana gelebilmektedir.

Aerosol seviyelerinin farklı emisyon senaryolarına olan hassasiyetini belirlemek için Brute zorlama metodu ile hassasiyet analizleri yapılmıştır. İlk önce tüm emisyonlar, sonra da sırası ile SO_2 , NO_x , NH_3 ve VOC emisyonları % 10 arttırılmış ve azaltılmış ve PM_{10} , sülfat, nitrat ve amonyum aerosollarının bu zorlamalara tepkisi tüm model alanı için hesaplanmıştır. Atmosferdeki kükürt ve azot miktarları, rüzgar alanları ve fotokimyasal aktivite, akış yönünde ve ters yöndeki aerosol seviyelerini farklı şekilde etkilemektedir. Genel bir değerlendirme yapıldığında, model performansının doğru olarak belirlenmesinde uzun dönemli simülasyonların göz önüne alınması gerektiği açıktır.

TABLE OF CONTENTS

ACKNOWLEDGEMENTS	iii
ABSTRACT	v
ÖZET	vii
LIST OF FIGURES	xii
LIST OF TABLES	xviii
LIST OF SYMBOLS/ABBREVIATIONS	xx
1. INTRODUCTION	1
1.1. Air Quality Modeling	9
1.1.1. Meteorological Modeling	12
1.1.2. Emission Modeling	15
1.1.3. Chemistry and Transport Models	17
1.1.3.1. Types of atmospheric chemical transport models	18
1.1.3.2. Initial and boundary conditions	18
2. LITERATURE REVIEW	22
3. MATERIALS AND METHODS	57
3.1. Episodic Period	57
3.2. Meteorological Modeling	61
3.2.1 Terrain	63
3.2.2 Regrid	63
3.2.3 Setting the Initial and Boundary Conditions (Interpf)	64
3.2.4 MM5	65
3.2.5. Horizontal and Vertical Grid Structures	65
3.2.6. Nesting	66
3.2.7. Lateral Boundary Conditions	68
3.2.8. Non-hydrostatic Dynamics versus Hydrostatic Dynamics	69
3.2.9. Land Use Categories	70
3.2.10. Data Required Running the Model	70
3.2.11. Basic equations of MM5	70
3.2.12. MM5 setup for the study	72

3.3. Emission Inventory	79
3.3.1. Anthropogenic Emissions	79
3.3.1.1. Combustion in energy and transformation industries	79
3.3.1.2. Non-industrial combustion plants	81
3.3.1.3. Combustion in manufacturing industry	81
3.3.1.4. Production processes	81
3.3.1.5. Extraction and distribution of fossil fuels and geothermal energy	81
3.3.1.6. Use of solvents and other products	81
3.3.1.7. Road transport	82
3.3.1.8. Other mobile sources and machinery	83
3.3.1.9. Waste treatment and disposal	84
3.3.1.10. Agriculture	84
3.3.2. Speciation	84
3.3.2.1. Temporal Allocation	84
3.3.3. Development of High Resolution Emission Inventory for the Greater Istanbul Area	88
3.3.3.1. Description of the emission processor	93
3.3.3.2. Quantification methodology	97
3.3.4. Vertical Layer Distribution	103
3.4. Chemistry and Transport Model	104
3.4.1. CMAQ System Components	107
3.4.2. Major CMAQ Programs	109
3.4.2.1. Photolysis Rate Preprocessor (JPROC)	110
3.4.2.2. Initial Conditions Processor (ICON)	110
3.4.2.3. Boundary Conditions Processor (BCON)	110
3.4.2.4. Meteorology-Chemistry Interface Processor (MCIP)	111
3.4.2.5. CMAQ Chemistry-Transport Model (CCTM)	111
3.4.3. Science in the CMAQ Modeling System	112
3.4.3.1. Gas-Phase Chemistry Solvers	113
3.4.3.2. Photolysis	114
3.4.3.3. Diffusion and Advection	115
3.4.3.4. Particulate Matter	116
3.4.4. CMAQ setup for the study	118

3.4.5. Sensitivity Analyses (Brute Force)	120
4. RESULTS	123
4.1. METEOROLOGICAL MODEL	123
4.1.1. Model Performance	123
4.1.2. Model results for the episode days	127
4.1.3. Back Trajectory Simulation Results	143
4.2. Emission Model	153
4.3. Chemistry and Transport Model	171
4.3.1. European and Balkan Domains	171
4.3.2. İstanbul Domain	174
4.3.3. Sensitivity Analyses	188
5. CONCLUSIONS	204
REFERENCES	208
APPENDICES	239
Appendix A Chemical Mechanisms Included in the CMAQ System	240
Appendix B CMAQ Predefined Vertical Profiles for Initial and Boundary Concentrations	249
Appendix C Aerosols	257

LIST OF FIGURES

Figure 1.1. Illustrative transport scales for PM and other atmospheric pollutants	4
Figure 1.2. Schematic picture of mass size distributions in different sands	7
Figure 1.3. Pathways of particle formation during the combustion of pulverized coal	9
Figure 1.4. Basic steps of air quality modeling	14
Figure 1.5. Illustration of a) Eulerian and b) Lagrangian approaches	19
Figure 1.6. General model data flow chart for the modeling system	21
Figure 3.1. The 24-hour PM ₁₀ concentrations between 10.01.2008-18.01.2008	57
Figure 3.2. Hourly PM ₁₀ concentrations at the İstanbul Greater Municipality stations	58
Figure 3.3. Comparison of daily average PM ₁₀ concentrations measured at the municipality stations with Boğaziçi University station	59
Figure 3.4. Distribution of the average concentrations of the aerosol species during the episode	61
Figure 3.5. MM5 modeling system flow chart	64
Figure 3.6. The vertical structure of MM5	67
Figure 3.7. The horizontal structure of the model	67
Figure 3.8. Example of a nesting configuration	68
Figure 3.9. Time splitting procedure in MM5	73
Figure 3.10. Map of the modeling domain	76
Figure 3.11. a) Terrain heights and b) Landuse categories of the mother domain in color scale	76
Figure 3.12. Map of the modeling domain 2	77
Figure 3.13. a) Map of the terrain heights and b) landuse categories of modeling domain 2 in color scale	77
Figure 3.14. Map of the modeling domain 3	78
Figure 3.15. a) Map of the terrain heights and b) landuse categories of modeling domain 3 in color scale	78

Figure 3.16. European PM ₁₀ emissions for January 12, 2008, 1600 UTC, on 30 km grid resolution	86
Figure 3.17. European emission of a) CO, b) SO ₂ , c) NO _x , d) NH ₃ , e) Toluene and f) Xylene for January 12, 2008, 1600 UTC, on 30 km grid resolution	87
Figure 3.18. Balkan Region PM ₁₀ emissions for January 12, 2008, 1600 UTC, on 10 km grid resolution	88
Figure 3.19. Schematic representation of the emission processor	95
Figure 3.20. Domain configuration in CMAQ chemistry and transport model	106
Figure 3.21. Schematic representation of the processors of the CMAQ model	109
Figure 3.22. Model construction in CMAQ	113
Figure 4.1. MM5 vs. observations for a) Temperature at 2 m at Kandilli, b) Temperature at 2 m at Finokalia, c) U component of wind at 10 m at Kandilli, d) U component of wind at 10 m at Finokalia, e) V component of wind at 10 m at Kandilli and f) V component of wind at 10 m at Finokalia	124
Figure 4.2. a) Sea level pressure and wind vectors, b) 850 mb level wind vectors and relative humidity, c) 1000 mb horizontal temperature, d) 24-hour precipitation e) vertical circulation vectors and f) vertical temperature variation on January 13, 2008, at 0200 LST	131
Figure 4.3. a) Sea level pressure and wind vectors, b) 850 mb level wind vectors and relative humidity, c) 1000 mb horizontal temperature, d) 24-hour precipitation, e) vertical circulation vectors and f) vertical temperature variation on January 14, 2008, at 0700 LST	134
Figure 4.4. a) Sea level pressure and wind vectors, b) 850 mb level wind vectors and relative humidity, c) 1000 mb horizontal temperature, d) 24-hour precipitation, e) vertical circulation vectors and f) vertical temperature variation on January 15, 2008, at 0300 LST	137

Figure 4.5. a) Sea level pressure and wind vectors, b) 850 mb level wind vectors and relative humidity, c) 850 mb horizontal temperature, d) 24-hour precipitation, e) vertical circulation vectors and f) vertical temperature variation on January 16, 2008, at 2000 LST	140
Figure 4.6. a) Sea level pressure and wind vectors, b) 850 mb level wind vectors and relative humidity, c) 850 mb horizontal temperature, d) 24-hour precipitation, e) vertical circulation vectors and f) vertical temperature variation on January 17, 2008, at 2200 LST	144
Figure 4.7. Back trajectory simulation results of January 13, 2008, 0200 LST for a) European, b) Balkan and c) İstanbul domains	148
Figure 4.8. Back trajectory simulation results of January 14, 2008, 0700 LST for a) European, b) Balkan and c) İstanbul domains	149
Figure 4.9. Back trajectory simulation results of January 15, 2008, 0300 LST for a) European, b) Balkan and c) İstanbul domains	150
Figure 4.10. Back trajectory simulation results of January 16, 2008, 2000 LST for a) European, b) Balkan and c) İstanbul domains	151
Figure 4.11. Back trajectory simulation results of January 17, 2008, 2200 LST for a) European, b) Balkan and c) İstanbul domains	152
Figure 4.12. Annual aggregated emissions per source category	153
Figure 4.13. Annual speciated PM emissions for each source category	154
Figure 4.14. Annual speciated NMVOC emissions for each source category	154
Figure 4.15. Source contribution to CO, NO _x , SO ₂ , NMVOC, PM ₁₀ and PM _{2.5} emissions	155
Figure 4.16. Spatial distribution of a) CO, b) NO _x , c) SO ₂ , d) NMVOC, e) PM ₁₀ (EC) and f) PM _{2.5} (EC) emissions from residential combustion	158
Figure 4.17. Spatial distribution of a) CO, b) NO _x , c) SO ₂ , d) NMVOC, e) PM ₁₀ (EC) and f) PM _{2.5} (EC) emissions from industrial combustion	159
Figure 4.18. Spatial distribution of a) CO, b) NO _x , c) PM ₁₀ (OC), d) PM _{2.5} (OC) and e) NMVOC emissions from industrial processes	160

Figure 4.19. Spatial distribution of a) CO, b) NO _x , c) SO ₂ , d) NMVOC, e) PM ₁₀ (OC) and f) PM _{2.5} (SO ₄) emissions from road transport	161
Figure 4.20. a) SO ₂ and b) NO _x emissions from cargo shipping emissions	162
Figure 4.21. Spatial distribution of a) NMVOC and b) NH ₃ emissions from solvent use	162
Figure 4.22. Spatial distributions of a) PM ₁₀ and b) PM _{2.5} emissions from coal extraction	162
Figure 4.23. Monthly variation of CO emissions from central heating, industrial processes and road transport	163
Figure 4.24. Monthly variation of NO _x emissions from central heating, industrial processes, road transport and cargo shipping	163
Figure 4.25. Monthly variation of SO ₂ emissions from central heating, industrial combustion and industrial processes	164
Figure 4.26. Monthly variation of NMVOC emissions from solvent use, road transport and waste disposal	165
Figure 4.27. Monthly variation of PM _{2.5} emissions from central heating, road transport and industrial processes	166
Figure 4.28. Daily variation of a) CO, b) NO _x , c) SO _x , d) NMVOC and e) PM _{2.5} from major contributors	167
Figure 4.29. Diurnal profiles of a) CO, b) SO ₂ , c) NMVOC and d) PM ₁₀	168
Figure 4.30. Diurnal profiles of CO from a) road transport and b) non-industrial combustion	168
Figure 4.31. Observed vs. modeled PM ₁₀ concentrations at a) Alibeyköy and b) Beşiktaş air quality stations at the 30 km resolution European domain	172
Figure 4.32. Observed vs. modeled PM ₁₀ concentrations at a) Alibeykoy and b) Beşiktaş air quality stations at 10 km resolution domains	174
Figure 4.33. 24-hour average PM ₁₀ concentrations for a) 13 th , b) 14 th , c) 15 th , d) 16 th and e) 17 th of January, 2008 for the European domain	175
Figure 4.34. 24-hour average PM ₁₀ concentrations for a) 13 th , b) 14 th , c) 15 th , d) 16 th and e) 17 th of January, 2008 for the Balkan domain	176
Figure 4.35. Observed vs. modeled PM ₁₀ concentrations at a) Alibeykoy and b) Beşiktaş air quality stations at 2 km resolution domain	178

Figure 4.36. 24-hour average PM ₁₀ concentrations for a) 13 th , b) 14 th , c) 15 th , d) 16 th and e) 17 th of January, 2008 for the İstanbul domain	181
Figure 4.37. Model results and observation for PM ₁₀ at Boğaziçi University from 13 to 17 January, 2008	182
Figure 4.38. Model results and observation of SO ₄ ²⁻ aerosols at Boğaziçi University from 13 to 17 January, 2008	183
Figure 4.39. 24-hour average sulfate (SO ₄ ²⁻) concentrations for a) 13 th , b) 14 th , c) 15 th , d) 16 th and e) 17 th of January, 2008 for the İstanbul domain	184
Figure 4.40. 24-hour average nitrate (NO ₃ ⁻) concentrations for a) 13 th , b) 14 th , c) 15 th , d) 16 th and e) 17 th of January, 2008 for the İstanbul domain	185
Figure 4.41. Model results and observation of NO ₃ ²⁻ aerosols at Boğaziçi University from 13 to 17 January, 2008	186
Figure 4.42. Model results and observation of NH ₄ ⁺ aerosols at Boğaziçi University from 13 to 17 January, 2008	187
Figure 4.43. 24-hour average ammonium (NH ₄ ⁺) concentrations for a) 13 th , b) 14 th , c) 15 th , d) 16 th and e) 17 th of January, 2008 for the İstanbul domain	189
Figure 4.44. 24-hour average PM ₁₀ changes in response to 10 per cent increase of all emissions for a) 13 th , b) 14 th , c) 15 th , d) 16 th and e) 17 th of January, 2008 for the İstanbul domain	194
Figure 4.45. 24-hour average PM ₁₀ changes in response to 10 per cent reduction of all emissions for a) 13 th , b) 14 th , c) 15 th , d) 16 th and e) 17 th of January, 2008 for the İstanbul domain	195
Figure 4.46. 24-hour average PM ₁₀ changes in response to 10 per cent increase of SO ₂ emissions for a) 13 th , b) 14 th , c) 15 th , d) 16 th and e) 17 th of January, 2008 for the İstanbul domain	196
Figure 4.47. 24-hour average PM ₁₀ changes in response to 10 per cent reduction of SO ₂ emissions for a) 13 th , b) 14 th , c) 15 th , d) 16 th and e) 17 th of January, 2008 for the İstanbul domain	197
Figure 4.48. 24-hour average PM ₁₀ changes in response to 10 per cent increase of NO _x emissions for a) 13 th , b) 14 th , c) 15 th , d) 16 th and e) 17 th of January, 2008 for the İstanbul domain	198

- Figure 4.49. 24-hour average PM_{10} changes in response to 10 per cent reduction of NO_x emissions for a) 13th, b) 14th, c) 15th, d) 16th and e) 17th of January, 2008 for the İstanbul domain 199
- Figure 4.50. 24-hour average PM_{10} changes in response to 10 per cent increase of NH_3 emissions for a) 13th, b) 14th, c) 15th, d) 16th and e) 17th of January, 2008 for the İstanbul domain 200
- Figure 4.51. 24-hour average PM_{10} changes in response to 10 per cent reduction of NH_3 emissions for a) 13th, b) 14th, c) 15th, d) 16th and e) 17th of January, 2008 for the İstanbul domain 201
- Figure 4.52. 24-hour average PM_{10} changes in response to 10 per cent increase of VOC emissions for a) 13th, b) 14th, c) 15th, d) 16th and e) 17th of January, 2008 for the İstanbul domain 202
- Figure 4.53. 24-hour average PM_{10} changes in response to 10 per cent reduction of VOC emissions for a) 13th, b) 14th, c) 15th, d) 16th and e) 17th of January, 2008 for the İstanbul domain 203

LIST OF TABLES

Table 1.1. Comparison of ambient particle fractions	3
Table 1.2. General descriptions of PM emissions and source types adapted from NARSTO (2004)	6
Table 3.1. Maximum PM ₁₀ concentrations at Istanbul Greater Municipality stations between 13-17.01.2008 (units in μgm^{-3})	60
Table 3.2. Chemical speciation of the PM ₁₀ samples (units in μgm^{-3})	62
Table 3.3. Description of 25-category (USGS) vegetation categories and physical parameters for N.H. summer (15 April-15 October) and winter (15 October-15 April)	73
Table 3.4. Physics options used in the MM5 simulation	80
Table 3.5. Sectors of anthropogenic emissions	80
Table 3.6. Chemical compounds of the emission inventory used in the European and Balkan domains	85
Table 3.7. Monthly temporal profiles for each source sector	90
Table 3.8. Weekly temporal profiles for each source sector	91
Table 3.9. Weekday and weekend hourly profiles for each source sector	92
Table 3.10. Input data used in the inventory, their geographical activity level and the spatial indicators used for the allocation of sources	94
Table 3.11. Annual fuel consumption in the study region	98
Table 3.12. Emissions factors used for the quantification of residential and industrial combustion emissions (Inside the parenthesis is the quality rating of the emission factor)	101
Table 3.13. Annual vessel traffic in the Bosphorus crossing and the Ambarli port	102
Table 3.14. Emissions factors (in gr ton^{-1} of fuel) used for the quantification of cargo shipping emissions	103
Table 3.15. Vertical distribution of anthropogenic emissions: Percentage of each sector allocated to the vertical layers of the air quality model (given as heights of layers, in meters)	104
Table 3.16. CB-IV species used for the study	119

Table 3.17. VOC speciation for the CBIV mechanism	121
Table 3.18. Aerosol species to calculate PM_{coarse} , $PM_{2.5}$ and PM_{10} concentrations	122
Table 4.1. Statistical comparison of MM5 simulated temperature, U and V with observations for Kandilli and Finokalia meteorological stations	126
Table 4.2. Comparison of land emissions (in tons yr^{-1}) with the other databases	170
Table 4.3. Statistical comparison of model results against observations for the İstanbul domain	179
Table 4.4. Per cent contributions of aerosol species to PM_{10} levels	182
Table 4.5. Statistical results for comparison of CMAQ results with observation for Boğaziçi University station	188
Table 4.6. Response (per cent) of aerosol levels to the emission scenarios for the whole domain and whole simulation period	193

LIST OF SYMBOLS/ABBREVIATIONS

$\frac{\partial p'}{\partial t}$: Change of pressure in time
p_0	: Reference pressure on earth's surface
ADOM	: The Acid Deposition and Oxidant Model
ALD2	: Acetaldehyde
ATDL	: Atmospheric Turbulence and Diffusion Laboratory
AQM	: Air Quality Model
BCON	: Boundary Condition Processors
BVOC	: Biogenic Volatile Organic Compound
CALGRID	: The California Grid Model
CALMET	: CALMET
CB4	: The Carbon Bond-IV photochemical mechanism
CB4_AE_AQ	: The CB4 gas-phase mechanism with AErosol and AQueous Chemistry
CCTM	: The CMAQ Chemistry Transfer Model
CLRTAP	: Convention on Long-Range Transboundary Air Pollution
CMAQ	: The Community Multiscale Air Quality Modeling System
CO	: Carbon Monoxide
CO₂	: Carbon Dioxide
CORINAIR	: CO-ordination d'Information Environnementale
D_u	: Diffusion in x-direction
D_y	: Diffusion in y-direction
D_w	: Diffusion in z-direction
DEM	: Digital Elevation Models
ECF	: Environmental Correction Factors
EEM	: EURAD Emission Model
EMEP	: The European Monitoring and Evaluation Program
EMEP/CCC	: Chemical Co-ordinating Centre of EMEP
EMIMA	: Global Emission Modeling
EMIMO	: EMIssion MOdel

ESCOMPTE	: Realization of Field Exp. to Const. Models of Atm. Poll.and Emis. Trans.
ETH	: Ethene
EU	: The European Union
EURAD	: The European Air Pollution Dispersion Model
<i>f</i>	: Coriolis force
EURAD-CTM	: EURAD Chemistry Transport Model
FCCC	: The Framework Climate Change Convention
FORM	: Formaldehyde
<i>G</i>	: Gravity term
GDAS	: Global Data Assimilation System
GENEMIS	: The Generation and Evaluation of Emission Data
GIS	: Geographic Information System
GLOREAM	: GLObal and REgional Atmospheric Modeling
HIRLAM	: Danish Meteorological Institute. The operational DMI-HIRLAM system
ICON	: The Initial Concentration
IIASA	: International Institute for Applied Systems Analysis
IPCC	: Intergovernmental Panel on Climate Change
I/O API	: Input/Output Applications Programming Interface
ISOP	: Isoprene
JPROG	: Photolysis Rates for CMAQ
LRTAP	: The Long Range Trans-boundary Air Pollution
<i>m</i>	: Map factor
MATCH	: Multi-scale Atmospheric Transport and Chemistry Model
MATCH-MPIC	: Model of Atm. Trans.and Chem., Max Planck Ins.for Chem.Version 3.0
MCIP	: Meteorology Chemistry Interface
MCNC	: Microelectronics Center of North Carolina
MCNC-SMOKE	: Microelectronics Center of North Carolina Sparse Matrix Ope. Ker. Emis.
MINOS	: The Mediterranean INTensive Oxidant Study
MM5	: Mesoscale Meteorological Model

MRF	: The Medium Range Forecast
MSA	: Methanesulphonate
N₂O	: Nitrous Oxide
NAO	: The North Atlantic Oscillation
NCAR	: National Center for Atmospheric Research
NCEP	: The National Centers for Environmental Prediction
NE-OPS	: The Northeast-Oxidant and Particle Study
NH₃	: Ammonia
NMVOOC	: Non Methane Volatile Organic Compounds
NO	: Nitric Oxide
NO₃	: Nitrate Radical
NOAA	: National Oceanic and Atmospheric Research
NO_x	: Nitrogen Oxides
NR	: Non-Reactive carbon atoms
O₃	: Ozone
OH	: Hydroxyl Radical
OLE	: Olefin
OVOC	: Other Volatile Organic Compounds
PAR	: Paraffin
PBL	: Planetary Boundary Layer
PM	: Particulate Matter
PMC	: Particulate Matter coarse fraction
PEC	: Particulate Matter elemental carbon fraction
POA	: Particulate Matter organic carbon fraction
PSO₄	: Particulate Matter sulfate fraction
PNO₃	: Particulate Matter nitrate fraction
PMFINE	: Particulate Matter fine fraction
PORG	: The United Kingdom Photochemical Oxidants Review Group
PRQA	: Regional Planning for Air Quality Management in Alsace
PEGASUS	: PNNL Eulerian Gas and Aerosols Scalability Unified System
PNNL	: The Pacific Northwest National Laboratory
QA/QC	: Quality Assurance/Quality Check
<i>r_{earth}</i>	: Radius of the earth

RADM	: The Regional Acid Deposition Model
RAINS	: Regional Air Pollution Information and Simulation
RELMAP	: The Regional Lagrangian Modeling of Air Pollution model
ROM	: The Regional Oxidant Model
RRTM	: The Rapid Radiative Transfer Model
σ	: Sigma coordinate
SATURN	: Studying Atmospheric Pollution in Urban Areas
SCAQS	: The Southern California Air Quality Study
SMOKE	: Sparse Matrix Operator Kernel Emissions
SO₂	: Sulfur Dioxide
SO₄²⁻	: Sulfate
SOA	: The Secondary Organic Aerosol
SO_x	: Sulfur Oxides
STEM	: The Sulfur Transport and Emissions Model
<i>T</i>	: Temperature
<i>T₀</i>	: Reference temperature on earth's surface
TAPOM	: The Transport and Air Pollution Model
TFS	: The German Tropospheric Research Program
TNO	: Netherlands Organization for Applied Scientific Research
TOL	: Toluene
TSP	: Total Suspended Particulate
<i>u</i>	: x component of wind vector
UAM	: Urban Airshed Model
UNECE	: United Nations Economic Commission for Europe
USEPA	: The U. S. Environmental Protection Agency
USGS	: The U.S. Geological Survey
<i>V</i>	: Horizontal wind speed
<i>v</i>	: y component of wind vector
<i>w</i>	: Vertical component of the wind vector
WHO	: The World Health Organization
XYL	: Xylene

1. INTRODUCTION

Gases or particular matters emitted into the atmosphere by human (anthropogenic) and natural activities cause many current and potential environmental problems, including acidification, air quality degradation, climate change, damage and soiling of buildings and other structures, stratospheric ozone depletion, human and ecosystem exposure to hazardous substances (Kindap, 2005). It is essential to have quantitative information on these emissions and their sources in order to define environmental priorities and identify the activities and actors responsible for the problems.

It is widely recognized that airborne particles bring about more health problems and more visibility degradation than gases do. Above all, an obvious connection between high levels of particle pollution and day-to-day excessive mortality rate attract the attention of researchers. At this point, urban areas, where extremely high levels of particulate matter (PM) are observed, might be given priority to be investigated immediately. Although urban areas themselves create poor air quality ambience by themselves, long-distance anthropogenic sources could significantly contribute to urban pollution. As a result of this, long-range aerosol transport has gained an outstanding importance in addition to local sources. Considering the importance of long-range transport, its evaluation is inevitable before taking any decision or making any policy regarding air quality.

Individual particles are characterized by their sizes, shapes and chemical composition. They can be solid or liquid, spherical or irregularly shaped, and can contain internal mixtures of species and phases. PM is typically composed of a complex mixture of chemicals, which is strongly dependent on source characteristics.

As indicated in Table 1.1, PM composition varies between the fine and coarse fractions (Wilson and Suh, 1997). The fine fraction, defined as particles smaller less than 2.5 μm , consists of constituents such as sulfate, nitrate, ammonium, metals, elemental carbon, and hundreds of different organic carbon compounds. The coarse fraction is

characterized by materials typical of the earth's crust (primarily fugitive dust and construction sources) and grinding processes (metals).

Particles directly emitted to the atmosphere are called primary particles. Such particles can be coarse or fine. Secondary PM results from the condensation / deposition of gaseous precursors to the particulate phase. Although direct nucleation from the gas phase definitely is a contributing factor, most secondary material accumulates on pre-existing particles in the 0.1 to 1.0 μm range and typically accounts for significant fractions of the $\text{PM}_{2.5}$ mass.

PM can be classified into four modes, which reflect particle origins. These include the coarse mode (particle diameter larger than $\sim 2 \mu\text{m}$), the accumulation mode (0.1 to 2 μm), the Aitken mode (10 to 100 nm) and the nucleation mode ($< 10 \text{ nm}$). Coarse – mode particles are lost rapidly by sedimentation, and ultrafine particles grow and coagulate, typically migrating into the Aitken mode as a result.

Atmospheric aerosol particles contain sulfates, nitrates, ammonium, organic material, crustal species, sea salt, hydrogen ions and water (Seinfeld and Pandis, 1998). Among these species, sulfate, ammonium, organic and elemental carbon and some metals are found predominantly in fine particles. Nitrate can be found both in fine and coarse particles. Typical urban aerosols contain sulfate, nitrate and ammonium in 0.1 to 1.0 μm size range (the condensation and droplet modes) and in a third mode of over 1 μm .

PM mass concentrations vary significantly on both temporal and spatial scales. The highest PM loadings, excluding dust storms and fires, are often found in major urban centers and small industrial areas where local sources strongly influence air quality. Long-range transport of PM and precursor gases has been documented for ground-level ozone and its precursors, as well as nitrate and sulfate compounds on regional, continental, and trans-oceanic scales. Figure 1.1 illustrates the potential for PM to be an issue at all spatial scales depending on the relative contributions of precursor gases and primary particles (NARSTO, 2004).

Table 1.1. Comparison of ambient particle fractions (from Kindap, 2005).

	Fine ($\leq 2.5 \mu\text{m}$)		Coarse ($2.5 - 10 \mu\text{m}$)
	Ultrafine ($< 0.1 \mu\text{m}$)	Accumulation ($0.1 - 2.5 \mu\text{m}$)	
Formed from:	Combustion, high – temperature processes, and atmospheric reactions		Break – up of large solids/droplets
Formed by:	Nucleation Condensation Coagulation	Condensation Coagulation Evaporation of fog and cloud droplets in which gases have dissolved and reacted	Mechanical disruption (crushing, grinding, and abrasion of surfaces) Evaporation of sprays Suspension of dusts Reactions of gases in or on particles
Composed of:	Sulfates Black carbon Metal compounds Low-volatility organic compounds	Sulfate, SO_4^- Nitrate, NO_3^- Ammonium, NH_4^+ Hydrogen ion, H^+ Black carbon Large variety of organic compounds Metals: compounds of Pb, Cd, V, Ni, Cu, Zn, Mn, Fe, etc. Particle – bound water	Suspended soil or street dust Fly ash from uncontrolled combustion of coal, oil, and wood Nitrates and chlorides from HNO_3 and HCl Oxides of crustal elements (Si, Al, Ti, and Fe) CaCO_3 , NaCl , and sea salt Pollen, mold, and fungal spores Plant and animal fragments Tire, brake pad, and road wear debris
Typical Atmospheric half-life:	Minutes to hours	Days to weeks	Minutes to hours
Important Removal processes:	Growth into accumulation mode Wet and dry deposition	Wet and dry deposition	Wet and dry deposition
Typical Travel distance:	< 1 to 10s of km	100s to 1000s of km	< 1 to 10s of km (100s to 1000s in dust storms)

PM varies both geographically and seasonally. Table 1.2 summarizes the major source contributions to primary and secondary PM. Varying source contributions and meteorological influences drive a large dynamic range of seasonal and diurnal variation in

PM mass concentration and composition. The origins of PM could be both anthropogenic and natural sources. Anthropogenic emissions can readily be identified with industrial sources, commercial operations, power plants, residential dwellings, and transportation. Natural emissions result from volcanic eruptions, wind-blown sea spray, dust storms from remote arid areas, and forest or brush fires initiated by lightning strikes. Other natural emissions include sulfur gases from terrestrial and marine sources, nitrogen oxides from soil respiration and lightning strikes, and organic vapors from vegetation.

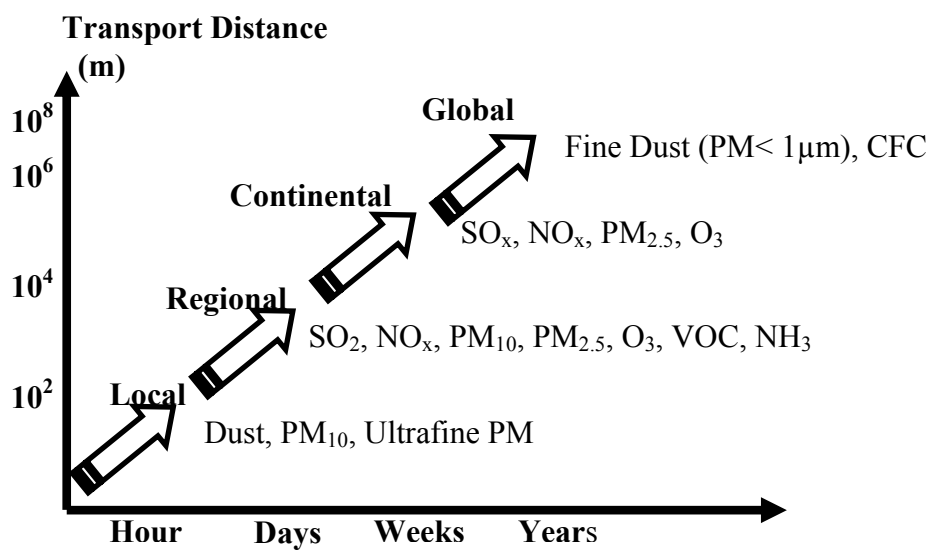


Figure 1.1. Illustrative transport scales for PM and other atmospheric pollutants (from Kindap, 2005).

Long-range transport of air pollutants has generally been studied in Europe under the framework of the European Monitoring and Evaluation Program (EMEP). As a result of these studies, long-range trans-boundary transport is responsible for a significant fraction of the particulate pollution in European cities as well as in rural areas (Baltensperger, 1999). Anthropogenic sources are dominant in Europe because of the urbanization of many countries and the large number of vehicle and combustion sources (industrial and residential). The industrial activities, high volumes of traffic and urbanization of the Continent of Europe had, as a result, the anthropogenic sources of PM to be predominant, mainly in urban areas (Lazaridis et al., 1999). Recently, there has been an extensive research and several regulations have been issued on PM focused air pollution mainly because of severe public health risks for susceptible members of the population, more

visibility reduction and damages to sensitive ecosystems in Europe. These studies have indicated a significant association between the long – range component of PM and a wide range of health damaging effects (EMEP/CCC-Report, 1999).

Compositions, morphology, physical and thermodynamic properties of aerosols vary between geographical places and seasons (Finlayson-Pitts and Pitts, 1986; Seinfeld and Pandis, 1998; Alpert and Hopke, 1981). Some studies have shown that in Northwestern Europe, aerosol concentrations between urban and non-urban areas do not exceed 20 per cent (Van Der Zee et al., 1998). Furthermore, a number of studies on wintertime concentrations of PM₁₀ and black smoke in 14 urban and 14 non-urban locations in Europe indicate a relatively small difference (on average 22 per cent for PM₁₀ and 43 per cent for black smoke) (Hoek et al., 1997). Similar observations on the regional character of PM are reported also in United States (EPA, 1996a). These results have indicated that there was a long-range transport of air pollutants. Long-range transport of PM has also been studied intensively in Southern Scandinavia (Pakkanen et al., 1996; Lannefors et al., 1983; Amundsen et al., 1992). Air masses originating from the British Isles, Central and Eastern Europe were mainly responsible for the long range transport of pollutions. Other studies show that long-range CO transport from both Western and Eastern Europe, mostly from fossil fuel use, contributes 60 to 80 per cent to the boundary-layer CO over the Mediterranean (Lelieveld and Siegmund, 2002). Hacidalihoglu et al. (1992) showed that during a field experiment near the Black Sea, 70 per cent of the mean concentrations of various pollutants have originated from Western and Central Europe. Sciare (2003) and his colleagues obtained the major contribution of aerosols of Central Europe to the Mediterranean region which was confirmed in terms of anthropogenic emissions. In addition Al-Momani (1997) and his colleagues demonstrated some indications of long-range transport from Europe to the Eastern Mediterranean.

Table 1.2. General descriptions of PM emissions and source types adapted from NARSTO (2004).

Emissions		General Source Types
Primary	Crustal / Soil Dust / Road Dust	Paved / unpaved roads, vehicle tire and brake wear, construction, agricultural and forestry operations, high wind events and fires.
	Salt (NaCl)	Oceans, road salt and salt pans / dry lake beds.
	Biogenic material	Pollen, spores and plant waxes.
	Metals	Industrial processes and transportation
	Black carbon	Fossil fuel combustion (especially diesel engines).
	Semi – volatile organic compounds (direct condensation of organic vapors at ambient conditions) and non – volatile organic compounds.	Contemporary and fossil fuel combustion, surface coatings and solvents, cooking, and industrial processes. Forest fires and biomass burning.
Semi- and volatile organic compounds (forming secondary organic aerosols)		
Secondary	Sulfur dioxide (forming sulfate particles)	Electrical utilities, transportation, mining and smelting, and industrial processes.
	Ammonia (contributing to formation of ammonium sulfate and ammonium nitrate)	Agriculture and animal husbandry, with minimal contributions from transportation and industrial processes.
	Nitrogen oxides (forming ammonium nitrate with ammonia)	All types of fossil fuel combustion and to minor degree microbial processes in soils.

Aerosol particles are generated through a combination of physical, chemical and biological processes in the atmosphere and in adjacent reservoirs (Heintzenberg, 1994). Among these processes, three different source types are distinguished. The first one is called Bulk-to-Particle Conversion (BPC). When the earth's crust is the solid based material for this type of process, it leads to the production of mineral dust particles. With natural water reservoirs as liquid based material, salt particles will be produced. Plant debris and pollen can also be classified under the BPC heading. In all BPC processes, physical, chemical and biological precursor processes are necessary for the division of bulk

material into particles before the proper emission processes can take over to make them airborne. The most important BPC process is the formation of sea salt particles. Small air bubbles are formed in the surface layer of the wind-stirred water. Each bubble produces 100-200 film drops with diameters between 1 and 100 μm . The second important natural BPC type of source generates particles from crustal material by means of a two-stage process. During the first stage, physico-chemical erosion processes divide the bulk material into small grains which are ejected into the atmosphere during the second stage. There are two models for stage one. The first one assumes slow processes dividing each grain at random into two different parts. It can be shown that this assumption leads to a binomial size distribution which will become a log-normal size distribution (Figure 1.2). The second model assumes fast processes which divide each grain at random into k parts yielding an exponential mass distribution size.

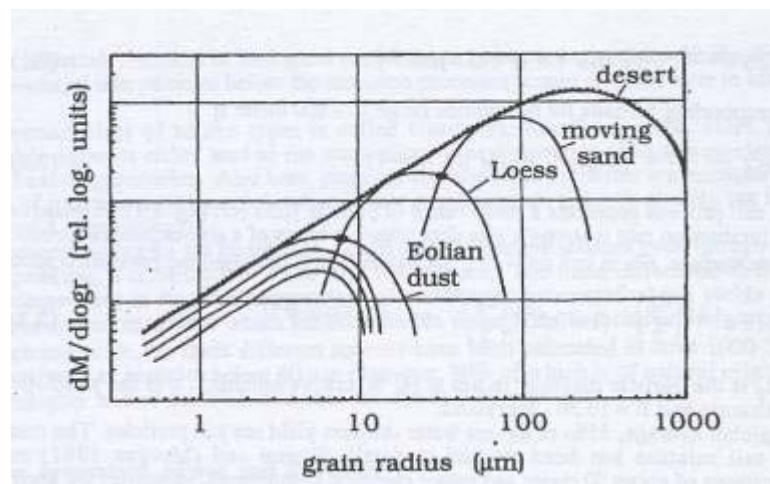


Figure 1.2. Schematic picture of mass size distributions in different sands (from Heintzenberg, 1994).

The second class of source types is called Gas-to-Particle Conversion (GPC). Condensable vapors either lead to the nucleation of new particles or to the condensational growth of existing particles. Physical and chemical processes are necessary for the accretion of precursors. These precursors are airborne already but too small to be counted as particles yet. There are two basic processes resulting from mass transfer from the gas phase to particulate phase. Pre-existing particles may grow through a material condensing from the gas phase or new particles may form through homogenous nucleation. The two

key parameters in the nucleation process are the curved particle/gas interface and the supersaturation ratio.

Combustion processes are the third class of particle sources even though they are a combination of the first two classes. The main differences to BPC and GPC processes lies in the high temperature of combustion processes which yields particles with shapes and compositions which are not possible through the first two processes. The combustion of all carbon-containing particles leads to the formation of soot particles containing elemental carbon (EC), partially-combusted fuel components and products of the high-temperature reactions in the flame. These primary soot particles are very small (< 10 nm), but they rapidly aggregate through coagulation, starting already in the flame. In the case of solid fuels, there are several pathways, leading to a variety of particle sizes, shapes and composition. The high-temperature fragmentation of burning coal and other solid fuels is a special case of a BPC-source process. Supersaturated vapors are formed in all combustion processes (Figure 1.3).

Atmospheric reactions modify the physical and chemical properties of emitted chemicals (Seinfeld and Pandis, 1998). Sulfur dioxide can be converted to sulfate by reactions in gas, aerosol and aqueous phases. The aqueous pathway is estimated to be responsible for more than half of the atmospheric sulfate concentrations and the rest is produced by gas-phase oxidation of SO_2 by OH (Walcek et al. 1990; Langner and Rodhe, 1991; Karamchandani and Ventkaram, 1992; Dennis et al., 1993). Fogs in polluted environments have the potential to increase aerosol concentrations. However, they also have the potential for the reduction of aerosols due to deposition of fog droplets (Pandis et al. 1990 and 1992). The low amount of liquid water in particles may trigger significant aqueous-phase conversion of SO_2 in such droplets, which can contribute to sulfate formation for very high relative humidity values above 90 per cent, and in areas close to ammonia or alkaline dust emissions. Sea-salt particles can also contribute to limited sulfate production (Sievering et al., 1992), as they are buffered by the alkalinity of sea water.

Atmospheric nitrate sources can also be distinguished into primary, gas phase, aqueous phase and aerosol phase. On the other hand, primary nitric acid emissions are too small and can be neglected (U.S. EPA, 1996). Gas-phase production of HNO_3 by reaction

of OH with NO_2 is well-established. The reaction of OH with NO_2 is 10 times faster than the reaction with SO_2 (Seinfeld and Pandis, 1998). A second pathway of nitrate formation is through reaction of NO_2 with O_3 , which operates only at nighttime. The gas-phase reaction of OH with NO_2 is the dominant daytime nitrate production.

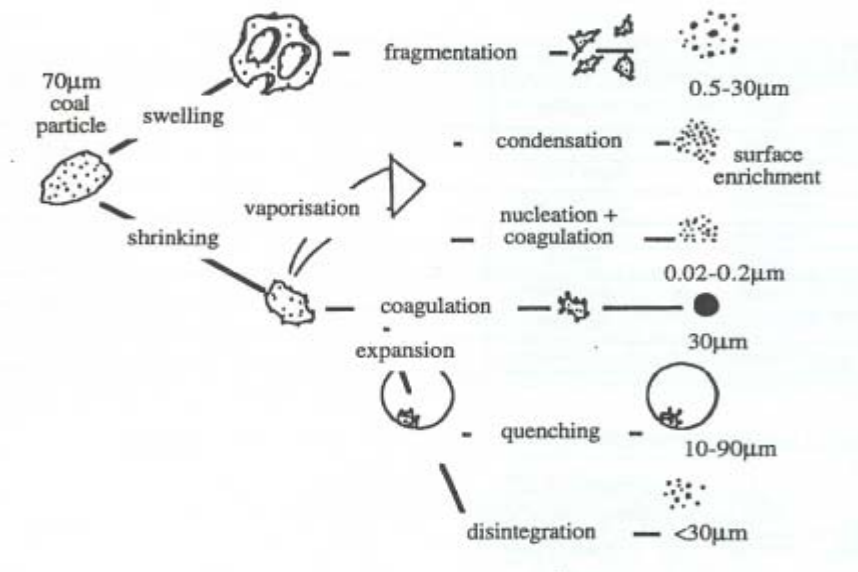


Figure 1.3. Pathways of particle formation during the combustion of pulverized coal (from Heintzenberg, 1994).

1.1. Air Quality Modeling

In order to develop air pollution control strategies, a better understanding of meteorological and chemical processes that contribute to the composition of atmosphere is required. Modeling studies can help in achieving this integration. Simulations of meteorological fields over urban or regional scales are gaining a more considerable place in estimation and evaluation of air pollution. The photochemical grid models aid in developing air pollution strategies (Chang and Cardelino, 2000).

The need for more detailed evaluation of air pollution in these scales is continuously increasing. In order to make estimations under complex terrain conditions, where an important portion of meteorological variables cannot be measured, high resolution and non-hydrostatic mesoscale meteorological models and chemical models that can work

coupled to these meteorological models are needed. The evaluation of complex mesoscale atmospheric flows and local circulations such as land and sea breezes, under synoptic processes are also gaining a more important place in regional transport models.

Air quality models are mathematical descriptions of the atmospheric transport, diffusion, and chemical reactions of pollutants. They operate on sets of input data that characterize the emissions, topography, and meteorology of a region and produce outputs that describe that region's air quality. Mathematical models for photochemical air pollution were first developed in the early 1970s and have been developed, applied, and evaluated since that time. Much of the field's history is described in reviews by Tesche (1983), and Seinfeld and Pandis (1988).

The region to be modeled is bounded on the bottom by the ground, on the top by the inversion base or some other height that characterizes the maximum extent of vertical mixing and on the sides by east-west and north-south boundaries, unless the coordinates are rotated. This space is then subdivided into a three-dimensional array of grid cells. The horizontal dimensions of each cell are usually a few kilometers for urban applications.

Vertical dimensions can vary, depending on the number of vertical layers and the vertical extent of the region being modeled. A compromise generally must be reached between the better vertical resolution afforded by the use of more vertical layers and the associated increase in computing time. Although aerometric data, such as the vertical temperature profile, that are needed to define the vertical structure of the airsheds are generally lacking, it is important to use enough vertical layers so that NO_x emissions from tall stacks are not overdiluted computationally. There are practical and theoretical limits to the minimum horizontal grid cell size. Increasing the number of cells increases computing and data acquisition effort and costs. In addition, the choice of the dimension of a grid cell implies that the input data-information about winds, turbulence, and emissions, for example -are resolved to that scale. In practice, most urban models use horizontal grid cell of a few kilometers, whereas regional models use horizontal grid cells of tens of kilometers.

There is a need for a set of directives about how to specify the size of the modeling domain, the horizontal grid spacing. These directives must be based on the exercise of models having a wide range of spatial resolutions and on the comparison of model performance against a wide variety of high-quality field data. It has been found that increasing the horizontal grid spacing in a photochemical air quality model will generally result in a reduction in the peak ozone concentration. It also is important to provide adequate vertical resolution-the order of five vertical layers or more for urban-scale applications. The minimum amount of meteorological and air quality data must be prescribed as modeling inputs. The choice of the size of the modeling domain will depend on the resolution available in the data, including the distribution of emissions in the region, the weather conditions, and, to some extent, the computational resources available.

The spatial resolution of the concentrations predicted by a grid-based model corresponds to the size of the grid cell. Thus, effects that have spatial scales smaller than those of the grid cell cannot be resolved. Such effects include the depletion of ozone by reaction with nitric oxide (NO) near strong sources of NO_x like roadways and power plants.

Air quality models (AQM) require three main steps of modeling:

- Meteorological modeling
- Emission modeling
- Chemistry and transport modeling

Each of these models produce outputs that enter as inputs in the next step of modeling (Figure 1.4). The principal output of an AQM system is the concentration levels of the considered atmospheric pollutants in a given domain and timescale. As described in various sections of tropospheric chemistry, understanding of photochemical pollution requires chemical and meteorological backgrounds that interact with each other. The tropospheric chemistry is triggered by UV radiation as well as the existence of numerous chemicals. Thus, the concentration levels of pollutants in a given domain are determined by both transport due to meteorological patterns and chemistry.

1.1.1. Meteorological Modeling

Meteorological models are developed to understand local, regional, or global meteorological phenomena and to provide the meteorological input required by the chemistry and transport models. Meteorological models can be divided into two categories (Zannetti P, 1990):

- Physical models: physical small scale models of atmospheric motion (e.g., wind tunnels)
- Mathematical models: a set of analysis techniques for solving a certain subset of meteorological equations

Mathematical models can be:

- Analytical models, in which exact analytical solutions are obtained
- Numerical models, in which approximate numerical solutions are found using numerical integration techniques

Numerical meteorological models can be divided into two groups:

- Diagnostic models, that are based on available meteorological measurements and contain no time-tendency terms
- Prognostic models, that contain full time-dependent equations and permit non-linear terms (e.g., advection) to create flow field that contains information not present in the observational analyses that are used to initialize the model

The performance of these models depends on the density of the meteorological observations in the given modeling domain. Diagnostic models contain very little physics whereas prognostic models incorporate atmospheric physics and are able to use the available observations to “nudge” the gridded meteorological observations.

Grid-based air quality models require, as input, the three-dimensional wind field for the episode being simulated. This input is supplied by a so-called meteorological module. Meteorological modules that construct wind fields for air-quality models fall into one of four categories (Tesche, 1983; Kessler, 1988):

- Objective analysis procedures that interpolate observed surface and aloft wind speed and direction data throughout the modeling domain.
- Diagnostic methods in which the mass continuity equation is solved to determine the wind field.
- Dynamic, or prognostic, methods based on numerical solution of the governing equations for mass, momentum, energy, and moisture conservation along with the thermodynamic state equations on a three-dimensional mesh.
- Hybrid methods that embody elements from both diagnostic and prognostic approaches

Objective analysis procedures are inexpensive and simple to use. Their disadvantage is that they contain no physics-based calculations, and the results are highly dependent on the temporal and spatial resolution of the observed wind speeds and directions. Results are often unsatisfactory in areas of the modeling domain where observations are either sparse or not representative of the physical geography. Areas of complex terrain, variations in land use, and ocean-land contrasts cannot be accounted for.

Diagnostic procedures impose mass consistency on the flow field through appropriate equations, and can crudely include terrain blocking effects or estimates of upslope and down-slope flows if observed values are entered into the analysis. Diagnostic procedures have modest computational requirements and can require fewer observations than does objective analysis to produce a three-dimensional wind field. Without representative data, however, diagnostic models cannot simulate such features as sea and land breezes.

Prognostic numerical prediction models are intended to simulate all relevant physical processes without requiring a significant amount of observed data. These models require specification of the large-scale flow, surface conditions, and the initial state of the

atmosphere. Because prognostic models simulate the temperature field in addition to the wind field, it is possible to determine atmospheric stabilities and mixing-height fields from the output. However, the computations performed by prognostic models can be expensive, and they do not necessarily reproduce available observations. Recent developments in data assimilation techniques could overcome the latter problem by forcing models to be more consistent with the available local observations, provided these observations can be shown to be truly representative of the actual meteorological field. Also, with better computer systems becoming available, it is increasingly practical to use full numerical prediction models.

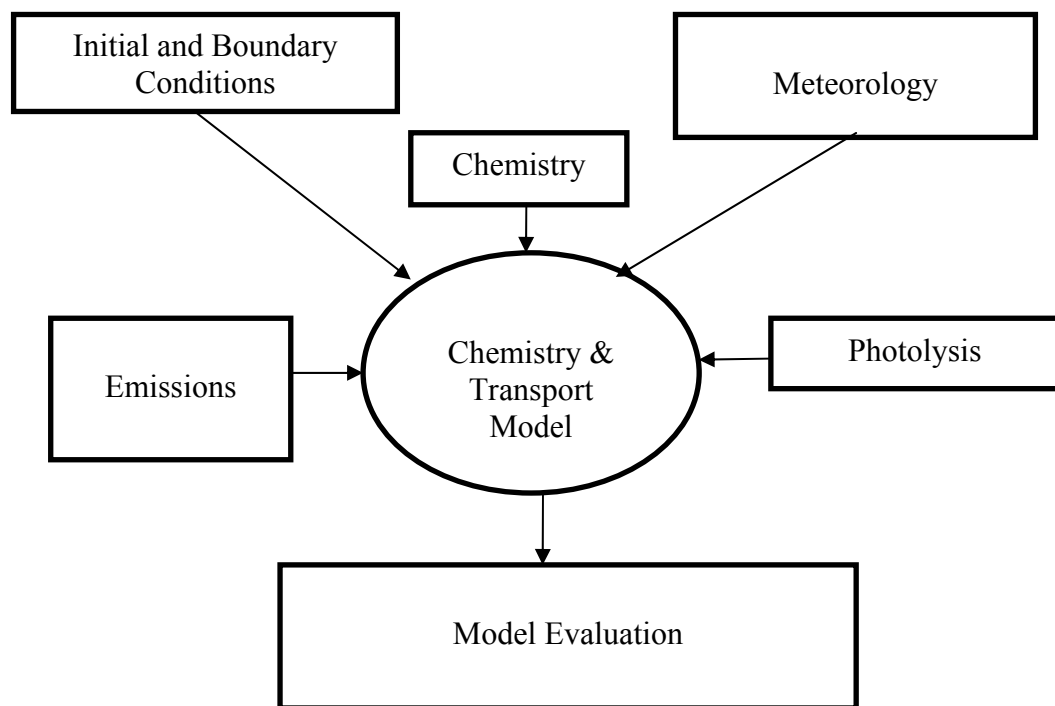


Figure 1.4. Basic steps of air quality modeling.

There are several important meteorological variables other than wind field. Of particular importance is the treatment of photolysis rates and of the effects on these rates of clouds, urban aerosols, and ozone aloft. Clouds have traditionally been neglected in photochemical grid models because these models have focused on gas-phase pollutants, even though clouds can have a significant effect on the vertical distribution of pollutants and on the attenuation (below cloud) or enhancement (near top of cloud) of photolysis

rates. Objective or diagnostic techniques and prognostic modeling also can be used to calculate mixing heights. The key questions relate to the level of accuracy of the spatial and temporal variability in mixing heights. There are no currently accepted procedures for calculating mixing heights, and the mixing height profile will strongly influence the predicted ozone concentrations in the modeling domain.

1.1.2. Emission Modeling

To have better model representations of the chemical processes that the pollutants undergo, we need detailed and up to date emission inventories. An emission inventory is a current, comprehensive listing, by source, of air pollutant emissions associated with a specific geographic area for a specific time interval. Emission inventories estimate the emissions of a species from a source based on a technique that uses emission factors that are based on source-specific emission measurements as a function of activity level regarding the source (Seinfeld and Pandis, 1998).

Emission inventories comprise a wide variety of sources depending on their characteristics of emitting. The sources of emissions can be divided to four main categories; (i) point sources, (ii) area sources, (iii) mobile sources, and (iv) biogenic sources.

Point sources are stationary and individual sources of emissions that can be identified by name and location. The major point source emissions categories are power plants, industrial boilers, petroleum refineries, industrial surface coatings and chemical manufacturing industries. Point sources' emissions are generated from stack emissions. Point sources are major emitters of nitrogen oxides (NO_x) and less important sources of VOCs.

Area sources are those emissions that are too small to be treated as point sources. Area sources' emissions can be generated from solvents used for surface coating operation, degreasing, graphic arts, dry cleaning and gasoline station (tank truck unloading and refueling). Area sources are the activities where aggregated source emissions information is maintained for the entire source categories instead of each point source. The category

also includes commercial buildings, residential buildings, and fuel combustion in non-road machinery, boats, and railroads. Waste disposal in the form of open burning, landfills and wastewater treatment are significant area sources. Though emissions from individual area sources are relatively small, collectively their emissions can be of concern-particularly where large numbers of sources are located in heavily populated areas. Area sources are responsible for particulate matter emissions and more than point or mobile sources for volatile organic compound (VOC) emissions, which contribute significantly to the formation of ground-level ozone.

Mobile sources are categorized as highway and off-highway sources. The highway sources include the automobile, buses truck and other vehicle traveling on local and highway roads. The emission from highway vehicles represents one third of the overall national (VOC) and 40 per cent of the overall (NO_x) emissions. Off-highway sources are any mobile combustion sources such as railroads, marine vessel, off-road motorcycle, snowmobiles, farm, construction, industrial and lawn/garden equipment. Emissions are determined based on a source activity variable. Mobile sources are responsible for about 75 per cent of carbon monoxide pollution, and more oxides of nitrogen emissions than area or point sources. In urban areas, the motor vehicle contribution to carbon monoxide pollution can exceed 90 per cent. In a typical urban area, at least half of the hydrocarbon and nitrogen oxide pollutants come from mobile sources.

Biogenic emissions are emissions from natural sources, such as plants and trees. The emissions are estimated as emissions of biogenic volatile organic compounds (BVOCs) from vegetation for natural areas, crops, and urban vegetation. BVOC emissions are functions of the species leaf mass, emission factors, temperature, and light conditions. Biogenic emission sources are needed to be accounted for in photochemical grid models, as most types are widespread and ubiquitous contributors to background air chemistry. Often only the emissions from vegetation and soils are included, but other relevant sources include volcanic emissions, lightning, and sea salt.

1.1.3. Chemistry and Transport Models

The atmosphere is an extremely complex reactive system where various physical and chemical processes occur simultaneously. Ambient measurements give only a snapshot of atmospheric conditions at a particular time and location. Such measurements are often difficult to interpret without a clear conceptual model of atmospheric processes. These measurements alone cannot be used directly by policymakers to develop effective control strategies for solving air pollution problems.

Mathematical models provide the necessary framework for integration of understanding of individual atmospheric processes and the study of their interactions. A combination of state-of-the-science measurements with state-of-the science models would be the best approach for making real progress toward understanding the atmosphere.

A model involving descriptions of emissions patterns, meteorology, chemical transformation and removal processes is an essential tool to provide a link between emission changes from source control measures and resulting changes in airborne concentrations. The main basic components of an atmospheric chemistry model are emissions, transport and physicochemical transformations.

Atmospheric models can be divided into two types: physical and mathematical models. Physical models are used to simulate atmospheric processes by means of small-scale representation of the actual system, for example, a small scale representation of an urban area. Mathematical models of atmospheric processes can be classified into two broad groups:

- Models based on the fundamental description of atmospheric physical and chemical processes.
- Models based on statistical analysis of data.

Statistical analysis of data gives valuable information of the current or past situation of the atmosphere. These models take advantage of the available databases and are relatively simple to apply. On the other hand, their reliance on past data is their major

weakness. Because these models do not explicitly describe casual relationships, they cannot be reliably extrapolated beyond the bounds of the data from which they were derived.

1.1.3.1. Types of atmospheric chemical transport models. A wide variety of atmospheric models have been used, some of which simulate changes in the chemical composition of a given air parcel as it is advected in the atmosphere, where there is not a fixed reference point, but the reference travels with the air parcel, and is referred as Lagrangian models. In a Lagrangian model, the air parcel moves with the local so that there is no mass exchange between the air parcel and its surroundings, with the exception of species emissions that are allowed to enter the parcel through its base. The parcel moves continuously, so the model actually simulates concentrations at different locations at different times. Another group of models describe the concentrations in an array of fixed computational cells, where there is a fixed reference point at $t=0$ step. These models are referred to as Eulerian models. An illustration of these two approaches is presented in Figure 1.5. Species in an Eulerian model enter and leave each cell through its walls and the model simulates the species concentrations at all locations as a function of time.

1.1.3.2. Initial and boundary conditions. The solution of the full atmospheric diffusion equation requires the specifications of the initial concentration fields of all species and side boundary conditions, two for each of the x, y and z directions, in three dimensions. In a modeling domain, there are practically never sufficient measurements that would represent the concentrations of each pollutant in each grid cell, so one needs to extrapolate from the few available data to the rest of the modeling domain. As the simulation proceeds, the impact of the initial concentrations decay exponentially, while does due to emissions or advection increases in the relative magnitude. Thus, even if the initial concentrations contain big errors, their effect is eventually lost and the solution is dominated by the emissions and the boundary conditions. It is therefore common in atmospheric simulations some period of time before that is actually of interest. This period is often called “start up” period or “spin up” period. This period is determined by the residence time of an air parcel in the modeling domain.

The boundary conditions, which are the initial concentrations at the boundaries of the modeling domain, are specified as a function of time. Unfortunately, specie concentrations are practically never known at all points of the boundary of a modeling domain. Unlike the initial conditions, the boundary conditions, especially at the upwind boundaries, continue to affect predictions throughout the simulation. The common practice, if applicable, is to set the boundaries of a domain to relatively clean areas, where the concentrations are relatively well known and have a small effect on model predictions. Uncertainties in an urban model as a result of boundary conditions may be reduced by use of larger scale models (e.g., regional models) to provide the boundary conditions to the urban scale model. This technique is called “nesting”.

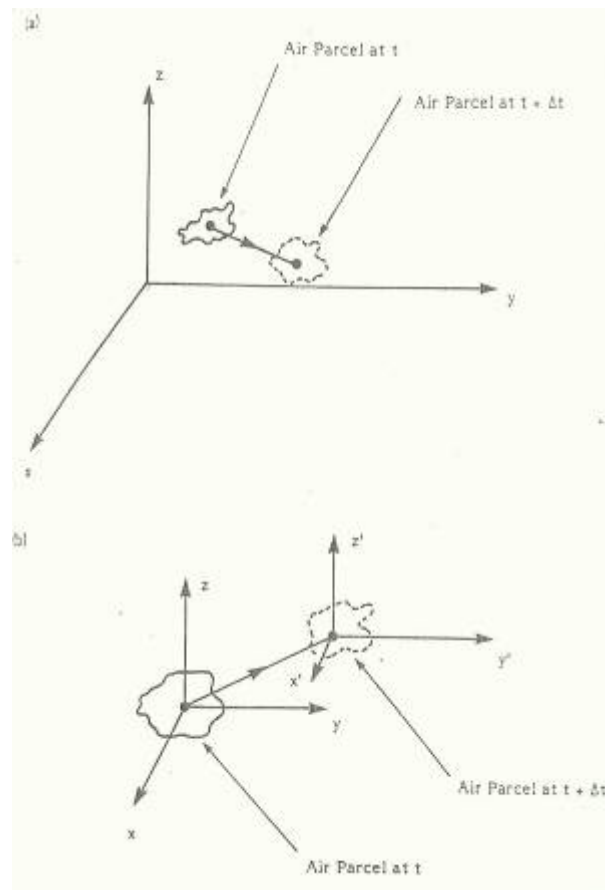


Figure 1.5. Illustration of a) Eulerian and b) Lagrangian approaches.

The assessment of Istanbul PM_{10} response to European countries has been performed by atmospheric models (Kindap et al., 2006). The whole forecast system included meteorological forecasting, emission modeling, and air quality modeling (Fig. 1.6). In this

study, air quality simulation with respect to a specific episode is performed for the European, Balkan and finally İstanbul scales with horizontal resolutions of 30, 10 and 2 km, respectively. The Fifth-Generation NCAR / Penn State Message Model (MM5; Grell et al. 1994) is used to provide meteorological fields to the Community Multiscale Air Quality Modeling System (CMAQ; Byun and Ching, 1999). For the European and Balkan domains, the emission inventory data of 30 and 10 km resolutions, compiled from the TNO inventory, is used in order to provide hourly input emission data. For the İstanbul domain, a 2 km resolution emission inventory is developed from various activity data and databases.

The study discussed in this thesis aims to investigate a winter episode of high PM_{10} levels from January 13 to January 17, 2008 in İstanbul. MM5 non-hydrostatic mesoscale model is used in order to produce the meteorological fields necessary for the chemistry and transport model, CMAQ. A high resolution modeling system is configured for the first time to study the pollution levels in the İstanbul area. In order to achieve this task, a model ready emission inventory is developed on high spatial, temporal and chemical resolution for the first time and validated for the particular episode. A base case and several emission scenarios are modeled to test the sensitivity of the CMAQ results to the emission change.

In light of the rapid development of atmospheric modeling, accurate simulations of the transport, diffusion, dry and wet deposition, and chemical transformations for gases and particulate matter are largely dependent on quality of meteorological and emission inventory data sets. Appropriate spatial and temporal evolution of the meteorological fields and emission inventories could be the first and most important step to get correct results of air quality.

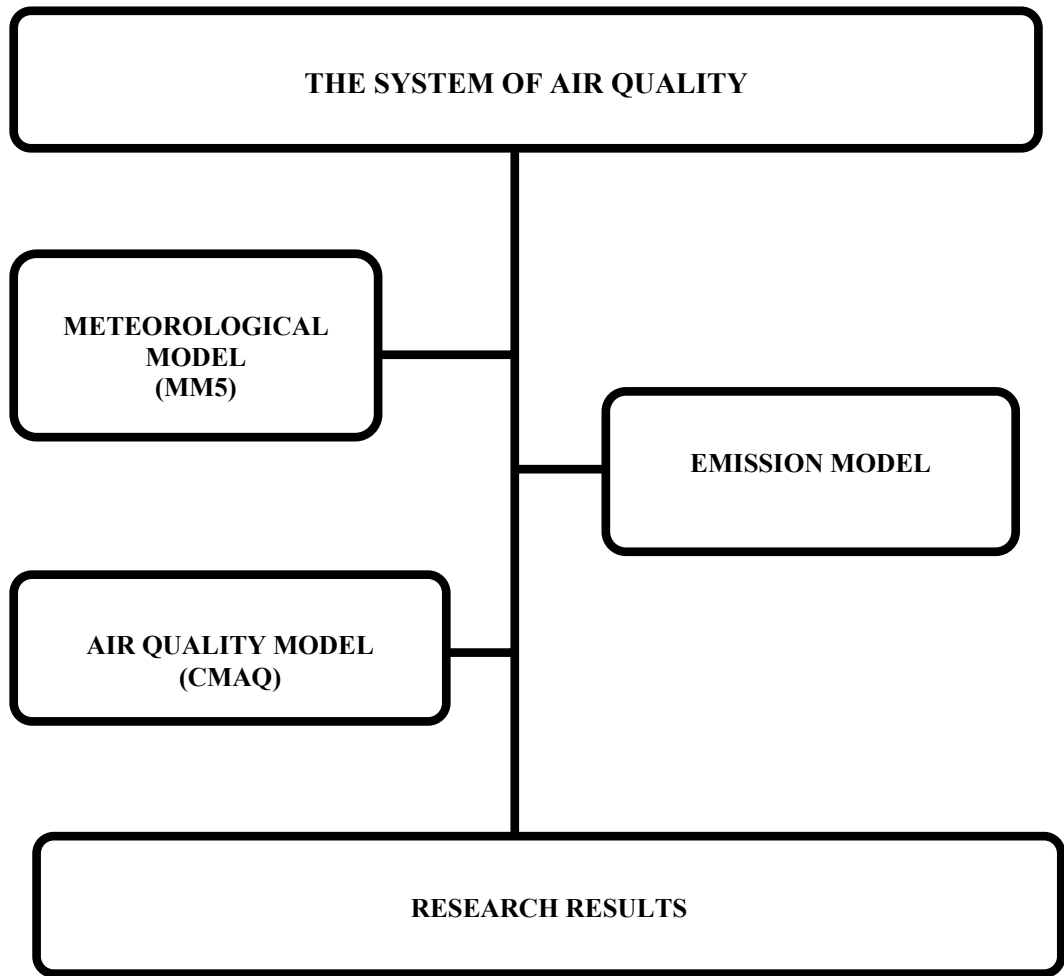


Figure 1.6. General model data flow chart for the modeling system (Kindap et al., 2006).

2. LITERATURE REVIEW

Meteorological models are used to simulate and forecast short-range meteorological conditions. In addition, operational use of weather prediction models has become widespread in recent years (Mass and Kuo, 1998). Moreover, prognostic meteorological models have been used to provide the meteorological inputs for air quality modeling studies (Pielke and Uliasz, 1998).

Alapaty et al. (1995) investigated the sensitivity of the US EPA Regional Oxidant Model (ROM) for different meteorological (prognostic MM4 and diagnostic model) inputs over Eastern U.S. The comparison of predicted concentrations of chemical species indicated higher values (1-5 ppb for NO_x and 1-25 ppb for reactive organic gases) when the prognostic model outputs were used.

Kumar and Russell (1996) investigated the impact of prognostic (MM4) and diagnostic meteorological inputs on photochemical air quality modeling performance for Southern California region during the Southern California Air Quality Study (SCAQS) period (27-29 August 1987). The results indicated that the temperature and mixing heights derived from the prognostic models agreed better with observations as compared to velocity data. However, the results obtained from the photochemical models were similar for both inputs except that a lower ozone peak was predicted using the prognostic meteorological inputs.

The necessity of correct description of the wind and turbulence fields used in air quality assessment models should be obvious (e.g., Svensson, 1996a; Berkowitz and Fast, 1996; Liu and Carroll, 1996). Otherwise, it was not possible to represent the transport, deposition, and dispersion of a chemical species and their concentration fields and chemical reactions accurately. Sistla et al. (1996) showed the influence of meteorological uncertainties with respect to ozone control strategies. Al-Wali and Samson (1996) illustrated the sensitivity of the Urban Airshed Model to the placement of boundary layer

measurements with respect to the location of emissions. Svensson (1996a-b) demonstrated that relative errors in meteorological variables simulated in chemical rate constants.

Pielke and Uliasz (1998) emphasized the importance of understanding how errors in the meteorological fields affect the results and conclusions from the air quality model. The importance of meteorological variability and uncertainty was described and discussed in the context of dispersion and chemistry of air pollution. They considered the importance of the spatial effects and temporal effects in terms of models. In the study, examples of uncertainty were given due to spatial resolution, model type and average time of the meteorological model-simulated fields. Their conclusion was not good to take full advantage of meteorological model – generated wind and turbulence fields.

The Norwegian Meteorological Institute has implemented the MM5 modeling system and it ran operationally with a 1 km resolution for the city of Oslo, Norway in order to produce high resolution meteorological data as input to an urban air pollution model during the winter season 1999/2000 (Berge et al., 2000). 22 days with calm winds during the winter of 1999/2000 were chosen to evaluate the prognosis of MM5 against screen level observations of wind, temperature and humidity and the ability of MM5 to improve the hydrostatic model (HIRLAM10) prognosis that was used as initial and boundary conditions. In order to investigate the gain by using higher resolution non-hydrostatic models, results during days with low winds and stable stratification are evaluated. Comparisons of 24 to 48 hour forecasts of wind, temperature and relative humidity for a 10 km resolution hydrostatic model (HIRLAM10) and 1 km forecasts with MM5 based on 24 hour forecasts from HIRLAM10 have been conducted. The finer resolution MM5 runs compared better for wind and relative humidity both with respect to bias and non-systematic errors.

Barna et al. (2000) ventured to utilize the MM5 output as an initial guess wind field for CALMET (The California Meteorological model/photochemical model) to create the meteorological fields for July 1996 in the Cascadia region. The predicted ozone concentration by the California Grid Model (CALGRID) agreed well with observations at the monitors located along the Interstate Highway No. 5 corridor.

Barna and Lamb (2000) also carried out three air quality simulations using CALGRID for an ozone episode which occurred in the Cascadia region of the Pacific Northwest during 11-14 July 1996. These simulations individually utilized the wind field obtained from the MM5 model without observational nudging, MM5 model output without observational nudging as an initial-guess field for CALMET and finally the MM5 model output with observational nudging. The results indicated that ozone predictions significantly improved when the MM5 output with observational nudging was used in comparison with the other two simulations.

Nielsen-Gammon (2002) produced MM5 simulations of the August-September 2000 ozone episode in the Houston-Galveston area. This episode was supported by special meteorological observations including three radiosonde launch site, six wind profiles, a Doppler Lidar, four instrumented aircraft, and special surface flux measurements. As a result, the MM5 successfully simulated the diurnal heating cycle. During the second half of the ozone episode, when a low-level jet was present, the MM5 gave a poor performance. But it was not surprising, since low-level jet was produced by a complex interaction between the diurnal variations of heating and turbulence.

Seaman (2000) studied meteorological modeling for the air quality assessments. Based on this review of current state-of-the-science models and projected demands for meteorological information for future air-quality assessments, the following major conclusions were made: (1) For most purposes, data-assimilating dynamical models are currently the best method available for generating reasonably accurate and dynamically consistent meteorological fields required for air quality applications. (2) The rapid expansion of remote sensing technology provides an outstanding opportunity to reduce errors in meteorological fields, but research is needed to learn how to best use these data in analysis and assimilation techniques. (3) As better land-surface schemes are introduced into meteorological models, considerable benefit may be gained by better coupling with emission models, perhaps leading to fully integrated meteorological emission modeling systems. (4) Rapid growth in computer technology has made it feasible to run multi-day regional meteorological model simulations having very fine grid resolutions. To take full advantage of this new technology, however, more research is needed to develop scale-appropriate physical parameterizations (land/surface fluxes, soil hydrology, boundary layer

fluxes, deep convection, and shallow clouds). (5) Mandated limits on long-term exposure to pollutants will require greater emphasis on long-range transport. This necessitates the re-evaluation of mesoscale models for inter-regional transport problems, particularly in episodes of poor air quality associated with weak dynamical forcing and convection. (6) Better coupling and interfacing of meteorological models and AQMs is a significant need, and preliminary efforts are being made to reduce errors due to model incompatibilities. Eventually, this should lead to fully integrated models that perform both meteorology and chemistry processing.

Thunis (2001) investigated the influence of the scale on modeled ground level O₃ concentrations for Europe. In the study, meteorological data requested to drive the TAPOM (Transport and Air Pollution Model) air quality model were simulated by the mesoscale non-hydrostatic model MM5. The comparison of air quality results obtained with different resolution meteorological datasets showed a similar pattern for the pollution plume although differences in resolution ranged from 1.5 to 50 km. Even a very coarse resolution of 50 km was able to capture the main features of the atmospheric circulations in the Milan region. On the other hand, the variability of O₃ levels as simulated with the different meteorological resolutions was shown to be significant and at least as important as the variability associated with the resolution of the air pollution model itself. In the area of Genova, where sharp changes in landuse were present (coastline), the impact of the spatial resolution of meteorology was shown to produce large errors in O₃ concentrations. Although these conclusions are valid only for the specific area of Milan and only for May 13th, 1998, one can expect a similar behavior in other conditions (Thunis, 2001).

Arellano et al. (2001) carried out observational evaluation of PBL (Planetary Boundary Layer) parameterization modeled by MM5. In this study, PBL schemes implemented in the mesoscale model MM5 were evaluated with the observational data set, because they emphasized that mesoscale models were currently used to simulate and forecast short-range meteorological and air pollution problems. As a result, the convective boundary layer modeled by MM5 strongly depends on the selected PBL scheme.

Mass et al. (2002) studied the effects of increasing horizontal resolution on the forecast skill by examining the results of two years of the University of Washington Real-

Time MM5 Modeling and Verification System over the Pacific Northwest. They found that decreasing grid spacing did improve the reliability of the results, but does not necessarily improve significantly the skill accuracy of the forecasts.

Concern for the potential economic cost from severe storms to the European Community has provided justification for increasing research and field studies with hopes of improving the ability to forecast these extreme events. To take this situation as a goal, Dailey and Keller (2002) made an approach and verification for extreme wind events by using the MM5 model. The model was initialized and bounded by the NCAR/NCEP (The National Center of Atmospheric Research/National Centers for Environmental Predictions) reanalysis data from 1958 to 1998 for each 36 hour-period that included at least one winter season mid-latitude cyclone passing over Europe. The MM5 model domain included two grids, 90 km and 30 km, respectively. Four-dimensional data assimilation (analysis nudging) was used to nudge the wind field to the reanalysis data. At the end of the research, they proved that MM5 is capable of producing a realistic wind climate for European winter storms.

In the troposphere, the long-range transport of pollutants into the Arctic was researched by Christensen et al. (2003). They used long-range transport modeling DEHM (The Danish Eulerian Hemispheric Model). The model system has two meteorological versions: Analyses version coupled with the MM5 and the ECMWF data and, forecast version coupled with Eta and NCEP data. The MM5 model was run with one nest for a period of 10 years 1993-2002 (150 km and 50 km resolution). The results for a 10 year period from 1993 to 2002 were compared with measurements from both EMEP data and Danish stations. The comparison showed good performance.

Anantharaman et al. (2003) evaluated the performance of a computationally efficient the MM5/CALMET (The California Meteorological model/photochemical model) system for developing wind field inputs to air quality models. Wind fields derived from this system were compared with the wind profiler observations from the Northeast-Oxidant and Particle Study (NE-OPS) field campaign over Philadelphia, undertaken during one of the summer ozone episodes in 1999 (23-24 July 1999). The MM5 simulations were performed on a nested grid (36, 12 and 4 km horizontal resolution) with 14 layers in the vertical

direction for the period 21 July 1999; 00 UTC to 25 July 1999; 05 UTC. The CALMET meteorological model was applied to 14 layers in the vertical direction, a horizontal resolution of 4 km and a domain which included New Jersey and the Philadelphia region and was employed in two modes. In the first mode, the MM5 model wind and mixing height output results (for 36, 12 and 4 km horizontal resolution) were ingested every hour into the CALMET diagnostic meteorological model along with an objective analysis procedure using all available observations. In the second mode, the MM5 results were utilized and the CALMET employed the objective analysis procedure. All the above simulations were compared with the wind profiler data collected during the NE-OPS program. The results of this study indicated that utilizing the coarsest prognostic meteorological model output in a diagnostic model provided an attractive option for generating accurate meteorological inputs for air quality modeling studies, especially for long-term simulations of periods lasting from several weeks to a year.

Srinivas et al. (2007) analyzed the sensitivity of mesoscale simulations of land-sea breeze to boundary layer turbulence parameterization for the south east coast in the Chennai region of India. MM5 mesoscale meteorological model was employed on nested domains. They tested four boundary layer turbulence parameterization schemes were selected for the study. These schemes were Blackadar (BK), medium range forecast (MRF), Mellor – Yamada (MY) and Gayno-Seaman (GS) schemes. BK and MRF schemes produced boundary layers that were more mixed than those produced with the MY and GS schemes. All schemes underestimated surface sensible heat fluxes during stable night conditions whereas daytime conditions were reasonably simulated by MRF and BK schemes. Among all the schemes, BK scheme has reasonably produced the PBL height, humidity and wind fields. The first order schemes (BK and MRF) have done equally well and better in the same-breeze flow simulation which is a simple case of atmospheric circulation.

Melas et al. (1998) investigated the sea-breeze circulation in Athens under weak large scale ambient winds under the MEDCAPHOT-TRACE campaign. The numerical simulations were performed using a three-dimensional, higher order turbulence closure model, MIUU. The model was configured for a 150 km resolution and topography and land use data with a resolution of 2 km and a model top was set to 7 km. The day chosen

for the simulation was 15th of September, 1994, which was characterized by high concentrations of both primary and secondary pollutants. They found that more than one sea-breeze system developed over Attica peninsula and the patterns produced by the model were consistent with the observations, with the most noticeable differences were found in small scale fluctuations of the near-surface winds.

Topçu et al. (2003) studied the surface ozone concentrations and their relation to wind field in İstanbul. They used the prognostic Systems Applications International Mesoscale Model (SAIMM) to produce three dimensional meteorological inputs to a chemistry transport model. 2 km horizontal resolution with 22 layers in vertical was defined in the model. They found that the circulation was clearly appearing during intense solar heating hours and disappearing at the late afternoon hours. The pattern at the noon hours was characterized by the sea breeze at the south of the city. At the evening hours around 1900 LST, winds from northeast dominated while very low wind speeds were experienced in the center of the city.

Accurate simulations of the transport, diffusion, dry and wet deposition and chemical transformations for airborne chemical species, aerosols and particulate matter are largely dependent on data sets that can properly resolve the spatial and temporal evolution of the meteorological fields on a wide range of scales. In recent years, the use of three-dimensional high frequency mesoscale data sets derived from the MM5 to drive air quality simulation models has been growing. The MM5 model proved to be a powerful tool for developing three-dimensional high-resolution meteorological fields for air quality assessments (Klausmann et al., 2003).

As described before, one of the key elements in air quality modeling is the estimation of emissions. Emissions represent the initial conditions within a domain and together with the meteorological fields produced by the meteorological models, are processed by the chemistry and transport models. Emissions are one of the most important sources of uncertainties in a modeling system and development of these emissions in high resolution and as realistic as possible is crucial for the model performance and evaluation. There are various techniques and tools in the modeling community that are developed to estimate the spatial and temporal allocation of the annual emissions, such as the geographic information

system (GIS). Researchers have recently put forth several studies to improve methods, models and emission factors for the generation of emission data to be used in the atmospheric models. Furthermore, the assessment of the accuracy of emission data has been performed for each study.

An emission inventory for NH₃ was constructed for the Danish county of Vejle (area about 3000 km²) with a spatial resolution of 100x100 m² (Asman et al., 1999). Also a newly developed atmospheric transport and deposition model for the total nitrogen deposition was calculated for the same area taking into account all Danish and foreign NH₃ and NO_x emissions. The aim of the research was to model the emission of ammonia from agricultural sources and its diurnal and seasonal variation. At the end of the study, they were able to generate emission inventory of ammonia for Denmark.

Baldasano et al. (1999) prepared an emission inventory for the Barcelona-Catalonia area, including both biogenic and anthropogenic emissions. These emissions were used as input in the coupled meteorological/photochemical modeling system to predict concentrations of pollutants over the Barcelona Geographical Area.

Another research was implemented by Friedrich et al. (1999) to calculate multi-scale high resolution emission data for Germany and Europe. The aim of the research was the improvement and further development of methods to calculate data on anthropogenic emissions of air pollutants with high a spatial and temporal resolution. For Germany and Europe, air pollutants NO_x, CO and VOC (in a detailed speciation) were covered. Emission data calculated with these models were used as input in the German tropospheric research program (TFS) for numeric simulations of atmospheric processes. The main conclusions were that emission data sets and their fast and flexible calculation remain to be vital for all modeling and evaluation issues being conducted within the Generation and Evaluation of Emission Data (GENEMIS) program. By improving the software and approaches for this calculation, it was possible to provide data sets with up to several greater Berlin areas of data within an acceptable time frame.

Within the scope of EUROTRAC/GENEMIS (A EUREKA Environmental Project/ The Generation and Evaluation of Emission Data), the study of Turkish emission inventory

covered by the Aegean Region was conducted by Müezzinoğlu et al. (1999). Inventories for these regions included the largest point sources (industries), domestic heating and traffic sectors. All emissions calculated with respect to four pollutant types (SO_x , NO_x , MVOC and CO) were evaluated in three pollutant source categories of point, area and line sources.

Ponche et al. (1999) worked on the improvement of the methodology of emission inventories and emission scenarios for air quality management. In the ESCOMPTE programme (realization of field experiments to constraint models of atmospheric pollution and emission transport), and with the support of the ADEME (Agence de l'Environnement et de la Maîtrise de l'Energie), improvements of emission inventory methodology consistent with the European emission databases have been started to facilitate emission database settlement for all regions in France. In the frame of the French ECODEV (Recherche Interdisciplinaire sur les Technologies pour l'Ecodéveloppement)-AGRICE (Agriculture pour la Chimie et l'Energie) programme and the PRQA Alsace (Regional Planning for Air Quality Management in Alsace), some scenarios have been elaborated to study respectively the impacts of some reformulated and oxygenated fuel car blends on the air quality and the impact of future European regulations (2015) at the regional scale.

Another study carried out in the related area was a new emission model EMIMO (EMission MOdel) based on the V2.0 version of EMIMA (Global Emission Modeling; San José et al., 1999) for general applications applied over the Bilbao and Madrid (Spain) domains. The IER (Institut für Energiewirtschaft und Rationelle Energieanwendung – Stuttgart, Germany) emission model (Schwarz and Friedrich) was also used to compare the emission data with both data bases. Both models followed the CORINAIR emission methodology. The results showed the importance of GIS data for final emission inventories. The ARC / INFO E00 maps from the Digital Chart of the World (1 km spatial resolution) and the DXF (100 m spatial resolution for only the Municipality of Bilbao) maps from the Municipality of Bilbao had been used to compare the emission data. The results showed that the DCW managed to obtain better comparisons with the IER emission data base than the DXF Municipality Maps which highlight the importance of having a homogeneous spatial distribution of geographical data.

The Technical University of Madrid (UPM) is currently studying the different alternatives to reduce air pollution in Spain. The policy design and decision – making for improving air quality are based on emission projections up to the year 2020 under several scenarios. The US/EPA CMAQ modeling system has been selected and therefore the SMOKE emission inventory information has been used to generate model – ready emission data. In spite of having a very flexible design, both modeling systems (CMAQ and SMOKE) have been developed, taking into account the inventory formats and particular conditions of the United States. This poses an obstacle for its application to other countries. Therefore, Borge et al. (2002) developed a specific methodology for the Spanish case. Their study showed the initial efforts to achieve a high quality emission data set suitable for modeling from the Spanish Emission Inventory.

Diem and Comrie (2001) illustrated the potential of a geographic information system (GIS) for enhancing an existing spatially-aggregated anthropogenic emission inventory and discussed the ozone-specific management implications of the resulting spatially-aggregated inventory. The main GIS methods include calculation of emissions for specific features, spatially disaggregating region-wide emission totals for area sources, and adding emissions from various point sources. Additionally, temporal allocation factors enable the addition of multi – temporal component to the inventory. The results showed that on-road motor vehicles accounted for approximately 50 per cent of VOC and NO_x emissions annually. On-road vehicles and wood burning were the largest VOC sources in the summer and winter months, respectively. The most noticeable weekday versus weekend VOC emissions differences were triggered by increased residential wood combustion and increased lawn and garden equipment use on weekends.

Landuse, topographic information and elevation data are very important input parameters for modeling anthropogenic and biogenic emissions. Several land-use data sets have been provided to the users within the GENEMIS (Generation and Evaluation of Emission Data), GLOREAM (GLObal and REgional Atmospheric Modeling) and SATURN (Studying Atmospheric Pollution in Urban Areas) subprojects. They include data at general categories as well as data at plant species-specific level. Smiatek et al. (1999) (Fraunhofer Institute for Atmospheric Environmental Research-Germany) provided appropriate landuse data for modeling anthropogenic and biogenic emissions by

using data from existing sources and data from remote sensing. In addition, how the biomass and leaf area index could be derived from remote sensing imagery was studied. The third task was to provide information on typical seasonal changes of vegetation. This data was needed to improve the accuracy of the modeling of biogenic emissions. At the end of the research, more than 44 different landuse data sets with 14 different nomenclatures, 30 data sets with vegetations index (VI) and leaf area index (LAI) data, 15 digital elevation models (DEM) were processed. More than 130 plant species names, 33 chemical compounds as well as 668 emission factors for biogenic VOC, 3600 records of information on forest area with 6 different nomenclatures and more than 400 regions were integrated into the relational data base.

Elbir and MÜezzinoğlu (2004) presented the air pollutant emission inventory of primary pollutants for Izmir, which is a highly industrialized area situated in the western part of Turkey. A proper emission inventory is very important for planning pollution control programs, particularly in coastal sites like Izmir, where environmental quality is of growing concern owing to their typical meteorological conditions. The sources were broadly classified as point, line and area sources in a systematic way. The data on activity levels of industries, fuel consumption in vehicles and domestic activities along with the respective emission factors were used for estimating the emissions for the year 2000. Their results showed that industry is the most polluting sector for sulfur dioxide (SO₂) in the study area contributing about 88 per cent of total emissions. On the other hand, domestic heating is the most polluting sector contributing about 56 per cent of total PM emissions, while traffic has the highest portion for NO_x emissions. Especially, emissions from industries located outside the metropolitan city center are much higher in amount. Industries located around Izmir metropolitan center contribute to the industrial SO₂ emissions by 93 per cent, PM emissions by 59 per cent and NO_x emissions by 80 per cent of the total.

Kesgin (2006) estimated the aircraft emissions during landing and take-off (LTO) at some biggest Turkish airports such as Atatürk International Airport (AIA) at İstanbul and Esenboğa Airport at Ankara. The model was based on flight data that was obtained from State Airports Authority and included the type and number of aircraft, number of passengers, and amount of cargo on daily basis. The International Civil Aviation

Organization engine emissions databank was used for the emission factors. By using first the minimum and then the maximum values from the data bank, two estimations of aircraft LTO emissions at Turkish airports were calculated. Total LTO emissions from aircrafts at Turkish airports were estimated to be between 7614.34 and 8338.79 t y⁻¹. These results were comparable with those from USA airports. Approximately half of these amounts were produced at AIA. To predict future emissions, it was estimated that an increase of 25 per cent in LTO cycles might cause a rise of between 31 and 33 per cent in emissions. The estimations showed that a decrease of 2 min in taxiing time results in a decrease of 6 per cent in LTO emissions.

Kesgin and Vardar (2001) estimated the exhaust gas emissions from ships in Turkish straits. İstanbul (Bosporus) and Çanakkale (Dardanelle) straits, which connect Black Sea and Aegean Sea, have a continuously increasing maritime traffic. Especially, the maritime traffic on Bosporus that connects the continents of Europe and Asia is too complex due to geographical conditions. The maritime traffic in the Turkish straits includes the ships, which are in use in domestic transport, the transit passing ships with various aims. Fuel consumption and exhaust gas emissions of NO_x, CO, CO₂, VOC, and PM, emitted transit vessels and passenger ships were calculated. The main engine systems, the fuel types, cruising times and speeds of all vessels were taken into consideration. The calculated NO_x emissions on the Bosporus were 2720 tons from domestic passenger ships and 4357 tons from transit ships. The results showed that the transit ships caused more than half of the total amount of emissions from ships on the Bosporus. The amount of NO_x emissions from domestic passenger ships used for public transport in Istanbul Strait was calculated to be equal to approximately 4 per cent of NO_x emissions from motor vehicles in Istanbul.

On a global scale, European biogenic emissions are not significant, a consequence of the climate and size (7 per cent of global land area) of Europe and of the destruction of natural ecosystems since prehistoric times. However, for the evaluation of the local budgets and for the photochemical oxidant modeling, natural/biogenic emissions can play an important role (Simpson et al., 1999). As a result, besides studying anthropogenic emissions, biogenic emissions should be researched as well.

As part of the work of the UNECE (United Nations Economic Commission for Europe) Task Force on Emission Inventories, a so called “Nature Panel” was set up to write a chapter for the EMEP/CORINAIR Atmospheric Emission Inventory Guidebook (McInnes, 1996) dealing with emissions from biogenic and natural sources. This Guidebook has been used by many European countries in reporting their national emissions to UN – ECE and the European Union.

The Mediterranean area is a region with high photochemical activity. The region is especially rich in aromatic plants emitting a lot of BVOCs, but the source strength is almost unknown. The BEMA-project on Biogenic Emissions in the Mediterranean Area has been initiated by the Joint Research Centre of the European Commission in collaboration with 12 European laboratories and is partially funded by the Environment and Climate Programme. The overall BEMA goal is to characterize the type and amount of VOC emissions from vegetation in the Mediterranean area and to assess their potential role in atmospheric chemistry and ozone formation (Versino, 1997). Within the general BEMA working concept, the goal of the Castelporziano study (An Overview of The Castelporziano Experiments; Seufert, 1997) as the initial BEMA field experiment was to develop the basic process understanding to parameterize biogenic emissions at the leaf and canopy levels; mesoscale transport and chemical transformation were treated only as preparatory activities for the more complete studies in BEMA. The core activities of the BEMA were field measuring campaigns on test sites representative of the Mediterranean vegetation cover in Italy, southern France and Spain. The starting action was a series of campaigns at the Castelporziano test site near Rome. Confirming the basic finding of the Castelporziano study, the monoterpenes made an important contribution to overall emissions and should not be omitted when considering the role of BVOCs in air chemistry.

Although some advanced methods have been used and a lot of researchers have focused on the topic, both of the emission inventories (Anthropogenic and Biogenic) bear still uncertainties. Furthermore, to get hourly data which is needed for air quality models, some processes must be performed on any given emission inventory which mean additional uncertainties in terms of emissions.

Comprehensive air quality models (AQMs) have been developed during recent decades to simulate the transport, chemical transformation and deposition of air pollutants on the regional scale. The first applications of AQMs have been performed for episodes, e.g. for the investigation of photo-oxidant formation or acid rain. In recent years the formation of secondary particles from gaseous precursors and particle dynamics has been added to the physical and chemical processes handled in AQMs (Binkowski and Shankar, 1995; Ackermann et al., 1998; Binkowski, 1999; et al., 2003). There are a number of chemistry models that are widely used by the modeling community, such as the California Photochemical Grid Model (CALGRID) (Yamartino et al., 1992), Urban Airshed Model (UAM) (Scheffe and Morris, 1993), Comprehensive Air Quality Model with Extensions (CAMx) (Environ International Corporation, 2002) and the Community Multi – scale Air Quality Modeling System (CMAQ) (Byun and Ching, 1999). These models are coupled online or offline to meteorological models in order to understand various physical and chemical phenomena such as the effect of complex terrain on regional transport or the transformation of air pollutants over a region (Jackson et al., 2006; Kim and Stockwell, 2007; Pirovano et al., 2007; Titov et al., 2007).

Nguyen et al. (1996) compared the performance of Eulerian and Lagrangian models on predictions of plume dispersion in complex terrains. For the Eulerian approach, they employed the CALGRID model. Considering the Lagrangian approach, they used a statistical approach to obtain the mean concentrations. The technique used the release of particles in the model to represent the mass of trace gas emissions. Particles were advected according to a specified windfield and diffused using a random walk procedure. They used the LADM model for this Lagrangian approach. The results showed that because of the different algorithms used for the release of pollutants into the model domain, LADM calculated initial concentrations at the release height one-third higher than in CALGRID. The Lagrangian approach simulated more realistic morning fumigation because in LADM, the elevated plume was mixed down to the surface rapidly, causing a sharp increase in ground level concentrations, whereas CALGRID-calculated concentrations increased gradually over a few hours. CALGRID simulated 40 per cent smaller daytime ground level concentrations than those predicted by LADM. For elevated point sources, Lagrangian approach simulated much better than Eulerian approach. On the other hand, due to the

relatively smaller turbulent eddies at the surface; CALGRID would agree much better for area sources that LADM would.

Air quality levels on European domain have been largely studied for the last two decades. Simpson (1992) conducted a long-period modeling study on the photochemical oxidants in Europe for July 1985. He proposed that in order to evaluate the performance of photochemical models, it would be useful to look at a range of meteorological conditions as possible, including not only the episodic days, but also the days with low ozone concentrations. The model used in the study was developed as a one-layer photochemical column trajectory model and the columns represented the atmospheric boundary layer (ABL). These columns were followed along specified 96-hour trajectories, picking up emissions of SO₂, NO_x, CO and VOC from the underlying grid. The meteorological data were obtained from the output of the Norwegian Numerical Weather Prediction (NWP) model. The chemistry consisted of about 100 reactions with 45 chemical species, including NO, NO₂, SO₂, CO, ethane, propylene, n-butane, o-xylene, isoprene and terpene. The results showed that due to the coverage of coniferous species in most of Europe, terpene emissions were higher than isoprene emissions. For northern and southern Europe countries, including Turkey, natural VOC rates were higher than anthropogenic emissions. He found that in general, ozone concentrations were not very sensitive to the assumed boundary conditions but convective clouds may have an important role as a sink mechanism for O₃. He calculated that on 95 percentile, 50 per cent of NO_x reduction led to 10 per cent, 50 per cent VOC reduction led to 11 per cent and 50 per cent reduction on both emissions led to 17 per cent reduction on ozone levels.

Simpson (1993) calculated the photochemical levels over Europe for two extended summer periods of April-September, 1985 and April-October, 1989. He used the EMEP MSC-W ozone model, which is a single-layer trajectory model that calculates concentrations of photochemical oxidants every 6 hours over whole Europe. The model domain covers the whole of Europe with a grid resolution of 150x150 km². The meteorological model was obtained from the NWP model. The chemical mechanism as well as the emissions was the same as those used in Simpson D. (1992). The modeled ozone concentrations compared good with the observational data, especially for the year 1989. On the other hand, the model significantly underpredicted observed concentrations of

NO₂. He also analyzed the sensitivity of ozone to 50 per cent reductions of NO_x and / or VOC. In general, both controls led to appreciable reductions of around 10 per cent on 6-month average ozone concentrations. The results showed that NO_x control produced more widespread reductions in ozone, whereas VOC reductions resulted in higher ozone reductions in northwest Europe, where greatest NO_x concentrations existed. The sensitivity of ozone concentrations to various parameters such as the emissions or the meteorological conditions have long been an important research area in air quality modeling community (Jiang et al., 1996; Pryor, S. C., 1998; Ziomas et al., 1998; Dabdub et al., 1999; Berge et al., 2001; Lee et al., 2007; Poupkou et al., 2008).

Brücher et al. (2000) simulated the traffic-induced air pollution on regional to local scales, using the Chemistry and Atmospheric Transport in Regional and Local Scales (CARLOS) model. CARLOS is an Eulerian modeling system that consists of the regional-scale EURAD system, which is a coupled system of MM5 and CTM2 models, as well as the combination of the non-hydrostatic prognostic flow model FOOT3D and CTM2F. The model application in this study contains a coarse domain over the Central Europe with a 27 km horizontal resolution, two EURAD nests of 9 and 3 km horizontal resolution over Germany and a third nest for FOOT3D/CTM2F model over Wuppertal. Initial and boundary conditions for MM5 were obtained from ECMWF analyses. A two-day spin-up period was run to initialize the concentrations. The emissions for the mother domain were taken from EMEP and for the other nests, an emission inventory of the North Rhine-Westphalian State Environment Agency (LUA-NRW) with a resolution of 1 km was used. The results showed that CARLOS was able to predict meteorological and chemical phenomena in a wide range of temporal and spatial scales. Although no measurements had been used to constrain the model chain, the results were quite satisfying. The simulations showed an overestimation of the morning peaks and the underestimation of the second evening peaks.

Andreani-Aksoyoglu et al. (2004) evaluated the performance of the aerosol module of the CAMx model in the northern Italy area. Concentrations of secondary aerosols were calculated for the particle size below 2.5 µm and compared with the data obtained from a field experiment that took place in May-June 1998. The results showed that the calculated concentrations of inorganic aerosols were comparable with the observations from the urban

and rural stations. Sensitivity analyses were also conducted and the results showed that the reduced anthropogenic NO_x and VOC emissions pointed that the secondary organic aerosols (SOC) behaved in the same way of ozone; decreasing with reduced VOC emissions and increasing with reduced NO_x emissions. Monoterpene emissions were predicted to contribute about 25 per cent of the SOC production in the forested areas of the domain.

In a research (Memmesheimer et al., 2004), the results of a long-term run carried out with the European Air Pollution Dispersion Model (EURAD; Jakobs et al., 2002a,b) were discussed with special emphasis on atmospheric particulate matter over Europe. Strongly polluted areas like North-Rhine-Westphalia have been considered in detail using nesting techniques. The results of the annual model run for the year 1997 had been analyzed with respect to the requirements of the EU directives on air quality for PM_{10} and other air pollutants, compared with observations. PM_{10} evidently was strongly influenced by transport whereas NO_x was controlled mainly by local sources.

A chain of global to mesoscale models focusing on Europe, Germany and Berlin-Brandenburg was applied by Langmann et al. (2003) for the investigation of the effect of long-range transport of pollution on surface air composition during a summer smog episode at the end of July 1994. The evaluation of model results with near-surface observations of ozone reveals a more realistic reproduction of the variability of simulated ozone mixing ratios with increasing horizontal resolution. Ozone mixing ratios simulated by the mesoscale models in the PBL and the free troposphere are considerably closer to observed levels when initial and lateral boundary conditions are taken from the global model simulation. However, the observed unusually high mixing ratios of ozone in the free troposphere are still underestimated in these model simulations. Also, when reducing anthropogenic emissions by 25 per cent (corresponding approximately to the emission reduction in Germany between 1994 and 2000) in a European-wide model simulation, a modification of 5-10 ppbv in maximum near-surface ozone over Central Europe was received again, a decrease in this case. From these results it was concluded that intercontinental transport of pollution can complicate the results of local efforts to reduce critical exposure levels of ozone during summer smog conditions. European pollution might also be reduced by decreasing emissions elsewhere due to the decreasing

contribution to the long-range transport of pollution. Other aspects that affect the long-range transport of pollution and its impact on European pollution levels are modifications in large scale dynamics.

Tesche et al. (2006), compared the performances of CAMx and CMAQ models on 2002 annual simulations over eastern US. The performance evaluation was conducted on operational, diagnostic and comparative levels for regional haze regulatory applications. Both models were exercised on nested 36/12 km grid resolutions and evaluated across a broad range of time and space scales for gas-phase and particulate species. The meteorological fields for both models were generated by MM5 model on the same grid resolutions. The gas-phase chemistry mechanism used was CB-IV and the aerosol chemistry used was ISORROPIA. Performance by both models for speciated fine particulate matter ranged from quite good (e.g. sulfate) to poor (e.g. soil). For most species, model bias was higher in winter and lower in the summer suggesting potential issues related to vertical mixing, temporal allocation of emissions and the model science. In general, both models yielded good performances for sulfate, elemental carbon PM₁₀ and PM_{2.5}.

Byun et al. (2007) also evaluated the model performances of CAMx and CMAQ for a high ozone episode in Houston metropolitan area. Both models used CB-IV chemistry mechanism in a nested grid resolution of 36, 12 and 4 km. In order to improve the baseline emissions, the amount of fugitive emissions of highly reactive VOCs (HRVOC) was scaled by multiplying by 3 to 12 times over the regular inventory values. With the base emissions, both models simulated similar ozone concentrations. On the other hand, with the improved HRVOC emissions, CMAQ predicted lower ozone peaks than CAMx in the vicinity and other highly HRVOC-rich areas. Based on analyses of sensitivity simulations of CMAQ with different emission inputs, and vertical diffusion algorithms in the model, it was found that the modeled atmosphere lacked reactivity to produce the observed high ozone event. Comparison of ozone precursor species with multi-species measurements revealed that there was serious mixing and transport problems with both models.

A real-time forecast system for atmospheric pollutants has been used based on the EURAD Model (European Air Pollution Dispersion Model) for Europe, Central Europe

and the German State of Northrhine-Westfalia. The whole forecast system includes the meteorological forecast (MM5) and an updated emission data base for the above mentioned regions. The results of the forecasts on the different regions have been published and are updated every day on the EURAD homepage. For about 15 years, the EURAD model was developed and improved for applications within numerous case studies on the regional scale in Europe (e.g. Jakobs et al., 1995; Ebel et al., 1997). The main purpose of the predictions was to answer the following questions: How reliable are the predictions and how can they be improved?

A simple model of atmospheric transport and an emissions inventory prepared by Netherlands Organization for Applied Scientific Research (TNO) were used to estimate the contribution of primary particulate material to PM_{10} and $PM_{2.5}$ concentration across Europe. The resulting population exposure was compared with that of secondary particulates, and it was noted that both primary and secondary contributions would be significantly reduced with the implementation of new protocols under the Convention on Long-Range Transboundary Air Pollution (CLRTAP). Since concentrations of primary PM_{10} could become elevated in episodic situations, when long-range transport of particulate could, on its own, exceed 24 hour average targets of $50 \mu\text{g m}^{-3}$ over large areas of Europe, such reduction was important for achievement of current air quality standards to control exposure to atmospheric particulate PM_{10} . These results presented only a preliminary step. A sophisticated atmospheric modeling and more refined emission inventories were recommended.

Between November 1995 and October 1996, particulate matter concentrations (PM_{10} and $PM_{2.5}$) were measured in 25 study areas in six Central and Eastern European countries: Bulgaria, The Czech Republic, Hungary, Poland, Romania and The Slovak Republic (Houthuijs et al., 2001). To assess annual mean concentration levels, 24-hour averaged concentrations were measured every sixth day on a fixed urban background site using Harvard impactors with a 2.5 and 10 mm cut-point. The concentration of the coarse fraction of PM_{10} was calculated as the difference between the PM_{10} and the $PM_{2.5}$ concentration. Spatial variation within study areas was assessed by additional sampling on one or two urban background sites within each study area for two periods of one month. QA/QC procedures were implemented to ensure comparability of results between study

areas. A two to threefold concentration range was found between study areas, ranging from an annual mean of 41 to 98 μgm^{-3} for PM_{10} , from 29 to 68 μgm^{-3} for $\text{PM}_{2.5}$ and from 12 to 40 μgm^{-3} for $\text{PM}_{10_{2.5}}$. The lowest concentrations were found in The Slovak Republic, the highest concentrations in Bulgaria and Poland. The variation in PM_{10} and $\text{PM}_{2.5}$ concentrations between study areas was about 4 times greater than the spatial variation within study areas suggesting that measurements at a single sampling site sufficiently characterize the exposure of the population in the study areas. PM_{10} concentrations increased considerably during the heating season, ranging from an average increase of 18 μgm^{-3} in The Slovak Republic to 45 μgm^{-3} in Poland. The increase of PM_{10} was mainly driven by increases in $\text{PM}_{2.5}$; $\text{PM}_{10_{2.5}}$ concentrations changed only marginally or even decreased. Overall, the results indicated high levels of particulate air pollution in Central and Eastern Europe with large changes between seasons, likely caused by local heating.

The Met Office's Lagrangian dispersion model ran over a regional scale for 1996 to predict both nitrate and sulfate aerosol (Redington and Derwent, 2002). Import to the UK from Europe has been quantified. The model validated by comparison with available measurement data and results from the EMEP Eulerian model. Results were presented in the form of daily time series of aerosol at two rural sites and one urban site. Annual average maps of sulfur dioxide, nitrogen dioxide, sulfate aerosol, nitrate aerosol and nitric acid were presented and were found to exhibit a reasonable agreement with the exception of sulfur dioxide which over-predicts substantially. The model results indicated the maximum contribution to secondary inorganic aerosol in the UK was in the southeast, where the annual average contribution was 14 μgm^{-3} (PM_{10}) based on 1996 data. On average, 30 per cent of UK aerosol was imported from Europe in the summer and 25 per cent in winter months.

During the winters of 1992/1993, 1993/1994 and 1994/1995 a monitoring study was performed in three urban and three non-urban areas in the Netherlands by van der Zee et al. (1998). PM_{10} , black smoke (BS), sulfate, nitrate, ammonium (non-organic secondary aerosols) and aerosol acidity were measured on a daily basis in both the urban and non-urban areas. The elemental composition of PM_{10} was analyzed. PM_{10} and BS concentrations were on average 13 per cent and 19 per cent higher in the urban areas than in the non-urban areas. $\text{PM}_{2.5}$ concentrations were similar in the urban and non-urban

areas. The small contrast in particle concentrations between urban and non-urban areas in the Netherlands was explained as a result of the small size of the country, the high population density, the lack of small-scale geographical and meteorological differences, and the importance of long-range transport of air pollutants. It was found that urban and non-urban differences depended strongly on wind direction. Easterly winds resulting in an influx of air masses from Central and Eastern Europe were associated with high concentrations and minimal urban-non-urban differences. Winds from the sea resulted in low concentrations but larger relative differences between urban and non-urban areas.

In the framework of the PEACE study, Hoek and his colleagues measured particles less than $10\mu\text{m}$ (PM_{10}) and black smoke (BS) in ambient at 28 sites in ten countries in Europe (1997). For about two months in the winter of 1993/94, 24-hour averaged measurements were conducted. Each center studied both an urban and a more rural site. The difference of particle concentrations across countries appeared to be considerably larger than the difference between the urban and rural locations within countries. The median PM_{10} concentration ranged from $11\ \mu\text{g}\text{m}^{-3}$ at three rural Scandinavian sites to $92\ \mu\text{g}\text{m}^{-3}$ in Athens, Greece. The median BS concentration ranged from $3\ \mu\text{g}\text{m}^{-3}$ in Umea, Sweden to $99\ \mu\text{g}\text{m}^{-3}$ in Athens, Greece. The most striking difference across countries was the low particle concentration found at the eight Scandinavian locations. PM_{10} and BS concentrations in the urban areas were on average 22 per cent and 43 per cent higher than the corresponding rural area concentrations, respectively. The correlation between the particle concentration measured at the urban and the more rural site exceeded 0.70 at almost all sites. PM_{10} concentrations from all Western and Central European locations were significantly correlated. Low or no correlation was found between these locations and the South-European and Scandinavian locations. PM_{10} and BS measured at the same site were highly correlated at most sites. However, the median PM_{10}/BS ratio ranged from 0.67 to 3.67 across sites. PM_{10}/BS ratios were close to unity for Athens, the Central European sites and Oslo. There was a tendency of lower PM_{10}/BS ratios in the urban area, consistent with the contribution of (diesel) motor vehicle emissions.

The study of Salisbury et al. (2003) presented measurements of acetonitrile, benzene, toluene, methanol and acetone made using the proton-transfer-reaction mass spectrometry (PTR-MS) technique at the Finokalia ground station in Crete during the Mediterranean

Intensive Oxidant Study (MINOS) in July-August 2001. Three periods during the campaign with broadly consistent back trajectories were examined in detail. First, air was advected from Eastern Europe without significant biomass burning influence. In the second period, the sampled air masses originated in Western Europe, and were advected approximately east-south-east, before turning southwest over the Black Sea and north-western Turkey. The third well-defined period included air masses advected from Eastern Europe passing east and south of/over the Sea of Azov, and showed significant influence by biomass burning, confirmed by satellite pictures. The mean toluene-benzene ratios observed in the three campaign periods described were 0.35, 0.37 and 0.22, respectively; the use of this quantity to determine air mass age was discussed. Methanol and acetone were generally well-correlated both with each other and with carbon monoxide throughout the campaign. Comparison of the acetone and methanol measurements with the MATCH-MPIC model (Model of Atmospheric Transport and Chemistry, Max Planck Institute for Chemistry version 3.0) showed that the model underestimated both species by a factor of 4, on average. The correlations between acetone, methanol and CO implied that the relatively high levels of methanol observed during MINOS were largely due to direct biogenic emissions, and also that biogenic sources of acetone were highly significant during MINOS (~35%). This in turn suggests that the model deficit in both species may be due, at least in part, to missing biogenic emissions.

Aerosol modeling is a challenging scientific problem aimed at improving current knowledge in the many complex processes involved in multiphase chemistry and transport. Correct simulations of aerosols are also required in order to elaborate particle emission reduction strategies. As a result, the CHIMERE chemistry transport model (Schmidt et al., 2001) has been improved to account for particle transport, formation and deposition at the European scale. The aerosol model has accounted both for inorganic and organic species of primary or secondary origin. Secondary organic aerosols from biogenic and anthropogenic gas precursors have been partitioned into gas and particulate phases through a temperature dependent partition coefficient. The modeling approach was presented in the study (Bessagnet et al., 2004) with preliminary simulation results over Europe. Comparisons with available data at background stations gave acceptable results on PM_{10} , with correlation coefficients usually exceeding 0.5 and normalized errors in the 30-80 per cent range in many regions. However, results on sulfate, nitrate and ammonium species

displayed less correct error statistics. Comparisons on sulfate concentrations gave normalized errors in the range 30-80 per cent in summer and less correct in winter. Temporal correlation coefficients usually ranged from 0.30 to 0.70. Nitrate concentrations were better simulated during winter than during summer. Difficulties in simulating heterogeneous and aqueous phase processes could explain model deficiencies. Moreover, temperature dependence of gas/particle partitioning processes for nitrate, ammonium and secondary organic species could mainly explain the seasonal variability of biases. Model deficiencies were observed in Southern countries, certainly due to natural dust emissions and resuspended particles. Finally, sea salts seemed to have a quite significant influence on error statistics in coastal areas.

The concentration of different species in the atmospheric aerosol is influenced significantly by human activities, so the study of the source origin of elements in aerosol particles is of crucial importance for environmental management on an urban scale. As a result, receptor modeling applied in the study (Bozo et al., 2002) provides quantitative estimates of the impacts of sources on ambient air. In contrast to dispersion modeling, only minimal meteorology and emission inventory information were applied. Based on ADMS dispersion model computations (Singles and Carruthers, 1999) spatial distribution of PM₁₀ was also estimated for Budapest to get a general picture on the particle pollution level at different locations in Budapest. It was concluded based on multiyear sampling and measurements that waste incineration provided the most significant contribution to the toxic metal load in Budapest (65-70 per cent). The relative contribution of traffic sources was between 11-17 per cent. Coal burning had no significant importance in Budapest regarding the contribution to the receptor profile. This could be explained by the fact that coal consumption was significantly reduced in Budapest during the past decades since it was replaced by natural gas at most of the industrial, residential and energy sources. In cooperation with The National Oceanic and Atmospheric Research (NOAA), three dimensional backward trajectories were also computed so as to estimate the origin of air masses on different days. It was found that episodes with relatively high concentrations of Ni and V measured in Budapest were accompanied by south winds indicating the effects of an oil refinery located 25 km South of Budapest.

Regional and local air quality models have become an important tool for environmental research and application to environmental assessment and policy questions. On one hand it is important to use air quality models as a tool to understand the simulations carried out with them, and on the other hand, evaluated, highly improved models should be used to forecast atmospheric pollutants in an operational state. The European Air Pollution Dispersion Model (EURAD) has been used to evaluate air quality problem for Europe. Since summer 2001 a real-time forecast system based on the EURAD Model has been tested and established to predict the main atmospheric pollutants on different scales in Europe. The EURAD forecast system consists mainly of the mesoscale meteorological model MM5 (PennState/NCAR mesoscale model Version 5), the emission Processor EURAD Emission Model (EEM) and the EURAD Chemistry Transport Model (EURAD-CTM). The EURAD forecast system consists mainly of the mesoscale meteorological model MM5 (PennState/NCAR mesoscale model Version 5), the emission Processor EEM (EURAD Emission Model) and the EURAD Chemistry Transport Model (EURAD-CTM). For about 15 years the EURAD model was developed and improved for applications within numerous case studies on the regional scale in Europe (e.g. Jakobs et al., 1995; Ebel et al., 1997). Every day, an extensive amount of data is produced by the EURAD forecast system. This includes the meteorological prediction variables and the concentrations of the atmospheric constituents at all model levels, as well. In order to compare later especially the concentrations of air pollutants, the main effort was made to visualize the near surface concentrations of the main air pollutants O₃, NO₂, SO₂, CO and PM₁₀ for the entirety of Europe. For assessment studies, the ranges for the concentration thresholds were selected according to the EU directives (Jakobs et al., 2002).

The RAINS (Regional Air Pollution INformation and Simulation) model has been developed by IIASA (International Institute for Applied Systems Analysis, Laxenburg, Austria) as a tool for the integrated assessment of alternative strategies to reduce atmospheric pollution in Europe (Schöpp et al., 1999). The current version of this model describes the pathways of emissions of sulfur dioxide, volatile organic compounds (VOC), nitrogen oxides, ammonia and particulate matter and explores health and ecosystems' impacts of particulate pollution, acidification, eutrophication and tropospheric ozone. This model has a strong political importance. It has been used several times since the beginning of the 1990s as a basis for the definition of European emission reduction strategies.

Klimont and his colleagues (2002) used RAINS model to evaluate particulate matter in the European Union (EU) and the non-EU countries. The model assumptions need further verification but its results already compare fairly well with published national and international inventories.

Vertical profiles, horizontal profiles and size distribution of airborne particulate matter were measured near major roads in Macao using DustTrak and TEOM monitors (Wu et al., 2002). A significant decrease in the concentrations of PM_{10} , $PM_{2.5}$ and PM_1 , as the height above the ground increases from 2 to 79 m, was found. At the height of 79 m, the concentrations of PM_{10} , $PM_{2.5}$ and PM_1 , decrease to about 60 per cent, 62 per cent and 80 per cent of the maximum occurrence at 2m above the ground, respectively. However, the horizontal profiles near another major road revealed there was no significant trend of decrease in concentrations of particulate matter as the distance from the road increases. Over the total measured distance (0-228 m), the maximum decreases of PM_{10} , $PM_{2.5}$ and PM_1 are only 7 per cent, 9 per cent and 10 per cent, of the maximum occurrence at 2m from the road, respectively. The daytime averaged $PM_{2.5}$ and PM_1 contribute 66-67 per cent and 51-60 per cent, respectively, of the total PM_{10} mass after the particle readings by DustTrak were recalibrated by TEOM. It showed that fine particles and submicrometer particles contributed a major part of PM_{10} at the roadside in Macao, which is most likely attributed to the combinations of local sources including exhausted particulate matter from vehicles and resuspended fine dust, and secondary particles (sulfate, nitrate and ammonium) of regional scales.

Field data were used to evaluate the vertical distribution of suspended particulates at different height levels in an urban area of Hong Kong (Chan et al., 2000). Four buildings in different street configurations and street environments were selected. According to the street configurations, they were classified into two groups: street canyon and open-street. In the street canyon, TSP and PM_{10} concentration varied with height exponentially. However, the rate of TSP, PM_{10} and $PM_{2.5}$ decrease with distance from the ground floor was in decreasing order of TSP, PM_{10} and $PM_{2.5}$. The particulate matter dispersion in street canyon was affected by the prevailing wind direction and the street configuration in particular the height-to-width ratio. In open streets, the vertical concentration depended on

the vertical mixing, local dilution and other external factors such as sea breeze, as well as the proximity of trunk road and construction activity.

On the basis of the recently estimated emission inventory for East Asia with a resolution of 1x1 degrees, the transport and chemical transformation of sulfur compounds over East Asia during the period of 22 February through 4 May 2001 was investigated by using the CMAQ modeling system with meteorological fields calculated by the regional atmospheric modeling system (Zhang et al., 2004). For evaluating the model performance, simulated concentrations of sulfur dioxide (SO_2) and aerosol sulfate (SO_4^{2-}) were compared with the observations on the ground level at four remote sites in Japan and on board aircraft and vessel during the transport and chemical evolution over the Pacific and Asian Pacific regional aerosol characterization experiment field campaigns. Analysis of model results shows that emission was the dominant term in regulating the SO_2 spatial distribution, while conversion of SO_2 to SO_4^{2-} in the gas phase and the aqueous phase and wet removal were the primary factors that controlled SO_4^{2-} amounts. The gas phase and the aqueous phase have the same importance in oxidizing SO_2 , and about 42 per cent sulfur compounds (~25 per cent in SO_2) emitted in the model domain was transported out, while about 57 per cent (~35 per cent by wet removal processes) was deposited in the domain during period of study.

The MM5-CMAQ model was used to assess the causes of weekday/weekend O_3 differences in the north-eastern Iberian Peninsula during an episode of photochemical pollution covering the whole Western Mediterranean Basin (Jimenez et al., 2004). The response of both ambient and simulated O_3 concentrations to day-of-week varied by location. Rural locations, dominated by medium-long range transport, depict similar O_3 concentrations. Both discrete and categorical model evaluations were shown in order to test the accuracy of the model for representing weekdays/weekends differences within the air basin. This study helped identify the major causes of the weekend effect in the considered domain, as the change in mass and time of precursor's emissions, and might be a useful tool to reduce ambient O_3 levels.

Hogrefe et al. (2006) studied the temporal features in observed and simulated meteorology and air quality over the eastern US by CMAQ and the regional modeling

system for aerosols and deposition (REMSAD) model. The meteorological fields were generated by MM5 meteorological model. Both meteorological and chemistry models had a horizontal grid resolution of 36 km. The spectral decomposition of total PM_{2.5} mass from TOEM observations and CMAQ and REMSAD model predictions revealed the days of high PM_{2.5} concentrations were in general characterized by positive forcing from fluctuations having periods equal to or greater than a day; diurnal, synoptic and longer-term components (Hogrefe et al., 2001). Both modeling systems did not capture most of the variability of the high-frequency, intra-day component, whereas other components were well captured. Both models exhibited greatest skills at capturing seasonal fluctuations of ozone, sulfate, and nitrate. The results suggested that boundary conditions and emissions could lead to problems on shorter time scales and that capturing meteorological fluctuations on all scales is a necessary but not sufficient for capturing pollutant fluctuations on all time scales, especially for PM_{2.5} simulations.

Jimenez and Baldasano (2004), evaluated the ozone response to precursor controls in very complex terrains in the northeastern Iberian Peninsula. They employed the MM5-EMICAT2000-CMAQ system to represent ozone formation with baseline emission rates of VOC and NO_x, and reducing anthropogenic VOC and NO_x emissions by 35 per cent. The results showed that areas downwind of the city of Barcelona benefit from NO_x reductions on a 10 ppb reduction of surface ozone concentrations. The same reductions caused an important increment of ozone in Barcelona (9 ppb) with a high industrial influence. The city of Barcelona benefited from VOC reductions (10 ppb) as well as the industrial zone of Alcover (20 ppb). The rest of the domain was practically insensitive to VOC reductions.

Jimenez et al. (2006) evaluated MM5-EMICAT2000-CMAQ system performance and the sensitivity in complex terrain. Horizontal grid resolutions of 8, 4 and 2 km² were used. The emission model had a high resolution of 1 km². The chemical transport model was used to compute the concentrations of photochemical pollutants for the episode of 13-16 August, 2000. The results showed that the outputs were sensitive to the grid size, presenting a higher dependence on horizontal grid than on the vertical resolution. Some small scale features appeared when using a grid spacing of 2 km that cannot be captured with coarser horizontal resolutions. The model met the ±20 per cent set by USEPA for prediction of the peak levels of ozone. Model sensitivity was evaluated by performing

simulations to represent ozone formation with baseline emission rates for VOCs and NO_x and reducing anthropogenic VOC and NO_x emissions by 35 per cent. Evaluation of ground-level ozone showed a good agreement when the model predicted dominant VOC-sensitive chemistry. Statistical parameters of ozone evaluation got worse when VOC emissions were reduced and improved in the 35 per cent-NO_x case, suggesting that the ozone production chemistry may not be sufficiently reactive.

Bell and Ellis (2004) conducted sensitivity analyses for tropospheric ozone to modified biogenic emissions over the mid-Atlantic region. The sensitivity runs were performed on a scenario with an additional 100 per cent increase in biogenic emissions and another scenario with additional 100 per cent increase in vehicle emissions together with the 100 per cent increase in biogenic emissions. The meteorological inputs were generated by the MM5 model on 108, 36 and 12 km grid resolutions. CMAQ runs were performed on two nests of 36 and 12 km. The results showed that biogenic VOCs had a greater impact than a comparable per cent increase in vehicle emissions. The 100 per cent increase in biogenic VOCs led to an additional 30 per cent higher maximum 1 hour ozone concentrations than the base case. On the other hand, the second scenario increased the ozone formation by 40 per cent in total.

Choi and Fernando (2008) modeled episodic high PM events along the US/Mexico border using the state-of-the-art CMAQ/MM5/SMOKE air quality modeling system. In their study, a time-dependent entrainment parameterization for wind-blown dust is implemented in the CMAQ-MM5-SMOKE modeling system with the hope of improving PM predictions. An approach for realizing wind-blown dust emission flux for each grid cell over the study domain on an hourly basis which accounts for the influence of factors such as soil moisture content, atmospheric stability and wind speed is employed. Comparison of model predictions with observational data taken at a pair of US/Mexico border towns shows a clear improvement of model performance upon implementation of the dust emission flux parameterization.

Bessagnet et al. (2005) investigated several wintertime pollution events due to particulate matter on the Paris Basin in 2003. High-pressure systems close to Scandinavia or the North Sea involve highly stable conditions with slight Northeasterly flux on France

leading to high airborne pollutant concentrations. An evaluation of the CHIMERE model results against observations over the Paris area showed that while PM_{10} , nitrate and ammonium seem fairly well reproduced, sulfate concentrations remain difficult to predict. A specific study, by removing Ile-de-France emissions, displays on 21 February and 21 March episodes an important ammonium nitrate contribution, mainly originating from outside the Paris area. According to the model results, the Paris Basin has also a large influence up to the Southwest of France. In a similar way, an investigation of the possible sources outside the Paris basin, displays a strong influence of emissions from Germany, the Netherlands and Belgium during these episodes. To a lesser extent, Italy has an influence on the Paris area at the end of the episodes. It is also demonstrated that in some situations, the contribution of locally produced or emitted particles is prevalent at the ground level. The influence of French emissions is also studied from 20 to 25 March displaying an influence on Spain and a strong impact at the end of the episode successively on Great Britain, Belgium, and the Netherlands when winds veer Southeast and West. This influence is also significant up to Eastern Europe.

Smyth et al. (2006) evaluated the performance of Models-3/CMAQ for the period of 9-20 August in 2001, for a domain centered about Vancouver and the Lower Fraser Valley in British Columbia, Canada, by comparing measurement data from the Pacific 2001 air quality field study. The model predicted O_3 concentrations reasonably well with a normalized mean bias (NMB) and normalized mean error (NME) of 13.3 per cent and 51.2 per cent over all measurement sites and hours. It showed an excellent performance in predicting daily O_3 peaks with a NMB and NME of 2.2 per cent and 24.3 per cent. The model also did well in predicting the time at which the peaks occurred. The model captured the diurnal variations and spatial distributions of O_3 concentrations very well, with some difficulty at locations deep in the valley. Model predictions of $PM_{2.5}$ concentrations over all sites and hours had a moderate NMB and NME of 30.9 per cent and 66.2 per cent. The model did well in predicting the general temporal trend of $PM_{2.5}$ concentration levels. However, the high hourly variability in $PM_{2.5}$ measurements was not possible for the model to capture. In addition, the temporal variations of modeled concentrations change more dramatically than the measured. The model performed poorly in predicting PM sulfate, ammonium, and nitrate concentrations. The extreme overprediction in nitrate concentrations was partially related to an overabundance of total ammonia in the system.

Sensitivity tests of NH₃ emission reductions showed that reducing NH₃ supply to the system could help reduce the overpredictions of both ammonium and nitrate concentrations, although the model science also needs to be improved. To evaluate the PM organics performance, carbon multiplication factors (CMFs) of 1.4 and 1.9 were applied to an urban site and an urban-to-rural transition site, respectively. The model showed satisfactory performance for PM_{2.5} organics with a NMB and NME of 6.0 per cent and 50.5 per cent.

The Regional Modeling System for Aerosols and Deposition (REMSAD) was employed to predict sulfate formation and transport in the Big Bend Regional Aerosol and Visibility Observational Study (BRAVO) by Barna et al. (2006). Fine particulate sulfate was the main component of haze measured at Big Bend National Park (BBNP) during the BRAVO field measurement campaign, which was conducted July–October 1999. Predicted sulfate was evaluated against measurements collected from BRAVO and CASTNet (Clean Air Speciation and Trends Network) monitors. During the four month study period, average observed and predicted sulfate concentrations at the 37 BRAVO sites were 3.1 and 3.3 μgm^{-3} , respectively, and 4.5 and 5.0 μgm^{-3} at the 62 CASTNet sites, respectively. Spatial and temporal biases were clearly apparent. Underestimations of sulfate during July and August were evident throughout the BRAVO monitoring network (fractional biases of -0.60 and -0.44, respectively), corresponding to a period of increased atmospheric transport from Mexico to Texas. Biases in estimated sulfate in the vicinity of BBNP may be attributed to an overestimation of predicted precipitation rates during July and August. Positive biases within the BRAVO network were apparent in October (fractional bias = 0.39), when atmospheric transport from the eastern US was more prevalent. Overall performance statistics for sulfate predictions relative to the BRAVO and CASTNet sites were: correlation coefficient = 0.61 and 0.90, respectively; fractional error = 0.56 and 0.35, respectively; fractional bias = -0.10 and 0.04, respectively. This simulation provided the basis for a series of emission sensitivity simulations that were used to estimate a sulfate source apportionment for BBNP.

Gego et al. (2006) compared the abilities of CMAQ and REMSAD to reproduce measured aerosol nitrate and sulfate concentrations during 2001 on a 36x36 km horizontal resolution. Model estimates were compared to observations reported by the interagency

monitoring of protected visual environment (IMPROVE) and the clean air status and trend network (CASTNet). Root mean squared errors were calculated for simulation/observation pairs from ten geographic regions and 12 seasons (months). Following the application of the Wilcoxon matched-pair signed rank test, they concluded that CMAQ is more skillful than REMSAD for simulation of aerosol sulfate. Simulations of particulate nitrate concentrations by CMAQ and REMSAD can seldom be differentiated, leading to the conclusion that both models perform equally for this pollutant specie.

The University of California at Davis (UCD) aerosol module, an internally mixed, sectional aerosol model with dynamic mass transfer between the gas and particle phases, has been coupled to the Community Multiscale Air Quality (CMAQ) model by Nolte et al. (2008). The study included the application of the CMAQ-UCD model to simulate air quality in Tampa, a large city with a population of 2 million on the west coast of Florida, USA. Modeled aerosol size and composition distributions are evaluated against size-segregated ambient measurements of SO_4^{-2} , NH_4 , NO_3^- , Na, and Cl^- collected at three Tampa-area sites during May 2002, and against semi-continuous HNO_3 and total aerosol SO_4^{-2} , NH_4^+ , NO_3^- , and Cl^- measurements collected at a single site. Sea-salt emissions over the open ocean and the surf zone are parameterized as a function of modeled wind speed and relative humidity. Modeled total aerosol sulfate and ammonium concentrations and size distributions agree with measurements, with an overall normalized mean bias (NMB) of 2 per cent and -23 per cent and normalized mean error (NME) of 46 per cent and 38 per cent, respectively, and correctly identifying the size bin in which the peak concentration is observed. Sea salt size distributions are also simulated well, with the distribution dominated by the coarse mode and total aerosol sodium and chloride NMB of 2 per cent and 17 per cent and NME of 32 per cent and 38 per cent. Though the model correctly identifies that nitrate is predominantly in the coarse ($D_p > 2.5 \mu\text{m}$) size sections, aerosol nitrate concentrations are underpredicted by a factor of two. The availability of highly time-resolved measurements provides a unique opportunity to evaluate the model's partitioning of total nitrate and the simulation of chloride depletion as a function of particle size.

Air quality levels in İstanbul have been widely investigated through measurements and statistical evaluation methods (İncecik, 1996; Tayanç M., 2000; Topçu and İncecik,

2002; İm et al., 2006 and 2008). However, there is very limited number of studies employing the air quality models to evaluate these levels. Combined SO₂ and total suspended particulate (TSP) concentrations from different locations in Istanbul province were used to investigate intense air pollution episodes from 1985 through 1991 (İncecik, 1996). Occurrence of intense episodes was found only after November 1989. These episodes were associated mainly with high-pressure systems, inversions and low wind speeds. The European side of the Bosphorus was found to be more polluted than the Asian side, probably because of weaker dispersion and the greater use of poor quality fuels.

Tayanç (2000) studied the SO₂ concentration levels in İstanbul in order to assess the air pollution during the heating seasons in which concentration of air pollutants reach high levels due to consumption of low quality fossil fuels. He analyzed the period between 1985 and 1991 and the results revealed that there was an increasing trend in the concentration levels during this period. Krigging technique was employed to obtain the spatial distribution of SO₂ over the area. The results indicated that monthly averages of SO₂ problem was specific to the heating season periods of 1993-94 and 1994-95, whereas the other months of the year (April to October) was characterized by clean air. The maximum concentration areas on both sides of the city were characterized by very high residential population densities. He also showed that shifting to natural gas in 1995-96 seasons led to considerable decrease in SO₂ concentrations.

Topçu and İncecik (2002) analyzed the surface ozone measurements and meteorological influences in the urban atmosphere of İstanbul. They used the hourly measurements of ozone concentrations between February 1998 and July 1999. They found that meteorological conditions favorable for high ozone concentrations were dominated high pressure systems. They calculated the annual, monthly and diurnal variations of ozone. They found that higher ozone levels were experienced in 1999 than in 1998. They found typical urban profile of diurnal variation of ozone in İstanbul; maximum concentrations in afternoon hours and minimum concentrations in traffic rush hours.

İm et al. (2006) analyzed the hourly ozone, NO_x and VOC concentrations, measured during 2001-2003 summer periods in order to examine the interaction patterns between the major photochemical pollutants in İstanbul. 34 high ozone days throughout the summer

periods of the three years were determined and examined in the study together with the meteorological parameters like temperature, wind and vertical structure of the atmosphere. The results showed that high levels of ozone are observed mostly under anticyclonic conditions with relatively low wind speeds. High ozone days generally experienced maximum concentrations at afternoon hours and minimum concentrations are reached at rush hours due to NO_x -titration by traffic emissions. High negative correlations with NO_x up to -0.84 were calculated for the Saraçhane station while higher correlations for VOC species, up to -0.75, were calculated for Kadıköy station. Some individual episodes experiencing high ozone concentrations up to $310 \mu\text{g m}^{-3}$ in the early morning hours were also studied. The results showed that decreasing inversion heights in the early hours of the day led to suppression of pollutants close to surface and thus, an increase in ozone concentrations was observed. Low wind speeds played a major role in the increase of pollution levels in the region. HYSPLIT model was applied to some particular episodes and the results show that the northeasterly transport to the region was dominant, especially in the early-morning maximums.

İm et al. (2008) investigated the hourly ozone, nitrogen oxide and hydrocarbon concentration levels measured between 2001-2005 in Kadıköy and Saraçhane, two urban districts in Anatolian and European sides of İstanbul. Episodes of three days or longer were especially focused in this study. The highest ozone concentrations were observed in summer periods having sunny days and maximum temperatures above 25°C , and the episodes were mainly characterized by the surface southwesterly winds during daytime and surface northeasterly winds during nighttime. Considering all high-ozone days, correlations of ozone with NO_x and VOC species were calculated to be -0.44 and -0.85 for Kadıköy, whereas they were estimated to be -0.84 and -0.39 for Saraçhane, respectively. High VOC/NO_x ratios in both of the stations point that NO_x -sensitive chemistry was dominant in the region. On the other hand, higher correlations of VOCs in Kadıköy, compared with those in Saraçhane, pointed that VOCs also have important contribution to ozone formation. High ozone days generally showed maximum concentrations at afternoon hours and minimum concentrations at rush hours due to NO_x -titration by traffic emissions. Trajectory model HYSPLIT was also employed backward for three long episodes and the results showed the north, northwest and northeasterly transport of the air masses to the city. Since the transportation is mainly from Black Sea and from the rural areas existing in the

north of İstanbul, the contribution of advection to the maximum levels of ozone in the city was believed to be low.

A modified version of the ATDL (Atmospheric Turbulence and Diffusion Laboratory) urban dispersion model was applied to estimate annual SO₂ and suspended particulate concentrations in the Golden Horn region of İstanbul (Erturk, 1986). The emissions were categorized as area sources (residential and commercial districts or small industries) and point sources (power plants and large industries). The area sources were distributed into a 3 km square grid pattern. The concentrations predicted from the model were compared with the observed concentrations. The results were found to be very reasonable. The model was used to estimate the effect of various control strategies on the reduction of SO₂ and suspended particulate levels, and the comparisons of these strategies were discussed.

UAM-V (Urban Airshed Model) modeling system was used to determine surface ozone over İstanbul in a Ph.D. thesis by Antepioglu (2000). In the study, meteorological variables were obtained from a mesoscale prognostic meteorological model. Emissions responsible for ozone formation over the region were assumed to be originated from highway vehicles only. EPA Mobile5 modeling system was utilized for emission factors and other requirements.

Kindap et al. (2006) studied the long-range transport of PM₁₀ from Europe to İstanbul by employing MM5 and CMAQ models. The models were configured for a single domain of 50 km. the emissions were obtained from 2001 EMEP inventory. The results showed the İstanbul background PM₁₀ levels to individual European countries ranged from 0.5 to 1.3 per cent. A 50 per cent change in the European anthropogenic emissions led to a response of maximum 26 per cent in İstanbul. The study demonstrated that the impact of Eastern European emissions to PM₁₀ levels in İstanbul might be significant under certain meteorological conditions. The trajectory analyses showed that episodes with relatively high PM₁₀ concentrations were related to northwesterly winds, especially from Eastern European countries. The overall results showed that the evaluation of PM₁₀ levels in Western or Northern Turkey should consider the contribution of long-range transport from Europe.

Kındap (2008) studied the SO₂ and NO₂ levels in İstanbul, regarding the impact of weather conditions. He used MM5 model to generate the meteorological fields and CMAQ for the concentration fields. He also conducted tracer analyses over the area of interest employing the online tracer model of MM5, MM5T. The physics options used in MM5 were; MRF for boundary layer mixing, Kain – Fritsch for cumulus convection, RRTM (Rapid Radiative Transfer Model) for radiation scheme and simple ice microphysics scheme. The modeling period covered 7-8 and 10-11, January, 2002. The tracer model indicated that pollutant transport to İstanbul took about a couple of hours from Bucharest; around one day from Kiev and about two days from Warsaw during the simulation period. The results obtained from the tracer study were quite reasonable and they supported the hypothesis that the transboundary transport from Eastern Europe can play an important role in both high pollutant events in İstanbul. A comparison of the simulated concentrations with the observations showed that the model reproduced the temporal variation of surface SO₂ and NO₂ concentrations at city monitoring stations with some success. However, the magnitudes of disagreement between the simulation and the observations indicated significant problems. The inaccurate or incomplete nature of emission inventory along with the limitations of the regional model could be the likely causes of this insufficient estimation. This points that a sophisticated emission inventory in a finer resolution and model development are required to improve the model simulation and to help further understand and explore the complex mechanism in long-range pollutant chemistry and transport.

3. MATERIALS AND METHODS

3.1. Episodic Period

Based on the daily PM₁₀ sampling conducted at the Boğaziçi University, Institute of Environmental Sciences, which are later analyzed physically and chemically at the University of Crete, Department of Chemistry, Environmental Chemical Processes Laboratory (ECPL), a 5-day PM₁₀ episode between 13 – 17.01.2008 is accounted as the base for the modeling setup. The 24-hour sample concentrations showed PM₁₀ concentrations varying from 92.8 $\mu\text{g m}^{-3}$ to 128.9 $\mu\text{g m}^{-3}$, which exceed the European Union standard for 24-hour PM₁₀ of 50 $\mu\text{g m}^{-3}$ (Figure 3.1). The details of the analysis procedure are discussed in Theodosi et al. (2009).

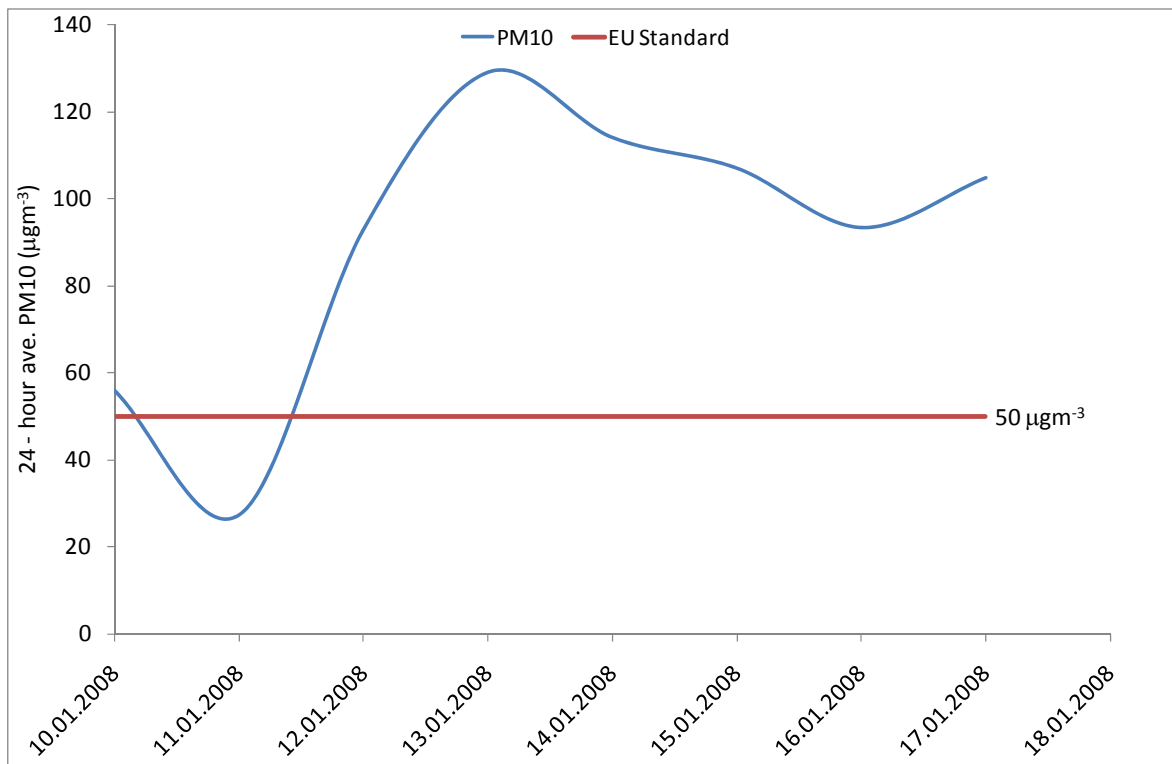


Figure 3.1. The 24-hour PM₁₀ concentrations between 10.01.2008-18.01.2008.

These 24-hour concentrations are also validated from the continuous hourly measurements of PM_{10} that are conducted by the Istanbul Greater Municipality at 10 different stations across İstanbul (Figure 3.2). As seen in Figure 3.2, hourly concentrations as high as $450 \mu g m^{-3}$ are observed within this period. The maximum hourly concentrations measured at each of these stations and the times of these maximums for each station during this period are demonstrated in Table 3.1. The comparison of the 24-hour averaged concentrations calculated from the hourly concentrations for each station with the Boğaziçi University station is presented in Figure 3.3.

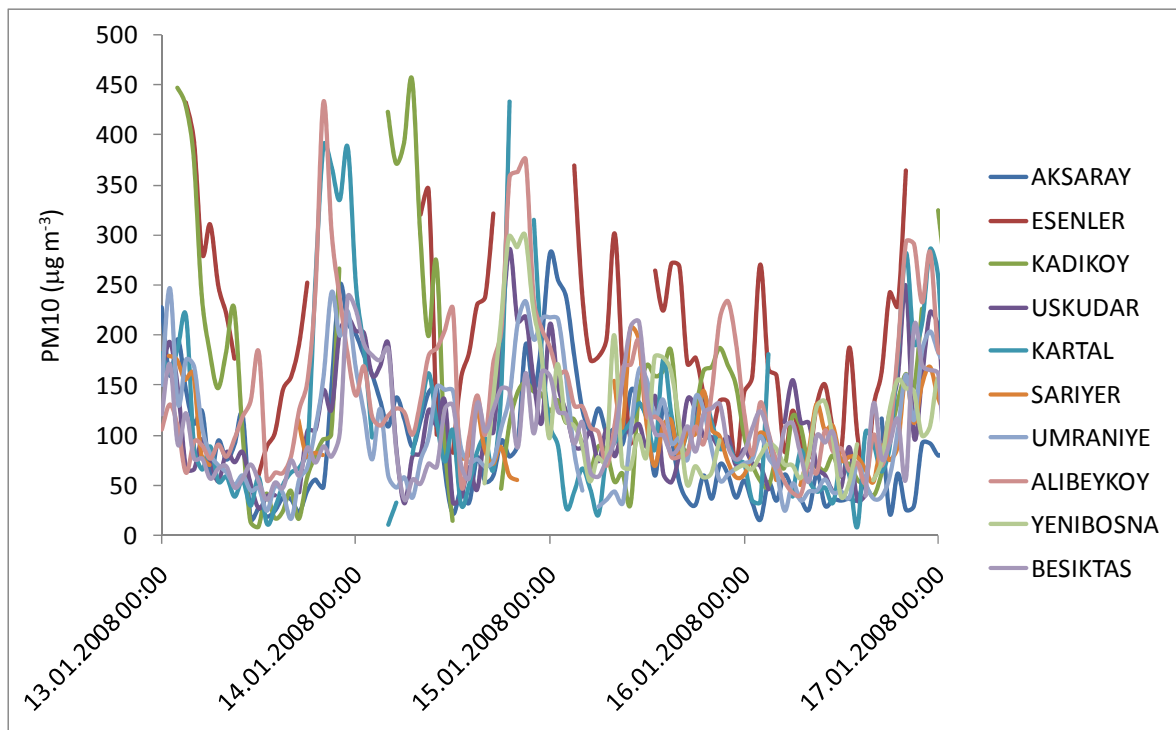


Figure 3.2. Hourly PM_{10} concentrations at the İstanbul Greater Municipality stations.

The chemical analysis conducted at ECPL analyzed the chemical speciation of the PM_{10} samples to get a better understanding of the characterization of the aerosol content during the episode. The results also provide better model performance evaluation since there are more details to validate the results. The chemical speciation of the PM_{10} samples are presented in Table 3.2. The average concentrations of the aerosol species during the episode is given in Figure 3.4. As can be seen from the concentrations and distributions of the species, water soluble organic carbon (WSOC) content of the samples covered the

dominant portion of the aerosol samples. Water soluble organic compounds (WSOC) in atmospheric aerosol contribute to the ability of aerosol particles to act as cloud condensation nuclei. This fraction of organic materials also plays an important role in the wet scavenging of atmospheric particles and formation of haze. On the other hand, since WSOC represents a group of compounds like dicarboxylic acids (C_2-C_6), dicarbonyls (C_2-C_3), oxo-carboxylic acids (C_2-C_{10}), pyruvic acid, C_2-C_7 polyols, C_2-C_6 amino acids, C_2-C_6 hydroxy amines, and monosaccharides and their derivatives, the major component of the aerosol samples become water soluble organics with 29 per cent, trace metals 18 per cent, sulfate aerosols with 17 per cent and nitrate aerosols with 12 per cent.

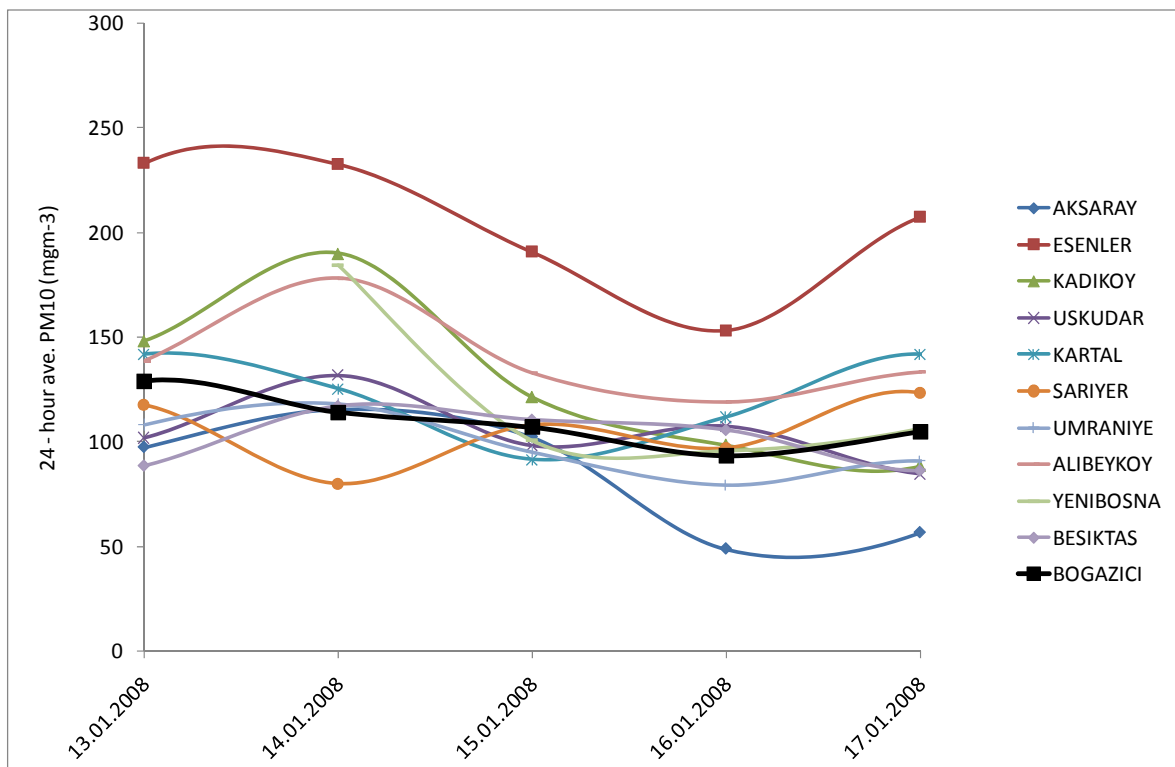


Figure 3.3. Comparison of daily average PM₁₀ concentrations measured at the municipality stations with Boğaziçi University station.

Table 3.1. Maximum PM₁₀ concentrations at Istanbul Greater Municipality stations between 13-17.01.2008 (units in µgm⁻³).

	13.01.2008	14.01.2008	15.01.2008	16.01.2008	17.01.2008
AKSARAY	250 (2200 LST)	201 (0000 LST)	282 (0000 LST)	117 (1700 LST)	129 (2100 LST)
ESENLER	438 (0100 LST)	353 (0500 LST)	369 (0300 LST)	364 (2000 LST)	450 (2200 LST)
KADIKOY	446 (0200 LST)	454 (0700 LST)	187 (2100 LST)	226 (2200 LST)	324 (0000 LST)
USKUDAR	217 (2300 LST)	286 (1900 LST)	211 (0000 LST)	249 (2000 LST)	221 (2000 LST)
KARTAL	389 (2000 LST)	433 (1900 LST)	176 (1400 LST)	286 (2300 LST)	311 (2000 LST)
SARIYER	179 (0200 LST)	125 (1500 LST)	206 (1000 LST)	168 (2300 LST)	243 (2000 LST)
UMRANIYE	246 (0100 LST)	233 (2100 LST)	217 (0000 LST)	203 (2300 LST)	223 (2100 LST)
ALIBEYKOY	432 (2000 LST)	374 (2100 LST)	233 (2200 LST)	292 (2000 LST)	443 (2200 LST)
YENIBOSNA	-	300 (2100 LST)	200 (0800 LST)	155 (1900 LST)	209 (2000 LST)
BESIKTAS	238 (2300 LST)	225 (0000 LST)	213 (1100 LST)	208 (2100 LST)	161 (0000 LST)

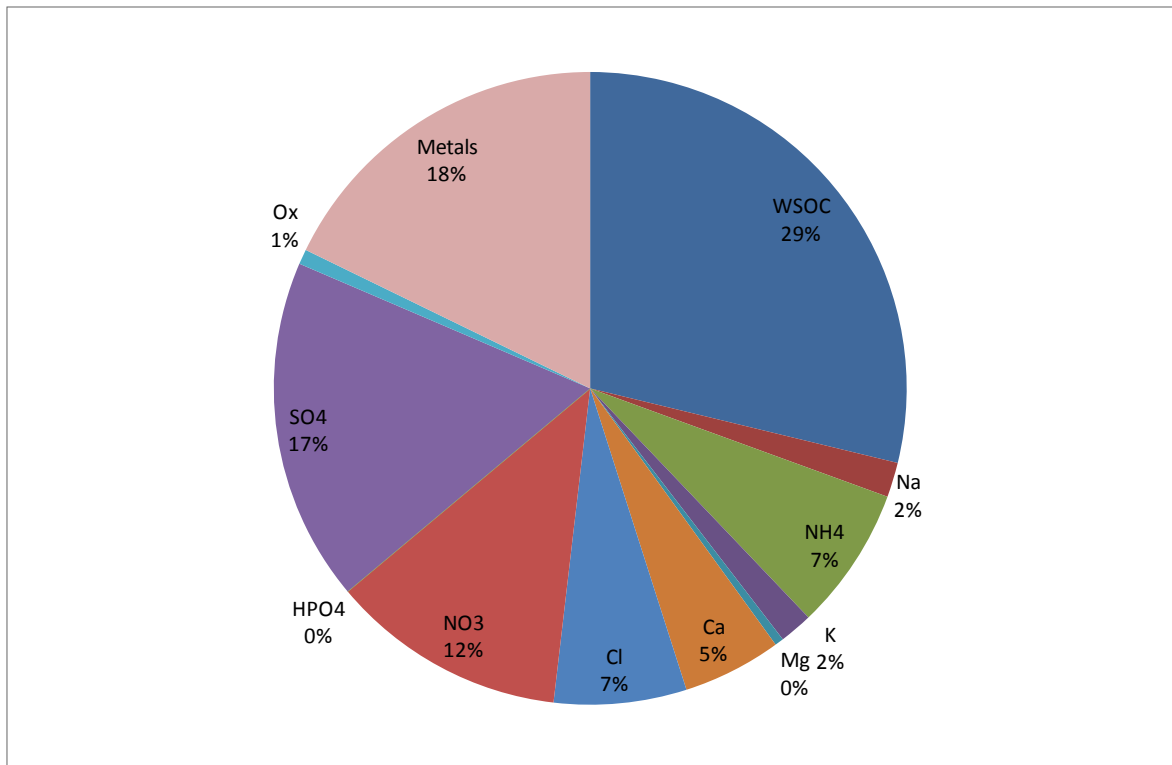


Figure 3.4. Distribution of the average concentrations of the aerosol species during the episode.

3.2. Meteorological Modeling

The simulations of the meteorological fields are conducted using the non-hydrostatic mesoscale model MM5 Version 3.7.0, which is developed by the Pennsylvania State University and National Center for Atmospheric Research (NCAR) (Grell et al., 1994). The initial and boundary conditions are provided from NCAR-NCEP reanalysis. The optimum physics and dynamics options are established for different cases and scenarios. Analysis nudging is employed in order to force the model to incorporate the surface and rawinsonde measurements into the simulations to get more realistic results.

MM5 is a mesoscale meteorological models that includes (i) multiple-nesting capability, (ii) non-hydrostatic dynamics and (iii) four dimensional data assimilation (PSU/NCAR, 2005). Terrestrial and isobaric meteorological data are horizontally interpolated by TERRAIN and REGRID programs, respectively, from a latitude-longitude

Table 3.2. Chemical speciation of the PM₁₀ samples (units in μgm^{-3}).

DATE	PM₁₀	WSOC	Na	NH₄⁺	K	Mg	Ca	Cl⁻	NO₃⁻	HPO₄²⁻	SO₄²⁻	O_x
10.01.2008	55.86	7.70	0.73	1.36	0.61	0.19	1.53	1.48	2.35	0.00	4.29	0.16
11.01.2008	27.27	4.96	0.48	0.87	0.32	0.12	0.82	0.69	1.63	0.00	2.89	0.13
12.01.2008	92.80	12.15	0.99	4.51	1.15	0.29	2.72	2.77	5.01	0.00	8.22	0.24
13.01.2008	128.87	16.73	1.09	4.32	1.02	0.28	2.84	5.06	6.91	0.00	9.49	0.32
14.01.2008	113.91	13.17	1.76	3.59	0.91	0.27	3.18	4.37	6.46	0.00	10.11	0.49
15.01.2008	106.87	15.01	0.86	5.79	1.30	0.19	1.71	4.22	8.41	0.00	11.17	0.35
16.01.2008	93.24	15.20	0.71	4.36	0.86	0.22	2.58	3.45	7.05	0.00	10.17	0.60
17.01.2008	104.68	21.23	0.60	2.65	0.69	0.31	3.96	2.05	5.22	0.00	8.64	0.37

grid to a mesoscale, rectangular domain on a Mercator, Lambert Conformal, or Polar Stereographic projection. Since the interpolation of the meteorological data does not necessarily provide much mesoscale detail, the interpolated data may be enhanced by programs LITTLE_R or RAWINS with observations from the standard network of surface and radiosonde stations using a successive-scan Cressman or multiquadric technique. Program INTERPF then performs the vertical interpolation from pressure levels to the σ – coordinate of the MM5 model. Alternatively, program 3DVAR may be used to ingest data on model σ levels. After a MM5 model integration, program INTERPB can be used to interpolate data from σ levels back to pressure levels, while program NESTDOWN can be used to interpolate model level data to a finer grid to prepare for new model integration. Graphic programs (RIP and GRAPH) may be used to view modeling system output data on both pressure and σ levels. The overall schematic representation of the MM5 modeling system is represented in Figure 3.5.

3.2.1 Terrain

TERRAIN makes use of high-resolution global terrain and land use data sets to create static files for the domain. The static files currently include values for each grid point for terrain height and land use specification (e.g., deciduous forest, desert, water). This is essential for an accurate run. It also defines the model domain and map projection that locates the area the model will simulate. Various types of terrain affect atmospheric circulation patterns. Therefore, the type of terrain and vegetation cover must be specified and accurately defined within the chosen domain for the simulation to produce accurate results (Guo and Chen, 1994).

3.2.2 Regrid

After the simulation domain had been established, the program REGRID is run to process the meteorological background fields. REGRID generated first-guess fields for the model simulation by horizontally interpolating a larger-scale data set (global or regional coverage) to the simulation domain. REGRID interpolated the background fields to the simulation domain throughout the simulation period; these files were used ultimately to generate lateral boundary conditions for the coarse-domain simulations.

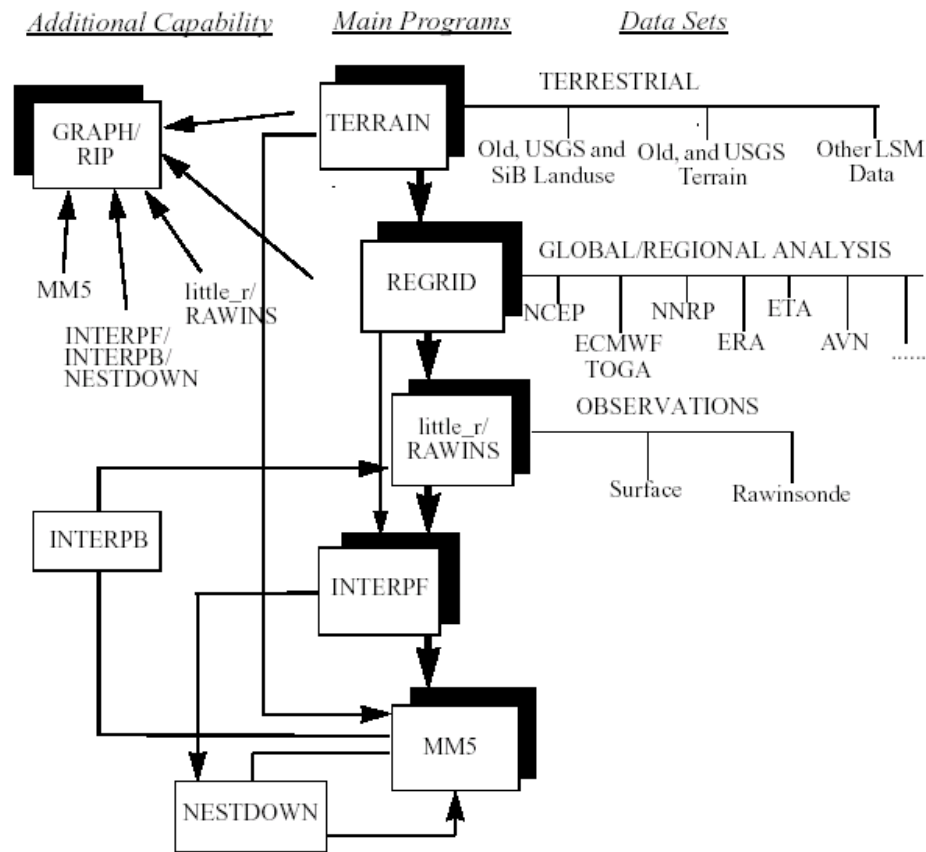


Figure 3.5. MM5 modeling system flow chart.

In brief, the main purpose of the program REGRID is to interpolate coarse-resolution global or hemispheric meteorological analyses horizontally to the mesoscale grid. The input analyses are obtained from the NCEP (The National Centers for Environmental Prediction) database. This data set is a global analysis beginning in 1948 using a single analysis system for the entire dataset. Analyses are available every six hours. Data are archived on a 1 x 1 degree latitude/longitude grid.

3.2.3 Setting the Initial and Boundary Conditions (Interpf)

The INTERPF program sets the initial and boundary conditions for the meteorology simulation. In the program, the analyses from one time were interpolated to provide MM5's initial conditions, while analyses from all running times were interpolated to get

MM5's lateral boundary conditions. This was the final step before the actual MM5 model could be run.

3.2.4 MM5

This is the numerical weather prediction part of the modeling system. MM5 can be used for a broad spectrum of theoretical and real-time studies, including applications of both predictive simulation and four-dimensional data assimilation to monsoons, hurricanes, and cyclones. On the smaller meso-beta and meso-gamma scales (2-200 km), MM5 can be used for studies involving mesoscale convective systems, fronts, land-sea breezes, mountain-valley circulations, and urban heat islands.

MM5 is based on primitive physical equations of momentum, thermodynamics, and moisture. The state variables are temperature, specific humidity, grid-relative wind components, and pressure. Several model physics options in MM5 are put together including radiation, convective parameterization, planetary boundary layer processes, surface layer processes and resolvable-scale microphysics schemes.

3.2.5. Horizontal and Vertical Grid Structures

The model analyzes the data on pressure surfaces but these have to be interpolated to the model's vertical coordinate before being input to the model. The vertical coordinate is terrain following meaning that the lower grid levels follow the terrain while the upper surface is flat. Intermediate levels progressively flatten as the pressure decreases toward the chosen top pressure. The sigma levels may mathematically be represented as following:

$$\sigma = \frac{p - p_t}{p_s - p_t} \quad (3.1)$$

where p is the reference-state pressure, p_t is a specified constant top pressure, and p_s is the reference-state surface pressure. It can be seen from the equation that σ is zero at the model top and one at the model surface, and each model level is defined by a value of σ .

All the above variables are defined in the middle of each model vertical layer, referred to as half-levels and represented by the dashed lines in Figure 3.6. Vertical velocity is carried at the full levels (solid lines). In defining the σ levels it is the full levels that are listed, including levels at 0 and 1. The number of model layers is therefore always one less than the number of full σ levels. Note also the I, J, and K index directions in the modeling system.

The horizontal grid has an Arakawa-Lamb B-staggering of the velocity variables with respect to the scalars. This is shown in Figure 3.7, where it can be seen that the scalars (T, q etc.) are defined at the center of the grid square, while the eastward (u) and northward (v) velocity components are collocated at the corners. The center points of the grid squares will be referred to as cross points and the corner points are dot points. Hence horizontal velocity is defined at dot points, for example, and when data is input to the model the preprocessors do the necessary interpolations to assure consistency with the grid.

3.2.6. Nesting

MM5 contains a capability of multiple nesting with up to nine domains running at the same time and completely interacting. A possible configuration is shown in Figure 3.8. The nesting ratio is always 3:1 for two-way interaction. Two-way interaction means that the nest's input from the coarse mesh comes via its boundaries, while the feedback to the coarser mesh occurs over the nest interior.

It can be seen that multiple nests are allowed on a given level of nesting (e.g. domains 2 and 3 in Figure 3.8.), and they are also allowed to overlap. Domain 4 is at the third level, meaning that its grid size and time step are nine times less than for domain 1. Each sub-domain has a "Mother domain" in which it is completely embedded, so that for domains 2 and 3 the mother domain is 1, and for 4 it is 3. Nests may be turned on and off at any time in the simulation, noting that whenever a mother nest is terminated all its descendent nests also are turned off. Moving a domain is also possible during a simulation provided that it is not a mother domain to an active nest and provided that it is not the coarsest mesh.

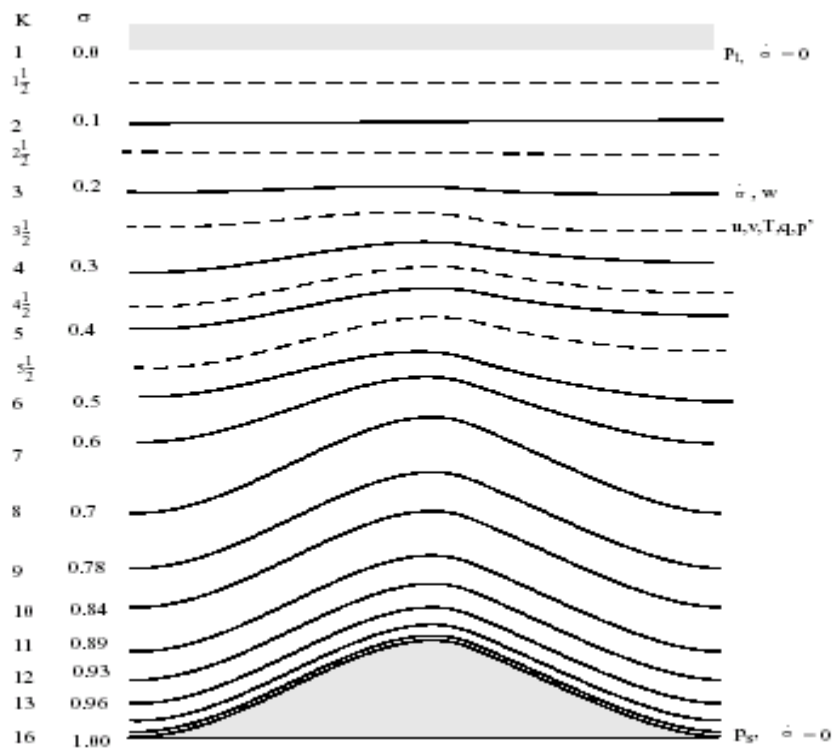


Figure 3.6. The vertical structure of MM5.

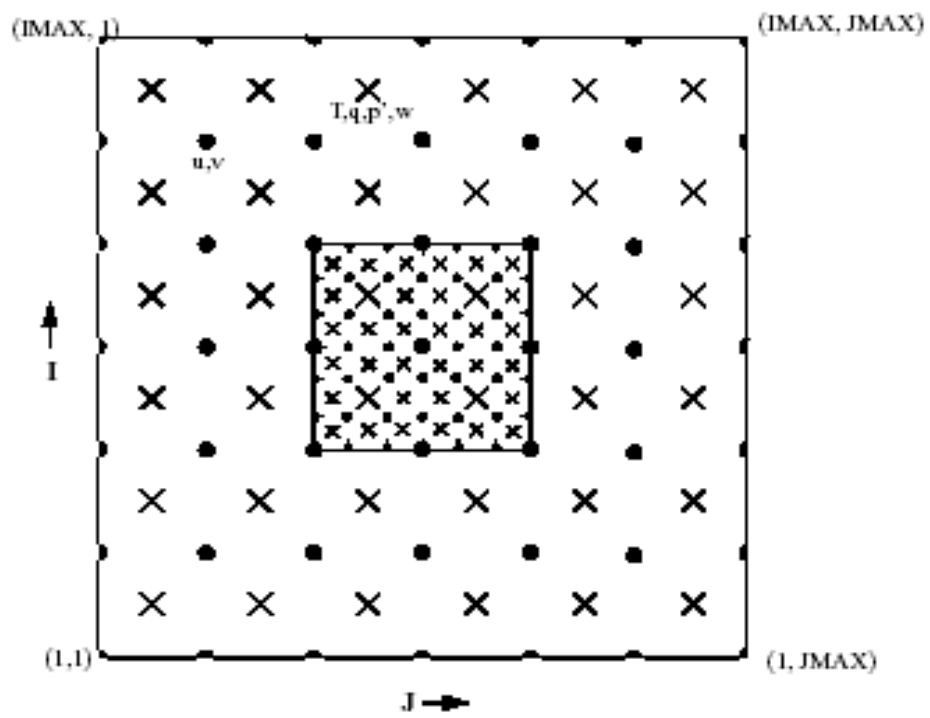


Figure 3.7. The horizontal structure of the model.

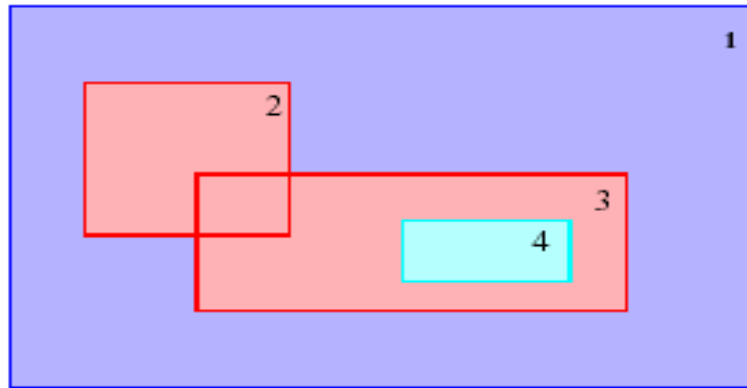


Figure 3.8. Example of a nesting configuration.

One-way nesting is also possible in MM5. Here the model is first run to create an output that is interpolated using any ratio (not restricted to 3:1), and a boundary file is also created once a one-way nested domain location is specified. Typically the boundary file may be hourly (dependent upon the output frequency of the coarse domain), and this data is time-interpolated to supply the nest. Therefore one-way nesting differs from two-way nesting in having no feedback and coarser temporal resolution at the boundaries. The one-way nest may also be initialized with enhanced-resolution data and terrain. It is important that the terrain is consistent with the coarser mesh in the boundary zone, and the TERRAIN preprocessor needs to be run with both domains to ensure this.

3.2.7. Lateral Boundary Conditions

To run any regional numerical weather prediction model requires lateral boundary conditions. In MM5 all four boundaries have specified horizontal winds, temperature, pressure and moisture fields, and can have specified microphysical fields (such as cloud) if these are available. Therefore, prior to running a simulation, boundary values have to be set in addition to initial values for these fields.

The boundary values come from analyses at the future times, or a previous coarser-mesh simulation (1-way nest), or from another model's forecast (in real-time forecasts). For real-time forecasts the lateral boundaries will ultimately depend on a global-model forecast. In studies of past cases the analyses providing the boundary conditions may be enhanced by observation analysis (LITTLE_R or RAWINS) in the same way as initial

conditions are. Where upper-air analyses are used the boundary values may only be available 12-hourly, while for model-generated boundary conditions it may be a higher frequency like 6-hourly or even hourly.

The model uses these discrete-time analyses by linearly interpolating them in time to the model time. The analyses completely specify the behavior of the outer row and column of the model grid. In the next four rows and columns in from the boundary, the model is nudged towards the analyses, and there is also a smoothing term. The strength of this nudging decreases linearly away from the boundaries. To apply this condition, the model uses a boundary file with information for the five points nearest each of the four boundaries at each boundary time. This is a rim of points from the future analyses described above. The interior values from these analyses are not required unless data assimilation by grid-nudging is being performed, so disk-space is saved by having the boundary file just contain the rim values for each field.

3.2.8. Non-hydrostatic Dynamics versus Hydrostatic Dynamics

Historically the Penn State/NCAR Mesoscale Model has been hydrostatic because typical horizontal grid sizes in mesoscale models are comparable with or greater than the vertical depth of features of interest. Therefore the hydrostatic approximation holds and the pressure is completely determined by the overlying air's mass. However when the scale of resolved features in the model have aspect ratios nearer unity, or when the horizontal scale becomes shorter than the vertical scale, non-hydrostatic dynamics cannot be neglected. MM5 Version 3 only supports the non-hydrostatic solver.

The only additional term in non-hydrostatic dynamics is vertical acceleration that contributes to the vertical pressure gradient so that hydrostatic balance is no longer exact. Pressure perturbations from a reference state together with vertical momentum become extra three-dimensional predicted variables that have to be initialized.

3.2.9. Land Use Categories

Each grid cell of the model is assigned a value for vegetation, desert, urban, water, ice, and etc... These land use properties determine the surface properties such as albedo, roughness length, longwave emissivity, heat capacity and moisture availability. These parameters are included in TERRAIN module but can also be manually input to the program.

3.2.10. Data Required Running the Model

Since the MM5 modeling system is primarily designed for real-data studies/simulations, it requires the following datasets to run:

- Topography and landuse (in categories);
- Gridded atmospheric data that have at least these variables: sea-level pressure, wind, temperature, relative humidity and geopotential height; and at these pressure levels: surface, 1000, 850, 700, 500, 400, 300, 250, 200, 150, 100 mb; Observation data that contains soundings and surface reports.
- MM5 user support system (Mesouser) provides a basic set of topography, landuse and vegetation data that have global coverage but variable resolution. The Data Support Section of Scientific Computing Division at NCAR has an extensive archive of atmospheric data from gridded analyses to observations.

3.2.11. Basic equations of MM5

The basic non-hydrostatic equations of MM5 in terrain following coordinates are given below:

Pressure:

$$\frac{\partial p'}{\partial t} - \rho_0 g w + \gamma p \nabla \cdot v = -V \cdot \nabla p' + \frac{\gamma p}{T} \left(\frac{Q}{c_p} + \frac{T_0}{\theta_0} D\theta \right) \quad (3.2)$$

Momentum (x-component):

$$\frac{\partial u}{\partial t} + \frac{m}{\rho} \left(\frac{\partial p'}{\partial x} - \frac{\partial p^*}{\partial x} \frac{\partial p'}{\partial \sigma} \right) = -V \cdot \nabla u + v \left(f + u \frac{\partial m}{\partial y} - v \frac{\partial m}{\partial x} \right) - ew \cos \alpha - \frac{uw}{r_{earth}} + D_u \quad (3.3)$$

Momentum (y-component):

$$\frac{\partial v}{\partial t} + \frac{m}{\rho} \left(\frac{\partial p'}{\partial y} - \frac{\partial p^*}{\partial y} \frac{\partial p'}{\partial \sigma} \right) = -V \cdot \nabla v + u \left(f + u \frac{\partial m}{\partial y} - v \frac{\partial m}{\partial x} \right) - ew \sin \alpha - \frac{vw}{r_{earth}} + D_v \quad (3.4)$$

Momentum (z-component):

$$\frac{\partial w}{\partial t} - \frac{\rho_0}{\rho} \frac{g}{p^*} \frac{\partial p'}{\partial \sigma} = -V \cdot \nabla w + g \frac{p_0}{p} \frac{T'}{T_0} - \frac{gR_d}{c_p} \frac{p'}{p} + e(u \cos \alpha - v \sin \alpha) + \frac{u^2 + v^2}{r_{earth}} + D_w \quad (3.5)$$

Thermodynamics:

$$\frac{\partial T}{\partial t} = -V \cdot \nabla T + \frac{1}{\rho c_p} \left(\frac{\partial p'}{\partial t} + V \cdot \nabla p' - \rho_0 g w \right) + \frac{Q}{c_p} + \frac{T_0}{\theta_0} D_\theta \quad (3.6)$$

Advection terms can be expanded as:

$$V \cdot \nabla A \equiv mu \frac{\partial A}{\partial x} + mv \frac{\partial A}{\partial y} + \dot{\sigma} \frac{\partial A}{\partial \sigma} \quad (3.7)$$

where

$$\dot{\sigma} = -\frac{\rho_0 g}{p^*} w - \frac{m\sigma}{p^*} \frac{\partial p^*}{\partial x} u - \frac{m\sigma}{p^*} \frac{\partial p^*}{\partial y} v \quad (3.8)$$

Divergence term can be expanded as:

$$\nabla \cdot V = m^2 \frac{\partial}{\partial x} \left(\frac{u}{m} \right) - \frac{m\sigma}{p^*} \frac{\partial p^*}{\partial x} \frac{\partial u}{\partial \sigma} + m^2 \frac{\partial}{\partial y} \left(\frac{v}{m} \right) - \frac{m\sigma}{p^*} \frac{\partial p^*}{\partial y} \frac{\partial v}{\partial \sigma} - \frac{\rho_0 g}{p^*} \frac{\partial w}{\partial \sigma} \quad (3.9)$$

The above equations are finite differenced over the grid. A second order leapfrog time-step scheme is used for these equations but some terms are handles using a time-splitting scheme. In the leapfrog scheme, the tendencies at time n are used to step the variables from time $n-1$ to $n+1$. This is used for most right hand-terms like advection, coriolis and buoyancy). A forward step is used for diffusion and microphysics where the tendencies are calculated at time $n-1$ and used to step the variables from $n-1$ to $n+1$. Some radiation and cumulus options use a constant tendency over periods of many model time steps and are only recalculated every 30 minutes. However, for certain terms the model time step is too long for stability (u, v, w, p') and these have to be predicted with a shorter step. When the time step is split, these variables are updated more frequently (Figure 3.9).

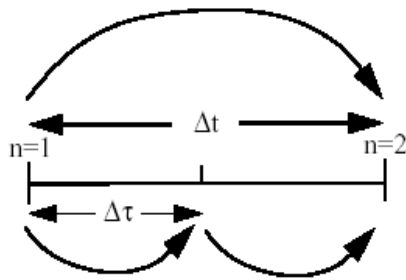
3.2.12. MM5 setup for the study

TERRAIN is configured to simulate a modeling domain that consists of 3 domains (Figure 3.10). The mother domain consists of 199 grids in x-direction and 175 grids in y-direction, with a grid resolution of 30 km. The domain covers Europe and Middle East, with central latitude of 55.00 degrees and central longitude of 13.00 degrees. The geographical information (terrain heights, landuse, etc...) is obtained from USGS on 3 minute (~19 km) resolution (Figure 3.11a and b). The map projection is set to Lambert Conformal projection. The landuse category includes 25 global-coverage landuse types and the descriptions of these categories are presented in Table 3.3.

The second domain covers the Balkan region of 10 km resolution (Figure 3.12). The domain has 181 grids on x-direction and 202 grids on y-direction. The terrain heights and landuse plots are presented in Figure 3.13a and b. The geographical data is downloaded from USGS on 4 minute (~9 km) resolution.

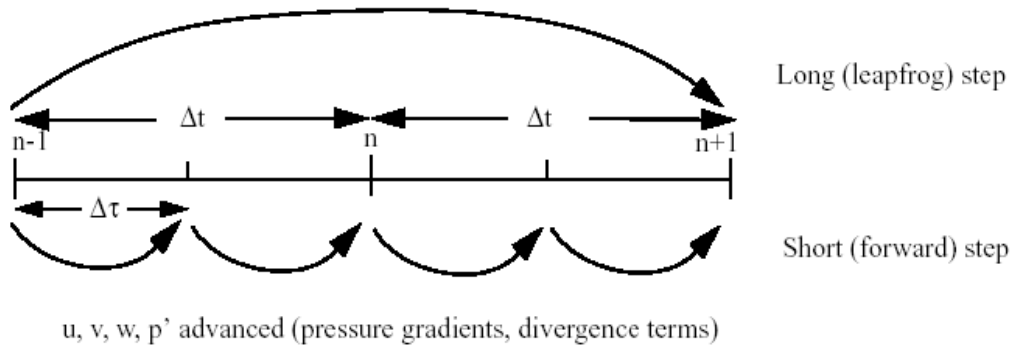
Finally, the inner most domain covers the north western part of Turkey on 2 km resolution, centered on İstanbul (Figure 3.14). The domain has 136 grids on x-direction and 111 grids on y-direction. The terrain heights and landuse plots are presented in Figures 3.15a and b, respectively. The geographical data is downloaded from USGS on 4 minute (~5 km) resolution.

First time step:



Time step n:

T, qv, qc, etc., advection, physics, boundary, coriolis, diffusion terms



Time step n+1:

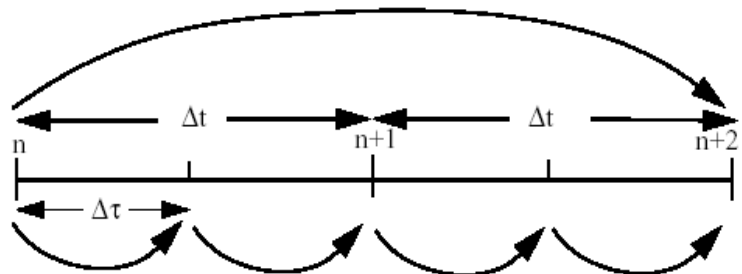


Figure 3.9. Time splitting procedure in MM5.

REGRID is configured for the time period of 10.01.2008-20.01.2008, for a 21600-minute time interval. The global reanalyzes is obtained from the NCEP Final Analyses (FNL) on 1° resolution and interpolated to the TERRAIN modeling domain. The domain is divided to 10 vertical pressure levels, with the pressure level at the top of the domain set to 100 hPa and the lowest vertical level to 950 hPa, and varying levels of 950, 925, 900, 800, 750, 650, 600, 550, 450 and 350 hPa.

Table 3.3. Description of 25-category (USGS) vegetation categories and physical parameters for N.H. summer (15 April-15 October) and winter (15 October-15 April).

Vegetation Integer Identification	Vegetation Description	Albedo(%)		Moisture Availability (%)		Emissivity (% at 9 μ m)		Roughness Length (cm)		Thermal Inertia (cal cm ⁻² k ⁻¹ s ^{-1/2})	
		Sum	Win	Sum	Win	Sum	Win	Sum	Win	Sum	Win
		1	Urban	15	15	10	10	88	88	80	80
2	Drylnd Crop. Past.	17	23	30	60	98.5	92	15	5	0.04	0.04
3	Irrg. Crop. Past.	18	23	50	50	98.5	92	15	5	0.04	0.04
4	Mix. Dry/Irrg.C.P.	18	23	25	50	98.5	92	15	5	0.04	0.04
5	Crop./Grs. Mosaic	18	23	25	40	99	92	14	5	0.04	0.04
6	Crop./Wood Mosec	16	20	35	60	98.5	93	20	20	0.04	0.04
7	Grassland	19	23	15	30	98.5	92	12	10	0.03	0.04
8	Shrubland	22	25	10	20	88	88	10	10	0.03	0.04
9	Mix Shrb./Grs.	20	24	15	25	90	90	11	10	0.03	0.04
10	Savanna	20	20	15	15	92	92	15	15	0.03	0.03
11	Decids. Broadlf.	16	17	30	60	93	93	50	50	0.04	0.05
12	Decids. Needlf.	14	15	30	60	94	93	50	50	0.04	0.05
13	Evergrm. Braodlf.	12	12	50	50	95	95	50	50	0.05	0.05

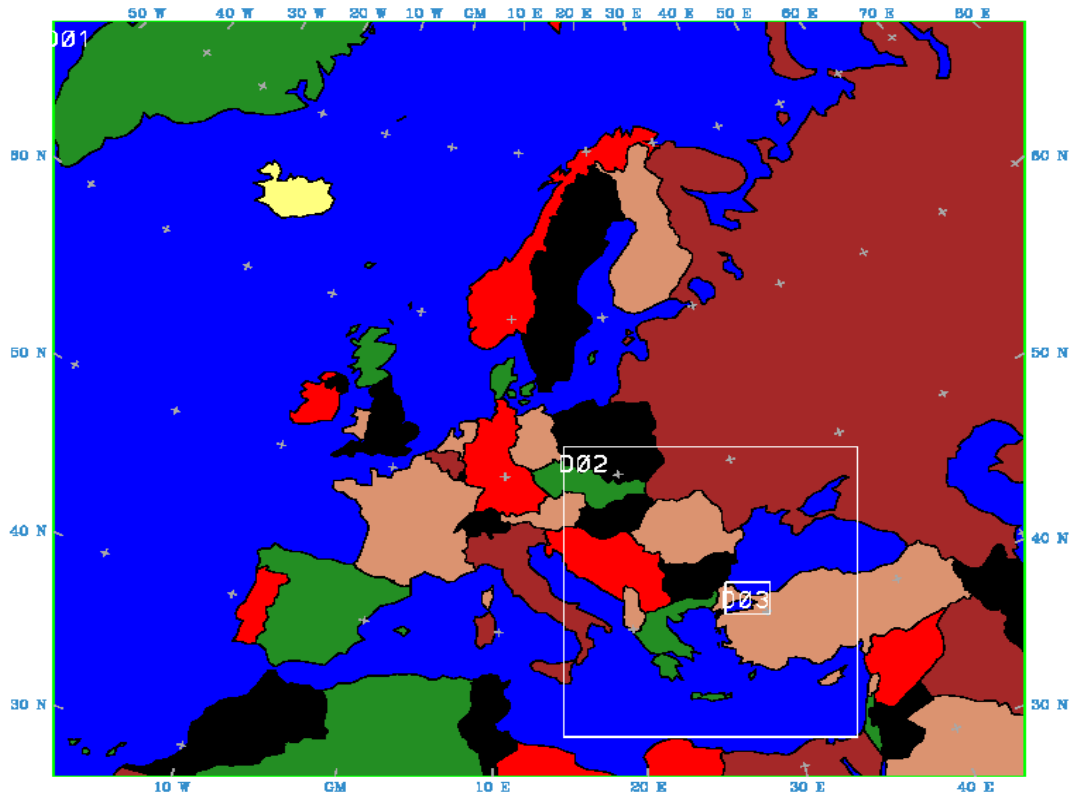


Figure 3.10 Map of the modeling domain.

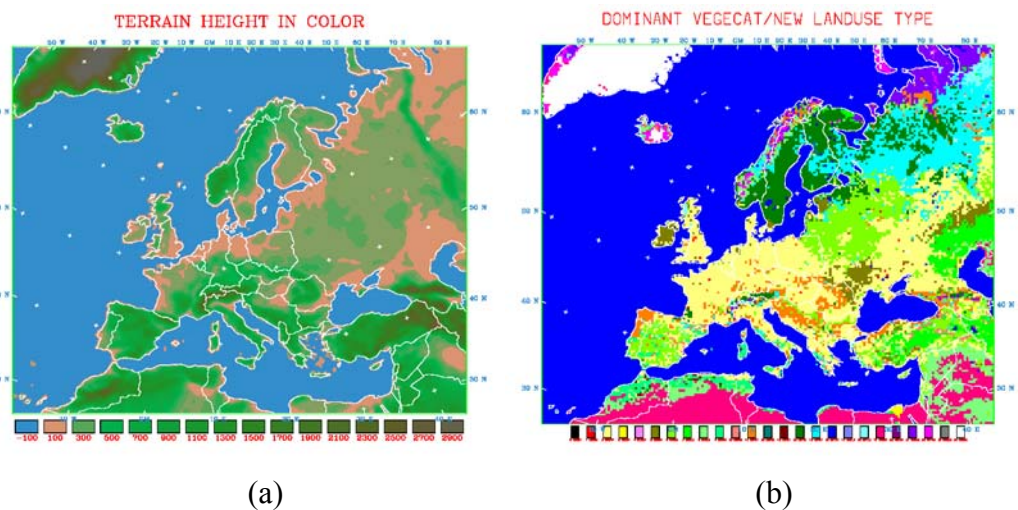


Figure 3.11. a) Terrain heights and b) Landuse categories of the mother domain in color scale.

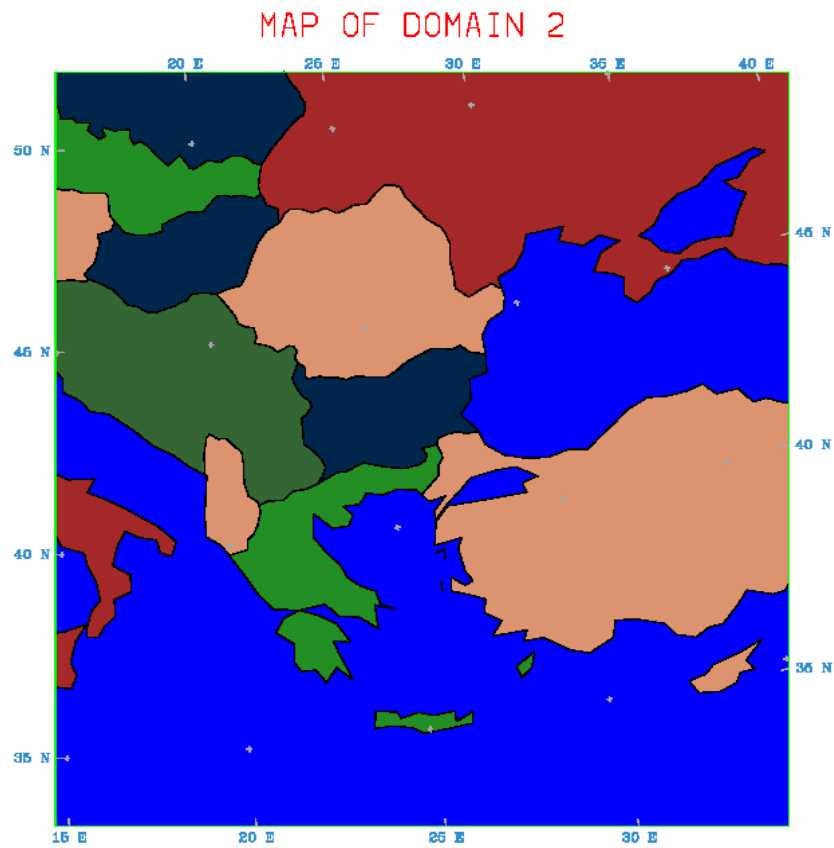
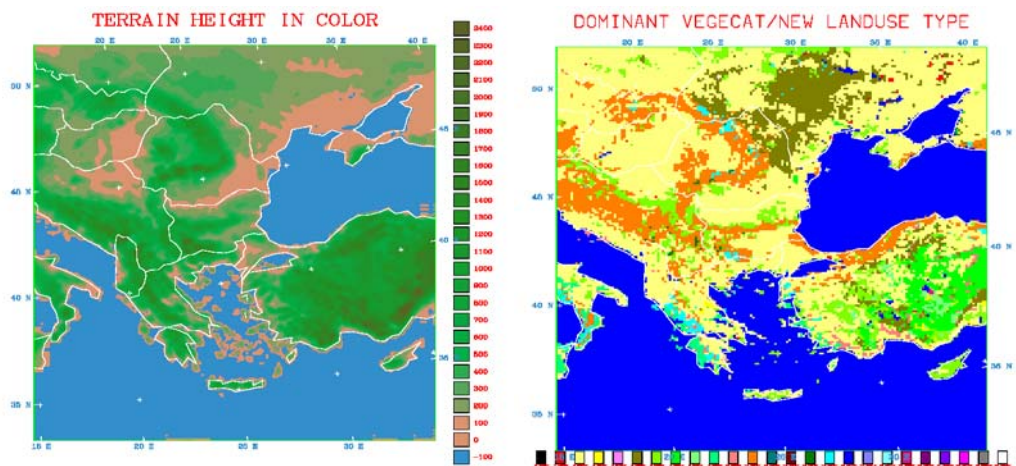


Figure 3.12 Map of the modeling domain 2.



(a)

(b)

Figure 3.13 a) Map of the terrain heights and b) landuse categories of modeling domain 2 in color scale.

MM5 is run for the above time period in 21600-minute time steps for domain 1 and domain 2. Since MM5 requires a 1:3 ratio between two domains, a configuration to downscale from 10 to 2 km resolution is not possible. Thus, NESTDOWN module is employed to generate the boundary conditions for the inner most domain covering İstanbul on 2 km resolution. The coarse domain D_t is set to $3 \times D_x$, where D_x is the grid resolution. The physics options used in the run are given in Table 3.4. NESTDOWN module is employed to generate the boundary conditions for the inner most domain covering İstanbul on 2 km resolution.

3.3. Emission Inventory

This study covers anthropogenic emissions on 3 domains. First domain includes 163×150 grids at x and y directions, respectively, on a 30×30 km² grid resolution, covering Europe and Middle East. The second domain covers the Balkan Domain, including 140×155 grids at x and y directions, respectively, on a 10×10 km² grid resolution. Finally, the inner domain covers the Greater Istanbul Area, on a 92×57 grids at x and y directions, respectively, on a 2×2 km² grid resolution. The methodology to calculate the spatial, temporal and chemically speciated emissions are presented in the following chapters.

3.3.1. Anthropogenic Emissions

In this study, gridded annual emission data which were obtained from Visschedijk et al., 2007 is used. The inventory was originally prepared for the Global and Regional Earth-System Monitoring using Satellite and in-situ data (GEMS) project (Hollingsworth et al., 2008) for the reference year of 2005 with a grid spacing of $1/8$ by $1/16$ degrees. The inventory was originally compiled to cover the European territory and a part of West Asia. The inventory is compiled on 30 km grid resolution and used for anthropogenic sources. This database provides emissions for 10 anthropogenic emission sectors. A list of these source categories are given in Table 3.6.)

3.3.1.1. Combustion in energy and transformation industries. Combustion in energy and transformation industries are taken into account as point sources or area sources depend on their capacities. Relevant pollutants are sulfur oxides (SO_x), nitrogen oxides (NO_x), carbon

dioxide (CO₂) and heavy metals. Emissions of volatile organic compounds (non-methane VOC and methane), nitrous oxide (N₂O), carbon monoxide (CO) and ammonia (NH₃) are also released through the stack.

Table 3.4. Physics options used in the MM5 simulation.

Physics Options	
Moisture Scheme	Mix Phase
Cumulus Scheme	KF2 (Kain, 2002)
PBL Scheme	MRF (Hong and Pan, 1996)
Radiation Scheme	RRTM (Mlawer et al., 1997)
Soil Temperature Model	Yes
Shallow Convection	No

Table 3.5. Sectors of anthropogenic emissions.

Sector No	Anthropogenic Sources
1	Combustion in energy and transformation industries
2	Non-industrial combustion plants
3	Combustion in manufacturing industry
4	Production processes
5	Distribution of fossil fuels and geothermal energy
51	Coal Extraction
6	Solvents and other product use
7	Road transport
81	Inter ferry lines
82	Cargo shipping
9	Waste treatment and disposal
10	Agriculture

3.3.1.2. Non-industrial combustion plants. Non-industrial combustion plants cover commercial and institutional plants, residential plants and plants in agriculture, forestry & aquaculture. A specific methodology for these activities has not been prepared by CORINAIR/EMEP, because the contribution to the total national emissions is thought to be currently insignificant, i.e. less than 1 per cent of national emissions of any pollutant.

3.3.1.3. Combustion in manufacturing industry. Combustion in manufacturing industry covers emissions released from that of combustion for furnaces with and without contact with different type of metals. Relevant pollutants are sulfur oxides (SO_x), nitrogen oxides (NO_x), carbon monoxide (CO), carbon dioxide (CO₂), nitrous oxide (N₂O) and heavy metals. Approximately, combustion in the manufacturing industry is responsible for 25 per cent SO₂, 24 per cent CO₂, 14 per cent NO₂ and 12 per cent CO of the all sectors.

3.3.1.4. Production processes. Production processes include processes in petroleum industries; iron & steel industries & collieries, non – ferrous metal industries, inorganic chemical industries, wood, paper pulp, food, drink and other industries; production of halocarbons and sulfur hexafluoride. This sector covers emissions of SO_x (3 per cent of all sectors), NO_x (2 per cent of all sectors), CO (5 per cent of all sectors), CO₂ (4 per cent of all sectors), NMVOC (6 per cent of all sectors), N₂O (19 per cent of all sectors), NH₃ (3 per cent of all sectors), PM and heavy metals.

3.3.1.5. Extraction and distribution of fossil fuels and geothermal energy. Extraction and distribution of fossil fuels and geothermal energy include processes in extraction and the first treatment of solid/liquid/gas fossil fuels; liquid/gasoline fuel distribution; gas distribution networks and geothermal energy extraction. This sector covers emissions of NO_x, CO₂, VOC, NMVOC and CH₄. When we compare the sector of extraction and distribution of fossil fuels with all sectors; its main contribution is 23 per cent CH₄, 6 per cent NMVOC and 1 per cent CO₂.

3.3.1.6. Use of solvents and other products. Solvent use is a major contributor to NMVOC emissions. On a European scale its contribution is roughly a quarter of the total anthropogenic NMVOC emission. The contribution of the sector to anthropogenic NMVOC emissions varies between 15 per cent and 30 per cent. Also, solvent use

contributes to the emissions of some heavy metals (Cd, Cu, Pb and Zn), CO, PM, SO_x and NO_x.

Most solvents are part of a final product, e.g. paint, and will sooner or later evaporate. This evaporation of solvents is a major source of NMVOC emission in any country, thus inventorying of this source is of great importance. The use of solvents, like that of other products, has three stages in which emissions occur: during production, during actual use and during disposal.

The NMVOC emission from solvent use is calculated based on per capita data for several source categories. The categories most used for this purpose are: paint, all applications; industrial degreasing; dry cleaning; glues & adhesives; graphic arts (ink); chemical industry (e.g. pharmaceuticals); household products (e.g. toiletries); rubber and plastics industry; vegetable oil extraction; leather industry; pesticides and other solvent uses.

3.3.1.7. Road Transport. Road Transport includes the emissions produced by the exhaust systems of road vehicles. It does not cover non-exhaust emissions such as fuel evaporation and component attrition. The vehicle category splits into base parts when we consider the report emissions from road transport to international bodies. However, from a technical point of view, it does not provide the level of detail considered necessary to collect emissions from road vehicles in a systematic way. This is because road vehicle power trains make use of a great range of fuels, engine technologies and after treatment devices. Thus, a more detailed vehicle category split is necessary and has been developed.

Pollutants covered include all major emission contributions from road transportation: Ozone precursors (CO, NO_x, and NMVOC), greenhouse gases (CO₂, CH₄, and N₂O), acidifying substances (NH₃, SO₂), particulate matter (PM), carcinogenic species (PAHs & POPs), toxic substances (dioxins and furans) and heavy metals. In detail, the sector covers exhaust emissions of CO, NO_x, NMVOC, CH₄, CO₂, N₂O, NH₃, SO_x, diesel exhaust particulates (PM), PAHs and POPs, Dioxins and Furans and heavy metals contained in the fuel (Lead, Cadmium, Copper, Chromium, Nickel, Selenium and Zinc). A detailed

NMVOC split is also included to distinguish hydrocarbon emissions as alkanes, alkenes, alkynes, aldehydes, ketones and aromatics.

Road transport poses significant environmental pressures. Until lately, air quality was the major issue of concern for road transport emissions but significant technological improvements have effectively alleviated the risks. Today, greenhouse gases (and energy consumption) from road vehicles arise as the main concern for sustainable road transport development. Available data show that in 1999, road transport contributed to about 24 per cent of total CO₂ emissions in EU and 47 per cent of total NO_x emissions. However, the trends in those two pollutants are opposite, with ~15 per cent increase and ~20 per cent decrease of CO₂ and NO_x in 1999 respectively, compared to 1990 levels. Other Mobile Sources and Machinery includes military, railways, inland waterways, agriculture, forestry, industry, household and gardening, other off-road, shipping activities and air traffic. These sectors cover emissions of NO_x, NMVOC, CH₄, CO, CO₂, NH₃, N₂O, PM, SO_x and some heavy metals.

3.3.1.8. Other mobile sources and machinery. On a European scale, SO₂ and NO_x emissions from national shipping can be important with respect to total national emissions. However, emissions from national shipping generally only represent a few percent of the emissions from shipping operating internationally. Globally, shipping is estimated to be responsible for around 5-12 per cent and 3-4 per cent respectively of anthropogenic NO_x and SO₂ emissions (extrapolations from Marintek (1990) and Lloyd's Register (1995)). Estimated total NO_x attributable to shipping in the Northeastern Atlantic is approximately equivalent to the national total for France and Denmark combined, and slightly greater than the emissions attributed to road transport in Germany in 1990. Total SO₂ emissions are estimated to be equivalent to the total emission from France and half that emitted by UK power stations in 1990. Shipping-generated exhaust emissions of hydrocarbons (VOC) and CO are relatively insignificant in comparison to national land based sources (Lloyd's Register, 1995). The total contribution of aircraft emissions to total global anthropogenic CO₂ emissions is considered to be about 2 per cent (IPCC, 1999). This relatively small contribution to global emissions should be seen in relation to the fact that most aircraft emissions are injected almost directly into the upper free troposphere and lower stratosphere. IPCC has estimated that the contribution to radiative forcing is about 3.5 per

cent. The importance of this source is growing as the volume of air traffic is steadily increasing.

3.3.1.9. Waste Treatment and Disposal. Waste treatment and disposal includes waste incineration, solid waste disposal on land, open burning of agricultural wastes, cremation and other waste treatment. The relative proportion of emissions contributed by the sector varies between pollutants. The emissions of compounds such as non methane volatile organic compounds (NMVOCs), NO_x, CO₂ and N₂O are unlikely to contribute significantly to total emissions. However, waste treatment and disposal have been a major source of emissions of CH₄ (19 per cent) and CO (6 per cent).

3.3.1.10. Agriculture. Agriculture is a branch of industry which cultivates land and keeps animals in order to produce food, fodder or raw materials used for industrial processes, and comprises arable agriculture, animal agriculture, horticulture, viticulture, etc., with a wide range of intensities. In principle, a sharp distinction between agriculture and natural systems is impossible, as even these systems are used intentionally for food, fodder or animal production and – at least in Europe – are almost everywhere subject to management measures.

3.3.2. Speciation

Raw emission inventories, in general, provide data for total VOCs, gaseous and particulate emissions. In order to be able to input data to air quality model, these raw values need to be speciated. For example, total VOCs should be divided into individual organic compounds (e.g., PAR, OLE, ALD etc). For this purpose, we used the source sector specific VOC speciation profile obtained from the TNO, 2005. The PM speciation factors were obtained from CARB, 2007. The species used in the inventory for the European and Balkan domains are listed in Table 3.6.

3.3.2.1. Temporal Allocation. Raw emissions inventories provide annual emissions, whereas air quality models require hourly values. In order to allocate emissions data temporally, temporal allocation factors need to be utilized. In this study, temporal allocation factors for monthly, weekly, weekdays-weekend diurnal variations are

determined. Then, annual emission data are multiplied with these factors. It should be noted that, temporal factors are source sector specific. Temporal allocation factors for the Europe, provided from Friedrich R. (1997) were used. The temporal profiles for monthly, weekly and diurnally are listed in Tables 3.7, 3.8 and 3.9, respectively.

Table 3.6. Chemical compounds of the emission inventory used in the European and Balkan domains.

Gaseous / PM Species	VOC Species
CO	Alcohols
NO _x	Ethane
SO ₂	Propane
VOC (aggregated)	Butanes
Organic Carbon (PM ₁₀)	Pentanes
Elemental Carbon (PM ₁₀)	Higher Alcanes
Sulfates (PM ₁₀)	Ethane
Nitrates (PM ₁₀)	Propene
Other Particles (PM ₁₀)	Ethyne
Other Particles (PM _{2.5})	Olefins
NH ₃	Benzene
	Toluene
	Xylenes
	Trimethylbenzene
	Other Aromatics
	Esters
	Ethers
	Chlorinated Hydrocarbons
	Formaldehyde
	Other Aldehydes
	Ketones
	Acids
	Other NMVOCs

The European PM₁₀ emissions on 30×30 km² grid resolution are presented in Figure 3.16. The figure clearly indicates the hot spots for particulate emissions, especially for the Eastern European countries. The northern parts of Italy, where very dense industrial activities take place is also demonstrated as a hot spot in both Figures. The Greater Istanbul Area is also a hot spot for both emissions. CO, SO₂, NO_x, NH₃, Toluene and Xylene emissions for the same time period are presented in Figure 3.17.

PM₁₀ emissions for the same time period in the second domain, which covers the Balkan Region on 10 km grid resolution, are presented in Figure 3.18. Three largest cities in terms of population and industry; İstanbul, Ankara and İzmir are clearly seen as hot spots for PM₁₀ emissions. Additionally, another important hot spot in the region, Athens, is also clearly distinguished.

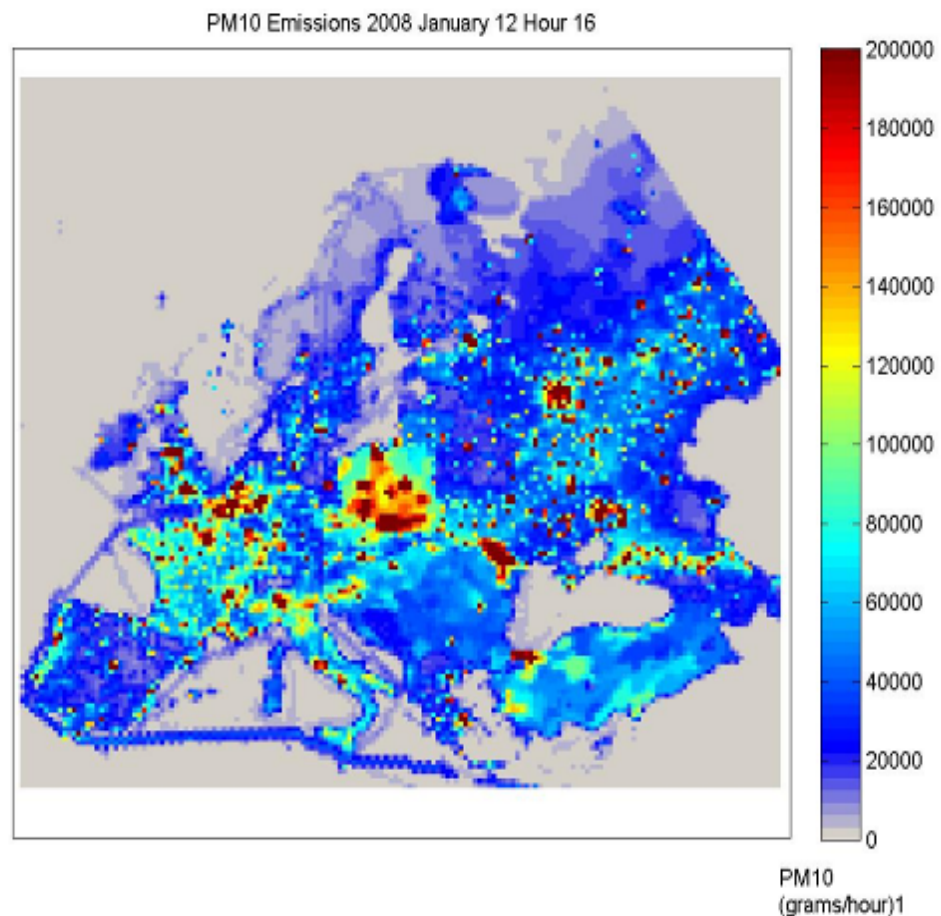


Figure 3.16. European PM₁₀ emissions for January 12, 2008, 1600 UTC, on 30 km grid resolution.

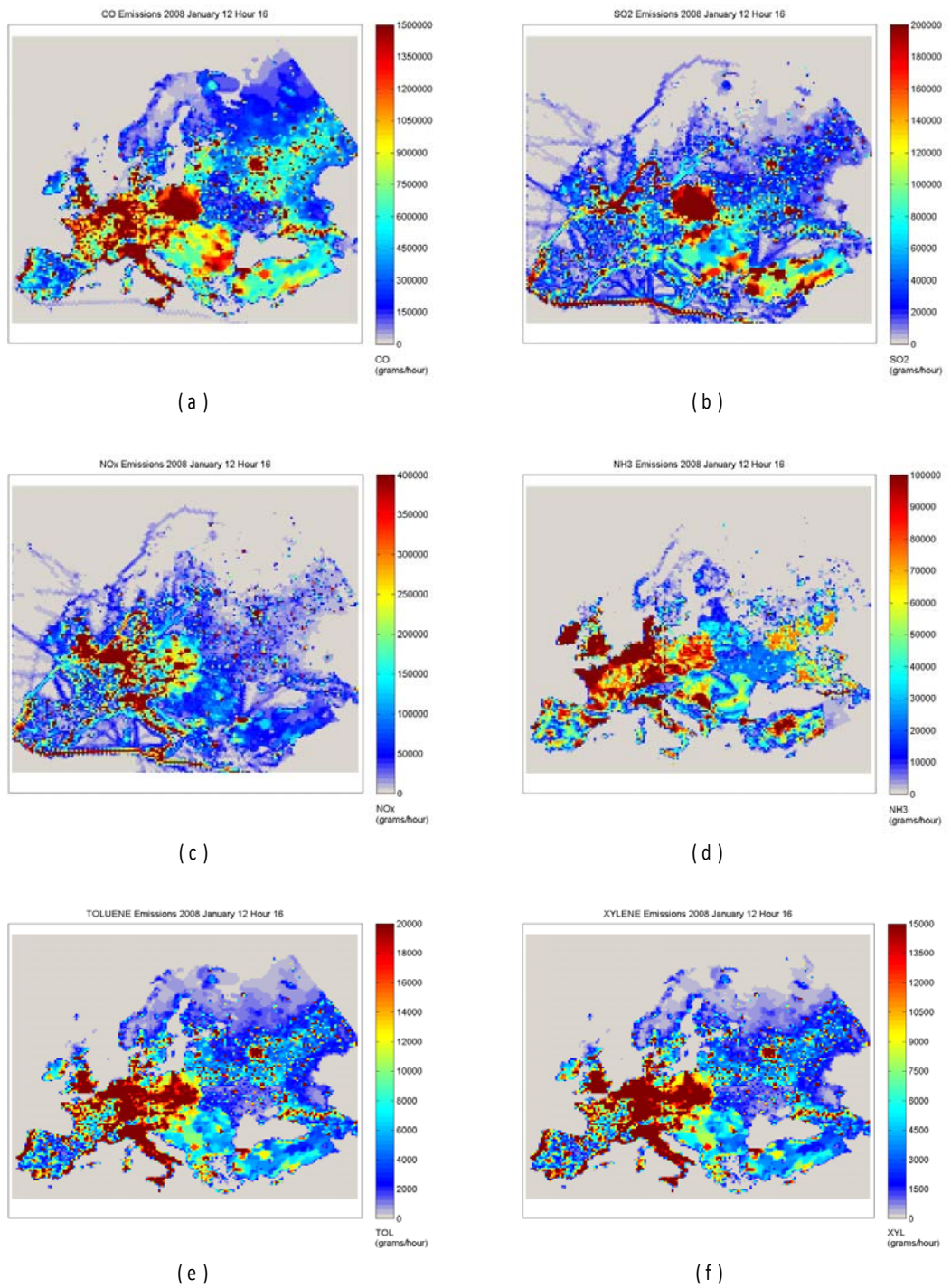


Figure 3.17. European emission of a) CO, b) SO₂, c) NO_x, d) NH₃, e) Toluene and f) Xylene for January 12, 2008, 1600 UTC, on 30 km grid resolution.

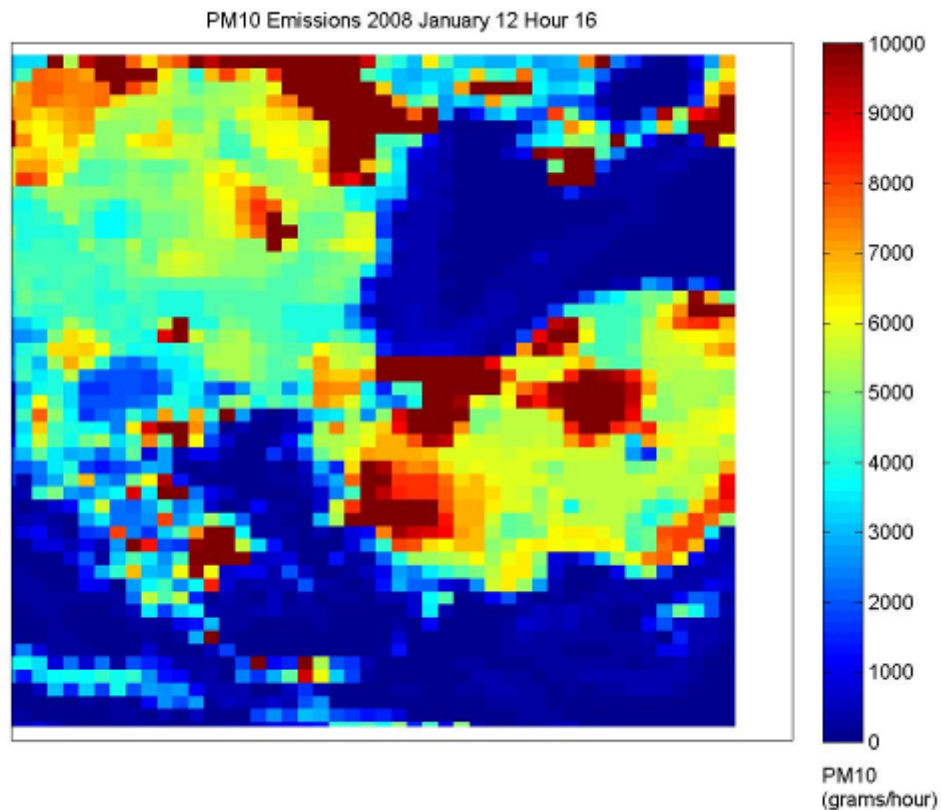


Figure 3.18. Balkan Region PM₁₀ emissions for January 12, 2008, 1600 UTC, on 10 km grid resolution.

3.3.3. Development of High Resolution Emission Inventory for the Greater Istanbul Area

An emission processor was developed in SQL / MapBasic programming language and was scripted into MapInfo 9.0 GIS software (Markakis et al., 2009). Each source sector was processed independently and in the first step emissions were calculated from the assembled activity data. Subsequently PM emissions were chemically speciated using look-up tables containing the IDs to links the emission sources with their chemical profile. The next step involved the spatial allocation of emissions. In order to fill for the remaining sources (for which activity data were not available) the high resolution gridded emission inventory of Visschedijk et al. (2007) was used. For the latter extracted emissions are reallocated to a higher spatial level with the help of the appropriate spatial indicator e.g. waste treatment emissions are allocated to neighborhood level using population statistics. Subsequently the emissions were reallocated to the final grid. The speciation of NMVOCs

followed and finally the emissions were temporally disaggregated per source sector down to weekly and diurnal level.

The emissions are spatially allocated over the Greater Istanbul Area using a grid spacing of 2 km. The emissions grid is created in Lambert Conformal Conic (LCC) projection covering an area of 20 976 km² (92 by 57 cells). The pollutants considered are nitrogen oxides (NO_x=NO+NO₂), carbon monoxide (CO), sulfur dioxide (SO₂), ammonia (NH₃), non-methane volatile organic compounds (NMVOCs), PM₁₀ and PM_{2.5}. The NMVOCs emissions are chemically speciated in 23 species based on the TNO, 2005 source sectoral profiles. Furthermore, splitting of PM emissions is needed for the characterization of their chemical composition. The chemical splitting was performed using source specific profiles derived from CARB, 2007. PM₁₀ emissions were chemically speciated in Organic and elemental carbon, nitrates, sulfates, ammonium and other particles. A constant NO/NO_x fraction with value of 0.9 was used for all NO_x emission sectors (USEPA 2002).

In order to derive annual emission estimates, the kernel uses either activity information or pre-existing emissions data originated either from official sources or older studies. Activity input data were available for the quantification of emissions for the sources presented in Table 3.10.

To compile the emission inventory various activity information and statistical data were gathered from local official authorities, experts, measurements, originated from other published studies in the region or extracted from international databases. Table 3.10 summarizes the input activity data used for the quantification of emission sources (residential and industrial combustion, solvents use, local sea basses/ferries and cargo shipping), emissions obtained from measurements (Esenyurt power plant), annual emissions originated from other national or local authorities (industrial sector), studies conducted in the area (road transport).

Table 3.7. Monthly temporal profiles for each source sector.

		MONTHS											
		JAN	FEB	MAR	APR	MAY	JUN	JUL	AUG	SEP	OCT	NOV	DEC
EMEP SECTORS	1	0.11	0.10	0.09	0.09	0.08	0.06	0.06	0.06	0.06	0.08	0.09	0.11
	2	0.17	0.19	0.15	0.10	0.05	0.03	0.02	0.02	0.02	0.05	0.08	0.13
	3	0.09	0.10	0.10	0.09	0.08	0.08	0.07	0.06	0.07	0.08	0.09	0.09
	4	0.08	0.09	0.09	0.09	0.09	0.09	0.08	0.07	0.08	0.09	0.09	0.08
	5	0.08	0.08	0.08	0.08	0.08	0.08	0.08	0.08	0.08	0.08	0.08	0.08
	6	0.08	0.08	0.08	0.09	0.09	0.09	0.08	0.07	0.08	0.09	0.09	0.09
	7	0.08	0.08	0.08	0.09	0.09	0.09	0.08	0.08	0.08	0.09	0.08	0.08
	8	0.07	0.08	0.08	0.09	0.09	0.09	0.09	0.08	0.08	0.09	0.08	0.08
	9	0.08	0.08	0.08	0.08	0.08	0.08	0.08	0.08	0.08	0.08	0.08	0.08
	10	0.01	0.02	0.09	0.13	0.08	0.06	0.05	0.06	0.14	0.19	0.13	0.04

Table 3.9. Weekday and weekend hourly profiles for each source sector.

HOURS OF THE DAY																										
		1	2	3	4	5	6	7	8	9	10	11	12	13	14	15	16	17	18	19	20	21	22	23	24	
EMEP SECTORS	1	0.03	0.03	0.03	0.03	0.04	0.04	0.05	0.05	0.05	0.05	0.05	0.05	0.05	0.05	0.05	0.05	0.04	0.04	0.04	0.04	0.04	0.04	0.04	0.03	
	2	0.02	0.02	0.02	0.02	0.03	0.05	0.06	0.06	0.06	0.05	0.05	0.04	0.04	0.04	0.04	0.04	0.05	0.06	0.06	0.06	0.05	0.03	0.02	0.02	
	3	0.03	0.03	0.04	0.04	0.04	0.04	0.05	0.05	0.05	0.05	0.05	0.05	0.05	0.05	0.05	0.04	0.04	0.04	0.04	0.03	0.03	0.03	0.03	0.03	
	4	0.03	0.03	0.04	0.04	0.04	0.04	0.05	0.05	0.05	0.05	0.05	0.05	0.05	0.05	0.05	0.04	0.04	0.04	0.04	0.03	0.03	0.03	0.03	0.03	
	5	0.03	0.03	0.04	0.04	0.04	0.04	0.05	0.05	0.05	0.05	0.05	0.05	0.05	0.05	0.05	0.04	0.04	0.04	0.04	0.03	0.03	0.03	0.03	0.03	
	6	0.01	0.01	0.01	0.01	0.02	0.04	0.05	0.06	0.06	0.06	0.06	0.06	0.06	0.06	0.06	0.06	0.06	0.06	0.05	0.04	0.04	0.04	0.03	0.03	0.02
	7	0	0	0	0.01	0.02	0.05	0.07	0.07	0.06	0.05	0.05	0.06	0.06	0.06	0.07	0.08	0.08	0.06	0.04	0.03	0.02	0.02	0.02	0.02	0.02
	8	0	0	0	0.01	0.02	0.05	0.07	0.07	0.06	0.05	0.05	0.06	0.06	0.06	0.07	0.08	0.08	0.06	0.04	0.03	0.02	0.02	0.02	0.02	0.02
	9	0	0	0	0.01	0.02	0.05	0.07	0.07	0.06	0.05	0.05	0.06	0.06	0.06	0.07	0.08	0.08	0.06	0.04	0.03	0.02	0.02	0.02	0.02	0.02
	10	0.02	0.02	0.03	0.03	0.03	0.03	0.04	0.05	0.06	0.06	0.07	0.07	0.07	0.07	0.06	0.05	0.04	0.04	0.03	0.03	0.02	0.02	0.02	0.02	0.02

To fill for the remaining source sectors (industrial processes, distribution of fuels, off-road vehicles and machinery, waste treatment and disposal and agriculture) the high resolution emissions of Visschedijk et al., (2007) are used. The inventory was originally prepared for the GEMS project for the reference year of 2005 with a grid spacing of 1/8 by 1/16 degrees. The inventory was originally compiled to cover the European territory and a part of West Asia. For the needs of this work a portion of it was extracted to cover the GIA.

The emissions are temporally resolved using monthly, weekly and diurnal profiles. For daily resolution, it was divided into Monday, Tuesday, Wednesday, Thursday, Friday, Saturday and Sunday. All temporal variation profiles used in the present study originate from Friedrich (1997) and were compiled within the scope of the EUROTRAC/GENEMIS project. The profiles were compiled for Turkey by SNAP source sector (EEA, 2001) for each of the pollutants in question. One exception is the diurnal variation for the road transport emissions provided by the EMBARQ study (EMBARQ, 2008) and the monthly variation of international cargo shipping emissions provided by the UMA (2007), as monthly vessel traffic. In addition, for the quantification of the residential and industrial combustion sector emissions the emission factors of USEPA were used. The latter are considered to be more representative for Turkey (Elbir and Muezzinoğlu, 2004) in comparison with the respective emission factors of European sources (EEA, 2003).

To provide easy updatability the inventory was compiled by each source sector or subsector using an emission processing kernel developed for this purpose. The emission processor is written in Mapbasic/SQL programming language and it is scripted into Mapinfo 9.0 GIS software. The processor is structured to yield spatially and temporally disaggregated emissions for 28 chemical species starting from input activity data or pre-existing annual/monthly emission totals.

3.3.3.1. Description of the emission processor. Figure 3.19 presents a schematic description of the emission processor. The processing is done by source sector and can be summarized in the following procedures.

Table 3.10. Input data used in the inventory, their geographical activity level and the spatial indicators used for the allocation of sources.

Source category (spatial analysis)	Input data	Spatial indicator
Energy (point sources)	Esenyurt Unit-hourly measured emissions rates Ambarli Unit-Annual consumption of fuel oil and natural gas	Geographical location
Residential combustion (area sources)	Annual consumption of fuels in 630 neighborhoods of the GIA Annual consumption of coal.	Area proportion
Industrial combustion (area sources)	Annual consumption of NG, fuel oil and coal in 142 OSB ^a	Area proportion
Solvents use (area sources)	Population statistics in 640 neighborhoods of the GIA	Population density
Road transport (area sources)	Annual emissions of (passenger cars, busses and trucks) in the GIA	Road segment length
Passenger ships/ferries (line sources)	Annual fuel consumption for 9 lines operated by sea busses and ferries	Route length
Cargo shipping (line sources)	Monthly vessel traffic in the Bosphorus strait and the Marmara sea Annual traffic in the Ambarli port	Route length
Aviation (point sources)	Annual emissions of the Ataturk International Airport ^b	Geographical location
1) Industrial processes 2) distribution of fossil fuels 3) Off-road vehicles and machinery^c 4) waste treatment and disposal 5) Agriculture	TNO emission database for the year 2005 provided in 1/8 by 1/16 degrees resolution grid	OBB (area proportion) Population density Population density Population density USGS landcover ^d

a Organized Industrial Areas.

b From Kesgin et al., 2002.

c agriculture, industrial, construction and household/gardening machinery.

d The source of the land use information was the Global Land Cover Characteristics database (GLCC version 2) distributed by US Geological Survey (USGS, 1992). The landcover elements characterized as crops or mixed (crops/forest) were used as the relevant landcover for this source.

The processor uses a number of pre-saved tables which contain the activity/statistical information necessary for the calculations in order to quantify the emissions from the

available activity data (e.g. from the gridded emissions of Visschedijk et al., 2007). For the sources that are not quantified but derived from pre-existing databases (e.g. from the TNO database), the processor opens pre-saved tables which contain the annual emissions to be processed in the next step.

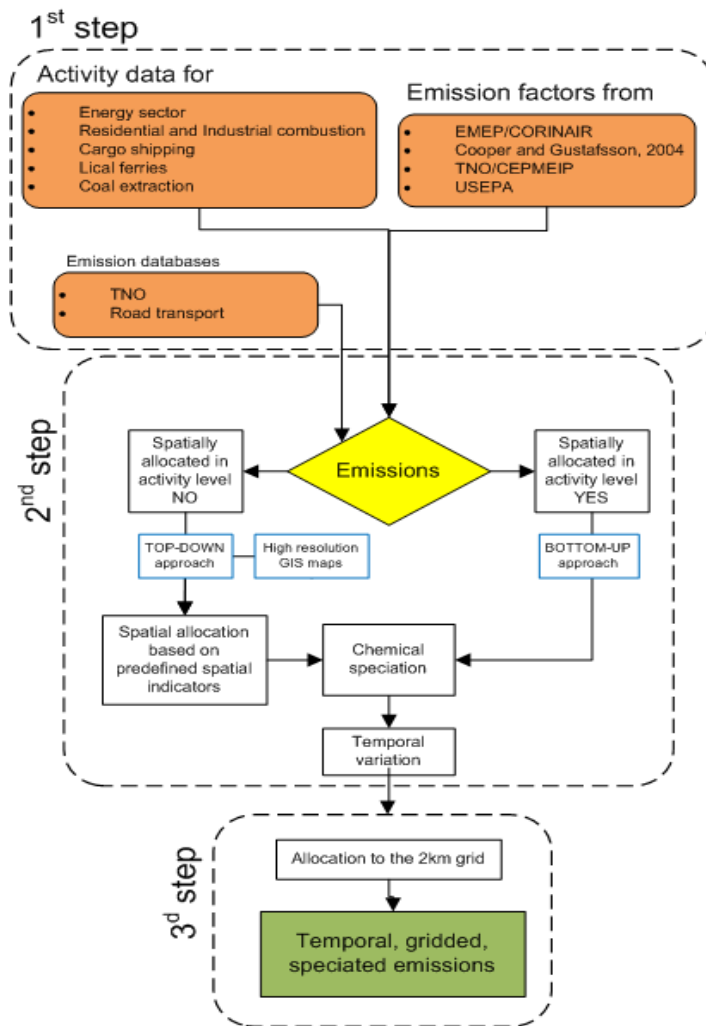


Figure 3.19. Schematic representation of the emission processor.

The next step is to introduce the spatial disaggregation of area sources emissions. To provide spatially resolved emissions, the processor handles geographical maps which are combined with source specific spatial indicators. A spatial indicator correlates a specific emission source with its activity in geographical terms. The spatial indicators are defined based either on geographically resolved official statistics (e.g. population density), data derived from GIS maps (e.g. road network) or on land use data (USGS, 2002). Table 3.10

summarizes the spatial indicators chosen for use in this work. In this step, spatial operations are performed with the aim to reallocate the emissions derived from the pre-existing databases to the highest possible spatial level e.g. in geographical terms the level which closest represents the actual activity of a given sector/subsector. For example, in order to reallocate the gridded TNO emissions (Visschedijk et al., 2007) of the distribution of fuels sector to the road network of Istanbul, the length of each road segment within each TNO grid cell is used as the appropriate spatial indicator. These emissions (e.g. the emissions allocated in the road segments) are finally reallocated to the final inventory grid.

As a next step PM emissions and NMVOCs are chemically speciated. To provide chemically resolved emissions, profile tables are used. The tables contain the chemical profiles which are linked to the emission tables based on source relevant chemical indicators e.g. the fuel burned (for residential/industrial combustion).

In the next step, the temporal variation of emissions is introduced (by source sector). The profile tables include all the factors to increase the temporal resolution (e.g. to scale the monthly emissions down to daily emissions, the code uses 7 factors one for each day of the week). The interaction between the emission data and the spatial indicators is possible through the use of spatial overlays which include:

- Point in polygon operations, to allocate point sources emissions (e.g. energy and industrial unit emissions) to the final grid.
- Line in polygon operations, to allocate line sources emissions to area polygons or vice versa. For example to allocate passenger/ferries emissions calculated along their cruising routes (lines) to the final grid (polygon) or to disaggregate the top – down estimation of the road transport sector emissions (calculated in a polygon representing the area of the country or the urban centers) to the road network (lines).
- Area in polygon operations, to allocate emissions calculated in a polygon e.g. ammonia emissions calculated in prefectural level, to another polygon e.g. polygons with the pasture landcover.

Finally the emissions of each source sector are aggregated to produce surrogate files for each pollutant in question. The system described above was implemented in order to

compile an emission inventory for 28 chemical compounds in a 2 km resolution grid over the GIA in monthly, weekly and hourly basis.

3.3.3.2. Quantification methodology.

Residential and Industrial combustion. The calculation of the emission rates derived from the residential and industrial combustion in the area was based on the annual consumption of natural gas, light fuel oil, coal and liquefied petroleum gas (LPG) and the emissions factors derived from EPA (USEPA, 1995). The consumption of residential natural gas was provided in a spatial level representing the neighborhoods of the GIA from the Istanbul Gas Distribution Corporation (IGDAS). In this study a high resolution digital database was used, provided in GIS format, which includes the boundaries of 958 administrative units representing the neighborhoods of the city. The total amount of coal used for residential space heating was provided from the Greater Municipality of Istanbul (IBB). To distribute the amount of coal, an inverse relationship with the consumption of NG was used. In the neighborhoods in which the penetration of NG was the lowest, the amount of the coal consumed was assumed to be higher. Consequently the municipality of Sultanbeyli was calculated to have the highest coal consumption rate, as expected. The municipality has a high and rapidly growing population and on the other hand, most of the provinces have not installed natural gas systems for residential heating (TUIK, 2007).

The annual consumption of coal, natural gas, LPG and Fuel Oil, used in the Organized Industrial Areas (OSB) are provided by IBB. Table 3.11 summarizes the amount of fuels used for the quantification of residential and industrial emissions and Table 3.12 tabulates the emission factors chosen for use in this work.

For the calculation of SO₂ emissions, the sulfur content of the fuel is necessary. For NG and LPG the value of 0.1 per cent wt was used and for residential/industrial fuel oil, it was taken equal to 1.5 per cent wt (Çetin et al., 2007). For industrial and residential coal, a value of 2.7 per cent wt was used. It was assumed that all industrial facilities in the area utilize local coal reserves. The properties of the extracted coal can vary significantly depending on the location of the extraction (Palmer et al., 2007). To derive a representative value for the coal consumed in the OBB, the average sulfur content of the coal extracted in

the mining sites of the North Marmara Sea (2.6 per cent wt) and the South Marmara Sea (2.8 per cent wt) were used. The latter values are provided in the study of Palmer et al., 2004 which presents a comprehensive analysis on the properties of the Turkish coals. The derived value is higher from the value used in other studies conducted in the area (Çetin et al., 2007) but lower from the national average of all coal mining sites in the country (2.9 per cent wt – median value of collected samples) (Palmer et al., 2004). The same approach was used to derive the ash content of the coal consumed. The value which was used in this study is 25 per cent wt, also reported by other studies (Say, 2006).

Table 3.11. Annual fuel consumption in the study region.

Fuel type	Residential	Industrial/ Energy
Coal (in kton)	1,000	1,402
NG (in million m³)	2,828	3,196
Fuel oil (in kton)	-	1,082
LPG (in million m³)	-	0.47

Public power generation plants. Two power generation plants were included in the emission inventory. For the natural gas power unit of Esenyurt (3 units, 130 MW each), the hourly emissions rates of CO, NO_x, SO₂ and TSP (total suspended particulates) were obtained from the emission reports provided to IBB. CO was measured by TS ISO 12039: 2005, SO₂ by TS ISO 7935: 1999, NO_x by EPA – CTM 022: 1998 and PM by TS ISO 9096: 2004. Flue gases were measured by Madur GA – 21 Plus flue gas analyzer and PM by Zambelli ISO 6000 Plus PM sampler. The measurements were conducted in August, 2003. In order to derive annual emissions from hourly measured rates, 7000 hours of annual operation was used (EEA, 2001) based on the assumption that Esenyurt power plant is a base load unit, which is under constant load except from the days in maintenance and the reduced operating load in some periods. Start – up emissions were not taken into account due to lack of the relevant information.

In order to estimate the emissions of the Ambarli power plant, which operates one 1350 MW unit burning natural gas and one 1205 MW unit burning oil, the annual consumption of natural gas (Table 3.11) and heavy fuel oil, provided from the Electric Generation Co. Inc. (EUAS, 2008), was multiplied with emissions factors from EPA (Table 3.12).

Road transport. Road transport data are obtained from the study conducted by EMBARQ and Istanbul Metropolitan Municipality. Continuous measurements of CO, CO₂, SO₂, HC and PM_{2.5} were done using Portable Emissions Measurement System (PEMS) for 29 trucks, 6 busses and 7 passenger vehicles for different models of vehicles on different road and driving conditions. Overall, 42 test drives have been done for diesel and 104 test drives have been done for gasoline vehicles.

Maritime. Istanbul is divided into the European and the Asian side by the Bosphorus, a sea water strait extending from Black Sea in north and the interior Marmara Sea in south. Local ferries play an important role in the transportation within the city. The Bosphorus strait serves as a passage linking Black Sea to Aegean and thus, Mediterranean Seas leading to intense transit international shipping through the city.

Maritime sector emissions were calculated for internal ferry lines and international cargo shipping (Table 3.10). Fuel consumption for 9 major cruising routes of sea busses and ferries were obtained from the Istanbul Fast Ferries Co. Inc. (IDO) for the year 2006 and 2007. The majority of these vessels are equipped with high speed engines (Deniz and Durmuşoğlu, 2008) and their emissions were calculated by employing the emission factors of EEA, 2001 methodology. Only cruising emissions were taken into account.

The quantification of international cargo shipping emissions was based on the monthly vessel (categorized in 8 vessel types) traffic in the Marmara Sea and the Bosphorus crossing for the year 2007 (Table 3.13). Annual traffic data in the port of Ambarli were also available (Kılıç, 2006). In order to be able to calculate the ships emissions the vessels had to be separated according to their engine type. The split was based on the 2003 world fleet statistics provided by Deniz and Durmuşoğlu (2008). Consequently, 2 per cent of the vessels are equipped with high speed diesel engines, 32 per cent are equipped with medium

speed diesel engines and 66 per cent are equipped with slow speed diesel engines while gas turbines and steam engines have a minimal share in the world fleet and were not taken into consideration. The emissions during the cruising mode as well as emissions during the hotelling and the maneuvering phases were quantified. The emission factors used for the aforesaid operating modes for all pollutants in question are summarized in Table 3.14. The emissions were calculated (Trozzi and Vacaro, 1998; EC, 2003) as the multiplication product of the relevant emissions factors (per mass of fuel) and the fuel consumption per vessel type (Trozzi and Vacaro, 1998) in each operating mode by using Equation 3.10:

$$E_i = \sum_{jkl} e_{ik} \times (F_{jkl} \times h_i) \times b_i \quad (3.10)$$

where E_i is the emissions of pollutant i , e_{ik} is the emissions factor per pollutant i and engine type k , F_{jkl} is the fuel consumption per hour at full power for each operating mode l and vessel type j , h is the total hours in operation for each mode l and b is the engine load factor per ship type j (USEPA 2000).

The operating time was assumed to be 0.5 hour for the hotelling phase (Deniz and Durmuşoğlu, 2008) and 0.5 hour for the maneuvering phase. The total cruising time was calculated using typical values for the cruising speed of each vessel type (Trozzi and Vacaro, 1998; Deniz and Durmuşoğlu, 2008) and the distance travelled.

The distance during the cruising mode was extracted from the GIS database available. The database contains the cursing lines of the vessels in the Marmara Sea and the Bosphorus crossing. In order for the distance to be calculated the vessels had to be separated in transit and non transit ships. A transit vessel passes through the Bosphorus and Canakkale strait while cruising in the Marmara Sea in between the crossings. A non-transit ship also passes the Turkish Straits but calls Marmara's ports (Ambarlı, Tekirdağ, İzmit, Haydarpaşa and Bandırma) for loading/unloading operations. After the ship finishes port operations, she cruises in the Sea of Marmara. Thus the vessels that pass through the Bosphorus crossing (56,606 in number) were assumed to cruise also in the Marmara Sea. Fig. 3 illustrates the area of the Marmara Sea and the largest ports to which non-transit vessels call for

loading/unloading operations. The split to transit and non-transit vessels was taken from Deniz and Durmuşoğlu, 2008 which utilized official data for the year 2003. The same split was assumed in this study for 2007.

Table 3.12. Emissions factors used for the quantification of residential and industrial combustion emissions. Inside the parenthesis is the quality rating of the emission factor.

Fuel type	CO	NO _x	SO _x ^a	NMVOC	PM ₁₀ /PM _{2.5}
	Residential				
Coal (kg/ton)^b	46.4	2.3	13.61 S	1.9	4 / 4
Light fuel oil (kg/10³ L)	0.6 (A)	2.16 (A)	17.28 S (A)	0.00856 (A)	0.048 ^b / 0.048 ^b
Natural gas (kg/million m³)	640 (B)	1504 (B)	9.6 (A)	51.2 (B)	121.6 (B) / 121.6 (B)
	Industrial/Energy				
Coal (kg/ton)^c	0.125 (C)	3.15 ^d (C)	15 S (C)	0.02 (C)	0.9 A ^e (E) / 0.26 A ^e (E)
Fuel oil^f (kg/10³ L)	0.6 (A)	LB: 5.64 ^g (B) SB No4: 2.4 (A) SB No6: 6.6 (A)	No4: 18.68 S (A) No6: 19.52 S (A)	No4: 0.024 (A) No6: 0.091 (A)	No4: 0.723 (D) / 0.471 (D) No6: 1.45 (D) / 0.942 (D)
Natural gas (kg/million m³)	1344 (B)	LB: 3040 ^h (A) SB: 1600 ^h (B)	9.6 (A)	51.2 (B)	121.6 (B) / 121.6 (B)
LPG (kg/10³ L)ⁱ	0.384 (E)	2.28 (E)	0.012 S (E)	0.036 (E)	0.072 (E) / 0.072 (E)

a S is the sulfur content of the fuel in % wt.

b From Woodfield 2003 (no quality rating provided).

c Uncontrolled.

d emission factor for Dry Bottom Wall Fired Boilers-Uncontrolled (post-NSPS).

e emission factor for uncontrolled Wall Fired Boilers, A is the ash content of fuel.

f For combustion in industries No4 fuel oil was used, normal firing. For the energy sector No6 heavy fuel oil was used.

g LB: Large boilers (>100 Million Btu/hr), SB: Large boilers (<100 Million Btu/hr).

h emission factor for Large Wall Fired Boilers-Uncontrolled (post-NSPS).

i Propane emission factors

Consequently, from the 56,606 cruising in the Marmara Sea and cross the Bosphorus strait, 61.7 per cent were transit vessels (34,926 ships) and 38.3 per cent were non-transit vessels (21,680 ships). Transit vessels cruise in the main line inside the Marmara Sea and their emissions were allocated along this line. The blue line represents the Bosphorus crossing from which both transit and non-transit vessels pass. From the 21,680 non-transit vessels a total number of 5601 vessels call the Ambarli port while the remainder (15,314 vessels) calls to the other ports of the Marmara Sea (Tekirdağ, İzmit and Bandırma). Unfortunately it was not possible to allocate the emissions of the remainder 15,314 vessels since both the traffic in the ports of İzmit and Bandırma as well as the exact routes in which they cruise were unknown. Their emissions were quantified by using the cruising distances provided by Deniz and Durmuşoğlu, (2008). The latter represent the cruised distance between each port and the Straights of Canakkale and Bosphorus.

Finally the chemical speciation of emissions was based on the chemical profiles of CARB, 2007 (per activity or source sub-sector) for PM and the profiles of the TNO for NMVOCs (23 species per source SNAP sector).

Table 3.13. Annual vessel traffic in the Bosphorus crossing and the Ambarli port.

Vessel type	Bosphorus crossing ^a	Ambarli port ^b
Tankers	9324	2239
General cargo	34,705	1305
Containers	2727	1725
LPG	800	-
Ro-Ro	439	155
Bulk Carriers	5144	-
Passenger	1702	-
Other	1765	177
Total	56,606	5601

a data for 2007 (UMA, 2007)

b data for 2005 (Kılıç, 2006)

Table 3.14. Emissions factors (in g ton⁻¹ of fuel) used for the quantification of cargo shipping emissions.

Engines type	CO	NO _x	SO _x ^a	NH ₃	NMVOC	PM
Cruising mode^b						
Slow speed	2545 ^c	87 136 ^d	46 000 S ^e	27 ^e	1525 ^c	6667 ^f
Medium speed	5063 ^c	61 657 ^d	46 000 S ^e	29 ^e	919 ^c	2326 ^f
High speed	5116 ^c	58 857 ^c	46 000 S ^e	14 ^e	930 ^c	2326 ^f
Hotelling mode^g						
Slow speed	99 000	35 000	20 000 S ^e	-	23 100	1200
Medium speed	99 000	23 000	20 000 S ^e	-	23 100	1200
High speed	120 000	28 000	20 000 S ^e	-	28 900	1500
Maneuvering mode^b						
Slow speed	4627 ^e	63 372 ^e	46 000 S ^e	25 ^f	2773 ^e	12 121 ^f
Medium speed	9206 ^e	44 841 ^e	46 000 S ^e	26 ^f	1671 ^e	4228 ^f
High speed	9302 ^e	42 805 ^e	46 000 S ^e	13 ^f	1691 ^e	4228 ^f

a Sulfur content of fuel (wt per cent) was taken equal to 2.3 (Cooper and Gustafsson, 2004).

b Emission factors for cruising and maneuvering modes from Cooper and Gustafsson, 2004.

c Uncertainty 10-20 per cent (Cooper and Gustafsson, 2004)

d Uncertainty 5-10 per cent (Cooper and Gustafsson, 2004)

e Uncertainty 20-50 per cent (Cooper and Gustafsson, 2004)

f Uncertainty >50 per cent (Cooper and Gustafsson, 2004)

g Emission factors from Trozzi and Vacaro., 1998.

3.3.4. Vertical Layer Distribution

Another important aspect of emission modeling is vertical distribution. This is especially critical for point sources that emit to higher layers than the surface. In this study, vertical distribution from EMEP study was utilized. Emissions were distributed vertically according to a default distribution based upon the sector codes, as shown in Table 3.15. These distributions have been based upon plume-rise calculations performed for different types of emission sources which are believed to be typical for different

emission categories, under a range of stability conditions (Calculations by S. Vidić, Croatian Meteorological Institute.).

Table 3.15. Vertical Distribution of Anthropogenic Emissions: Percentage of each sector allocated to the vertical layers of the air quality model (given as heights of layers, in meters)

No	Sources	Height of Emission Layer (m)					
		0–92	92–184	184–324	324–522	522–781	781–1106
1	Combustion in energy and transformation industries	0	0	8	46	29	17
2	Non-industrial combustion plants	50	50				
3	Combustion in manufacturing industry	0	4	19	41	30	6
4	Production processes	90	10				
5	Extraction and distribution of fossil fuels and geothermal energy	90	10				
6	Use of solvents and other products	100					
7	Road transport	100					
8	Other mobile sources and machinery	100					
9	Waste treatment and disposal	10	15	40	35		
10	Agriculture	100					

3.4. Chemistry and Transport Model

The U.S. Environmental Protection Agency's Community Multiscale Air Quality (CMAQ) model is a three-dimensional Eulerian (i.e., gridded) atmospheric chemistry and transport modeling system that simulates ozone, acid deposition, visibility, and fine particulate matter throughout the troposphere. Designed as a one-atmosphere model, CMAQ can address the complex couplings among several air quality issues simultaneously

across spatial scales ranging from local to hemispheric. The CMAQ source code is highly transparent and modular to facilitate extensibility through community development.

CMAQ is a third-generation air quality model that is designed for applications ranging from regulatory and policy analysis to understanding the complex interactions of atmospheric chemistry and physics. First-generation air quality models simulated air quality using simple chemistry at local scales, and Gaussian plume formulation was the basis for prediction. Second-generation models covered a broader range of scales (local, urban, regional) and pollutants, addressing each scale with a separate model that often focused on a single pollutant (e.g., ozone). Third-generation models, like CMAQ, treat multiple pollutants simultaneously up to continental or larger scales, often incorporating feedback between chemical and meteorological components.

Air quality models integrate our understandings of the complex processes that affect the concentrations of pollutants in the atmosphere. Establishing the relationships among meteorology, chemical transformations, emissions, and removal processes in the context of atmospheric pollutants is the fundamental goal of an air quality model (Seinfeld and Pandis, 1998). In contrast to statistical air quality models that use historical trends in observed atmospheric conditions to predict air pollution, CMAQ uses coupled mathematical representations of actual chemical and physical process to simulate air quality. Based upon the underlying concept of preserving mass through a series of contiguous three – dimensional grid cells covering a fixed model grid, CMAQ belongs to the Eulerian class of mathematical models that calculate a mass balance within each grid cell by solving the transport across each cell boundary and chemical transformations within each cell during a given time period (Figure 3.20).

CMAQ incorporates grid nesting, which means that pollutant concentration information propagates into and out of all grid nests during model integration. Any number of grid nests can be specified in a single run, while grid spacings and vertical layer structures can vary from one grid nest to another. The nested grid capability of CMAQ allows cost-effective application to large regions in which regional transport occurs, yet at the same time providing fine resolution to address small-scale impacts in selected areas. Each grid nest is defined over a subset of master (coarsest) grid cells.

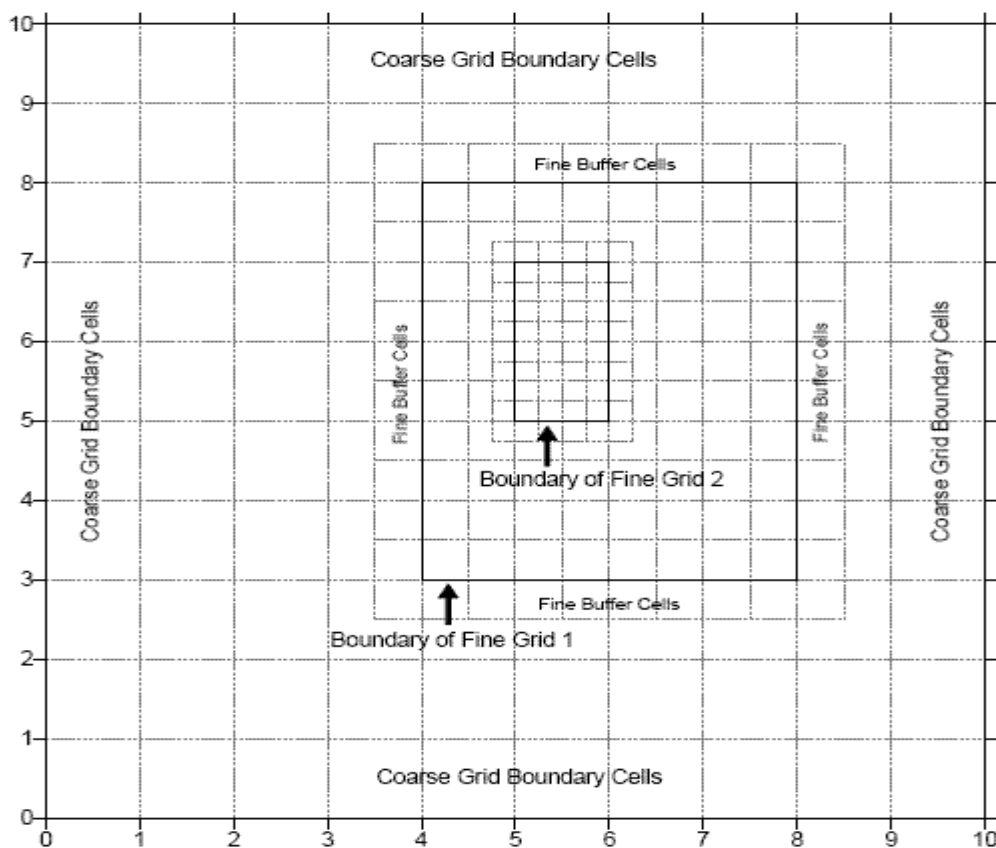


Figure 3.20. Domain configuration in CMAQ chemistry and transport model.

As a framework for simulating the interactions of multiple complex atmospheric processes, CMAQ thus requires two major types of inputs: meteorological information and source emissions rates.

With weather conditions contributing the primary physical driving forces in the atmosphere (such as the changes in temperature, winds, cloud formation, and precipitation rates), representative gridded meteorology forms the basis of all 3-D air quality model simulations. The meteorology inputs dictate the following CMAQ configuration parameters:

- Horizontal grid coordinate and projection
- Horizontal grid resolution
- Maximum spatial coverage

- Vertical grid extent (model top)
- Temporal extent (start/end date/time, time step length)

CMAQ emissions inputs must be on the same horizontal and vertical spatial scales and cover the same time period used in the air quality model simulation. The emissions inputs to CMAQ must also represent VOC emissions using a chemical parameterization supported by CMAQ; currently supported photochemical mechanisms are the Carbon Bond IV (CB-IV) mechanism (Gery et al., 1989; Dodge, 1989; Carter, 1996), the 2005 update to the Carbon Bond mechanism (CB-V) (Yarwood et al., 2005), and the Statewide Air Pollution Research Center (SAPRC-99) mechanism (Carter, 1990, 2000).

3.4.1. CMAQ System Components

CMAQ is a suite of FORTRAN-90 programs that work in concert to estimate ozone, particulate matter (PM), toxic compounds throughout the troposphere as well as acidic deposition. The five main CMAQ programs are

- The initial conditions preprocessor (ICON)
- The boundary conditions preprocessor (BCON)
- The clear-sky photolysis rate calculator (JPROC)
- The Meteorology-Chemistry Interface Processor (MCIP)
- The CMAQ Chemistry – Transport Model (CCTM)

Eulerian chemistry transport models use coupled ordinary differential equations to solve the changes in concentration of pollutants throughout a three-dimensional grid that is fixed relative to a selected map projection. The changes in concentration in each grid cell are affected by the following processes:

- Emissions from sources
- Horizontal and vertical advection
- Horizontal and vertical diffusion
- Chemical transformations
- Deposition

Mathematically, these processes relate to the concentration change in each grid cell through the continuity equation, which is presented in Equation 3.11, below:

$$\begin{aligned} \frac{\partial C_i}{\partial t} = & -\nabla_H \cdot V_H C_i + \left[\frac{\partial(C_i \eta)}{\partial z} - C_i \frac{\partial}{\partial z} \left(\frac{\partial h}{\partial t} \right) \right] + \nabla \cdot \rho K \nabla (C_i / \rho) \\ & + \left. \frac{\partial C_i}{\partial t} \right|_{\text{Chemistry}} + \left. \frac{\partial C_i}{\partial t} \right|_{\text{Emission}} + \left. \frac{\partial C_i}{\partial t} \right|_{\text{Removal}} \end{aligned} \quad (3.11)$$

where V_H is the horizontal wind vector, η is the net vertical “entrainment rate”, h is the layer interface height, ρ is atmospheric density, and K is the turbulent exchange (or diffusion) coefficient. The first term on the right-hand side represents horizontal advection, the second term represents net resolved vertical transport across an arbitrary space-and time-varying height grid, and the third term represents sub-grid scale turbulent diffusion. Chemistry is treated by simultaneously solving a set of reaction equations defined from specific chemical mechanisms. Pollutant removal includes both dry surface uptake (deposition) and wet scavenging by precipitation.

In CMAQ, the advection and emissions terms are calculated based on input files generated by the meteorology and emissions models, respectively; the diffusion, chemical transformation, and loss process terms are calculated within the CTM.

The Eulerian representation of the modeling domain is a series of contiguous grid cells that form a limited-area box on a subset of the globe, so the domain lateral boundary must define advection into the modeling grid. CMAQ currently accounts for advection into the domain only from the horizontal (i.e., lateral) boundaries, assuming there is no exchange through the top boundary of the domain. These spatial boundary conditions are estimated in CMAQ using the boundary conditions preprocessor, BCON. As a temporal boundary condition, the first time step of a model simulation is estimated in CMAQ using the initial conditions preprocessor, ICON. To model solar radiation, which provides the energy source for photolysis reactions, the program JPROC calculates clear-sky photolysis rates at various latitude bands and hours based on sun angles. Output from these CMAQ programs is used with output files from the emissions and meteorology models and other CMAQ preprocessors to form the required data for running the CCTM.

3.4.2. Major CMAQ Programs

The input data for the CCTM are developed using the five processors shown in Figure 3.21. CMAQ uses the MCIP processor to prepare the meteorological fields for the CCTM. The ICON and BCON processors generate the initial and boundary conditions for a CCTM simulation. JPROC computes the photolysis rates that will be used when simulating photochemical reactions in the CCTM. The PDM generates plume information for emissions sources that use a subgrid Plume-In-Grid (PinG) treatment to characterize their emissions. Emissions for CMAQ must be prepared with a modeling system that generates emissions for direct input to the CCTM.

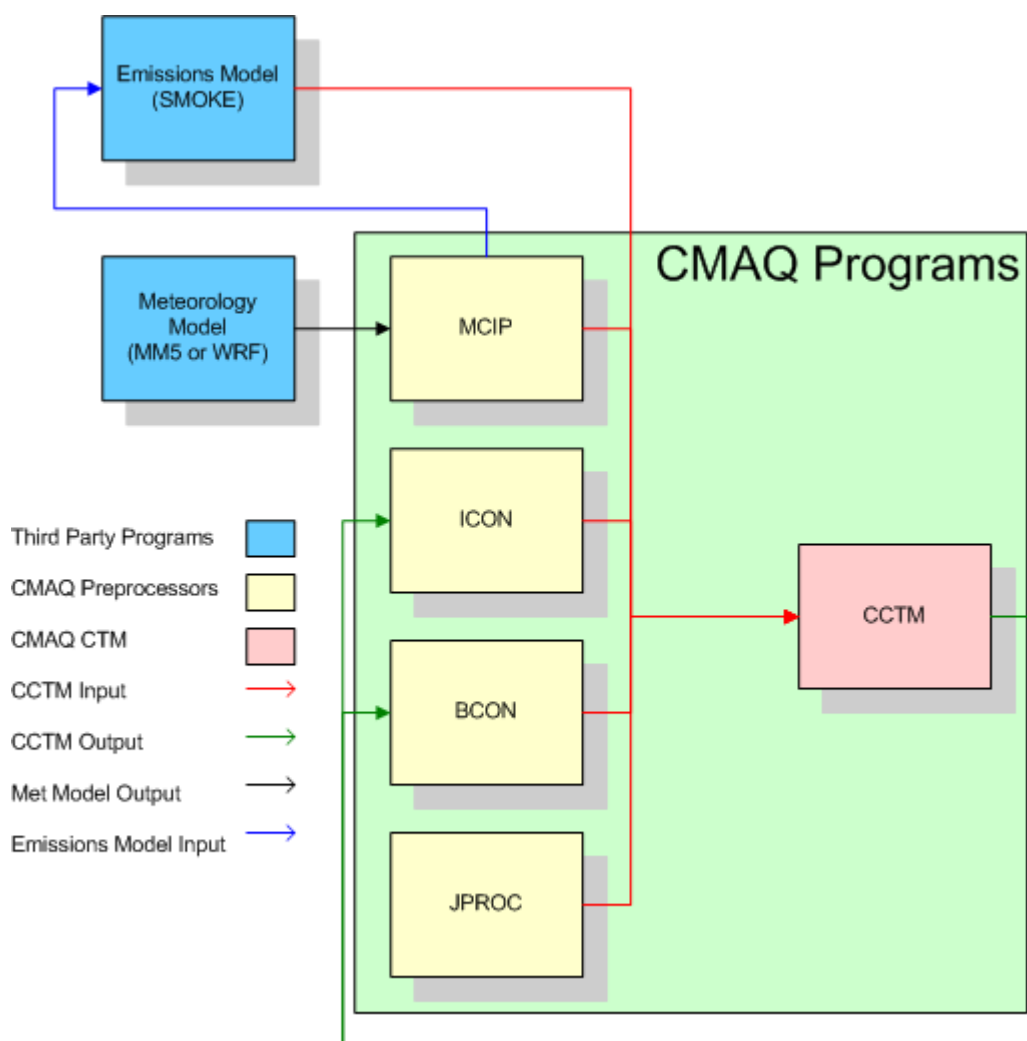


Figure 3.21. Schematic representation of the processors of the CMAQ model.

3.4.2.1. Photolysis Rate Preprocessor (JPROC). JPROC calculates chemical-mechanism-specific clear-sky photolysis rates at fixed altitudes, hour angles, and latitude bands from tabulated absorption cross-section and quantum yield (CSQY) data. The only configuration option required for JPROC is the selection of the chemical mechanism to model. Output from JPROC is an ASCII lookup table of photolysis rates that the CCTM uses to calculate gas-phase chemical transformations and pollutant concentrations.

3.4.2.2. Initial Conditions Processor (ICON). ICON generates a gridded binary netCDF file of the chemical conditions in the modeling domain for the first hour of a simulation. It can generate these initial conditions from either an ASCII file of vertically resolved concentration profiles or from an existing CTM output file. If the ASCII profiles do not have the same vertical structure as the CTM configuration, ICON will interpolate the data to a vertical structure consistent with the CTM's. Using an existing CTM output file to generate initial conditions is applicable when extrapolating initial conditions from a coarse to a fine grid simulation, as may occur when setting up nested simulations. The configuration options for ICON include selecting the chemical mechanism to model, defining the horizontal and vertical grids, and choosing whether the initial conditions are generated from an ASCII profile or from an existing CCTM output file.

3.4.2.3. Boundary Conditions Processor (BCON). BCON generates a gridded binary netCDF file of the chemical conditions along the horizontal boundaries of the modeling domain. These boundary conditions can be either static or time-varying, and (as with ICON) can be generated from either an ASCII file of vertically resolved concentration profiles or from an existing CTM output file. BCON differs from ICON in that it can generate time-varying (i.e., dynamic) boundary conditions. Dynamic boundary conditions are typically extracted from CTM outputs from a coarse grid simulation for nested simulations or from a CTM simulation using a global-scale model. The file structure of the ASCII input profiles can also support the creation of dynamic boundary conditions, but generally these files are used for creating static data. The configuration options for BCON include selecting the chemical mechanism to model, defining the horizontal and vertical grids, and choosing whether the boundary conditions are generated from an ASCII profile or from an existing CTM output file.

3.4.2.4. Meteorology-Chemistry Interface Processor (MCIP). MCIP uses MM5 or WRF output files to create netCDF-based input meteorology for the emissions model and the CTM. MCIP prepares and diagnoses all meteorological fields that are required for the emissions model and the CTM. In addition, MCIP is currently used to calculate the time-varying, species-dependent dry deposition velocities that are used in the CTM. MCIP can be used to uniformly trim cells off the boundary of the domain defined by the meteorological model, or to window in on a subset of that domain. MCIP can also decrease the vertical resolution of the meteorological data by “layer collapsing”, although this option should be used with caution as it can degrade the quality of the data if used incorrectly. Configuration options for MCIP include the time periods over which to extract data from the meteorological model output files, horizontal and vertical grid information, and selections for either passing through certain MM5-calculated variables unaltered or recalculating these variables within MCIP.

3.4.2.5. CMAQ Chemistry-Transport Model (CCTM). The CCTM integrates the output from all of the preprocessing programs, including the emissions and meteorology models, to simulate continuous atmospheric chemical conditions. The concentrations of relevant species can be captured for output at a user-definable frequency (typically hourly). The CCTM output files (some of which are “optional”) are all binary netCDF files of gridded and temporally resolved air pollutant information, such as gas and aerosol-phase species mixing ratios, hourly wet and dry deposition values, visibility metrics, and integral-averaged concentrations. The spatial and temporal extent of the CCTM output is dictated by the input meteorology. The science configuration is specific to each application of the model and can be adjusted to optimize model performance both computationally and in the numerical reproduction of observed air quality trends. Configuration options for the CCTM include the temporal coverage of the simulation, the chemical mechanism to model, the physics scheme to use for modeling pollutant transport, heterogeneous and aqueous chemistry options, plume-in-grid options, and diagnostic options (such as process analysis). The CCTM has the largest number of configuration options of all the CMAQ programs.

3.4.3. Science in the CMAQ Modeling System

CMAQ is a multi-pollutant, multi-scale air quality modeling system that can simulate the transport and chemistry of ozone, particulate matter, toxic airborne pollutants, and acidic and nutrient pollutant species. CMAQ uses state-of-the-science techniques and has many new and important features that are not available in previous modeling systems. CMAQ is capable of modeling complex atmospheric processes affecting transformation, transport, and deposition of air pollutants using a system architecture that is designed for fast and efficient computing.

CMAQ allows users to easily construct models with different characteristics, such as different chemical mechanisms or alternative cloud treatments, in order to address a specific air quality issue (Figure 3.22). This modeling configuration will allow CMAQ to retain its state-of-the-science status over time with future implementations of new science modules as appropriate. At the same time, CMAQ can be employed for regulatory applications by using approved standard configurations of the modeling platform that represent the best available modeling technology at a given time. CMAQ has been developed to meet the needs of both the research and application communities.

CMAQ's current coding structure is based on a modularity level that distinguishes its main driver, science modules, data estimation modules, and control/utility subroutines in the CCTM. The distinction remains at a division between the science models (including submodels for meteorology, emissions, chemistry and transport models), and analysis and visualization subsystems. In the CCTM, the process modules that affect the pollutant concentration fields are classified as follows:

Science Modules:

- Horizontal advection (hadv).
- Vertical advection (vadv).
- Mass conservation adjustments for advection processes (adjc).
- Horizontal diffusion (hdiff).

- Vertical diffusion (vdiff).
- Gas-phase chemical reaction solver (chem).
- Aqueous-phase reactions and cloud mixing (cloud).
- Aerosol dynamics and size distributions (aero).
- Plume chemistry effects (ping).

Control/Utility Modules:

- Model data flow and synchronizing of fractional time steps (ctm).
- Unit conversion (gencoor).
- Initialization (init).
- Process analysis (pa).

Data Estimation Modules:

- Aerosol deposition velocity estimation (aero_depv).
- Photolytic rate computation (phot).

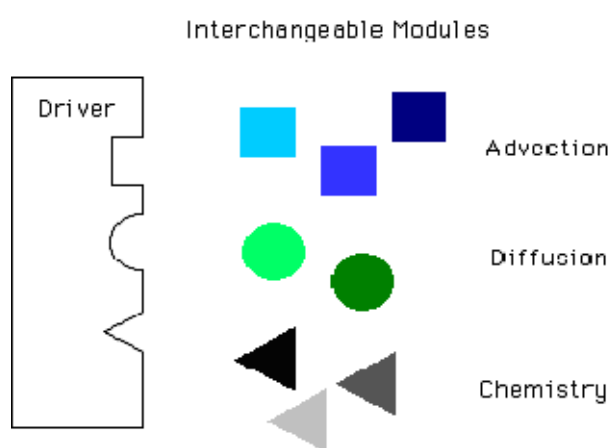


Figure 3.22. Model construction in CMAQ.

3.4.3.1. Gas-Phase Chemistry Solvers. Various modules for simulating tropospheric gas-phase chemistry within CMAQ have been developed, ranging from simple linear and nonlinear systems for engineering model prototypes to comprehensive chemistry representations for detailed chemical pathways related to atmospheric acid and oxidant

formation. In CMAQ Version 4.6, gas-phase chemistry can be simulated with the Carbon Bond IV (CB-IV), the 2005 update to the Carbon Bond mechanism (CB-V) (Yarwood et al., 2005), or the Statewide Air Pollution Research Center, Version 1999 (SAPRC99) photochemical mechanisms. Because of CCTM's modularity, users can modify the existing photochemical mechanisms or add new mechanisms. To compute time-varying species concentrations and their rate of formation or depletion (called chemical kinetics), equations governing chemical reaction kinetics and species conservation need to be solved for the entire species set. CCTM uses special numerical techniques called chemistry solvers that compute these concentrations and rates at each time step.

3.4.3.2. Photolysis. Photolysis (or photo dissociation) of trace gases initiates most chemical reactions that take place in the atmosphere. Photolysis splits gas-phase chemical species with energy from sunlight. Photolysis is involved in the formation of smog, an air pollution problem that affects human, animal, and plant health. Simulating photochemical reactions accurately is therefore a key issue that strongly influences air quality model performance.

CCTM uses state-of-the-science techniques to simulate photolytic reactions in the Phot module. Photolysis reactions and their rates of reaction are driven by sunlight. Similar to kinetic reaction rates for non-photochemical reactions, the photolysis rate quantifies how much reactant is produced from a photolytic reaction in a given amount of time. The rate of photolysis is a function of the amount of solar radiation (called actinic flux), which varies based on the time of day, season, latitude, and terrestrial features. The amount of solar radiation is also affected by the amount of cloudiness and by aerosol absorption and scattering in the atmosphere. The photolysis rate also depends on species-specific molecular properties like the absorption cross-section (the effective molecular area of a particular species when absorbing solar radiation, which results in a shadow region behind the particle) and quantum yield (the number of molecules that dissociate for each light photon incident on the atmosphere). These molecular properties depend on the wavelength of the incident radiation and the temperature (and hence, on the available photon energy). Thus, estimating the photolysis rate is further complicated by these temperature and wavelength dependencies.

3.4.3.3. Diffusion and Advection. Pollutant transport includes both advection and sub-grid scale diffusion. Advection has to do with pollutant transport due to the mean wind fields, and diffusion involves sub-grid scale turbulent mixing of pollutants. If a plume is transported primarily by advection, then it may travel a long distance without much change in pollutant concentrations. On the other hand, if a plume is transported primarily by diffusion, then the pollutants will mix more quickly and nearer to the source, which will result in substantial changes to pollutant concentrations.

In CCTM, the advection process is divided into horizontal and vertical components. This distinction is possible because mean atmospheric motion is mostly horizontal. Often, the vertical motion is related to the interaction of dynamics and thermodynamics. The advection process relies on the mass conservation characteristics of the continuity equation. Data consistency is maintained for air quality simulations by using dynamically and thermodynamically consistent meteorology data from MCIP. A new mass continuity scheme, similar to that used in the air quality forecasting version of CMAQ, has been implemented for the 2005 release. This scheme is globally mass-conserving and uses the piecewise parabolic method (PPM) (Colella and Woodward, 1984) advection scheme for horizontal advection, deriving a vertical velocity component at each grid cell that satisfies the mass continuity equation using the driving meteorology model's air density. This algorithm is based on the finite volume subgrid definition of the advected scalar. In PPM, the subgrid distribution is described by a parabola in each grid interval. PPM is a monotonic and positive definite scheme. Positive definite schemes maintain the sign of input values, which means, in this case, that positive concentrations will remain positive and cannot become negative.

The mixing ratio correction step, used in previous CMAQ versions, is not needed with this method. Note that, the former advection scheme, with the same horizontal advection but also using PPM for the vertical velocity component, is still available, along with the mixing ratio correction step.

The vertical advection modules solve for the vertical advection with no mass-exchange boundary conditions at the bottom or top of the model. CMAQ also uses PPM as its vertical advection module. In CCTM, the PPM algorithm with a steepening procedure is

implemented for vertical advection as the default because of the strong gradients in the tracer species that are observed in photochemical air quality conditions.

In CCTM, turbulent fluxes are expressed in terms of the mixing ratios and an air-density-weighted Jacobian to handle atmospheric diffusion processes with generalized coordinates. This approach is convenient for numerically solving the flux-form turbulence mixing because most flux-based closure algorithms use parameterizations of turbulent fluxes of conserving quantities, such as mass mixing ratios. In CMAQ version 4.5, Eddy diffusion is implemented for representing vertical diffusion. Eddy diffusivity is a local mixing scheme and is estimated using the same planetary boundary layer (PBL) similarity-based algorithm as in the Regional Acid Deposition Model, RADM, (Chang et al., 1987). In CCTM, the deposition process is simulated as a flux boundary condition that affects the concentration in the lowest layer. By treating the deposition process as the loss of mass due to the diffusion flux at the bottom of the model, one can relate the bottom boundary condition in the generalized coordinate system to that in the Cartesian coordinate system.

In CMAQ, horizontal diffusion is implemented with a single eddy diffusion algorithm that is based on local wind deformation and is scaled to the grid cell size. The horizontal eddy diffuseness is assumed to be uniform but dependent on the grid size of the model. The diffusivity is larger for a higher resolution run where the numerical diffusion due to the advection process is smaller.

3.4.3.4. Particulate Matter. CCTM uses a modal approach to simulate $PM_{2.5}$ (particulate matter of diameter equal to or less than 2.5 microns), coarse particulate matter (particulate matter of diameter greater than 2.5 microns and equal to or less than 10 microns), and PM_{10} (particulate matter of size equal to or less than 10 microns). $PM_{2.5}$ is further divided into the Aitken and accumulation modes. Coarse particulate matter is represented currently by fugitive dust and a generic anthropogenic species. PM_{10} is the sum of the $PM_{2.5}$ and coarse particulate matter.

Particulate matter in the atmosphere can either be primary or secondary. Primary particulate matter is emitted directly into the atmosphere from natural or anthropogenic emissions. Secondary particulate matter is formed in the atmosphere either from

precursors, as a result of chemical reactions, or from condensation or deposition onto primary particles that are already present in the atmosphere. CCTM can predict fine particulate speciated concentrations of sulfate, nitrate, ammonium, organics, and aerosol water, and it includes methods for simulating nucleation, dry deposition, and cloud processes. The 3rd generation CMAQ aerosol module (AERO3) takes chemical species concentrations and reactivity rates from the chemistry solvers and primary particulate concentrations from the emissions processor to compute fine and coarse particulate concentrations.

Invoking the AERO3 module will influence the sulfate, ammonia, and nitric acid concentrations predicted by the gas phase chemistry module. The sulfate is partitioned between the vapor (sulfuric acid) and particle phases. The greater part of the sulfate is put into the aerosols with a very small residual amount remaining in the vapor phase. Nitric acid and ammonia are equilibrated with the aerosol species.

The aerosol module in CMAQ version 4.5 is called AERO4. The difference between AERO4 and AERO3 is that AERO4 includes consideration of sea salt aerosols. Emissions of sea salt from the open ocean are calculated as a function of wind speed and relative humidity. These emissions are speciated into sodium, chloride, and sulfate, and are distributed by size to the accumulation and coarse modes by fitting the emission parameterization to a bimodal distribution. Note that sea salt emissions are calculated within the CMAQ model and do not require special preprocessing in SMOKE. Equilibrium between the accumulation mode (which now contains sodium and chloride) and the gas phase (which now contains hydrochloric acid) is calculated within the ISORROPIA thermodynamic module. As in previous CMAQ releases, mass transfer is not simulated between the coarse mode and the gas phase. These sea salt processes can be activated by selecting the AERO4 module and deactivated by using AERO3. For easier comparison of CMAQ output with measurement, AERO4 provides three new variables (PM25AT, PM25AC, and PM25CO) that are the fractional amounts of the Aitken, accumulation, and coarse modes, respectively, that are composed of particles less than 2.5 μm in aerodynamic diameter.

Unlike gases, the deposition velocity for particles must be calculated from the aerosol size distribution, as well as meteorological and land-use information. The `aero_dep_v2` module calculates the size distribution from the mass and number concentration for each of the three modes and calculates the dry deposition velocity. The dry-deposition algorithm has been modified to include an impaction term in the coarse and accumulation modes. Finally, two diagnostic tools, for tracking the sulfate budget and sources of elemental and primary organic carbon have been added.

CCTM's AERO module is also useful for evaluating visibility. CCTM integrates Mie scattering (a generalized particulate light-scattering mechanism that follows from the laws of electro-magnetism applied to particulate matter) over the entire range of particle sizes to obtain a single visibility value for each model grid cell at each time step.

3.4.4. CMAQ setup for the study

CMAQ is run on three domains covering Europe in a 163×150 grid system of 30 km resolution, Balkan region in a 140×155 grids domain of 10 km resolution and GIA in a 92×57 grids domain of 2 km resolution.

MCIP was used to cut the MM5 produced fields to the emission domain's sizes for a number of vertical layers. The vertical sigma layers used in the study are 1, 0.988, 0.976, 0.958, 0.933, 0.901, 0.862, 0.816, 0.763, 0.703, 0.636, 0.562, 0.481, 0.392, 0.302, 0.225, 0.165, 0.12, 0.08, 0.04 and 0. MCIP produced the necessary 2D and 3D meteorological and grid fields required for CMAQ for the user-requested horizontal and vertical grids.

ICON and BCON were used to produce the initial and boundary conditions of the concentrations for the coarse domain, in order to initialize for $t=0$. The necessary file required for ICON includes the concentrations of the chemical species for requested vertical sigma layers at each horizontal grid cell. On the other hand, for BCON, a profile data including the vertical concentrations at boundaries at each direction is provided. These data files for ICON and BCON are presented in Appendixes A and B. The concentrations files were prepared based on CBIV gaseous chemistry and AERO3 for aerosol chemistry. 6

sigma layers were used to calculate the vertical concentrations of species by the CCTM model. These layers were 1, 0.98, 0.93, 0.84, 0.60, 0.30 and 0.

JPROC was employed to calculate the photolysis rates for the fixed vertical sigma layers. CB-IV and AERO4 chemistry mechanisms were used in order to calculate these photolysis rates. The CBIV chemistry mechanism is presented in Appendix C.

The model ready emissions were prepared based on the requirements of the CMAQ model. CMAQ requires 4-dimensional emissions files, including time step, layer, rows and columns. The emissions should be prepared in units of moles sec⁻¹ for the gaseous species and gr sec⁻¹ for particulate species. Table 3.16 presents the species used in this study. Emissions of these species were calculated from the raw species presented in Table 3.5, based on Oliver et al. (2001). This methodology is described in Table 3.17.

Table 3.16. CB-IV species used for the study.

Gaseous Species (moles sec⁻¹)	Particulate Species (gr sec⁻¹)	VOC Species (moles sec⁻¹)
CO	PMC	ETOH
NO	POA	MEOH
NO2	PEC	PAR
SO2	PSO4	OLE
NH3	PNO3	TOL
	PMFINE	XYL
		ETH
		FORM
		ALD2

For the aerosol species, AERO4 mechanism was used in the study. An important aspect of this mechanism is that CMAQ can calculate sea salt emissions, which contribute to aerosol levels especially in the coastal regions. In order to provide the sea salt emissions,

CMAQ requires a 2-D file including the grids that are covered by water bodies and land. This file was produced by using the GRIDCRO2D file generated by the MCIP model. This file includes a variable (LWMASK) showing which grid cell is covered by ocean and which by land. A MATLAB code was written to read this file and extract the variable to process it into the OCEAN_FILE required by CMAQ.

CMAQ model outputs a number of chemical species including various gaseous species in units of ppmV and aerosols species in units of micrograms per meter cube. Among these species, the aerosol species that the model produces and are used in order to calculate PM_{coarse} , $PM_{2.5}$ and PM_{10} are listed in Table 3.18.

3.4.5. Sensitivity Analyses (Brute Force)

In order to quantitatively examine the response of PM_{10} levels and aerosol species to changes in local emissions, CMAQ is rerun with perturbed emission data. An increase and decrease of 10 per cent on all anthropogenic emissions is conducted to see the relative changes of aerosol levels from the base case. In order to find the governing chemistry for the aerosol species of sulfate, nitrate and ammonium, same amount of increases and reductions are tested individually for NO_x , SO_2 , NH_3 and VOC emissions. This kind of scenario analyses also gives us the opportunity to see the responses to the various air quality control strategies.

Table 3.17. VOC speciation for the CBIV mechanism.

VOCs GROUP	DOMINANT COMPOUNDS	CB4 MOLAR SPLIT
Methane	Methane	0.01 PAR
Alcohols	Half by mass Ethanol and Methanol	Ethanol = 1 ETOH
		Methanol = 1 MEOH
Ethane	Ethane	0.4 PAR
Propane	Propane	1.5 PAR
Butanes	n-Butane	4 PAR
Pentanes	2-Methylbutane, n-Pentane	5 PAR
Hexanes and higher alkanes	Alkane with mean molecular weight 106.8	7.5 PAR
Ethene	Ethene	1 ETH
Propene	Propene	1 OLE + 1 PAR
Ethyne	Ethyne	1 PAR
Other alk(adi)enes and alkynes (olefines)	One third by mass 1-Butene, 2-Butene and 1,3-Butadiene	1-Butene = 1 OLE + 2 PAR
		2-Butene = 2 ALD2
		1,3-Butadiene = 2 OLE
Benzene	Benzene	1 PAR
Methylbenzene (toluene)	Toluene	1 TOL
Dimethylbenzene (xylenes)	Dimethylbenzene isomers	1 XYL
Trimethylbenzene	Trimethylbenzene isomers	1 PAR + 1 XYL
Other aromatics	C10 Aromatics	2 PAR + 1 XYL
Esters	Non-speciated	4.1135 PAR + 0.0113 ALD2
Ethers	Oxygenates	4 PAR
Formaldehyde	Formaldehyde	1 FORM
Other alkanals (aldehydes)	One third by mass 2-Methylpropanal, Ethanal and Butanal	2-Methylpropanal = 2 PAR + 1 ALD2
		Ethanal = 1 ALD2
		Butanal = 2 PAR + 1 ALD2
Ketones	Butanone	4 PAR
Alkanoic acids	Ethanoic acid	1 PAR

Table 3.18. Aerosol species to calculate PM_{coarse} , $PM_{2.5}$ and PM_{10} concentrations*.

PM_{coarse}	$PM_{2.5}$	PM_{10}
ACORS	ASO4J (Sulfate)	PM_{coarse}
ASOIL (Soil – derived aerosol)	ASO4I (Sulfate)	$PM_{2.5}$
ANAK (Sodium)	ANH4J (Ammonium)	
ACLK (Chloride)	ANH4I (Ammonium)	
ASO4K (Sulfate)	ANO3J (Nitrate)	
	ANO3I (Nitrate)	
	AORGAJ (Anthropogenic organic aerosol)	
	AORGAI (Anthropogenic organic aerosol)	
	AORGPAJ (Anthropogenic primary organic aerosol)	
	AORGPAI (Anthropogenic primary organic aerosol)	
	AORGBJ (Biogenic organic aerosol)	
	AORGBI (Biogenic organic aerosol)	
	AECJ (Elemental aerosol)	
	AECI (Elemental aerosol)	
	A25J ($PM_{2.5}$)	

* J and I stand for accumulation and Aitken modes, respectively

4. RESULTS

4.1. METEOROLOGICAL MODEL

In this study, three nested domains are used in order to produce the meteorological fields required for the chemistry and transport model. The coarse (mother) domain has 199 grids in x-direction and 175 grids in y-direction, with a resolution of 30 km. The second domain has 181 grids in x-direction and 202 grids in y-direction, with a resolution of 10 km. Finally, the inner domain has 136 grids in x-direction and 111 grids in y-direction, with a resolution of 2 km. The National Centers for Environmental Prediction (NCEP) Global Data Assimilation System (GDAS) data (with 1 degree by 1 degree resolution) are used for MM5 boundary and initial conditions. The model integrated days start from 00:00 UTC January 10, 2008 and end on 00:00 UTC January 20, 2008. The physical options used in the model were mix phase moisture scheme, KF2 cumulus scheme, MRF PBL scheme and RRTM radiation scheme.

4.1.1. Model Performance

The time series of temperature and U and V components of winds are compared with hourly observations provided from one meteorological station from Istanbul: Kandili meteorological station (41.06 N and 29.06 E), which falls into the inner most MM5 domain, and one meteorological station from Crete: Finokalia meteorological station (35.20 N and 25.40 E), which falls into the Balkan domain. The MM5 grid cells that cover these meteorological stations are $i=57$ and $j=81$ grid cell for Kandilli station at Istanbul domain and $i=31$ and $j=98$ grid cell for Finokalia meteorological station at Balkan domain. The comparison between MM5 results and actual observations of temperature at 2 m, and U component of wind at 10 m and V component of the wind at 10 m are presented in Figure 4.1.

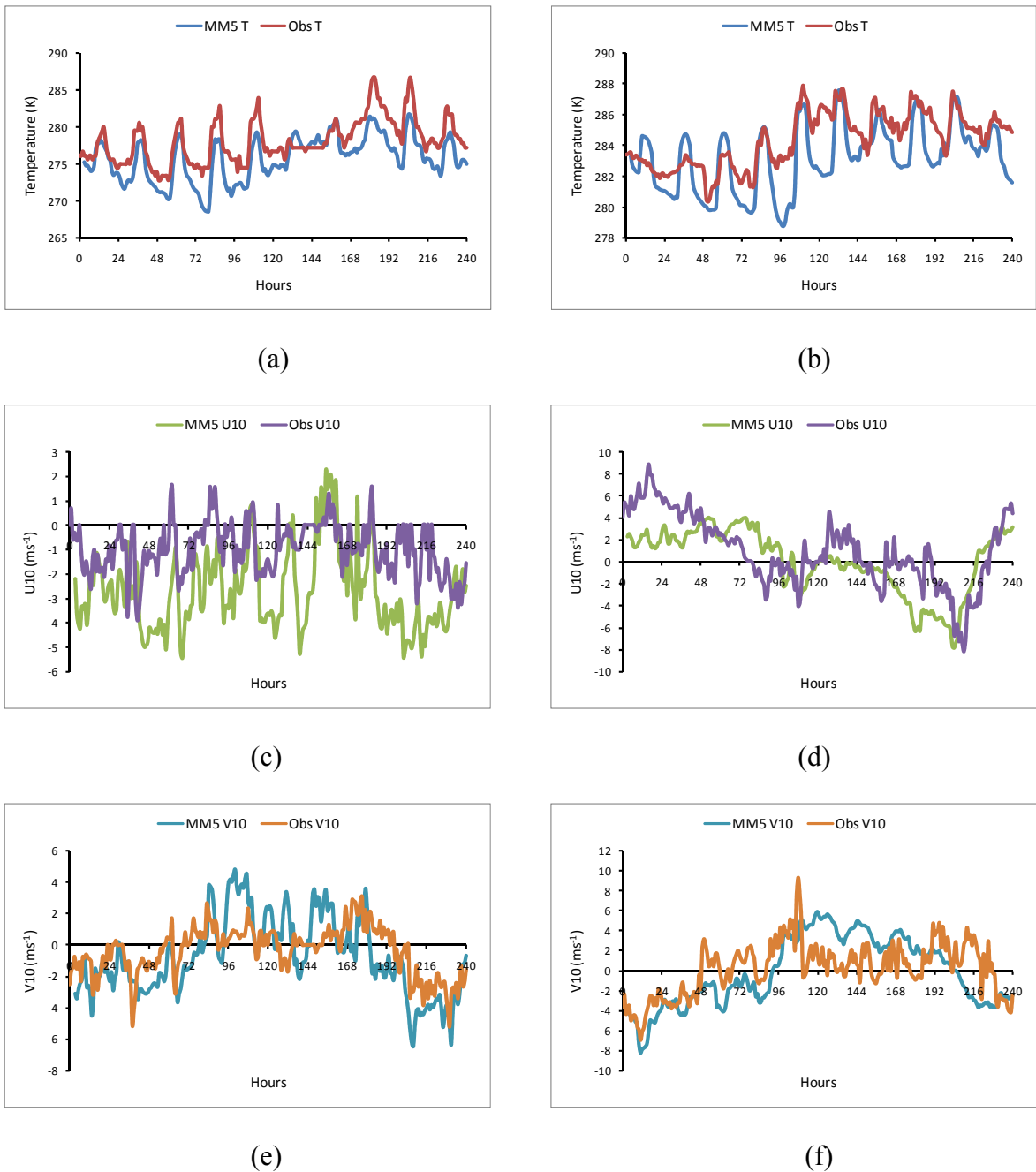


Figure 4.1. MM5 vs. observations for a) Temperature at 2 m at Kandilli, b) Temperature at 2 m at Finokalia, c) U component of wind at 10 m at Kandilli, d) U component of wind at 10 m at Finokalia, e) V component of wind at 10 m at Kandilli and f) V component of wind at 10 m at Finokalia.

As seen from Figure 4.1, MM5 underestimated temperatures for both stations, but on the other hand, the trend is well captured, especially for the Kandilli station. Although correct prediction of low level winds is not easy, the results showed that the model was

capable of correctly simulating U and V components. These differences between the observations and MM5 simulation are due to the averaging of the values to the cross point of the particular grid. This means that the model calculates one value for each meteorological variable as an average of the 4 km² grid cell, for instance. On the other hand, the observations represent the meteorological conditions for a particular geographical point at a certain latitude and longitude.

In order to mathematically express the differences between observations and MM5 simulation for each variable, the Pearson correlation factors are calculated and presented in Table 4.1. Besides correlation factors, three basic statistical measures, two of which are aspects of error and one skill score, are used in order to calculate the model performance. These statistical measures are mean bias (BIAS), absolute error (ABSE), root-mean-square error (RMSE) and index of agreement (IOA). These measures are defined as follows:

$$\text{BIAS} = \frac{1}{MN} \sum_{j=1}^M \sum_{k=1}^N (\phi_{j,k}^m - \phi_{j,k}^o) \quad (4.1)$$

$$\text{ABSE} = \frac{1}{MN} \sum_{j=1}^M \sum_{k=1}^N |\phi_{j,k}^m - \phi_{j,k}^o| \quad (4.2)$$

$$\text{RMSE} = \frac{1}{M} \sum_{j=1}^M \left[\sqrt{\frac{1}{N} \sum_{k=1}^N ((\phi_{j,k}^m - \phi_{j,k}^o))^2} \right] \quad (4.3)$$

$$\text{IOA} = 1 - \left(\frac{\sum_{k=1}^N ((\phi_{j,k}^m - \phi_{j,k}^o))^2}{\left(\left(|\phi_{j,k}^m - \overline{\phi_{j,k}^m}| \right) + \left(|\phi_{j,k}^o - \overline{\phi_{j,k}^o}| \right) \right)^2} \right) \quad (4.4)$$

where ϕ^m is a model variable and ϕ^o is the corresponding observation. M is the total number of locations and N is the total number of times that the model data is compared with observation data. These statistical measures are chosen among other error measures that are used for model performance assessment and evaluation for two reasons. First, these measures are simple and have physical meanings clearly defined. They permit easy understanding and direct comparison of results from other studies. Second, they all share

the same physical unit of the specific variable to be assessed. Thus, these measures lead to new derivatives that can enhance the understanding of model performance (Mao et al., 2006). The measures calculated are also presented in Table 4.1. The derived aspects ratios of error are defined as the ratio of BIAS to ABSE (R_1) and the ratio of ABSE to RMSE (R_2). It is obvious that the aspect ratio of error R_1 is bounded between $-1 \leq R_1 \leq 1$. The equality holds when the model data are persistently negatively biased. R_1 can be zero when model equals the observation which represents a preferred model performance. Aspect ratio of error R_2 is bounded between $0 < R_2 \leq 1$. R_1 and R_2 results of the two datasets are presented in Table 4.1.

Table 4.1. Statistical comparison of MM5 simulated temperature, U and V with observations for Kandilli and Finokalia meteorological stations.

Measures	Kandilli			Finokalia		
	T 2 (K)	U 10 (ms ⁻¹)	V 10 (ms ⁻¹)	T 2 (K)	U 10 (ms ⁻¹)	V 10 (ms ⁻¹)
Correlation	0.84	0.38	0.65	0.74	0.64	0.59
Observed Mean	278.13	-0.99	-0.38	284.41	0.91	0.31
Model Mean/Obs. Mean	0.99	2.74	1.97	0.99	-0.02	-0.32
Observed STDEV	2.97	1.06	1.55	1.78	3.24	2.62
Model STDEV/Obs. STDEV	0.99	1.54	1.58	1.18	0.91	3.44
BIAS	-2.38	-1.72	-0.37	-1.28	-0.93	-0.41
ABSE	2.56	1.99	1.58	1.57	2.36	2.39
RMSE	2.91	2.33	1.89	1.92	2.80	2.85
R1	-0.92	-0.85	-0.25	-0.81	-0.38	-0.17
R2	0.90	0.90	0.84	0.84	0.86	0.83
IOA	0.74	0.11	0.74	0.74	0.76	0.75

The results show that MM5 simulated temperatures highly correlate with observations. The results also point that the higher the spatial resolution is, more accurately MM5 simulates the meteorological conditions. The model calculates the average parameter

within a grid cell so that the smaller the area of the grid becomes, the average approaches the actual observation. Higher correlation factor for the 2 m temperature and 10 m V component is calculated for Kandilli station (0.84 and 0.65, respectively) than Finokalia station (0.74 and 0.59) due to the higher resolution. These results also explain the underestimation of meteorological parameters calculated by MM5. On the other hand, all models employ various approximations in order to solve the transport equations. Thus, when the resolution of a grid cell is lower, the errors originated from these approximations are also averaged, leading to possible better results for highly fluctuating variables like low level winds on lower resolution grids, as is the case for U component. Confirming Figure 4.1, the correlation for U component of wind is poor, particularly for Kandilli station (0.38) whereas better correlations are calculated for V component. The calculated U and V values are not as biased as temperature. T, U and V values for Kandilli station are clearly negatively biased, pointing that MM5 underestimated temperature and wind fields. For the Finokalia station, the highest R_1 is calculated for temperature, whereas U and V results are closer to center, suggesting a better reproduction of winds. These results overall suggest that even with a coarse resolution, MM5 model is capable of successfully simulating the meteorological variables. IOA values indicate good agreement for almost all meteorological parameters, giving agreements around 75 per cent, except for U component of wind for Kandilli station, with a calculated IOA of 0.11, where Pearson's correlation factor is also calculated low and BIAS are higher, compared to other parameters. Finally, the ratios of calculated standard deviations to observed standard deviations show good agreement between the model and observations. This ratio is desired to be 1 to represent perfect simulation and for most of the cases, these ratio do not fluctuate highly around 1.

4.1.2. Model results for the episode days

The MM5 simulations for the 10-day period from January 10 to 20, 2008, are conducted. The first three days of the run is considered as spin-up period and not included in the analyses. The episodic period between January 13 and 17, 2008, is extracted from the outputs. The horizontal wind vectors at sigma level 1 (near surface), relative humidity distribution at 850 mb level, horizontal temperature at 850 mb level, 24-hour total precipitation, potential temperature, vorticity and circulation vectors, and vertical

temperature, dew point temperature and wind direction on each day for the Istanbul domain are presented in Figures 4.2 to 4.6.

The meteorological conditions on January 13, 2008, at 0200 LST, are presented in Figure 4.2. Complex wind patterns, especially in the Kocaeli Gulf and around Bosphorus strait are very clear in Figure 4.2a. The easterlies over the Black Sea and the low pressure system at the center of the Marmara Sea are visible. The channeling of the winds through the Çanakkale strait is also clear. Figure 4.2b shows that the humidity levels were below 70 per cent and no precipitation is detected. The 1000 mb level temperatures, which can be considered as ground level temperatures, were around 4 to 6 °C degrees range around İstanbul and around 0 °C degree and below on the western parts of the domain as well as the eastern parts (Figure 4.2c). The easterlies over the Black Sea and İstanbul and the north easterlies on Marmara Sea are clearly visualized. The figure also confirms the complexity of the wind patterns around Kocaeli Gulf. The south easterly winds coming to Marmara Sea turns south west here so that the transport becomes north easterly. The 24 hour-precipitation is presented in Figure 4.2d. The figure shows that the precipitation amount across the domain was low and there was no precipitation over İstanbul except for the northern part of the European side. A cross section, starting from $i=30$ and $j=57$ to $i=120$ and $j=57$, (see Figure 4.2a, red line) and passing over the Bosphorus is taken and the vertical circulation vectors are plotted over this cross section (Figure 4.2e). The easterlies on all vertical levels are clearly seen in the figure. Finally, on the Figure 4.2f, the vertical variation of temperature (red line) and dew point temperature (blue line) are presented. An inversion layer below the 900mb level is visible in the figure, leading to an increase in pollutant concentrations. Additionally, temperature and dew point temperature lines do not intersect, suggesting that no precipitation had occurred at that time and confirming Figure 4.2d.

The horizontal wind, humidity, temperature, precipitation and vertical temperature and wind variation plots for January 14, 2008, 0700 LST are presented in Figure 4.3. The southerly winds over İstanbul and Marmara Sea is dominating for the time period (Figure 4.3a). The easterly winds from Kocaeli Gulf turn north on Marmara Sea. On the other hand, the complex wind patterns around Kocaeli Gulf arise from the complex topography of the area. The 850 mb level relative humidity plot shows no precipitation at the hour of

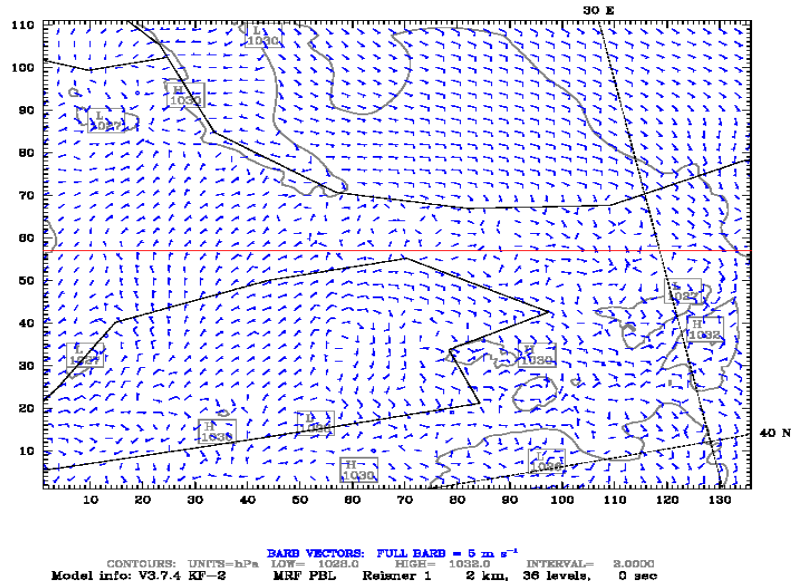
the maximum concentration and the humidity level was below 70 per cent (Figure 4.3b). The wind vectors clearly show south westerly transport over the Marmara Sea and the Bosphorus strait whereas on the Kocaeli Gulf region, due to the high pressure, the clockwise turning of the winds is visible. The temperatures were as high as above 6 °C degrees but were in the 4 to 6 °C degrees range on most of the domain (Figure 4.3c). On the other hand, the eastern and southern parts of the domain were below 0 °C degree, decreasing down to -6 °C degrees. It is also clear that the temperature variation follows the terrain height within the domain, which was presented in Figure 3.15a. The higher terrain heights lead to decrease of temperature. The southerly winds all across the domain as well as the complex wind patterns around the Kocaeli Gulf are also presented in the figure. The model simulated no precipitation over İstanbul except for the northern parts of the European side (Figure 4.3d). A cross section, starting from $i=30$ and $j=57$ to $i=120$ and $j=57$ (see Figure 4.3a, red line), and passing over the Bosphorus is taken and the vertical circulation vectors are plotted over this cross section (Figure 4.3e). The westerlies on all vertical levels are clearly seen in the figure. Finally, on the Figure 4.3f, the vertical variation of temperature (red line) and dew point temperature (blue line) are presented. An inversion layer below the 900 mb level is visible in the figure, leading to an increase in pollutant concentrations. Additionally, temperature and dew point temperature lines do not intersect, suggesting that no precipitation had occurred at that time.

The meteorological conditions on January 15, 2008, at 0300 LST, are presented in Figure 4.4. The complex wind patterns over the region are clearly visible in Figure 4.4a. There were southerly winds over Black Sea region and south easterly winds over Marmara Sea. On 850 mb level, the southerly winds are clearly seen. The southerly winds carry humidity and over the western part of the domain, the relative humidity levels are around 80-90 per cent (Figure 4.4b). The 850 mb humidity levels point to precipitation in the region. The southerly winds on 850 mb level turn east over Black Sea. On the other hand, the area around Bosphorus Strait shows no sign of precipitation and humidity levels below 70 per cent. The temperature distribution over the area shows temperatures up to 8 °C degrees, especially on İstanbul, Black Sea and Marmara Sea (Figure 4.4c). Lower temperatures on southeastern parts of the domain, due to higher topography were simulated by the model. Turning of winds coming from eastern parts to southerlies over İstanbul are clearly seen in the figure. Figure 4.4d shows precipitation over the western parts of the

domain, including north western parts of İstanbul. On the other hand, the precipitation records from the Kandilli meteorological station showed 6.4 mm of precipitation. A cross section, starting from $i=30$ and $j=57$ to $i=120$ and $j=57$ (see Figure 4.4a, red line), and passing over the Bosphorus is taken and the vertical circulation vectors are plotted over this cross section (Figure 4.4e). The westerlies on all vertical levels are clearly seen in the figure. Additionally, a vertical circulation around the center of the cross section on mid – altitudes between 850 and 550 mb levels can be seen in the figure. Finally, on the Figure 4.4f, the vertical variation of temperature (red line) and dew point temperature (blue line) are presented. Temperature and dew point temperature lines do not intersect, suggesting that no precipitation had occurred at that time. This vertical change represents the variation from a particular point, Atatürk Airport in this case. Thus, the absence of precipitation is valid for the area close to this point.

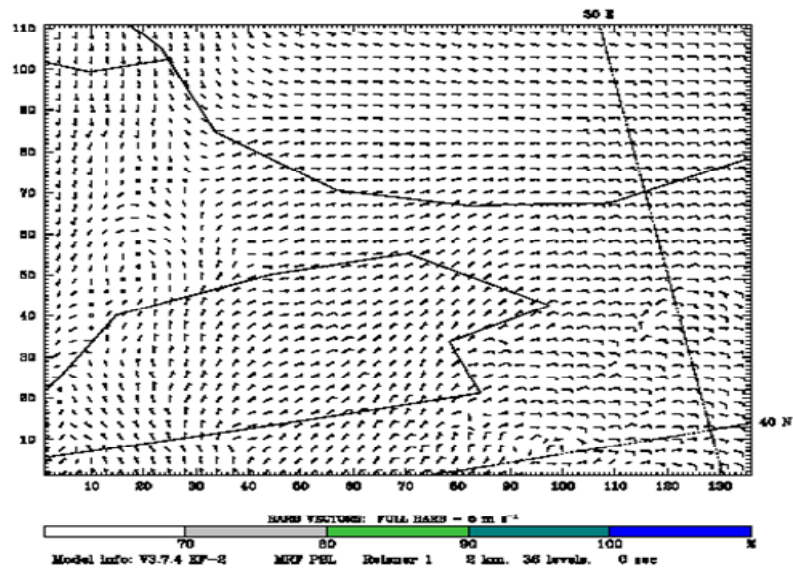
The horizontal wind, humidity, temperature, precipitation and vertical temperature and wind variation plots for January 16, 2008, 2000 LST are presented in Figure 4.5. The easterly winds over Marmara Sea and the complex wind patterns around İstanbul and Kocaeli Gulf can be seen in Figure 4.5a. The 850 mb level relative humidity plot shows the humid air parcels around south eastern parts of the domain, transported by the southerlies (Figure 4.5b). The humidity level was below 70 per cent on the western parts of the domain. Eastern parts of İstanbul and some local areas around Bosphorus strait can be seen in the figure. The temperatures were above 6 °C degrees on most of the eastern parts domain, whereas the temperatures were around 4 °C degrees on western parts (Figure 4.5c). The winds were blowing southerly on the western parts of the domain whereas highly varying wind vectors on the eastern part of the domain were calculated by the model. The 24-hour precipitation plot on Figure 4.5d shows that there was precipitation on the southern parts of the domain, whereas there was no precipitation over İstanbul. The vertical circulation vectors are plotted in Figure 4.5e (see cross section in Figure 4.5a, red line). The westerlies on all vertical levels are clearly seen in the figure. The wind speeds were significantly low close to earth surface. Finally, on Figure 4.5f, the vertical variation of temperature (red line) and dew point temperature (blue line) are presented. Additionally, temperature and dew point temperature lines do not intersect, suggesting that no precipitation had occurred at that time.

Dataset: RIP: press humidity Init: 0000 UTC Thu 10 Jan 08
 Fcst: 72.00 h Valid: 0000 UTC Sun 13 Jan 08 (0200 LST Sun 13 Jan 08)
 Sea-level pressure
 Horizontal wind vectors at k-index = 36



(a)

Dataset: RIP: press humidity Init: 0000 UTC Thu 10 Jan 08
 Fcst: 72.00 h Valid: 0000 UTC Sun 13 Jan 08 (0200 LST Sun 13 Jan 08)
 Relative humidity (w.r.t. water) at pressure = 850 hPa
 Horizontal wind vectors at pressure = 850 hPa



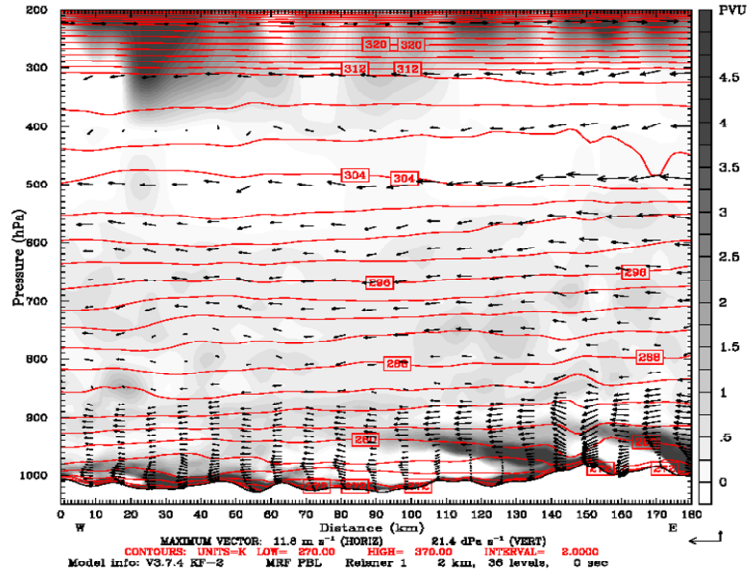
(b)

Figure 4.2. a) Sea level pressure and wind vectors, b) 850 mb level wind vectors and relative humidity, c) 1000 mb horizontal temperature, d) 24-hour precipitation e) vertical circulation vectors and f) vertical temperature variation on January 13, 2008, at 0200 LST.

Dataset: RIP: vertical
Fest: 72.00 h
Potential vorticity
Potential temperature
Circulation vectors

Valid: 0000 UTC Sun 13 Jan 08 (0200 LST Sun 13 Jan 08)
XY= 30.0, 57.0 to 120.0, 57.0
XY= 30.0, 57.0 to 120.0, 57.0
XY= 30.0, 57.0 to 120.0, 57.0

Init: 0000 UTC Thu 10 Jan 08

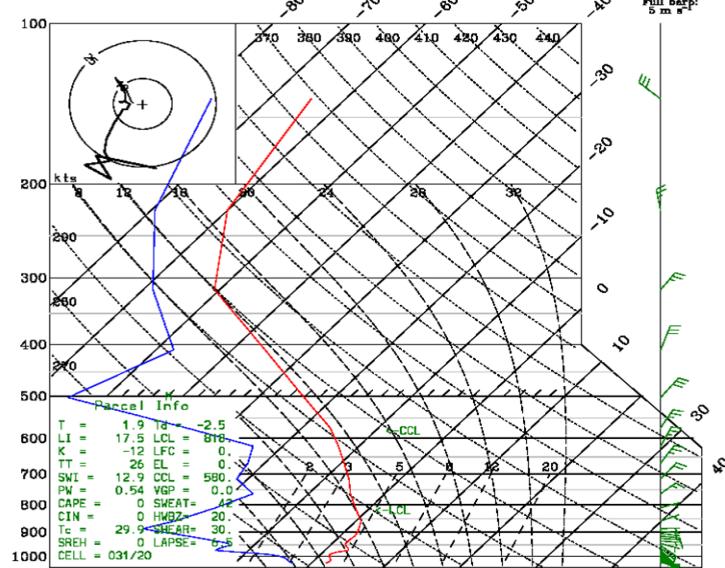


(e)

Dataset: RIP: vertical
Fest: 72.00 h
Temperature
Dewpoint temperature
Horizontal wind vectors

Valid: 0000 UTC Sun 13 Jan 08 (0200 LST Sun 13 Jan 08)
x,y= 70.14, 53.32 lat,lon= 40.97, 28.82 stn=LTA,17080
x,y= 70.14, 53.32 lat,lon= 40.97, 28.82 stn=LTA,17080
x,y= 70.14, 53.32 lat,lon= 40.97, 28.82 stn=LTA,17080

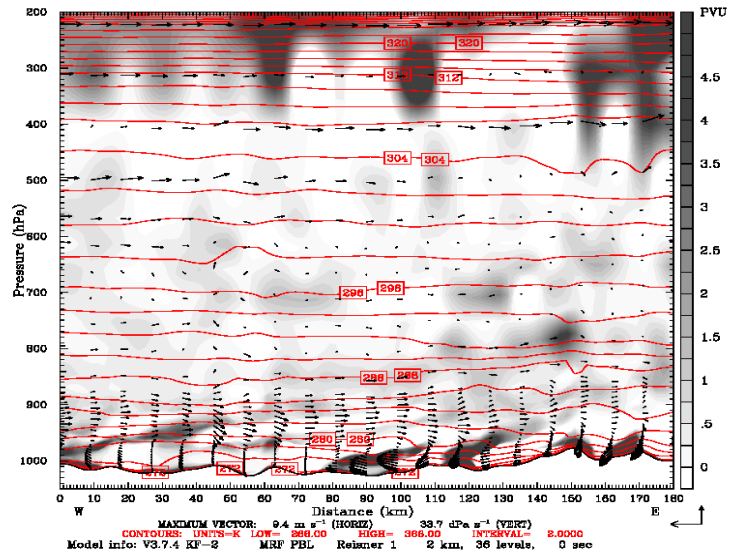
Init: 0000 UTC Thu 10 Jan 08



(f)

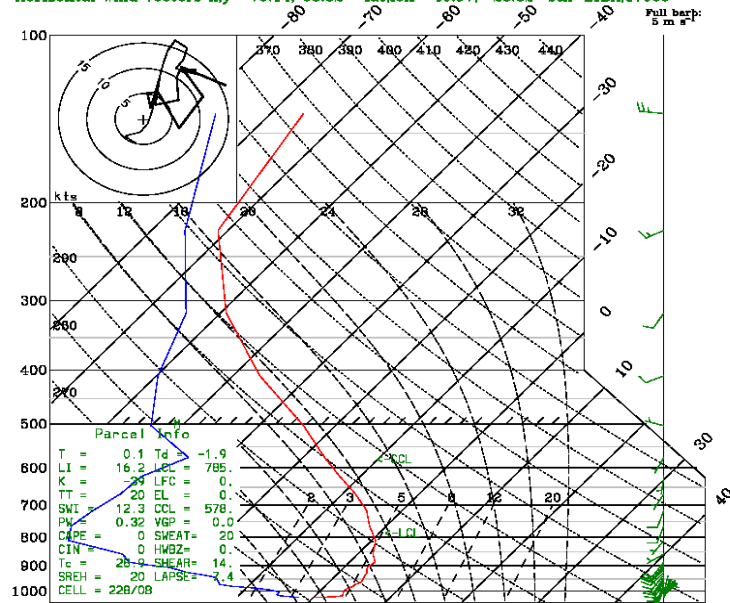
Figure 4.2. a) Sea level pressure and wind vectors, b) 850 mb level wind vectors and relative humidity, c) 1000 mb horizontal temperature, d) 24-hour precipitation e) vertical circulation vectors and f) vertical temperature variation on January 13, 2008, at 0200 LST (continued).

Dataset: RIP: vertical Init: 0000 UTC Thu 10 Jan 08
 Fcst: 101.00 h Valid: 0500 UTC Mon 14 Jan 08 (0700 LST Mon 14 Jan 08)
 Potential vorticity XY= 30.0, 57.0 to 120.0, 57.0
 Potential temperature XY= 30.0, 57.0 to 120.0, 57.0
 Circulation vectors XY= 30.0, 57.0 to 120.0, 57.0



(e)

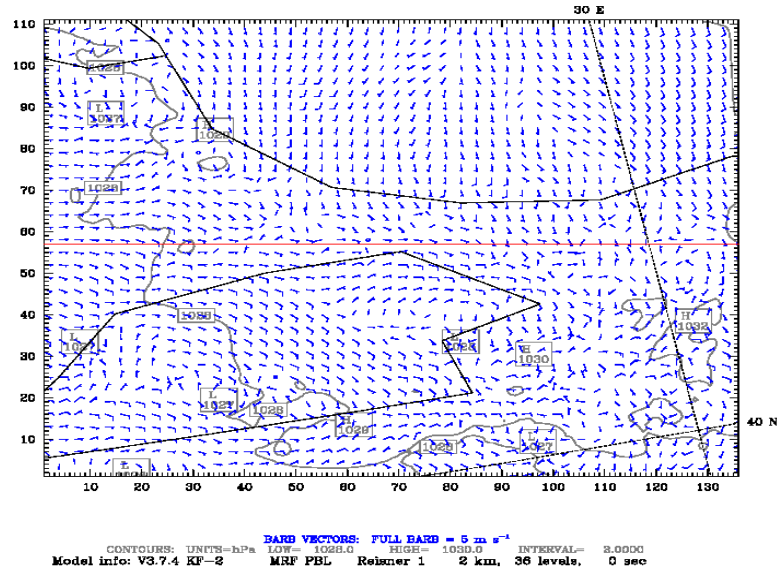
Dataset: RIP: vertical Init: 0000 UTC Thu 10 Jan 08
 Fcst: 101.00 h Valid: 0500 UTC Mon 14 Jan 08 (0700 LST Mon 14 Jan 08)
 Temperature x,y= 70.14, 53.32 lat,lon= 40.97, 28.82 stn=LTEA.17060
 Dewpoint temperature x,y= 70.14, 53.32 lat,lon= 40.97, 28.82 stn=LTEA.17060
 Horizontal wind vectors x,y= 70.14, 53.32 lat,lon= 40.97, 28.82 stn=LTEA.17060



(f)

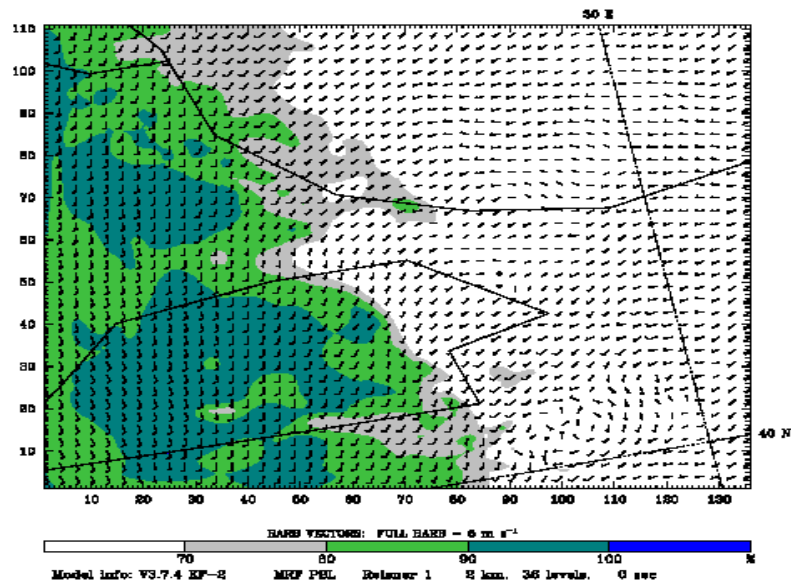
Figure 4.3. a) Sea level pressure and wind vectors, b) 850 mb level wind vectors and relative humidity, c) 1000 mb horizontal temperature, d) 24-hour precipitation, e) vertical circulation vectors and f) vertical temperature variation on January 14, 2008, at 0700 LST (continued).

Dataset: RIP: press humidity Init: 0000 UTC Thu 10 Jan 08
 Fcst: 121.00 h Valid: 0100 UTC Tue 15 Jan 08 (0300 LST Tue 15 Jan 08)
 Sea-level pressure
 Horizontal wind vectors at k-index = 36



(a)

Dataset: RIP: press humidity Init: 0000 UTC Thu 10 Jan 08
 Fcst: 121.00 h Valid: 0100 UTC Tue 15 Jan 08 (0300 LST Tue 15 Jan 08)
 Relative humidity (w.r.t. water) at pressure = 850 hPa
 Horizontal wind vectors at pressure = 850 hPa

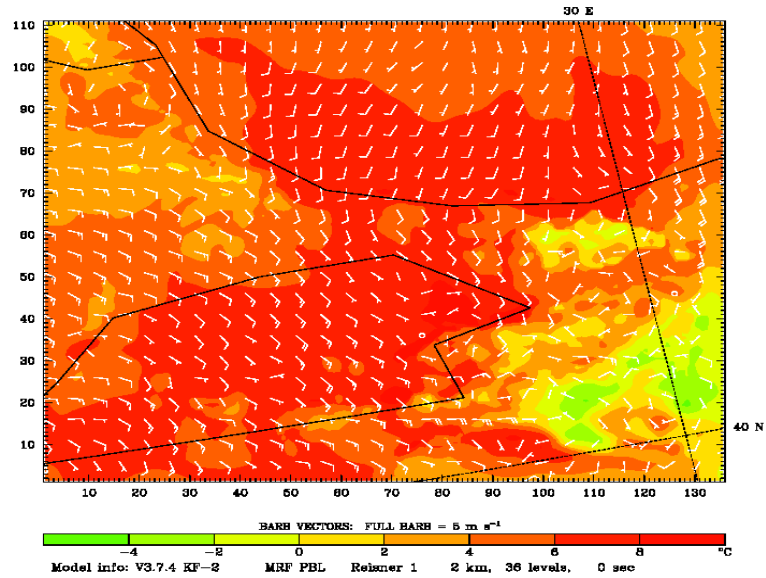


(b)

Figure 4.4. a) Sea level pressure and wind vectors, b) 850 mb level wind vectors and relative humidity, c) 1000 mb horizontal temperature, d) 24-hour precipitation, e) vertical circulation vectors and f) vertical temperature variation on January 15, 2008, at 0300 LST.

Dataset: RIP: temp
 Fcst: 121.00 h
 Temperature
 Horizontal wind vectors

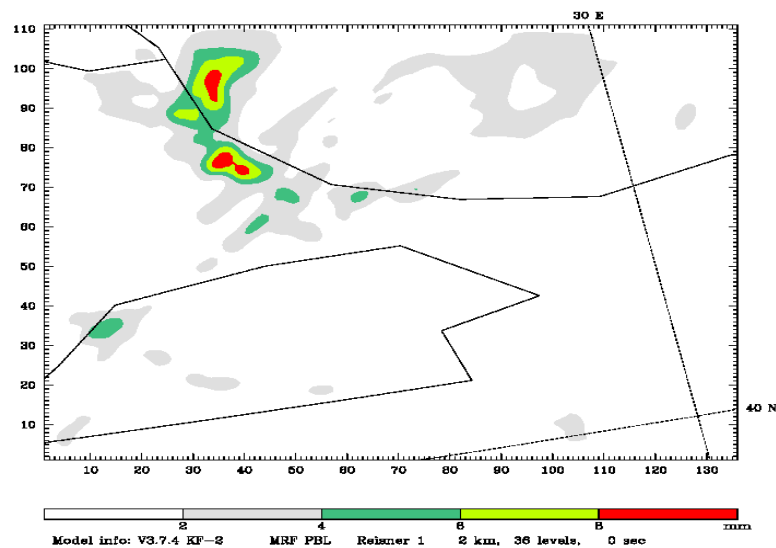
Init: 0000 UTC Thu 10 Jan 08
 Valid: 0100 UTC Tue 15 Jan 08 (0300 LST Tue 15 Jan 08)
 at pressure = 1000 hPa
 at pressure = 1000 hPa



(c)

Dataset: RIP: precip
 Fcst: 121.00 h
 Total precip. since h 24

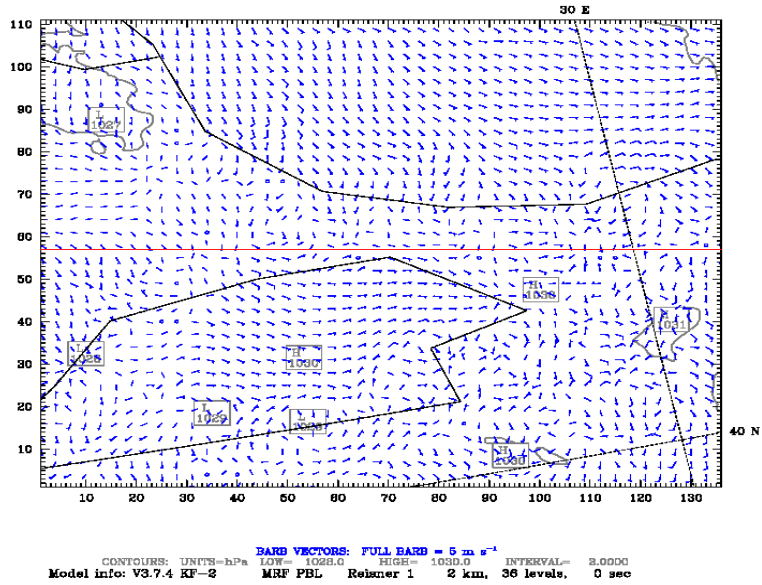
Init: 0000 UTC Thu 10 Jan 08
 Valid: 0100 UTC Tue 15 Jan 08 (0300 LST Tue 15 Jan 08)



(d)

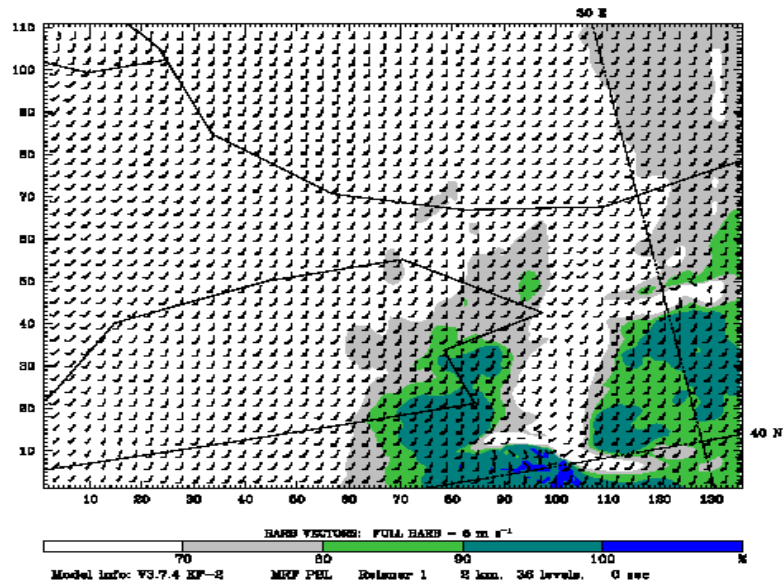
Figure 4.4. a) Sea level pressure and wind vectors, b) 850 mb level wind vectors and relative humidity, c) 1000 mb horizontal temperature, d) 24-hour precipitation, e) vertical circulation vectors and f) vertical temperature variation on January 15, 2008, at 0300 LST (continued).

Dataset: RIP: press humidity Init: 0000 UTC Thu 10 Jan 08
 Fcst: 162.00 h Valid: 1800 UTC Wed 16 Jan 08 (2000 LST Wed 16 Jan 08)
 Sea-level pressure
 Horizontal wind vectors at k-index = 36



(a)

Dataset: RIP: press humidity Init: 0000 UTC Thu 10 Jan 08
 Fcst: 162.00 h Valid: 1800 UTC Wed 16 Jan 08 (2000 LST Wed 16 Jan 08)
 Relative humidity (w.r.t. water) at pressure = 850 hPa
 Horizontal wind vectors at pressure = 850 hPa

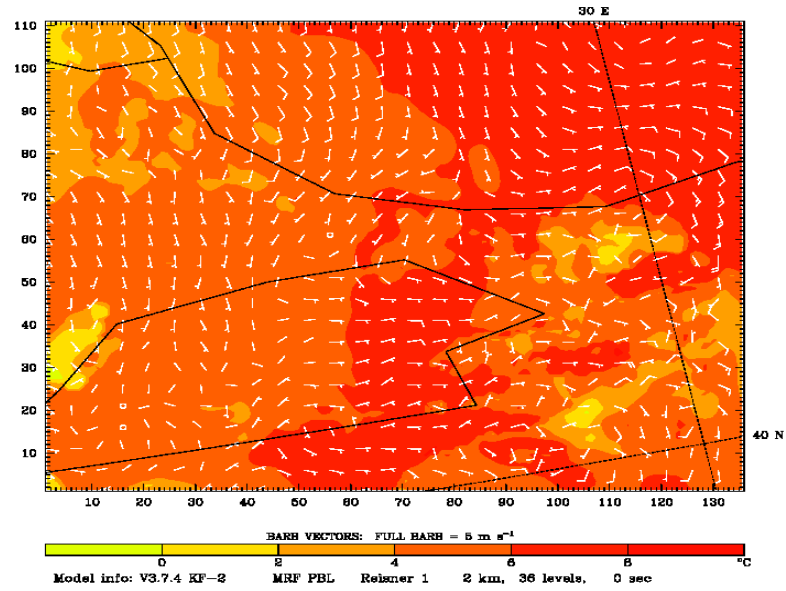


(b)

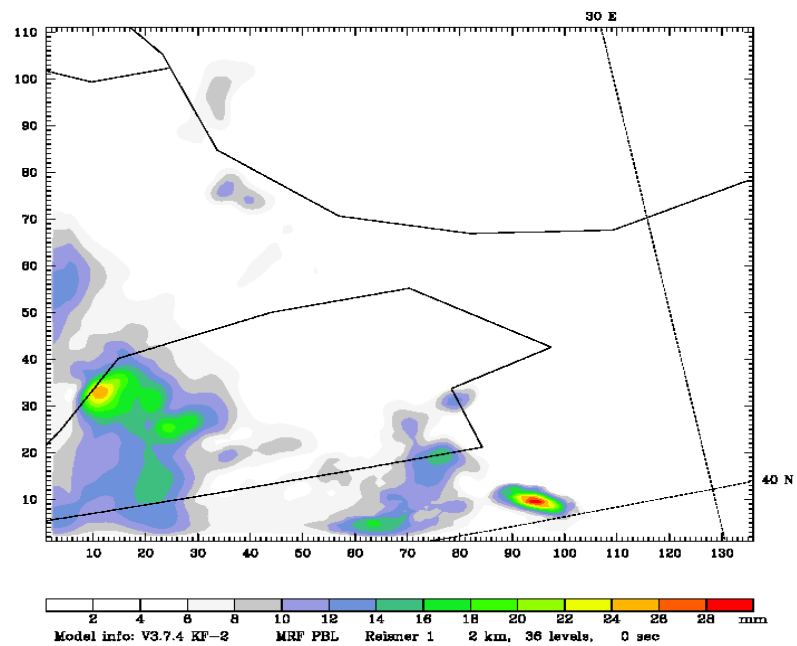
Figure 4.5. a) Sea level pressure and wind vectors, b) 850 mb level wind vectors and relative humidity, c) 850 mb horizontal temperature, d) 24-hour precipitation, e) vertical circulation vectors and f) vertical temperature variation on January 16, 2008, at 2000 LST.

Dataset: RIP: temp
 Fcst: 162.00 h
 Temperature
 Horizontal wind vectors

Init: 0000 UTC Thu 10 Jan 08
 Valid: 1600 UTC Wed 16 Jan 08 (2000 LST Wed 16 Jan 08)
 at pressure = 1000 hPa
 at pressure = 1000 hPa



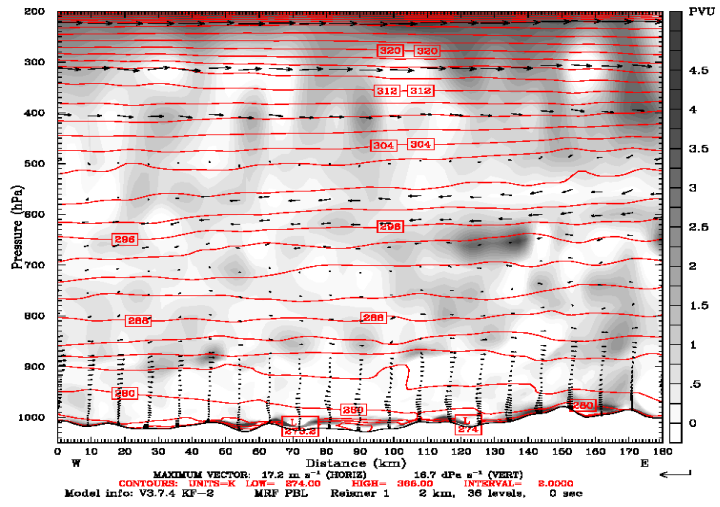
(c)



(d)

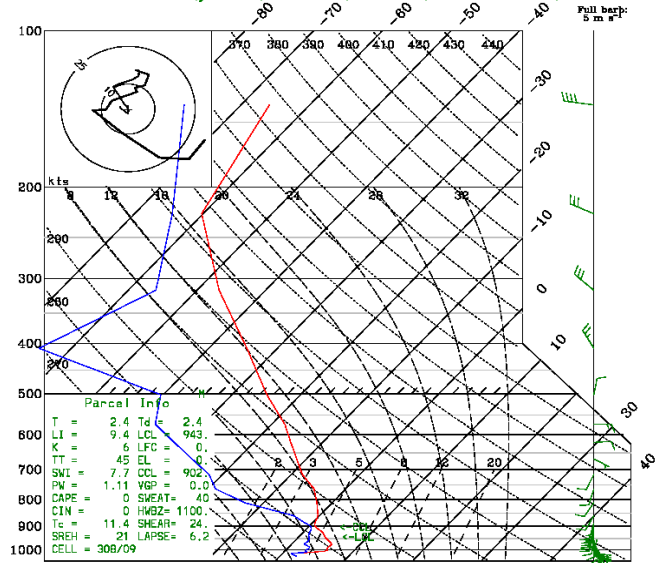
Figure 4.5. a) Sea level pressure and wind vectors, b) 850 mb level wind vectors and relative humidity, c) 850 mb horizontal temperature, d) 24-hour precipitation, e) vertical circulation vectors and f) vertical temperature variation on January 16, 2008, at 2000 LST (continued).

Dataset: RIP: vertical Init: 0000 UTC Thu 10 Jan 08
Fest: 162.00 h Valid: 1800 UTC Wed 16 Jan 08 (2000 LST Wed 16 Jan 08)
Potential vorticity XY= 30.0, 57.0 to 120.0, 57.0
Potential temperature XY= 30.0, 57.0 to 120.0, 57.0
Circulation vectors XY= 30.0, 57.0 to 120.0, 57.0



(e)

Dataset: RIP: vertical Init: 0000 UTC Thu 10 Jan 08
Fest: 162.00 h Valid: 1800 UTC Wed 16 Jan 08 (2000 LST Wed 16 Jan 08)
Temperature x,y= 70.14, 53.32 lat,lon= 40.97, 28.82 stn=LTBA,17060
Dewpoint temperature x,y= 70.14, 53.32 lat,lon= 40.97, 28.82 stn=LTBA,17060
Horizontal wind vectors x,y= 70.14, 53.32 lat,lon= 40.97, 28.82 stn=LTBA,17060



(f)

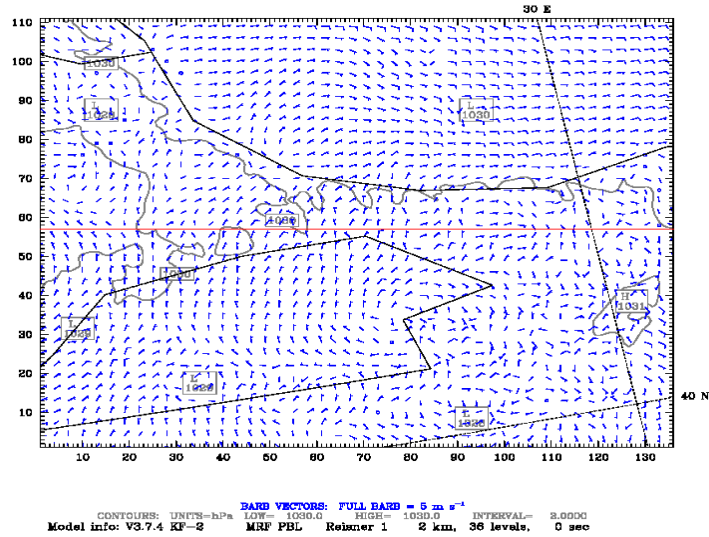
Figure 4.5. a) Sea level pressure and wind vectors, b) 850 mb level wind vectors and relative humidity, c) 850 mb horizontal temperature, d) 24-hour precipitation, e) vertical circulation vectors and f) vertical temperature variation on January 16, 2008, at 2000 LST (continued).

The horizontal wind, humidity, temperature and vertical temperature and wind variation plots for January 17, 2008, 2200 LST are presented in Figure 4.6. The turning of easterly winds from Black Sea to northerlies over İstanbul and Marmara Sea and finally to westerlies is visible in Figure 4.6a. The complex wind patterns around İstanbul and Kocaeli Gulf can be seen in the figure. The 850 mb level relative humidity plot in Figure 4.6b shows that the humidity levels were above 80 per cent across the domain and around Bosphorus strait and eastern parts of İstanbul, above 90 per cent. The southerly winds on İstanbul can be seen in the figure. The temperatures were above 4 °C degrees on most of the domain (Figure 4.6c). The area around Bosphorus strait and the eastern parts of the domain experienced temperatures above 8 °C degrees. Easterly winds on the northern half of the domain can be seen as well as the complex patterns around Kocaeli Gulf. The counter clockwise circulation of winds due to a low pressure system on eastern parts of the Marmara Sea is clearly seen in the figure. The vertical circulation vectors are plotted in Figure 4.6e (see cross section in Figure 4.6a, red line). The westerlies on all vertical levels are clearly seen in the figure. The wind speeds were significantly low close to earth surface. Finally, on Figure 4.6f, the vertical variation of temperature (red line) and dew point temperature (blue line) are presented. As seen in the figure, temperature and dew point temperature lines intersect around 900 mb level, suggesting that occurrence of precipitation at that time. This is also confirmed by Figure 4.6b, which shows humidity levels above 90 per cent above İstanbul, strongly pointing to precipitation.

4.1.3. Back Trajectory Simulation Results

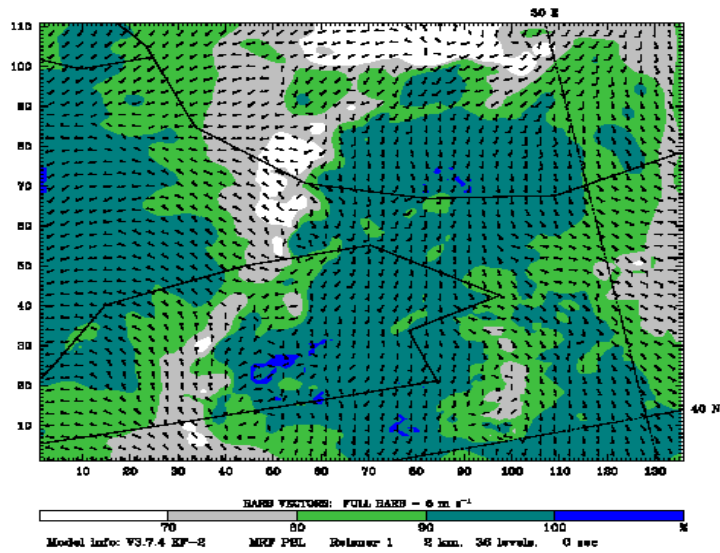
The model back trajectory simulations are conducted individually for the hours of the maximum concentrations measured for each day on European, Balkan and İstanbul grids. The back trajectories are calculated from the hourly outputs of the MM5 simulation, for a 72-hour period. The back trajectory results for January 13, 2008 are presented in Figure 4.7 a-c for European, Balkan and İstanbul domains, respectively. There is northerly transport to the area as seen in Figure 4.7a and b. The air masses travel from Eastern Europe, mainly from Poland and Ukraine, and through Black Sea, they enter Turkey. Figure 4.7b shows that the air masses arrive to İstanbul through highly polluted industrial parts of Kocaeli, carrying pollutants within.

Dataset: RIP: press humidity Init: 0000 UTC Thu 10 Jan 08
 Fcst: 188.00 h Valid: 2000 UTC Thu 17 Jan 08 (2200 LST Thu 17 Jan 08)
 Sea-level pressure
 Horizontal wind vectors at k-index = 36



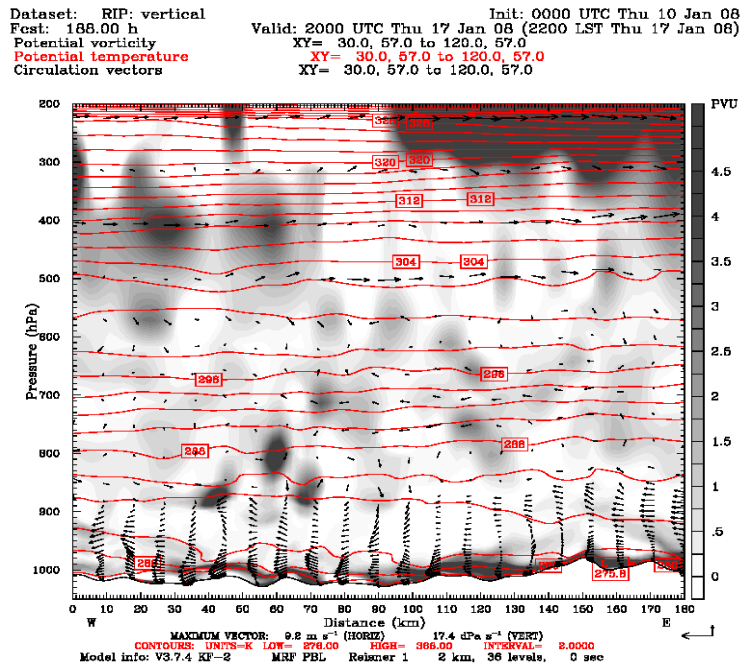
(a)

Dataset: RIP: press humidity Init: 0000 UTC Thu 10 Jan 08
 Fcst: 188.00 h Valid: 2000 UTC Thu 17 Jan 08 (2200 LST Thu 17 Jan 08)
 Relative humidity (w.r.t. water) at pressure = 850 hPa
 Horizontal wind vectors at pressure = 850 hPa

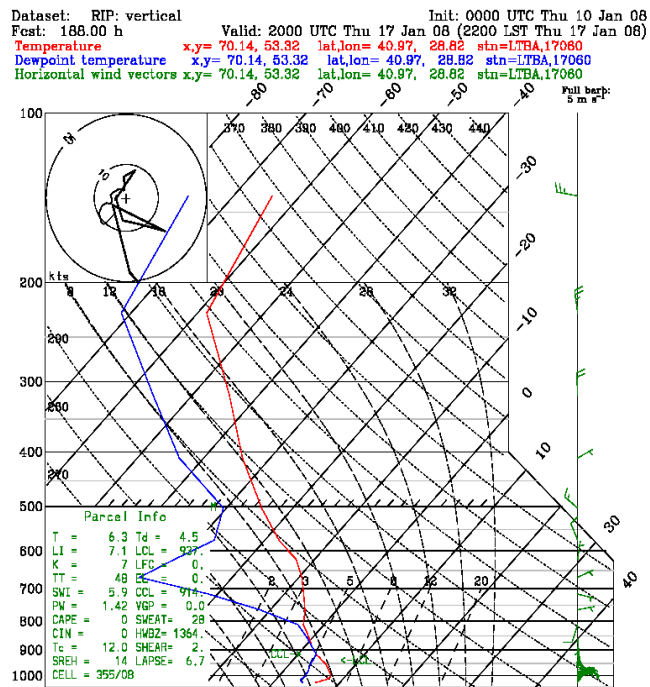


(b)

Figure 4.6. a) Sea level pressure and wind vectors, b) 850 mb level wind vectors and relative humidity, c) 850 mb horizontal temperature, d) 24-hour precipitation, e) vertical circulation vectors and f) vertical temperature variation on January 17, 2008, at 2200 LST.



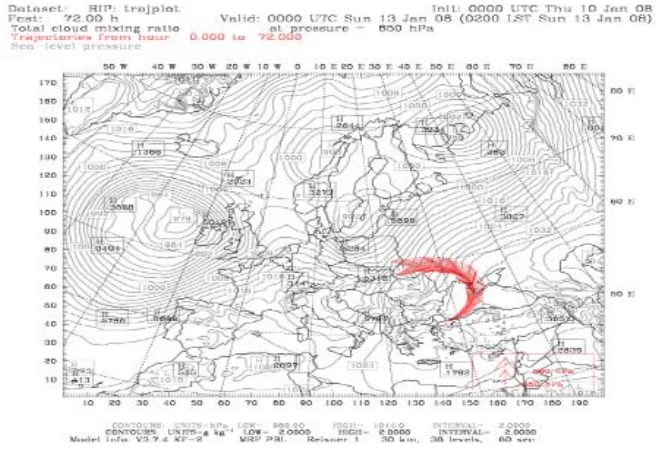
(e)



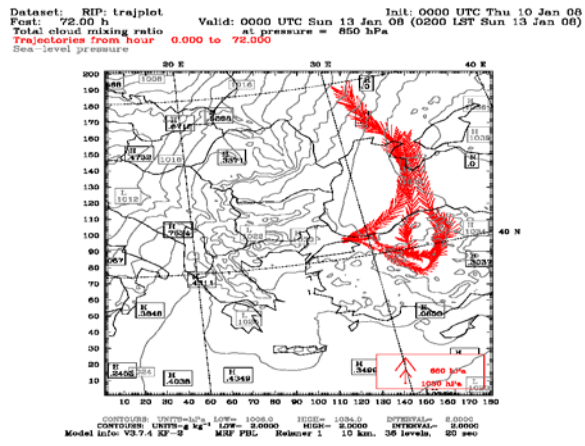
(f)

Figure 4.6. a) Sea level RIP pressure and wind vectors, b) 850 mb level wind vectors and relative humidity, c) 850 mb horizontal temperature, d) 24-hour precipitation, e) vertical circulation vectors and f) vertical temperature variation on January 17, 2008, at 2200 LST (continued).

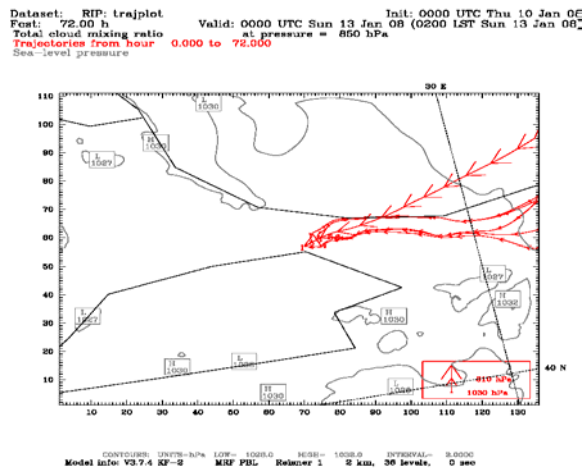
Back trajectories are calculated for European, Balkan and İstanbul domains trajectory plots are produced for January 14, 2008 episode. The back trajectories are presented in Figure 4.8 a-c for each domain. Air masses are transported from Russia and enter Turkey from eastern Black Sea (Figure 4.8a). The air masses travel through Blacksea coast and central Anatolia (Figure 4.8b) and arrive to İstanbul through Kocaeli Gulf, carrying the pollutants from the highly industrial regions (Figure 4.8c). As seen in Figure 3.16, there are important sources on the Black Sea coasts for Russia, especially around southern Ukraine. The polluted air masses from these regions may travel to İstanbul, and increase the air quality levels. For the January 15, 2008 episode, the back trajectories are calculated for European, Balkan and İstanbul domains and the results are presented in Figure 4.9 a-c. The transport to İstanbul on this episode is relatively short ranged compared to the previous two days of the episode (Figure 4.9a). However, in a more detailed investigation, similar transport patterns are easily observed. The travel of air masses through Blacksea and central Anatolia region and the transport from the Kocaeli Gulf is clearly seen. Another trajectory, coming from Black Sea, extending up to the Mediterranean Sea and the recirculation back to İstanbul is presented in Figure 4.9b. The transport of air masses from Kocaeli Gulf to İstanbul is clearer in Figure 4.9c. The back trajectory simulation results for the January 16, 2008 episode are presented in Figures 4.10 a-c. The results show that a different route characterized the transport to İstanbul. The air masses travelled through Adriatic Sea and through Greece, they arrive to İstanbul (Figure 4.10a). With a more detailed look, it is clearly seen that the air masses travel southeast over Thessaloniki and enter Turkey turning northeast over Çanakkale and passing from southern parts of the Marmara Sea, they arrive to İstanbul (Figure 4.10b). Another similar trajectory with the previous days is from central Anatolia region. The air masses concentrate over Marmara Sea and travel north to İstanbul (Figure 4.10c). The transport of air masses from over the Mediterranean Sea through southern parts of Greece is presented in Figure 4.11a. This trajectory may lead to PM episodes on the pathway due to the fact that it may contain aerosols from northern Africa and sea salt from Mediterranean Sea. There are also trajectories from southern coasts of Turkey, close to Antalya and also Mediterranean region of Turkey (Figure 4.11b). In Figure 4.11c, it is seen that the air masses to İstanbul travel north and pass over the highly industrial regions of the Kocaeli Gulf.



(a)



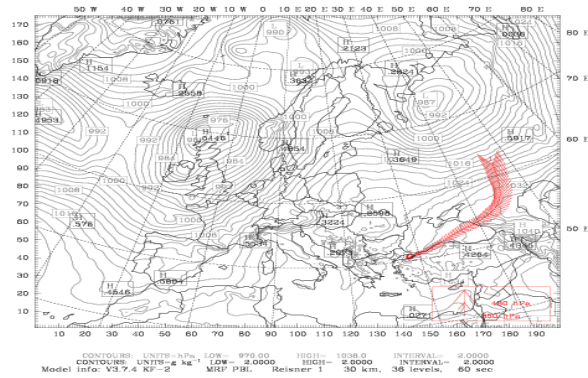
(b)



(c)

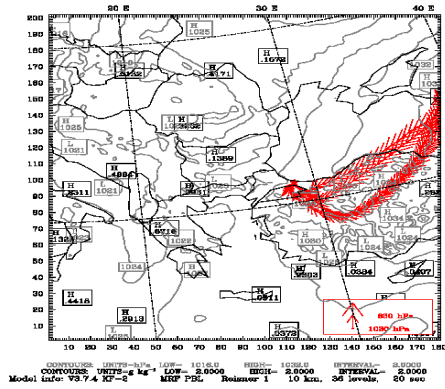
Figure 4.7. Back trajectory simulation results of January 13, 2008, 0200 LST for a) European, b) Balkan and c) İstanbul domains.

Dataset: RIP: trajplot Valid: 0500 UTC Mon 14 Jan 08 Init: 0000 UTC Thu 10 Jan 08
Fest: 101.00 h Total cloud mixing ratio at pressure = 850 hPa
Trajectories from hour 29.000 to 101.000
Sea-level pressure



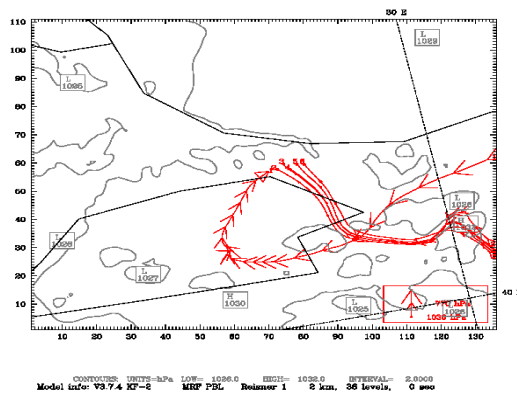
(a)

Dataset: RIP: trajplot Valid: 0500 UTC Mon 14 Jan 08 Init: 0000 UTC Thu 10 Jan 08
Fest: 101.00 h Total cloud mixing ratio at pressure = 850 hPa
Trajectories from hour 29.000 to 101.000
Sea-level pressure



(b)

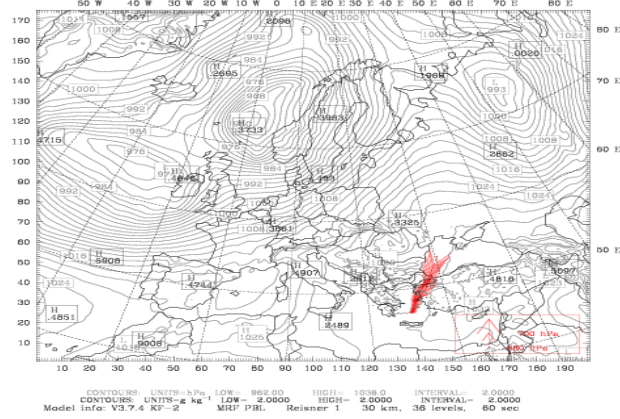
Dataset: RIP: trajplot Valid: 0500 UTC Mon 14 Jan 08 Init: 0000 UTC Thu 10 Jan 08
Fest: 101.00 h Total cloud mixing ratio at pressure = 850 hPa
Trajectories from hour 29.000 to 101.000
Sea-level pressure



(c)

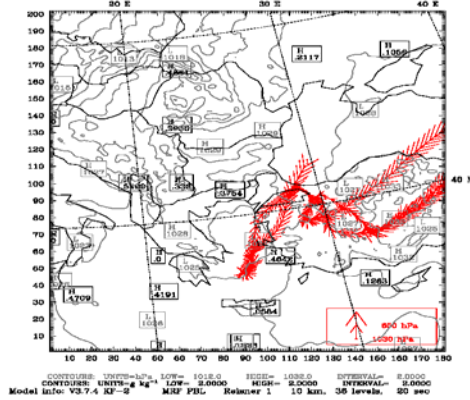
Figure 4.8. Back trajectory simulation results of January 14, 2008, 0700 LST for a) European, b) Balkan and c) İstanbul domains (continued).

Dataset: RIP: trajplot Valid: 0100 UTC Tue 15 Jan 08 Init: 0000 UTC Thu 10 Jan 08
Fest: 121.00 h at pressure = 850 hPa
Total cloud mixing ratio
Trajectories from hour 49.000 to 121.000
Sea-level pressure



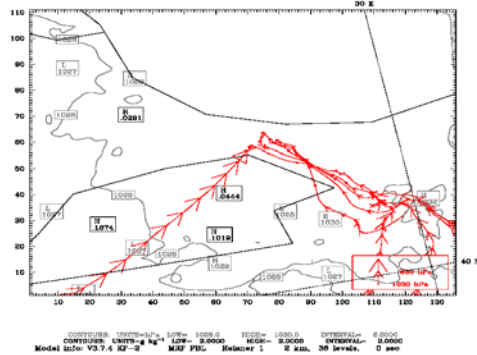
(a)

Dataset: RIP: trajplot Valid: 0100 UTC Tue 15 Jan 08 Init: 0000 UTC Thu 10 Jan 08
Fest: 121.00 h at pressure = 850 hPa
Total cloud mixing ratio
Trajectories from hour 49.000 to 121.000
Sea-level pressure



(b)

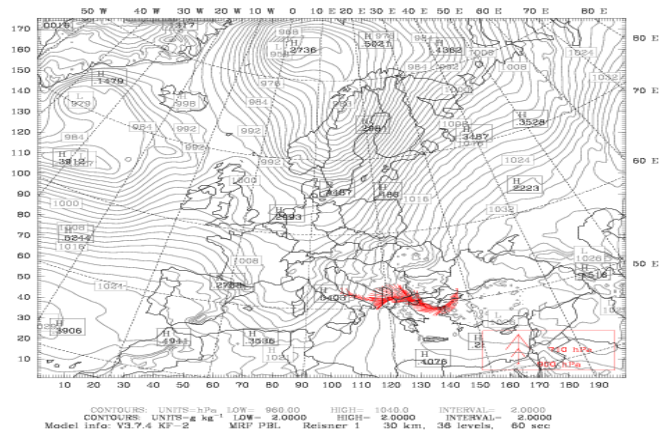
Dataset: RIP: trajplot Valid: 0100 UTC Tue 15 Jan 08 Init: 0000 UTC Thu 10 Jan 08
Fest: 121.00 h at pressure = 850 hPa
Total cloud mixing ratio
Trajectories from hour 49.000 to 121.000
Sea-level pressure



(c)

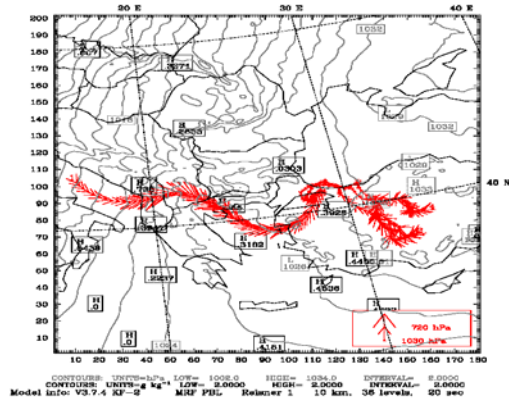
Figure 4.9. Back trajectory simulation results of January 15, 2008, 0300 LST for a) European, b) Balkan and c) Istanbul domains (continued).

Dataset: RIP: trajplot Valid: 1800 UTC Wed 16 Jan 08 Init: 0000 UTC Thu 10 Jan 08
 Fcst: 162.00 h at pressure = 850 hPa (2000 LST Wed 16 Jan 08)
 Total cloud mixing ratio
 Trajectories from hour 90.000 to 162.000
 Sea-level pressure



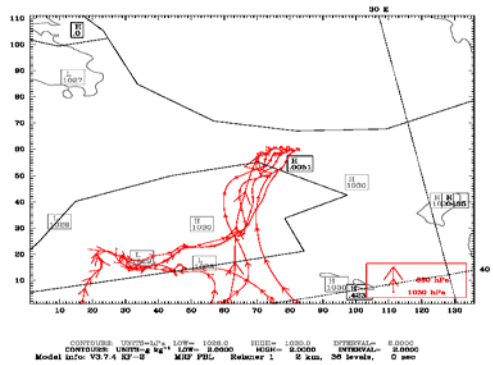
(a)

Dataset: RIP: trajplot Valid: 1800 UTC Wed 16 Jan 08 Init: 0000 UTC Thu 10 Jan 08
 Fcst: 162.00 h at pressure = 850 hPa
 Total cloud mixing ratio
 Trajectories from hour 90.000 to 162.000
 Sea-level pressure



(b)

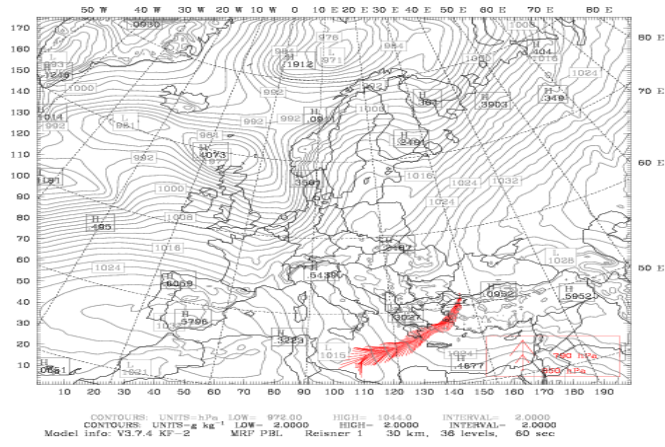
Dataset: RIP: trajplot Valid: 1800 UTC Wed 16 Jan 08 Init: 0000 UTC Thu 10 Jan 08
 Fcst: 162.00 h at pressure = 850 hPa
 Total cloud mixing ratio
 Trajectories from hour 90.000 to 162.000
 Sea-level pressure



(c)

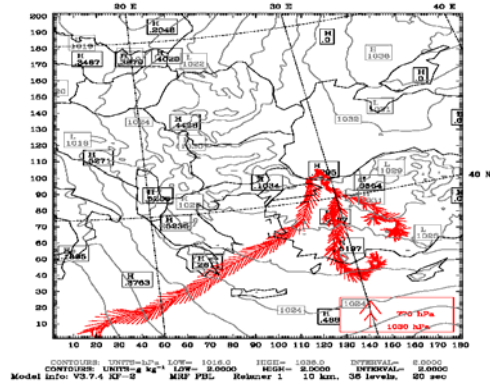
Figure 4.10. Back trajectory simulation results of January 16, 2008, 2000 LST for a) European, b) Balkan and c) İstanbul domains (continued).

Dataset: RIP: trajplot Init: 0000 UTC Thu 10 Jan 08
Fcast: 188.00 h Valid: 2000 UTC Thu 17 Jan 08 (2200 LST Thu 17 Jan 08)
Total cloud mixing ratio at pressure = 850 hPa
Trajectories from hour 116.000 to 188.000
Sea-level pressure



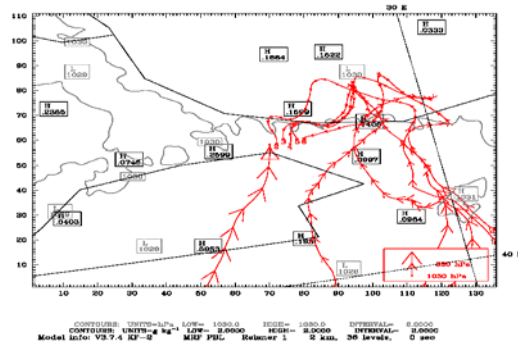
(a)

Dataset: RIP: trajplot Init: 0000 UTC Thu 10 Jan 08
Fcast: 188.00 h Valid: 2000 UTC Thu 17 Jan 08 (2200 LST Thu 17 Jan 08)
Total cloud mixing ratio at pressure = 850 hPa
Trajectories from hour 116.000 to 188.000
Sea-level pressure



(b)

Dataset: RIP: trajplot Init: 0000 UTC Thu 10 Jan 08
Fcast: 188.00 h Valid: 2000 UTC Thu 17 Jan 08 (2200 LST Thu 17 Jan 08)
Total cloud mixing ratio at pressure = 850 hPa
Trajectories from hour 116.000 to 188.000
Sea-level pressure



(c)

Figure 4.11. Back trajectory simulation results of January 17, 2008, 2200 LST for a) European, b) Balkan and c) Istanbul domains (continued).

4.2. Emission Model

The annual emission estimates for the aggregated pollutant groups of CO, NO_x, SO₂, NMVOC, NH₃, PM₁₀ and PM_{2.5} for each source category are presented in Figure 4.12. The figure clearly shows that road transport plays the main role among all other sectors. Road transport, alone, is responsible for 57 per cent of CO emissions (272 000 tons). Another important CO emitter is the residential combustion, emitting 29 per cent of the total CO emissions (47 399 tons). Solvent use is the second important sector, contributing to 77 per cent of the total NMVOC emissions (84 973 tons). The figure also shows that 40 per cent of SO₂ emissions come from industrial combustion and 32 per cent come from point sources. In Figure 4.13, the annual speciated PM emissions are presented. As seen in the figure, the organic portion of both PM₁₀ (69 per cent) and PM_{2.5} (69 per cent) dominates over other subspecies of PM. On the other hand, elemental carbon constitutes 26 per cent of both PM₁₀ and PM_{2.5}. Road transport is the major source category contributing to PM₁₀ (60 per cent) and PM_{2.5} levels (73 per cent). Point sources from industrial processes also contribute to the PM emissions (40 per cent and 52 per cent for PM₁₀ and PM_{2.5}, respectively)

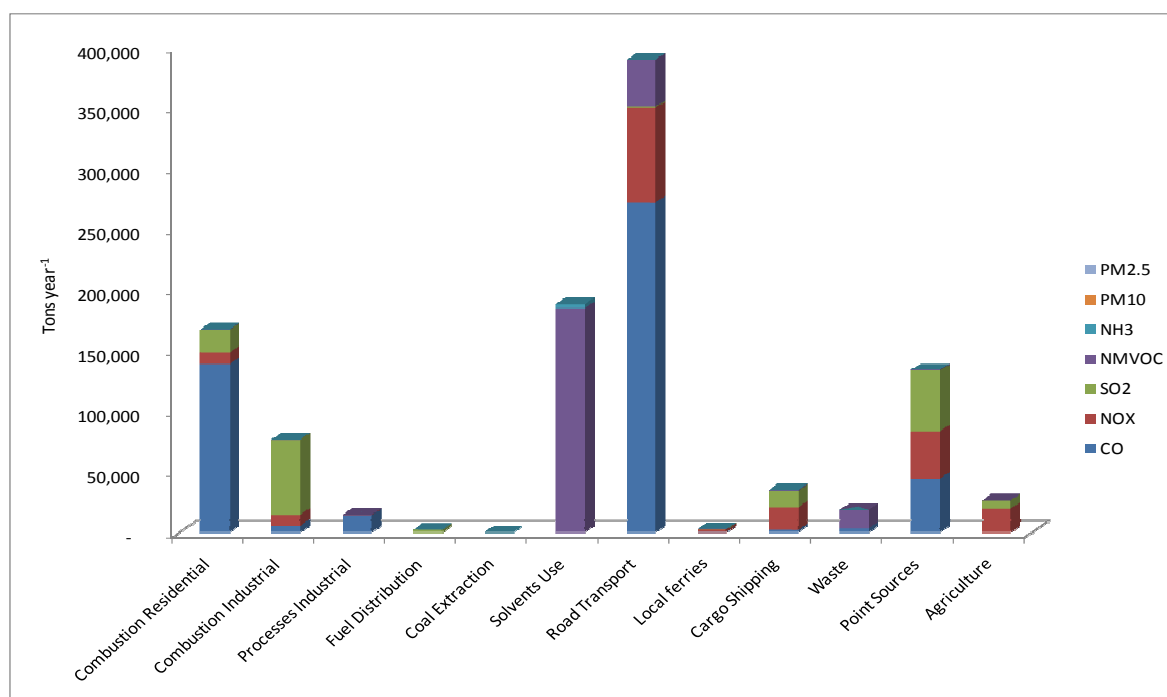


Figure 4.12. Annual aggregated emissions per source category.

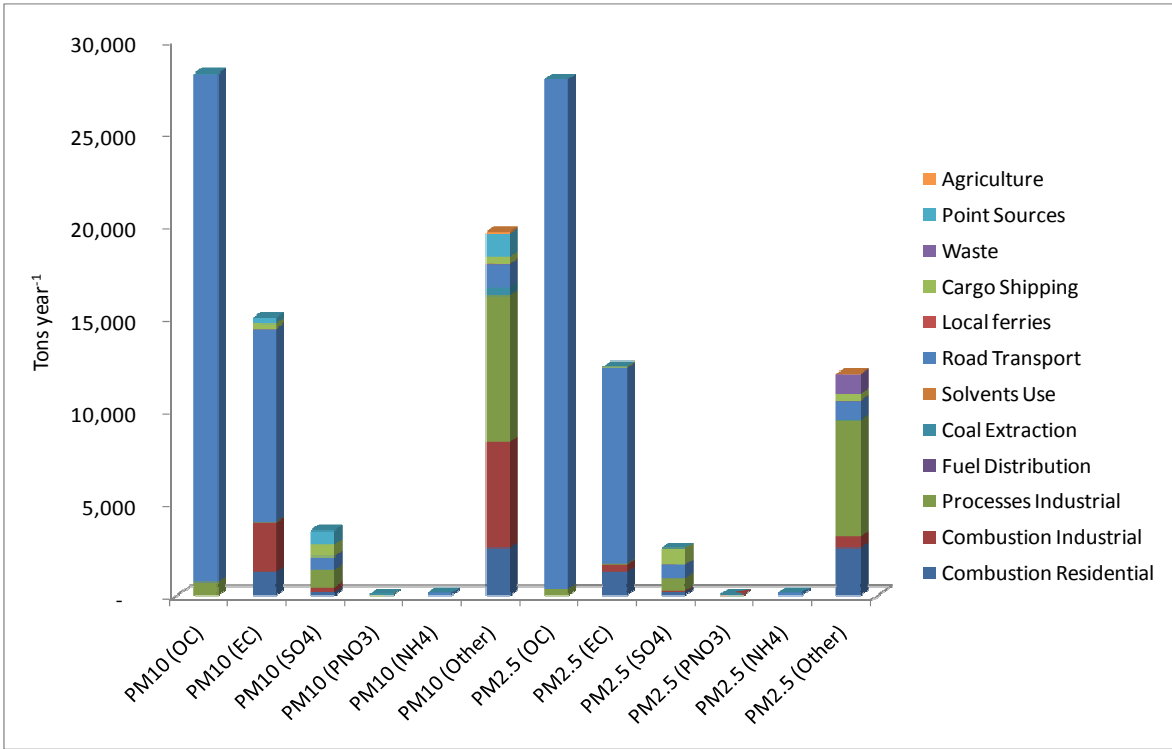


Figure 4.13. Annual speciated PM emissions for each source category.

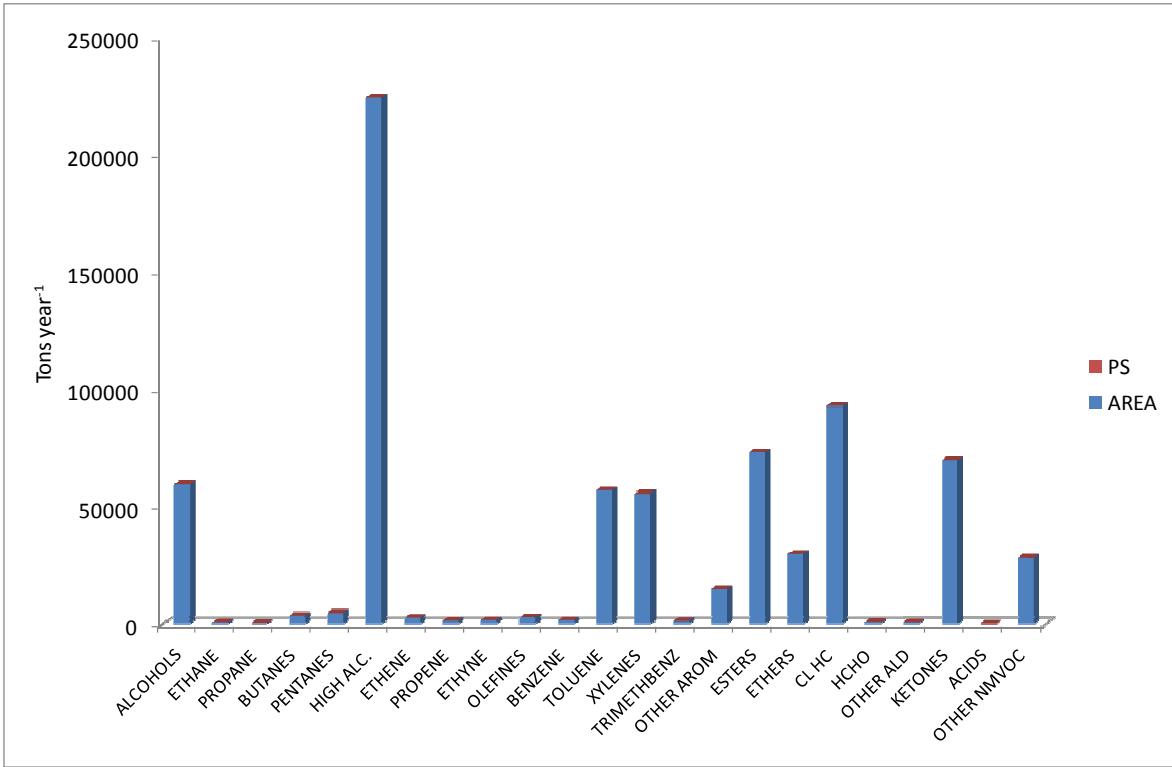


Figure 4.14. Annual speciated NMVOC emissions for each source category.

In Figure 4.14, the annual speciated NMVOC emissions are presented. The figure shows the domination of area sources over point sources. 31 per cent of NMVOC emissions come from higher alkanes, whereas 8 per cent come from alcohols, 8 per cent from toluene, 8 per cent from xylene, 10 per cent from esters, 13 per cent from chlorinated hydrocarbons, 10 per cent from ketones, and finally, 4 per cent originate from other NMVOCs.

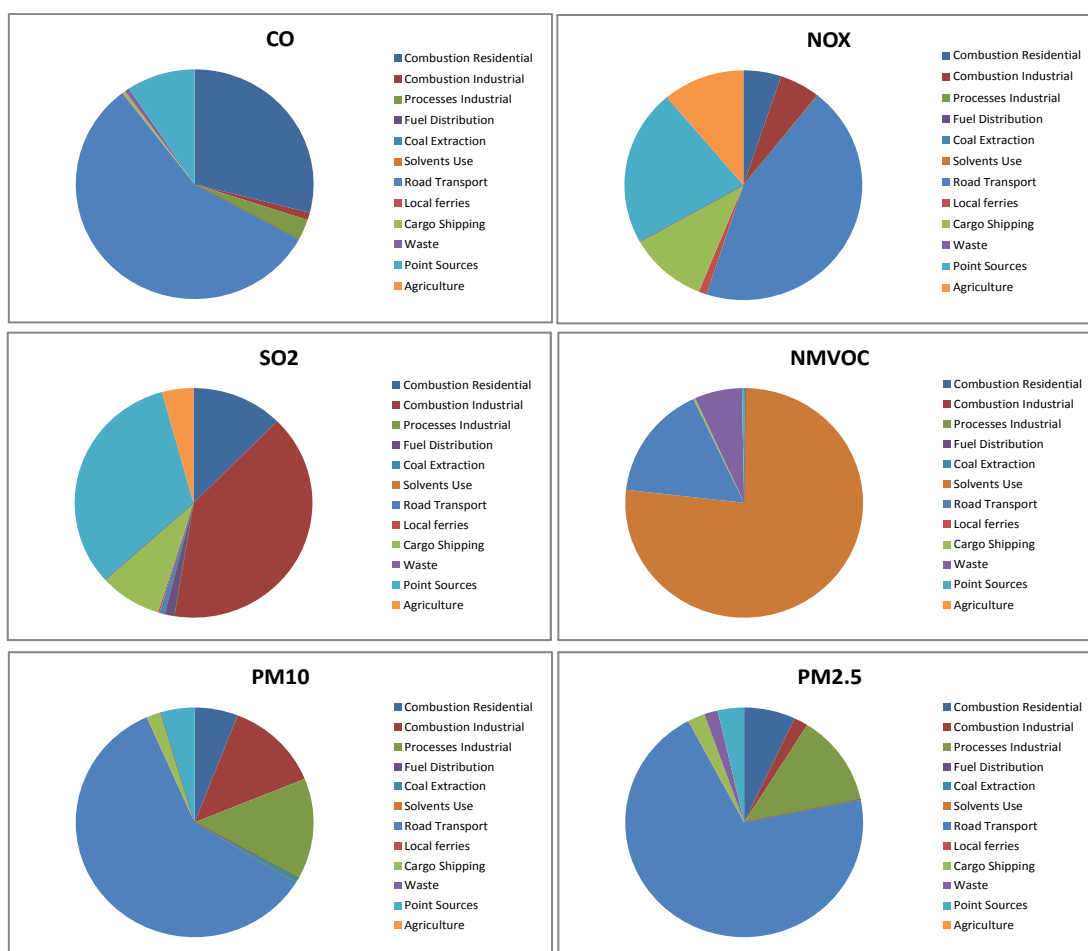


Figure 4.15. Source contribution to CO, NO_x, SO₂, NMVOC, PM₁₀ and PM_{2.5} emissions.

Figure 4.15 demonstrates the important sources of CO, NO_x, SO₂, NMVOC, PM₁₀ and PM_{2.5} emissions in the area. As stated above, road transport plays the major role in CO (57 per cent), NO_x (44 per cent), PM₁₀ (60 per cent) and PM_{2.5} (70 per cent) emissions, where as solvent use is the main contributor of NMVOC emissions (77 per cent). Road

transport contributes 16 per cent of NMVOC emissions. Industrial combustion plays the major role in SO₂ emissions (40 per cent).

The spatial distributions of CO, NO_x, SO₂, NMVOC, PM₁₀ and PM_{2.5} from residential heating are presented in Figure 4.16. The figure clearly shows that CO emissions from the residential combustion originate from the two coastal sides of the Bosphorus strait, where most of the population resides. The old centers of the city at the European side and Kadıköy region on the Asian side are where the main and the oldest residential areas are located.

The spatial distribution of emissions from industrial combustion and industrial processes are presented in Figures 4.17 and 4.18, respectively. As mentioned before, the industrial activities were assumed to be present only in the organized industrial areas. The figures show that the highest rate of emission comes from the İkitelli industrial region, as expected, which hosts the highest amount of industrial complexes in the city. SO₂ emissions are dominant over other pollutant emissions due to combustion of fossil fuels (coal and fuel oil) in the industry. The amount of CO emissions is in the same magnitude as emissions from residential heating whereas industrial NO_x emissions are one order of magnitude higher than residential NO_x emissions. SO₂ emissions from industrial combustion are 10 orders of magnitude higher than residential SO₂ emissions. The PM emissions from industry are more than one order of magnitude higher than those from residential heating.

In Figure 4.19, the emissions from road transport are presented. The very dense traffic network inside the city leads to the occurrence of maximum on-road traffic emissions around the residential and commercial regions of the domain. As discussed before, the figure shows that CO is the main pollutant emitted from on-road traffic sources (272 000 tons year⁻¹). Monthly emissions from cargo shipping are calculated and the emissions of SO₂ and NO_x for January are presented in Figure 4.20. As seen in the figure, the highest emissions are released from the Bosphorus strait.

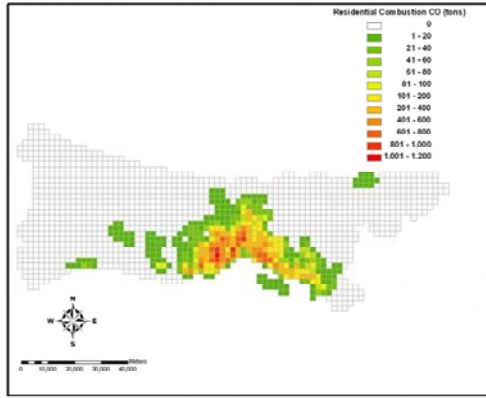
The solvent use is directly proportional to the population distribution and emits NH₃ (3 256 tons year⁻¹) and NMVOCs (84 793 tons year⁻¹). The spatial distribution of NH₃ and

NMVOCs from solvent use is presented in Figure 4.21. Elemental carbon emissions from coal extraction sites, in both PM₁₀ and PM_{2.5} portion, are presented in Figure 4.22.

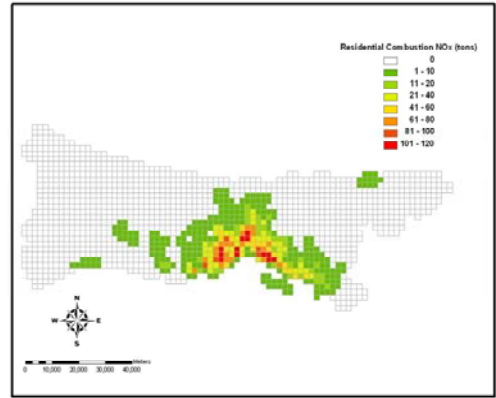
The monthly variations of CO, NO_x, NMVOCs, SO₂, PM₁₀ and PM_{2.5} for the major source categories are presented in Figures 4.23 to 4.26. Figure 4.23 shows the monthly variation of CO for central heating, industrial processes and road transport as well as the total CO emissions. As seen in the figure, the total CO emissions follows a seasonal pattern; an increase of emissions in winter time, especially during the heating season, then a decrease in the summer months. This points that the variation of CO emissions is most significantly determined by the variation in residential heating emissions. As expected, the CO emissions from industrial process do not vary much throughout the year. A small decrease in the summer months can be seen from the figure. On the other hand, the traffic emissions tend to increase from winter to spring, then decrease in summer months and finally, increase in autumn.

The monthly variation of NO_x emissions from central heating, industrial processes, road transport and cargo shipping, as well as the total amount is presented in Figure 4.24. The variation of total NO_x emissions from all sectors, as well as the emissions from central heating sector, follows the seasonal trend, as was the case for CO emissions. NO_x emissions from road transport follows the same variation trend as do traffic originated CO emissions in Figure 4.23. The cargo originated and industrial processes originated NO_x emissions do not vary much throughout the year.

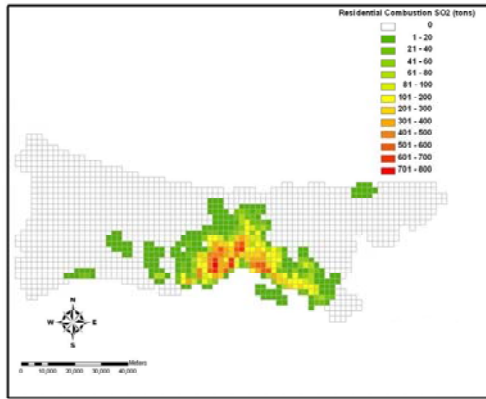
In Figure 4.25, the monthly variation of SO₂ from central heating, industrial combustion and industrial processes are presented. The significant variation of the total SO₂ emissions is clearly seen in the figure. The trend follows the same seasonal pattern that the central heating originated SO₂ emissions follow; maximums in winter and minimums in summer. All source categories make their minimums in summer period as can be seen from the figure.



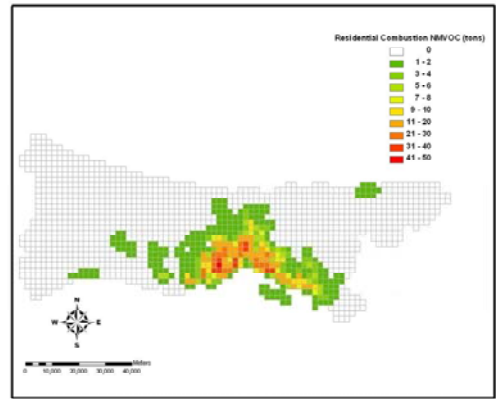
(a)



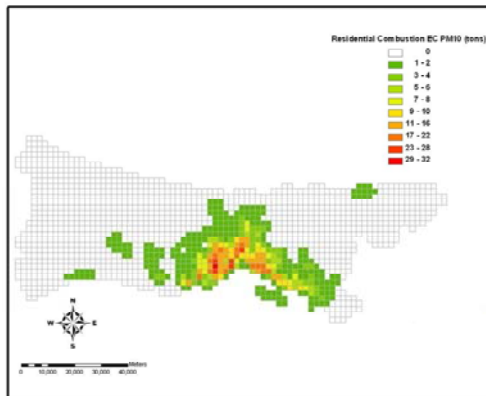
(b)



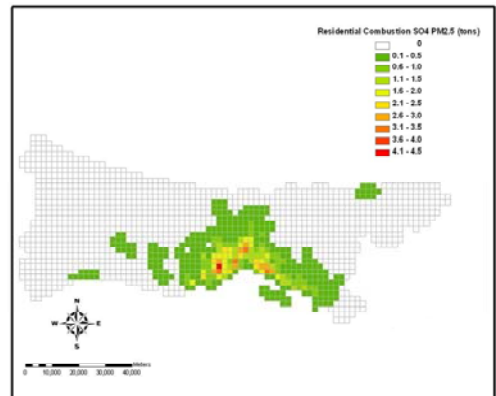
(c)



(d)

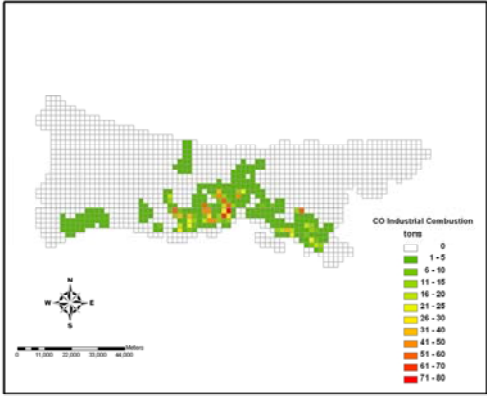


(e)

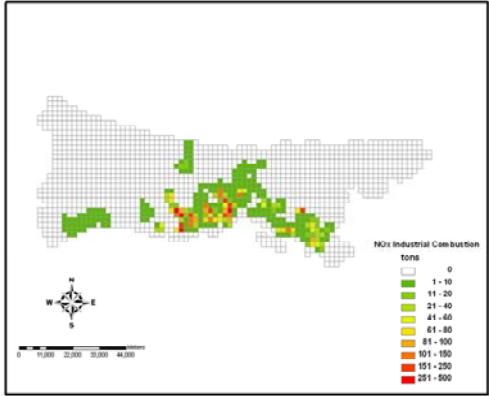


(f)

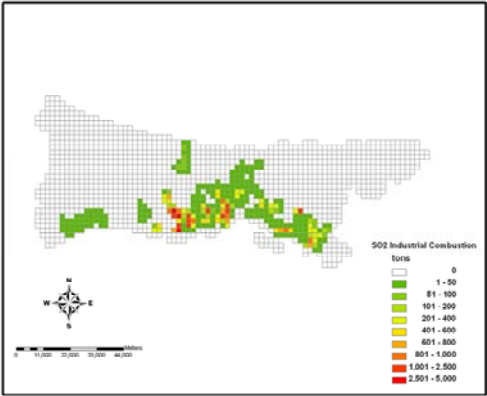
Figure 4.16. Spatial distribution of a) CO, b) NO_x, c) SO₂, d) NMVOC, e) PM₁₀ (EC) and f) PM_{2.5} (EC) emissions from residential combustion.



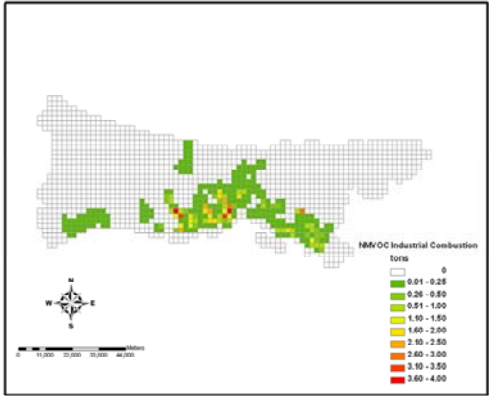
(a)



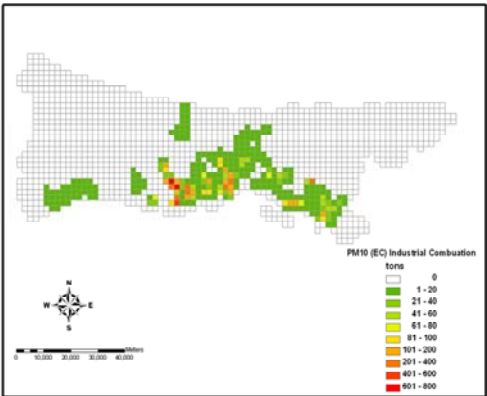
(b)



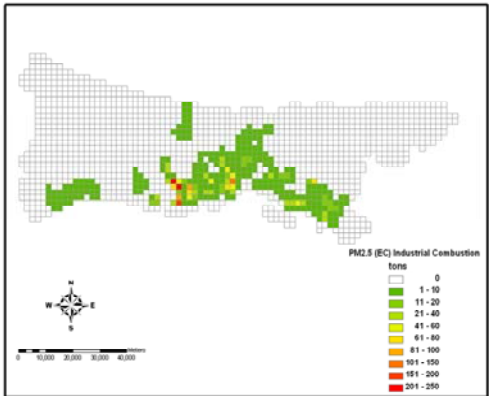
(c)



(d)

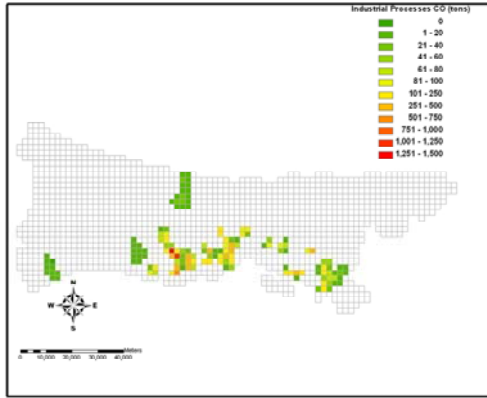


(e)

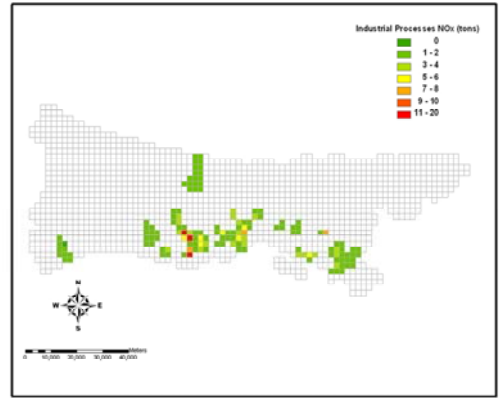


(f)

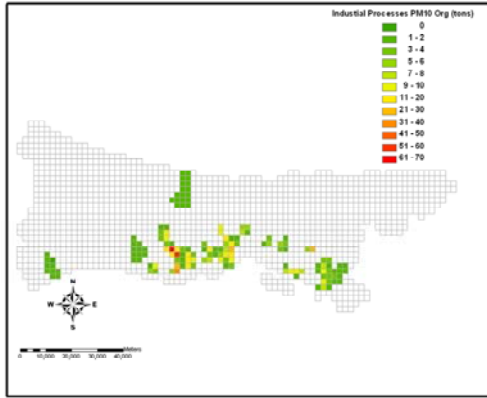
Figure 4.17. Spatial distribution of a) CO, b) NO_x, c) SO₂, d) NMVOC, e) PM₁₀ (EC) and f) PM_{2.5} (EC) emissions from industrial combustion.



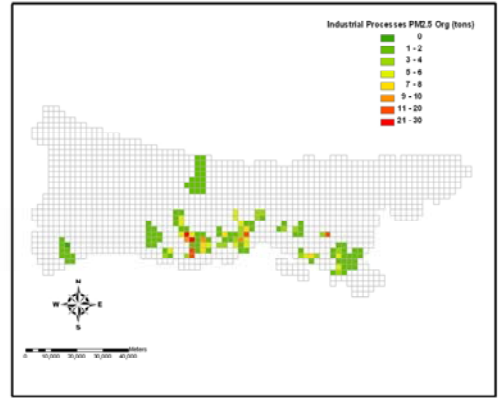
(a)



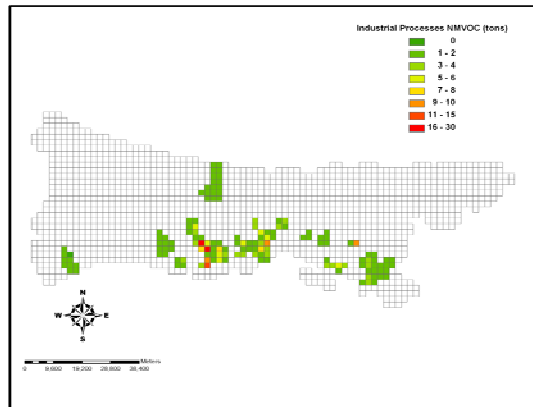
(b)



(c)

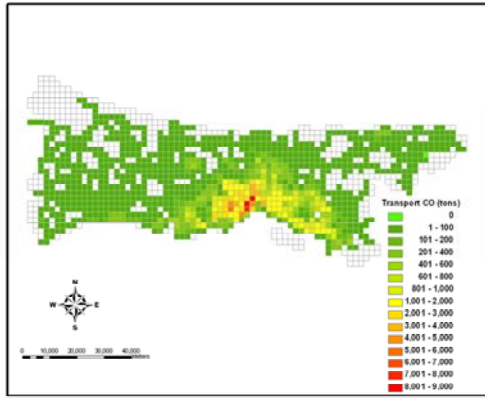


(d)

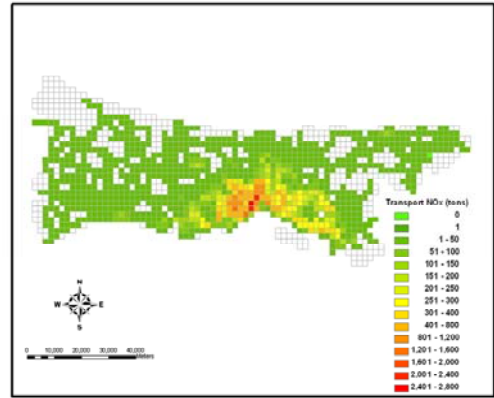


(e)

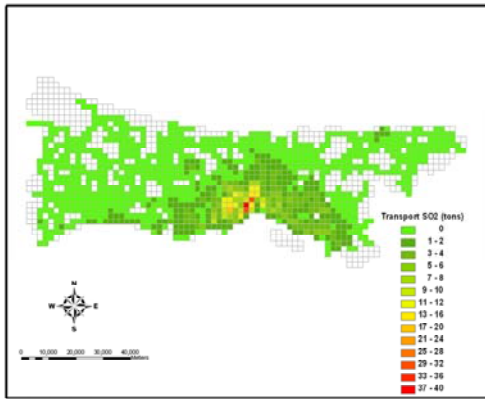
Figure 4.18. Spatial distribution of a) CO, b) NO_x, c) PM₁₀ (OC), d) PM_{2.5} (OC) and e) NMVOC emissions from industrial processes.



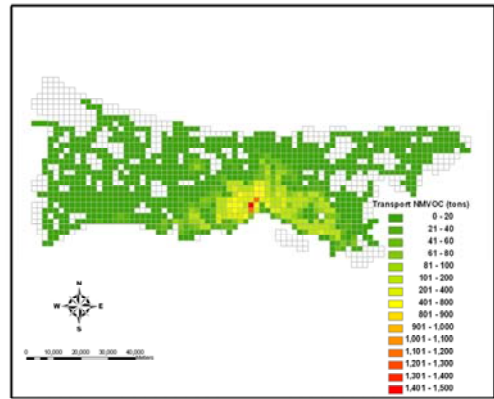
(a)



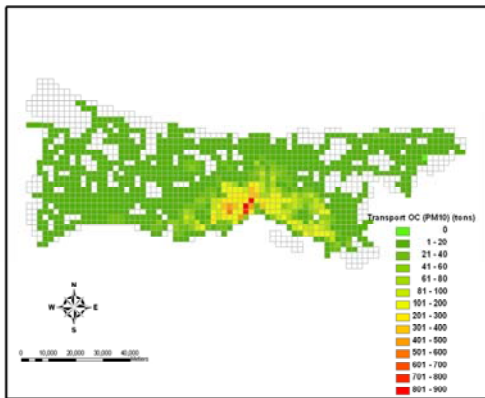
(b)



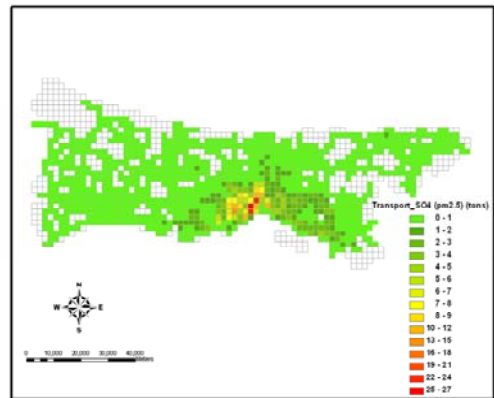
(c)



(d)



(e)



(f)

Figure 4.19. Spatial distribution of a) CO, b) NO_x, c) SO₂, d) NMVOC, e) PM₁₀ (OC) and f) PM_{2.5} (SO₄) emissions from road transport.

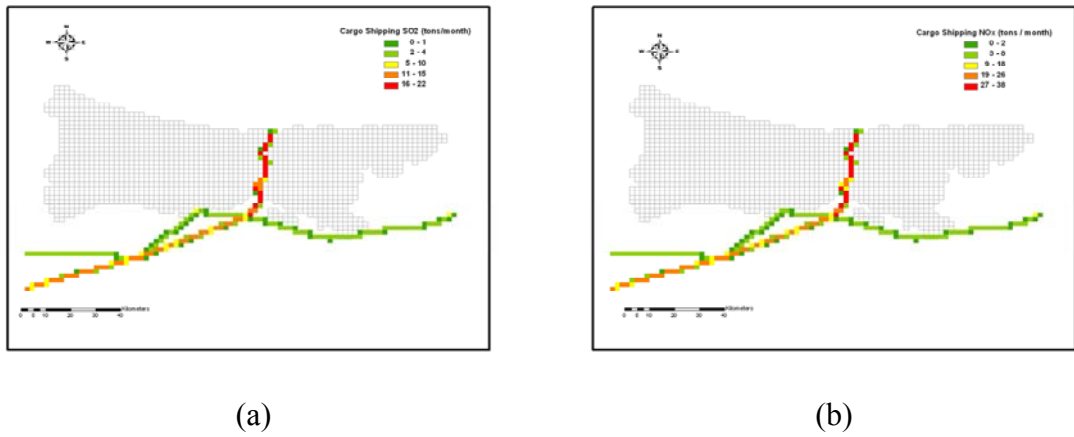


Figure 4.20. a) SO₂ and b) NO_x emissions from cargo shipping emissions.

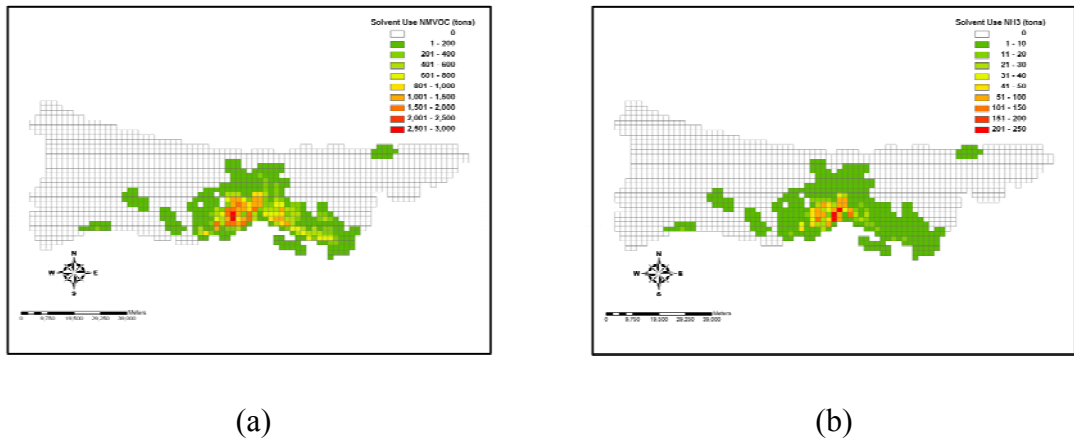


Figure 4.21. Spatial distribution of a) NMVOC and b) NH₃ emissions from solvent use.

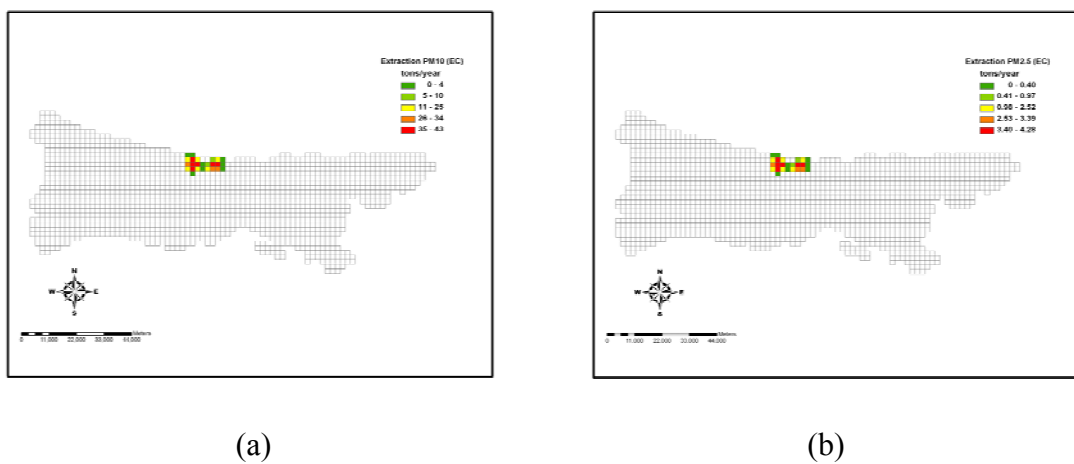


Figure 4.22. Spatial distributions of a) PM₁₀ and b) PM_{2.5} emissions from coal extraction.

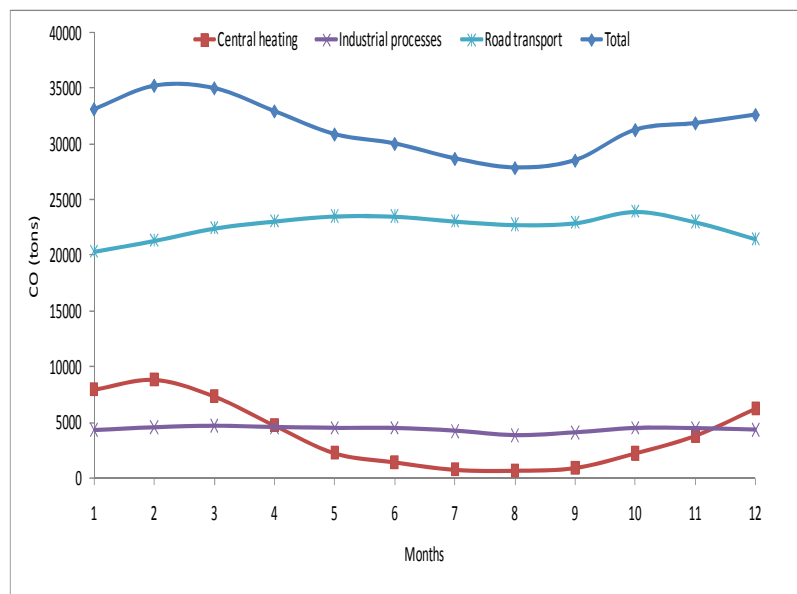


Figure 4.23. Monthly variation of CO emissions from central heating, industrial processes and road transport.

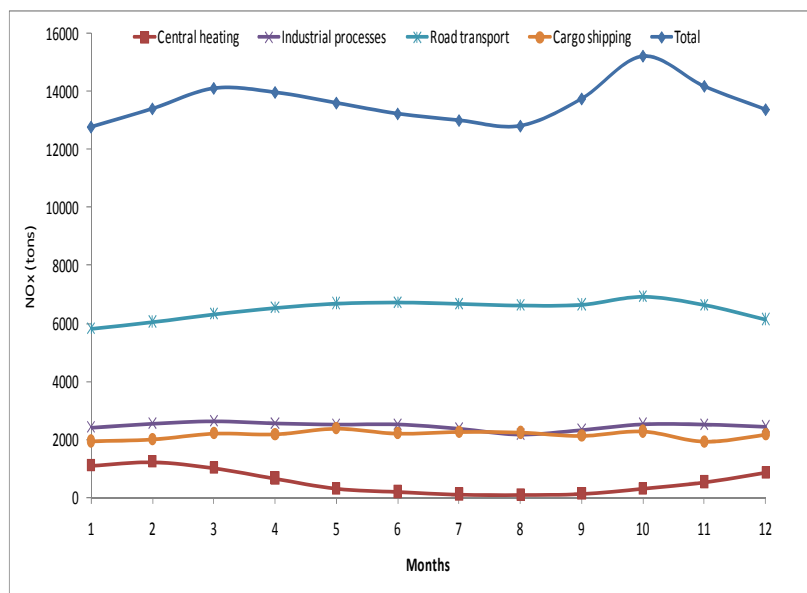


Figure 4.24. Monthly variation of NO_x emissions from central heating, industrial processes, road transport and cargo shipping.

Monthly variation of NMVOCs is presented in Figure 4.26. As stated before, the majority of NMVOCs originate from solvent use. The NMVOC emissions are produced

due to evaporation from solvents so that temperature is an important factor controlling the rate of emissions. Thus, it is expected to have higher emissions in summer period than winter and Figure 4.26 confirms this. The emission profile from road transport follows the same trend as the other road transport originated pollutants do. Finally, the monthly variation of $PM_{2.5}$ is presented in Figure 4.27. The figure clearly shows that the profile for the $PM_{2.5}$ from all sectors follows the seasonal trend again. $PM_{2.5}$ emissions from road transport, industrial processes and central heating shows similar trends as did the other pollutants.

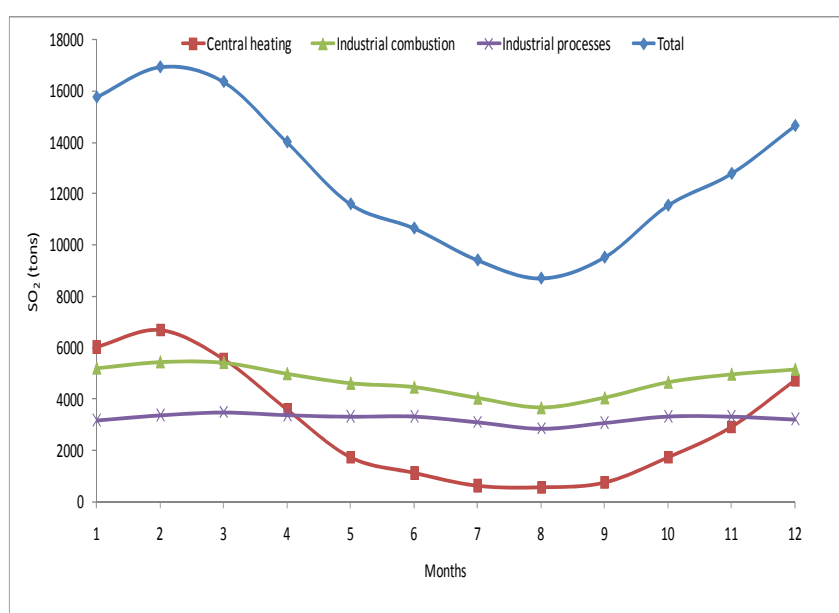


Figure 4.25. Monthly variation of SO_2 emissions from central heating, industrial combustion and industrial processes.

The variation of daily emissions is less than 1 per cent during the weekdays, while emissions drop during weekends (within 17 to 22 per cent for all pollutants in question) due to the reduced anthropogenic activity. This trend applies to all pollutants considered although the emission sectors which control the reduction as well as the relative amounts of emissions during the weekends compared to weekdays varies with the location and the period. The reduction of CO (by 17.3 per cent) is attributed to road transport (for which emissions drop about 15 per cent). For SO_x emissions the weekend reduction is larger (22 per cent) due to the reduction in the industrial sector (for which emissions drop about 25

per cent on weekends). The reduction of NMVOC presents the highest reduction (by 42%) attributed to the rapid drop of solvent use emissions. Figure 4.28 presents the daily variations of CO, NO_x, SO_x, NMVOC and PM_{2.5} emissions from the major contributors. As seen in the figure, the emissions from residential heating do not change from weekdays to weekend.

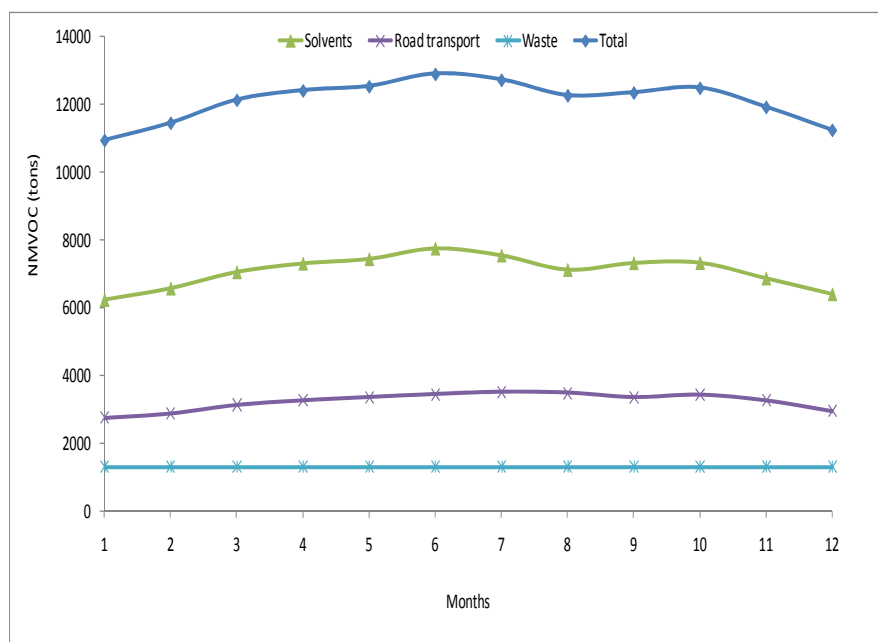


Figure 4.26. Monthly variation of NMVOC emissions from solvent use, road transport and waste disposal.

The diurnal variation of CO, NO_x, SO_x, NMVOC and PM_{2.5} are presented in Figure 4.29. As seen in the figure, the variation trends fit with the social habits: the emissions reach the maximum levels in morning hours, along with the start of traffic and residential heating. The second peak is seen at the evening hours, together with the increase of traffic, residential heating and cooking activities. As expected, the rush hours clearly affect the emissions trends in area. This effect is clearly demonstrated in Figure 4.30, where CO emissions from road transport and non-industrial combustion are presented. The maximum emissions are CO, PM_{2.5} and NMVOC emissions as seen in Figure 4.30. PM_{2.5} and CO emissions follow the above trend where as NMVOC emissions do not change much in the day time. This is due to the fact that NMVOCs are mostly released from solvent use and secondly from road transport.

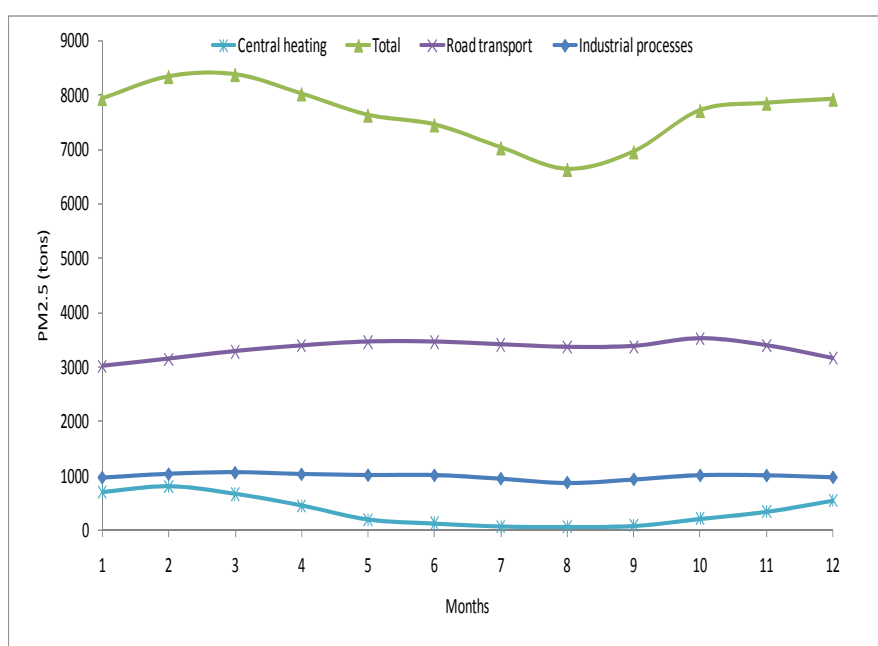


Figure 4.27. Monthly variation of PM_{2.5} emissions from central heating, road transport and industrial processes.

Regarding the quantification of combustion emissions the use of the emission factors is expected to introduce the larger uncertainties due to both the inherited uncertainty of the emissions factors as well as the selection of representative emission factors for the area. Quality rating of the emission factors used for fuel combustion emissions was tabulated in Table 3.14. The largest uncertainty is associated with the particulate matter emissions of the industrial combustion sector for which the emissions factors are classified as E in EPA's quality rating. The uncertainty associated with the appropriate selection of the emissions factors are due do limitations in the provided data e.g. there was no information regarding the share of smaller and larger boilers in the industries, the control efficiency implemented as well as the firing technique in the boilers (normal firing, tangential firing). Based on the contribution of each pollutant combustion emissions as well the fuel type contribution this deficiency is expected to affect NO_x and SO_x emissions related to coal combustion. In this study we have assumed 50 per cent use of smaller boilers and 50 per cent larger boilers with no control efficiency. In addition the use of uncontrolled emission factors for PM are expected to introduce large uncertainties. Large industrial units equipped with ESP filters are expected to have a reduced emission rate of more than 80per cent.

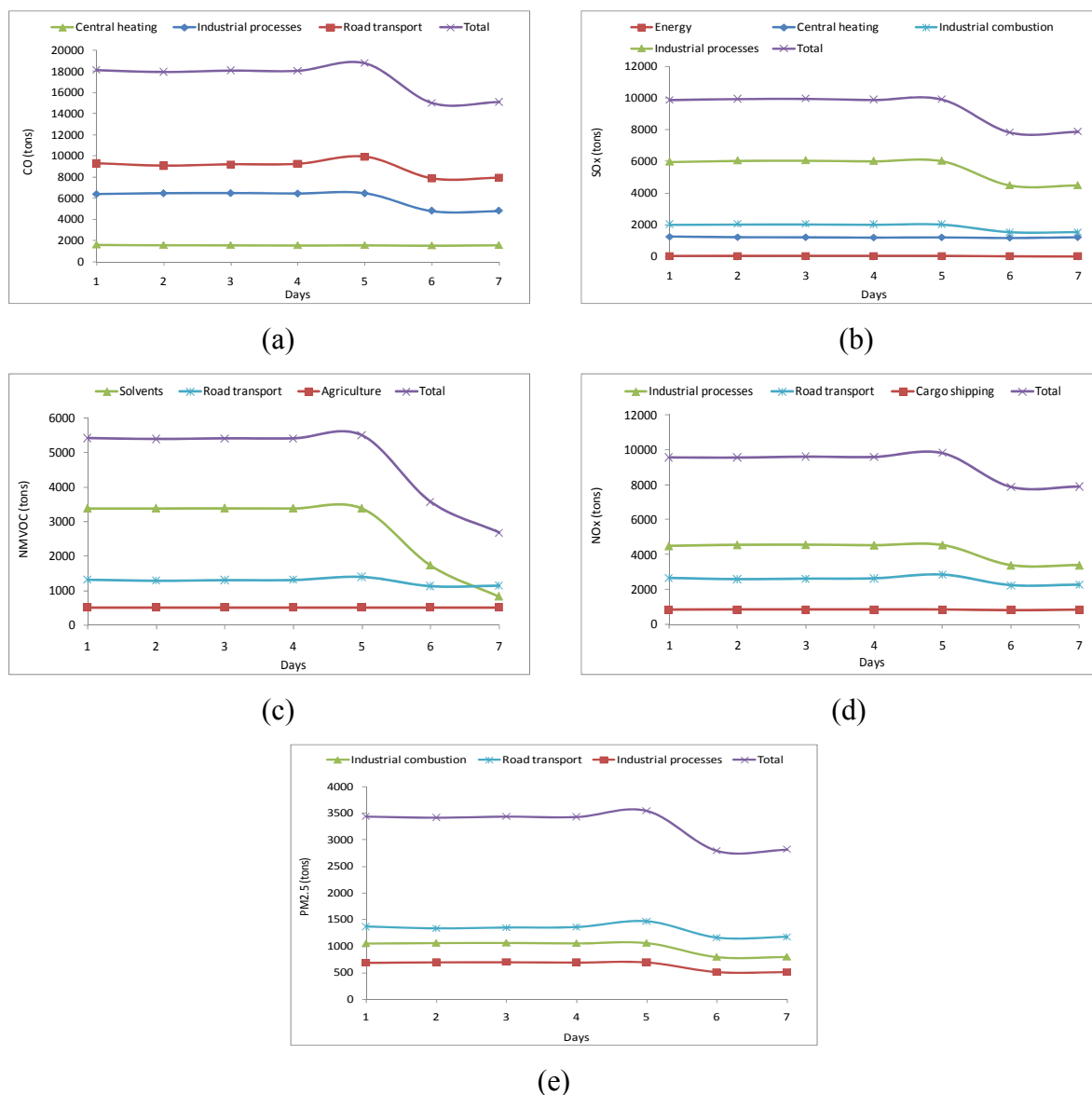


Figure 4.28. Daily variation of a) CO, b) NO_x, c) SO_x, d) NMVOC and e) PM_{2.5} from major contributors.

The uncertainties in the quantification of the maritime sector and in particular the cargo shipping emissions are mainly associated with the utilization of average daily consumption of fuel per vessel type. The latter can introduce deviations since the fuel consumption can be substantially different among vessels of the same type due to differences in the engine power output. In addition the quality rating of the emission factors used, indicate that the emission factor of NO_x (Table 3.14) which is a major source

during the cruising mode from the latter sector is considered quit reliable (in the order of 5-10 per cent) while for the less important SO₂ is in the order of 20-50 per cent.

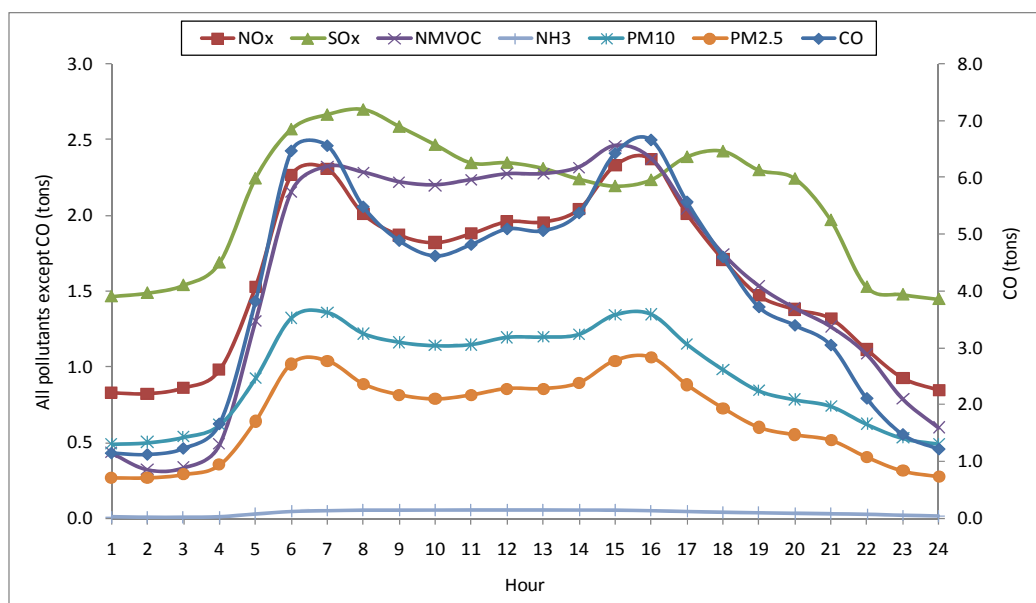


Figure 4.29. Diurnal profiles of a) CO, b) SO₂, c) NMVOC and d) PM₁₀.

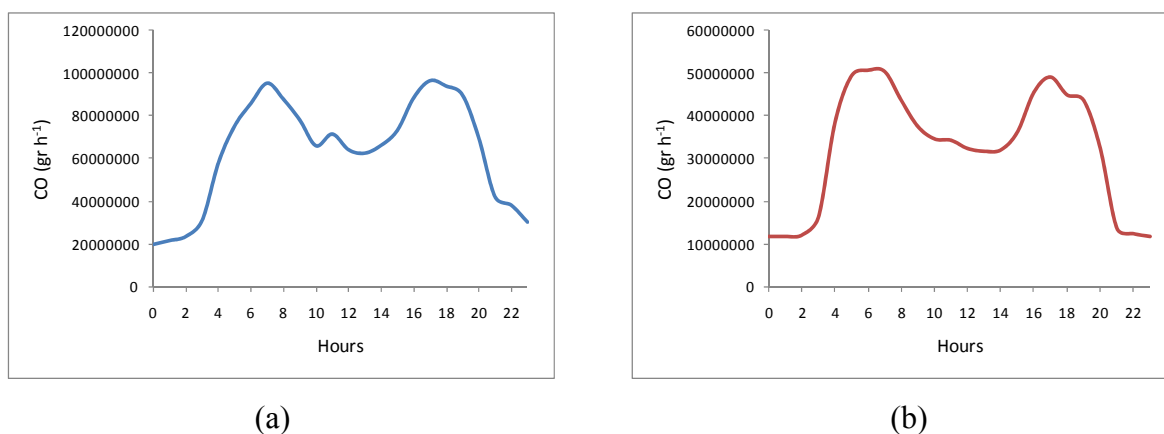


Figure 4.30. Diurnal profiles of CO from a) road transport and b) non-industrial combustion.

The quantified emissions from the use of solvents are probably lower than the expected provided that a number of emission sources are missing. According to EEA, 2001 the most important emission sources are the paint application, household products and chemical industry (Western Europe average). It is expected that a relatively large amount is

missing from the industrial application of paint. In addition, SO₂ emissions from the production processes are expected to be underestimated. The annual amount which was used in this study originating from Visschedijk et al. (2007) are not considered representative for the area being in the order of a few tons. This is probably due to the lack of reliable production statistics. Based on the İstanbul Chamber of Industry reports, 30 per cent of the industrial activities in İstanbul originate from the metal industry. Other studies have indicated the importance of the metal industry as a source of SO₂ (Pham et al., 2008). Moreover the calculated rates of SO₂ from the residential sector are expected to be lower than the real ones. The reason for the latter is the large amounts of low quality (high sulfur content) smuggled coal mostly used in the outer parts of the city center where the least developed areas are located. The latter was also reported by Çetin et al. (2007) which has developed of emission inventory for the nearby Kocaeli region.

The emission inventory compiled for the city of İstanbul is compared with other studies in the literature and the emission databases of EMEP and Visschedijk et al. (2007). The EMEP cells (in 50 km grid spacing) which cover the city of İstanbul were extracted from the on-line database for the year 2003 (Vestreng et al., 2006) in order to compare with the land emissions of this study. The comparisons show that the emissions compiled for İstanbul highly exceed the emissions of EMEP. CO emissions are calculated to be 3 times higher than EMEP (211 per cent), whereas NO_x emissions exceed by 4 times (333 per cent), SO_x emissions 4 times (291 per cent), NMVOC emissions 8 times (741 per cent), NH₃ emissions nearly 3 orders of magnitude (28,546 per cent), and PM₁₀ and PM_{2.5} by 2 times (92 and 89 per cent, respectively) (Table 4.2). Larger discrepancies are seen in the road transport sector which is calculated in this study to exceed by 6 to 16 times (NO_x to PM_{2.5}, respectively). CO emissions from residential combustion in EMEP inventory are slightly higher from the results of this study (49,014 tons to 47,465 tons, respectively), whereas SO_x emissions from this study are 35 times higher than EMEP inventory (36,133 to 1,283 tons, respectively). The EMEP value for PM emissions from residential combustion is higher than the results of this study, whereas PM emissions from other sources in this study highly exceed the EMEP emissions.

The comparison with the emissions database of Visschedijk et al., (2007) (no maritime emissions) presents much lower discrepancies than those of EMEP. The

emissions of SO_x and NH₃ between the studies are quite close (12 per cent and 9 per cent, respectively) while CO and NMVOCs emissions show differences in the order of 60 and 50 per cent, respectively. The larger discrepancies are observed for particle emissions for both modes with the emission rates of Visschedijk et al. (2007) to be 3 times less than the findings of this study.

Table 4.2. Comparison of land emissions (in tons yr⁻¹) with the other databases.

Pollutant	EMEP, 2003^a	TNO, 2003^b	This study
CO	126 728 (128 165)	221 875	344 729 (346 102)
NO _x	19 943 (23 365)	69 522	110 552 (140 814)
SO _x	10 216 (10 491)	104 231	115 995 (131 954)
NMVOC	16 536 (16 857)	95 685	108 164 (143 609)
NH ₃	23 (23)	7 266	6 505 (6 514)
PM ₁₀	37 974 (39 837)	33 022	88 650 (90 159)
PM _{2.5}	29 142 (30 906)	23 520	64 442 (66 283)

^a Data extracted for 2003 (Vestreng et al., 2006). International shipping included in the parenthesis

^b The inventory is representative for 2003 (Visschedijk et al., 2007).

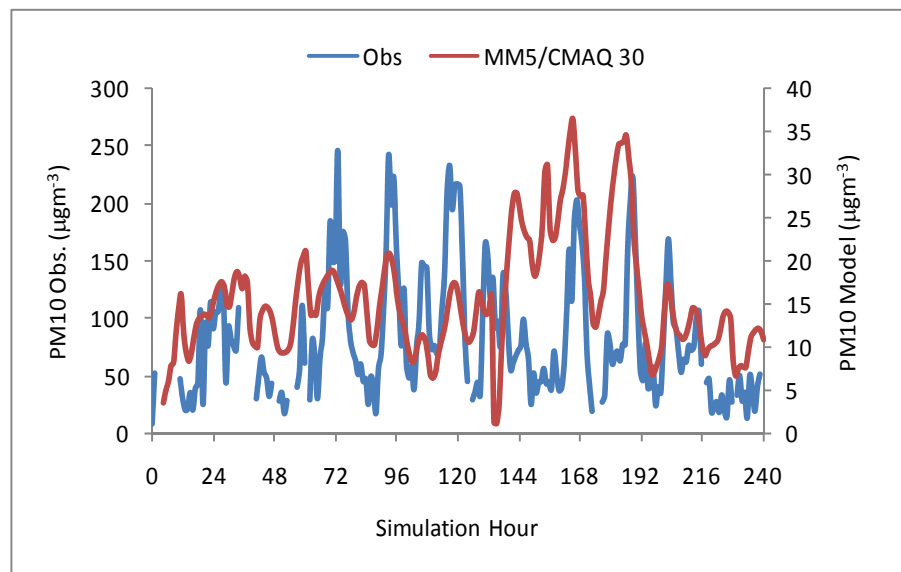
Finally, the shipping emissions calculated in this study are compared with the findings of Deniz and Durmuşoğlu (2008) and shipping database of EMEP. Deniz and Durmuşoğlu (2008) calculated the total emissions from the Marmara Sea and Bosphorus strait covering international shipping and local ferries, as well as the shipping emissions from the Çanakkale strait. The results show that the emissions calculated in this study were lower than the emissions from Deniz and Durmuşoğlu (2008), except for PM₁₀ emissions. CO emission of this study is 153 per cent lower than the findings of Deniz and Durmuşoğlu (2008), whereas NO_x are 9 per cent lower; SO_x 57 per cent lower, and NMVOC 128 per cent lower. On the other hand, PM₁₀ emissions of this study are 28 per cent higher than those of Deniz and Durmuşoğlu (2008). The comparisons with the EMEP emissions shows that the CO emissions of this study are 31 per cent lower than those of EMEP, whereas NO_x emissions are 69 per cent, SO_x 79 per cent, NMVOCs 77 per cent and PM₁₀ 79 per cent higher than the emissions of the EMEP inventory.

4.3. Chemistry and Transport Model

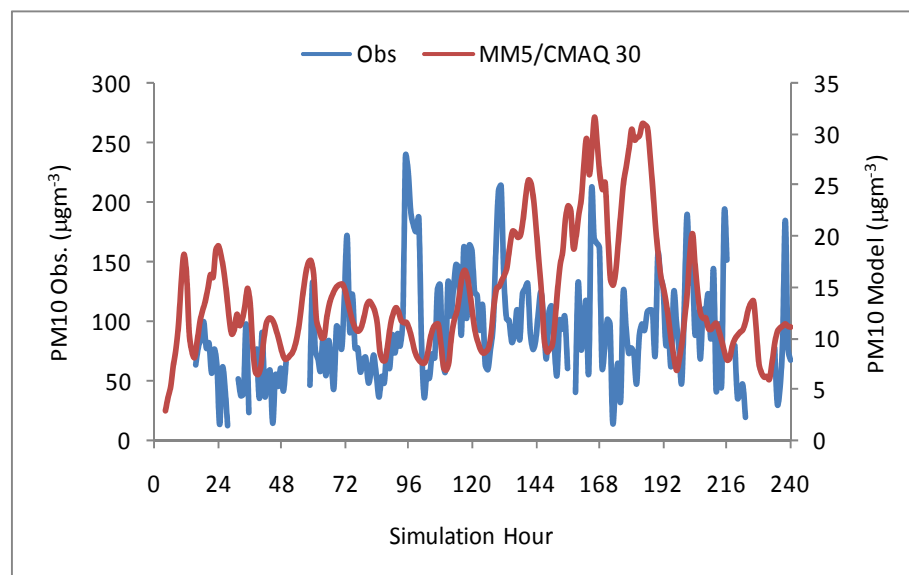
4.3.1. European and Balkan Domains

The CMAQ chemistry and transport model is run for the European domain of 30 km resolution on 163 and 150 grids at x and y axis, respectively. The model calculated PM₁₀ results are compared with Alibeyköy (28.95 latitude, 41.07 longitude) and Beşiktaş (29.01 latitude and 41.05 longitude) air quality stations on hourly basis (Figure 4.31). As seen from the figure, the model successfully simulated the hourly trends of the observed data. However, there are large differences between model results and observations in terms of magnitude. The differences between the hourly profiles mainly arise from the temporal profiles that are used for the compilation of emissions. These profiles do not particularly represent the temporal profiles of the activity levels in Istanbul, leading to shifts of variations of concentrations. The differences between the concentration values of the model and observations come mainly from the coarse resolution of the domain configuration. It should be noted that the evaluation is based on comparison of point measurements with an average value calculated for a grid cell. Thus, it is expected that the model underestimates the observed values. Similar differences were also seen between observations and modeled PM₁₀ concentrations in the study conducted by Kındap et al. (2006) using the EMEP emissions on 50 km resolution.

The simulations for the Balkan domain, covering 140 grids in x-direction and 155 grids in y-direction with a 10 km resolution did not much improve the results as expected (Figure 4.32). The emissions on 10 km resolution were compiled using surrogates to downscale 30 km resolution European emission, keeping the total amounts of emissions on the same levels. However, since the resolution of the model configuration is increased, the model calculated concentrations are expected to be better representing the actual levels. The results show that the 10 km simulation produced slightly higher PM₁₀ concentrations than the 30 km simulation; however, the results are still well below the observed concentrations.



(a)



(b)

Figure 4.31. Observed vs. modeled PM_{10} concentrations at a) Alibeyköy and b) Beşiktaş air quality stations at the 30 km resolution European domain.

Other possible reasons for differences come from the sources of emissions used in the study. It should be noted that only anthropogenic emissions are used in this study, and biogenic emissions and other natural emissions such as resuspension of dust are not taken into account. Biogenic emissions can significantly contribute to the formation of secondary

organic aerosols. Origins and types of the uncertainty of the air quality modeling can be summarized as following (Kindap et al., 2006):

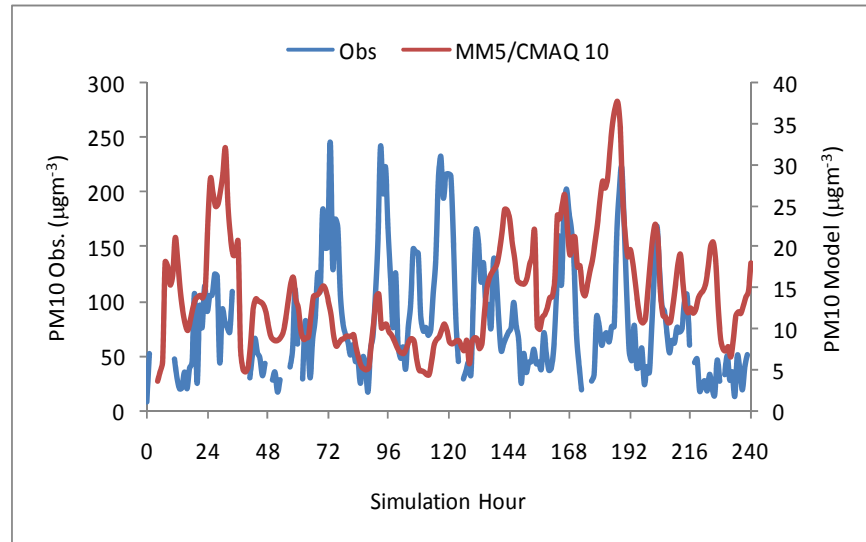
- Model uncertainty
- Emission uncertainty
- Spatial and temporal averaging
- Lumping in chemical mechanism
- Errors in measurements

The 24-hour European PM₁₀ concentrations calculated by the model for the period from 13 to 17 January, 2008 are presented in Figure 4.33. All figures clearly show the poor air quality levels over İstanbul. İstanbul is a clear hot spot considering the PM₁₀ levels in Europe, together with eastern and southern regions of Greece, particularly Athens. The central parts and western coasts of Turkey also experience high PM₁₀ levels. In order to focus closer to İstanbul and the surrounding area on the Balkan scale, the 10 km simulation results for the 24-hour PM₁₀ concentrations are presented in Figure 4.34. İstanbul and Athens are more clearly seen as important hot spots, where poor air quality levels are observed in terms of PM₁₀ concentrations. Especially, between 13 and 17 January, 2008, high PM₁₀ concentrations are simulated for the Greater İstanbul Area. The southerly wind vectors simulated by the MM5 meteorological model (Figures 4.33 and 4.34), for 14th and 15th of January, agree with the concentration distribution simulated by the CMAQ model. The relatively low wind speeds observed over İstanbul on 15, 16 and 17th of January 2008, which are also simulated by the MM5 model, lead to the accumulation of pollutants over the area. On 14th of January, higher southerly wind speeds transported the pollutants to İstanbul (Figure 4.33b and 4.34b).

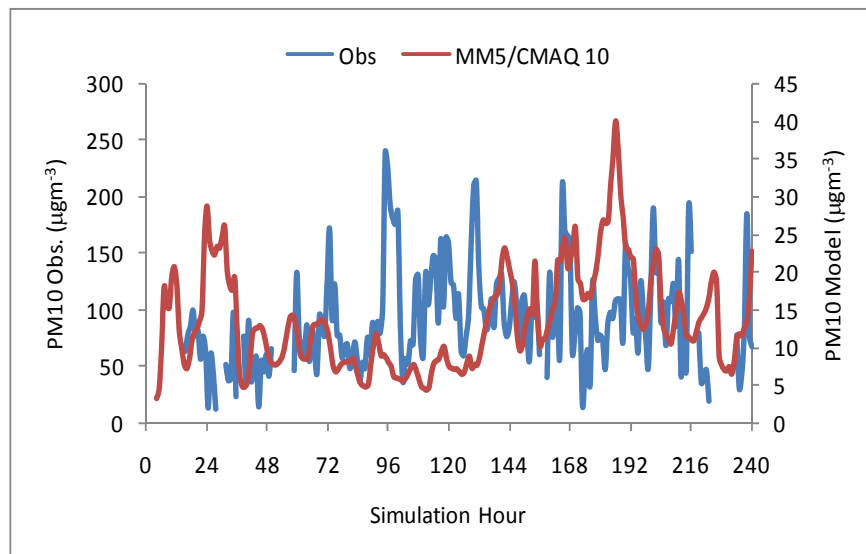
4.3.2. İstanbul Domain

This study is mainly focused on the analyses of results from this 2 km resolution domain in order to make the first evaluations of the high temporal, spatial and chemical

emission inventory developed for the Greater İstanbul Area. The boundary conditions are interpolated from each hour of the previous Balkan domain simulations and the initial conditions are taken from each time step of the previous run of the İstanbul domain.



(a)



(b)

Figure 4.32. Observed vs. modeled PM₁₀ concentrations at a) Alibeyköy and b) Beşiktaş air quality stations at 10 km resolution domains.

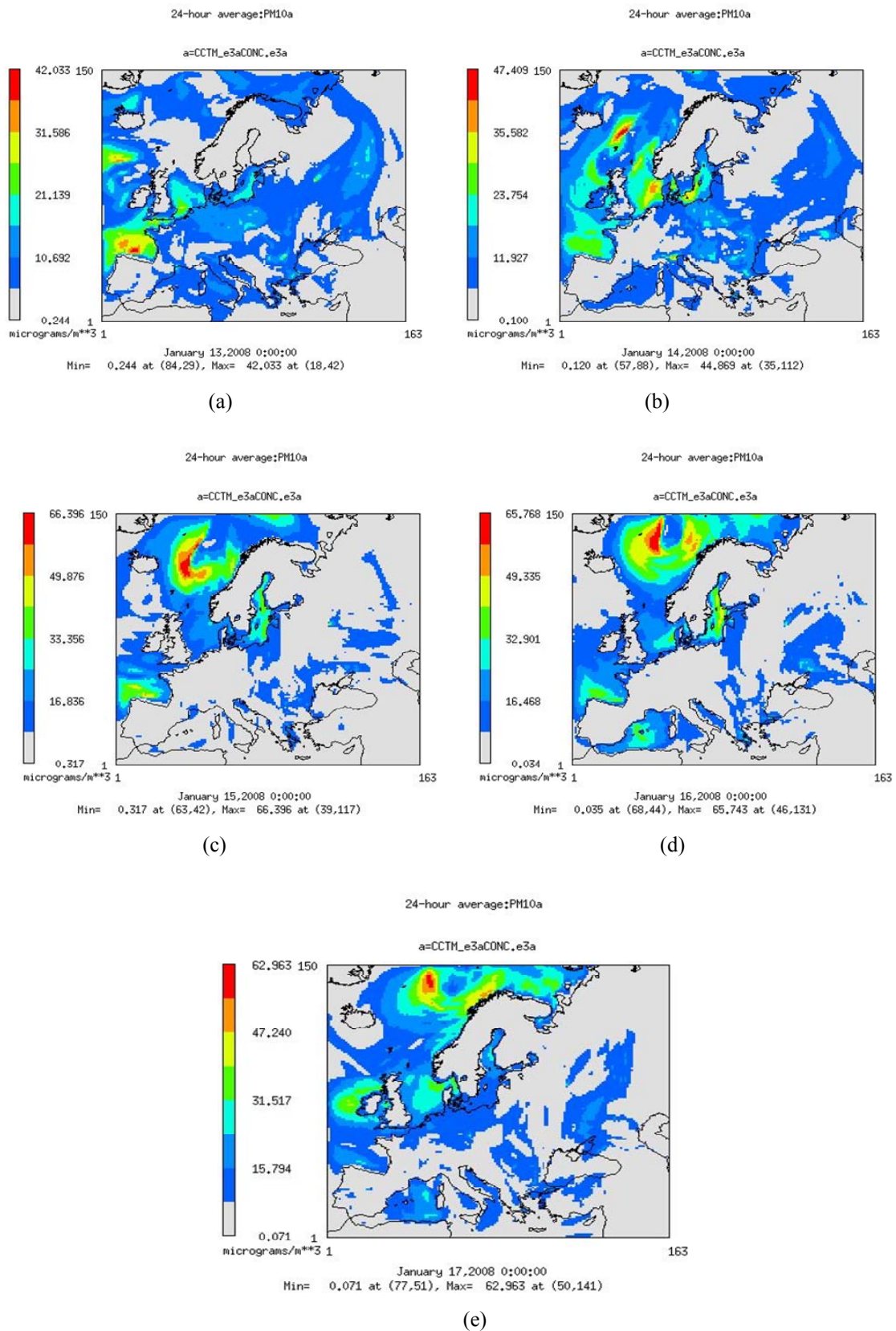


Figure 4.33. 24-hour average PM₁₀ concentrations for a) 13th, b) 14th, c) 15th, d) 16th and e) 17th of January, 2008 for the European domain.

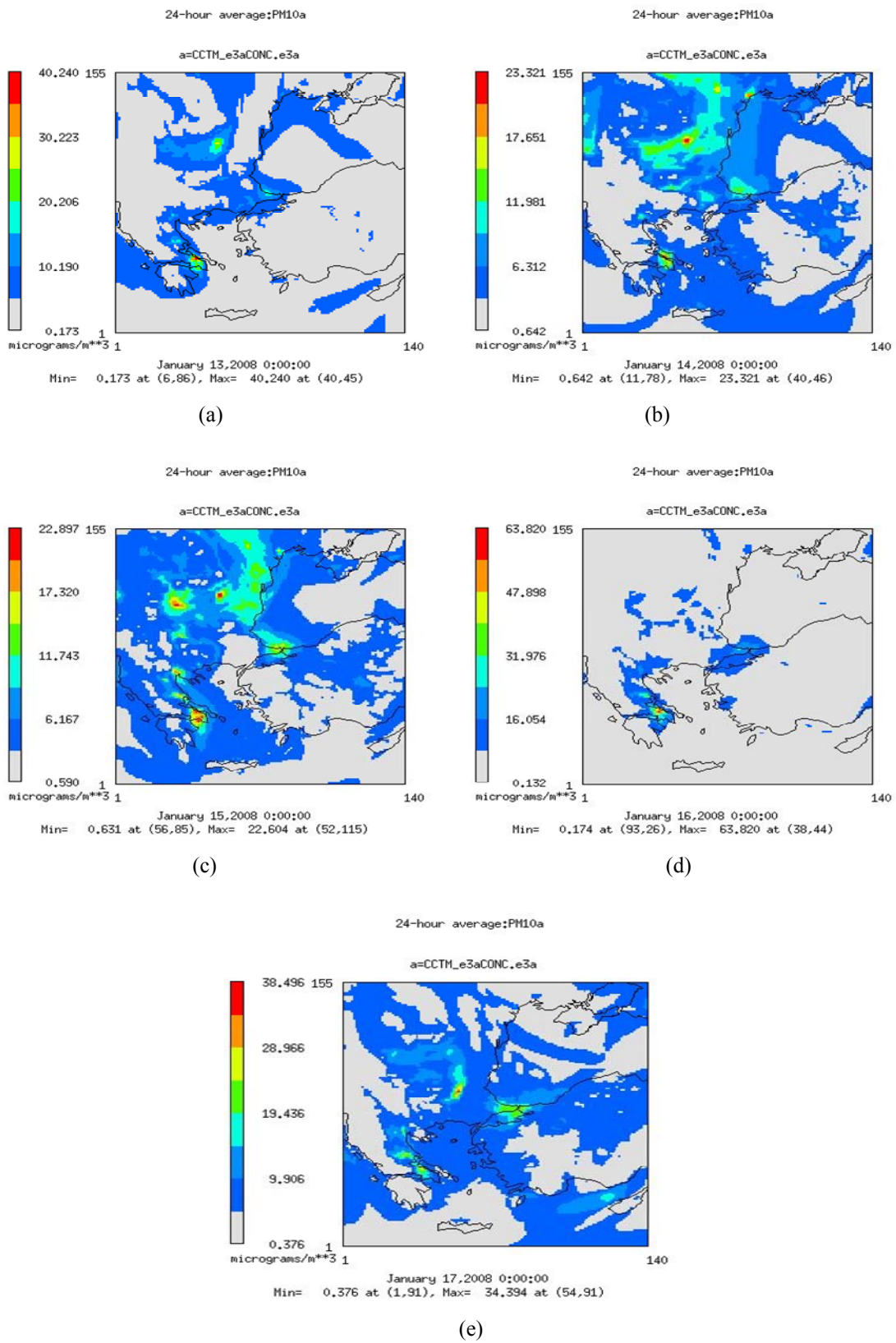
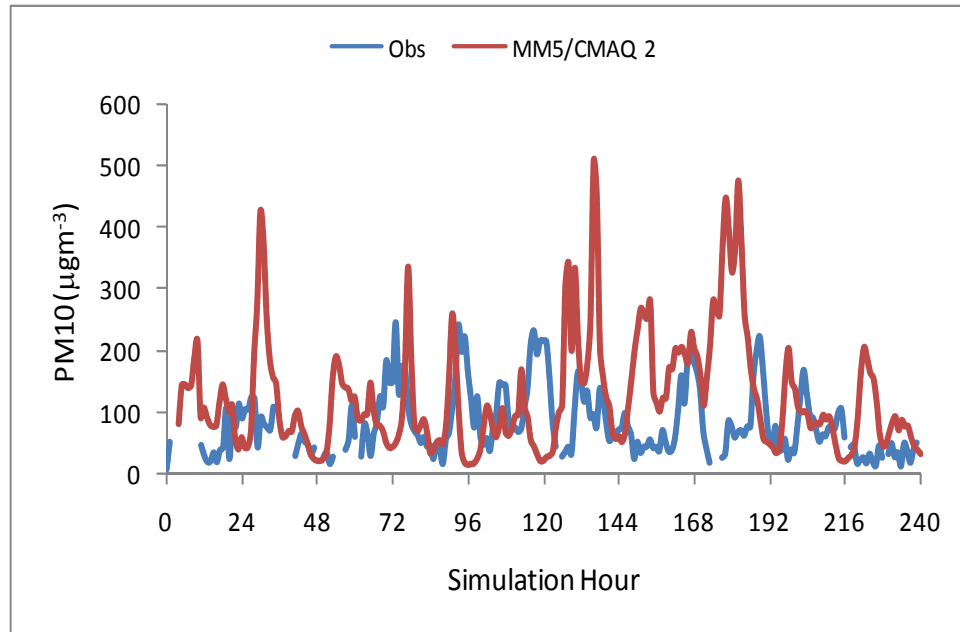


Figure 4.34. 24-hour average PM₁₀ concentrations for a) 13th, b) 14th, c) 15th, d) 16th and e) 17th of January, 2008 for the Balkan domain.

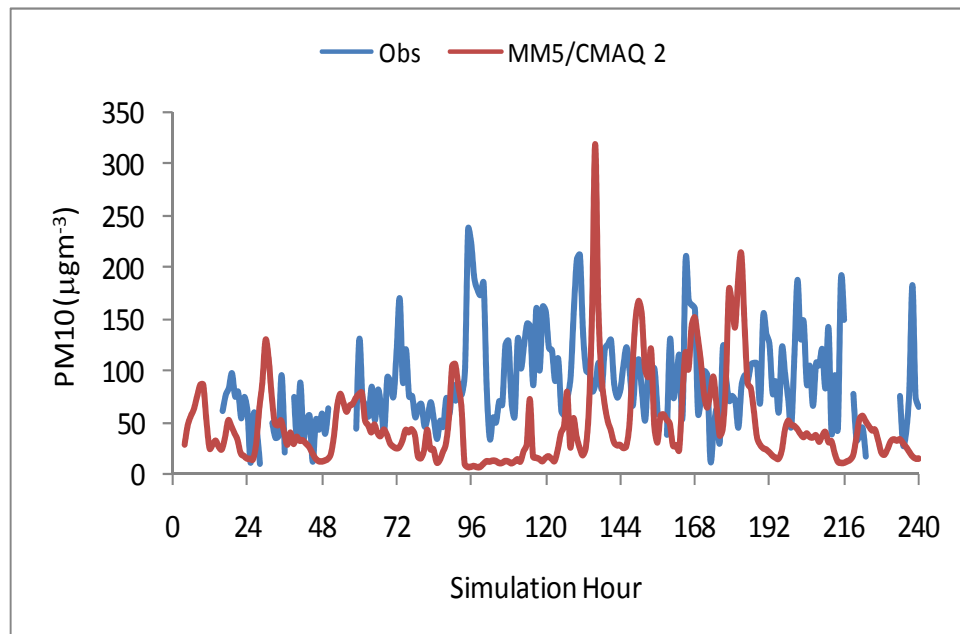
CMAQ results for İstanbul domain are compared with the observed PM_{10} concentrations measured at Alibeyköy and Beşiktaş air quality stations, as was the case for the evaluation of European and Balkan domains. The time series plots for the whole simulation period show that the concentration calculated for the İstanbul domain are more realistically estimated (Figure 4.35). The comparisons between the model and the observations for Alibeyköy stations clearly show that the model over estimated the observations whereas the Beşiktaş comparisons indicate that the model underestimated the measurements. The different biases calculated for the two different air quality stations may arise from the estimation of the high resolution emissions developed. The PM emissions from the road traffic, which represent a significant contribution to the total PM emissions, are highly uncertain due to the presence of trucks in the inventory. As there was little information for the activity levels for trucks, the emission estimates are highly uncertain. These uncertain PM emissions might be a reason for the over estimations of aerosol levels. It should be noted that aerosols from road traffic contain significant amounts of $PM_{2.5}$ than PM_{coarse} . The results showed that around 90 per cent of PM_{10} concentrations were of $PM_{2.5}$ origin, which agrees that the over estimations are most probably due to traffic emissions.

The statistical measures that were also used to evaluate the MM5 model performance are used in order to calculate the model performance. The results are presented in Table 4.3. The correlations are very poor, indicating that the trends in variations of PM_{10} concentrations do not match on hourly basis. However, it is known that modeling particulate matter by photochemical models is a challenging issue. Low agreements are frequently achieved between model results and observations (Smyth et al., 2009). This inconsistency may occur due to the temporal profiles that are used in the emission model. As discussed before, there are no studies yet to develop local temporal profiles of pollutants on sectoral bases. The profiles used in this study represent a European averaged temporal change which may not represent the conditions in Turkey. The results confirm that the model over estimated for Alibeyköy and under estimated for Beşiktaş air quality station, both around $40 \mu g m^{-3}$. The RMSE is a measure of the differences between values predicted by the model and actual observations. The results show that the error was smaller for the Beşiktaş air quality station compared to Alibeyköy air quality station. This most probably results from the spatial distribution of emissions, where Alibeyköy has higher emissions compared to Beşiktaş. As seen in the Table, the IOA values are around 25 per

cent, indicating a poor agreement. However, the mean and standard deviation ratios between the model results and the observations show that in terms of magnitude, the model successfully simulated the observations.



(a)



(b)

Figure 4.35. Observed vs. modeled PM₁₀ concentrations at a) Alibeyköy and b) Beşiktaş air quality stations at 2 km resolution domain.

Table 4.3. Statistical comparison of model results against observations for the İstanbul domain.

Measures	Alibeyköy	Beşiktaş
Correlation	0.11	0.05
Observed Mean	81.74	89.24
Model Mean/Obs. Mean	1.53	0.54
Observed STDEV	53.87	44.52
Model STDEV/Obs. STDEV	1.76	0.96
BIAS	44.49	-40.8
ABSE	87.69	59.7
RMSE	123.56	75.9
R1	0.51	-0.64
R2	0.71	0.79
IOA	0.24	0.25

24- hour average concentration distribution maps of PM₁₀ (Figure 4.36) show that the highest PM₁₀ concentrations are calculated for the region surrounding Alibeyköy area. This mainly arises from the spatial distribution of emissions developed for the Greater İstanbul Area. The emission maps from various source categories indicate that the area around Alibeyköy and İkitelli are hot spots for most of the pollutants. İkitelli area is the largest industrial combustion source as discussed before. Industrial combustion is an important contributor to elemental carbon emissions, which agrees with the model calculated concentration contributions listed in Table 4.4.

The samplings at Boğaziçi University were conducted for 24-periods, from 1100 LST each day to 1030 LST next day. However, due to the lack of a continuous PM₁₀ measurement system, hourly profiles are not available. Thus, in order to compare between model system and observations, 24-hour averages are calculated from the model results for the above hour intervals for PM₁₀, SO₄²⁻, NO₃⁻ and NH₄⁺. Figure 4.37 presents the comparison of the model calculations and observations of PM₁₀. It is clearly seen that the model produced a second peak on January 16, 2008, whereas the observations do not show

such a peak. The correlation factor calculated for this period is 0.62, which points to a moderate agreement between the model and observations. It is also clear that the model underestimates the observations. It is important to note that statistical measures for such a short period and number of data may not represent the overall performance of a model. Additionally, it is known that some of the VOCs from biogenic sources, such as monoterpenes, can be oxidized by hydroxyl radicals (OH), nitrate radicals (NO₃) and ozone (O₃), and directly take part in the secondary organic aerosol (SOA) formation processes. Others can indirectly affect SOA formation in the air (Kulmala et al., 1998, Griffin et al., 1999). Nitric oxide (NO), resulting from nitrifying bacteria activities in the upper few centimeters of soil, is another chemical that can affect the atmospheric chemistry. In addition to anthropogenic sources, emissions from biogenic sources can contribute to PM pollution. Thus, the underestimation in the results might be decreased by adding the biogenic emissions to the system.

The amounts of contribution of each chemical specie on model calculated PM₁₀ levels are presented in Table 4.4. The table shows that primary anthropogenic organic carbon constitutes 36.67 per cent of the PM₁₀ simulated by the model. Elemental carbon is the second main contributor with 21.40 per cent. Primary PM_{2.5} is the third largest source for simulated PM₁₀ concentrations with 18.15 per cent and sulfate aerosols are the fourth main contributors with 13.86 per cent each. Ammonium aerosols with 4.02 per cent and nitrate aerosols with 3.33 per cent are also important aerosol species in the region. The largest source for the primary anthropogenic organic carbon and elemental carbon is calculated to be road traffic, which confirms that the concentration contributions presented in Table 4.6 are traffic induced concentrations. Figure 4.13 shows that organic and elemental portions of both PM₁₀ and PM_{2.5} come from road transport. Industrial combustion is also an important contributor of elemental carbon, which has the second largest share in model calculated aerosol concentrations. Ikitelli industrial region is the hot spot for industrial PM emission sources as was seen in Figure 4.17.

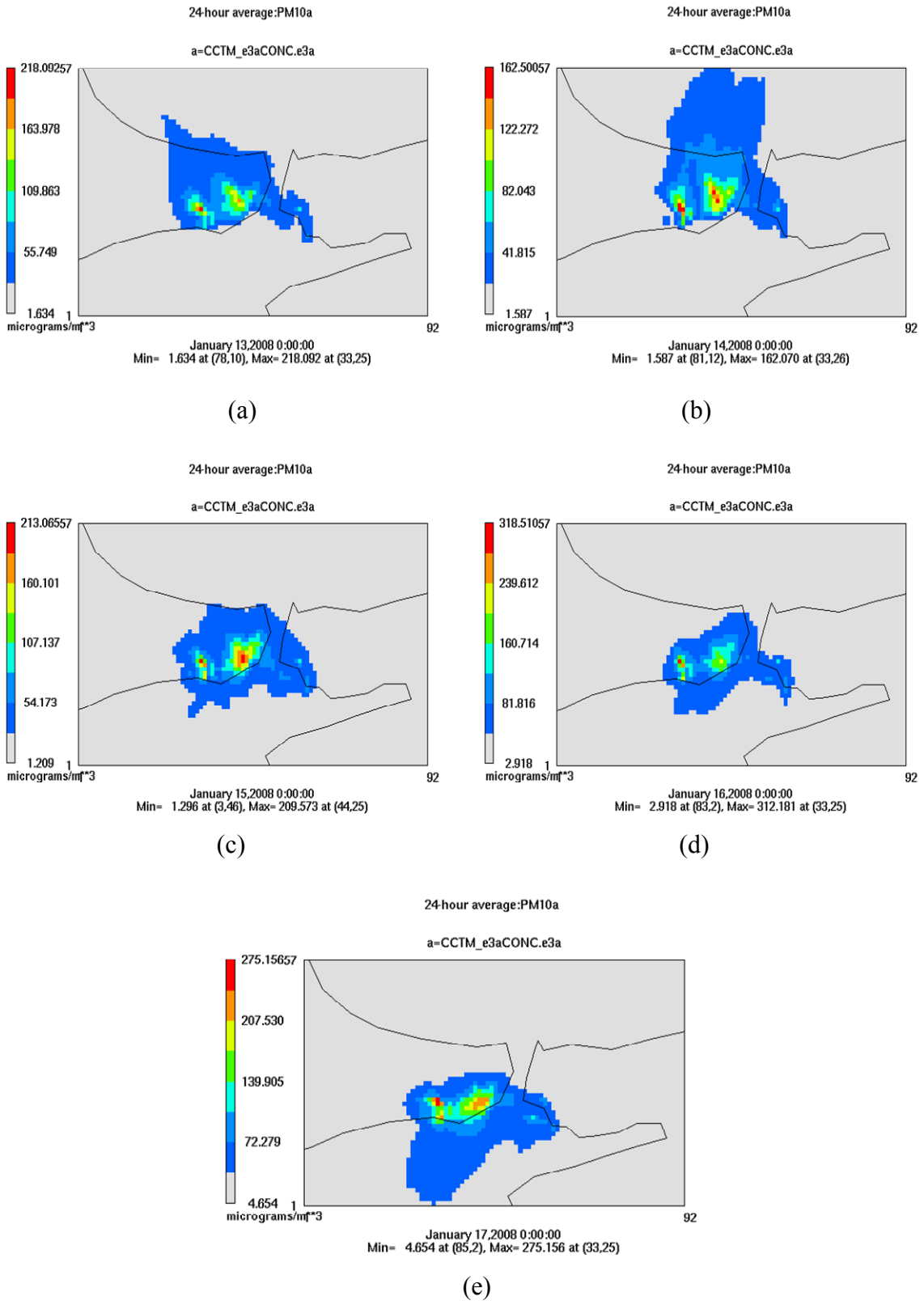
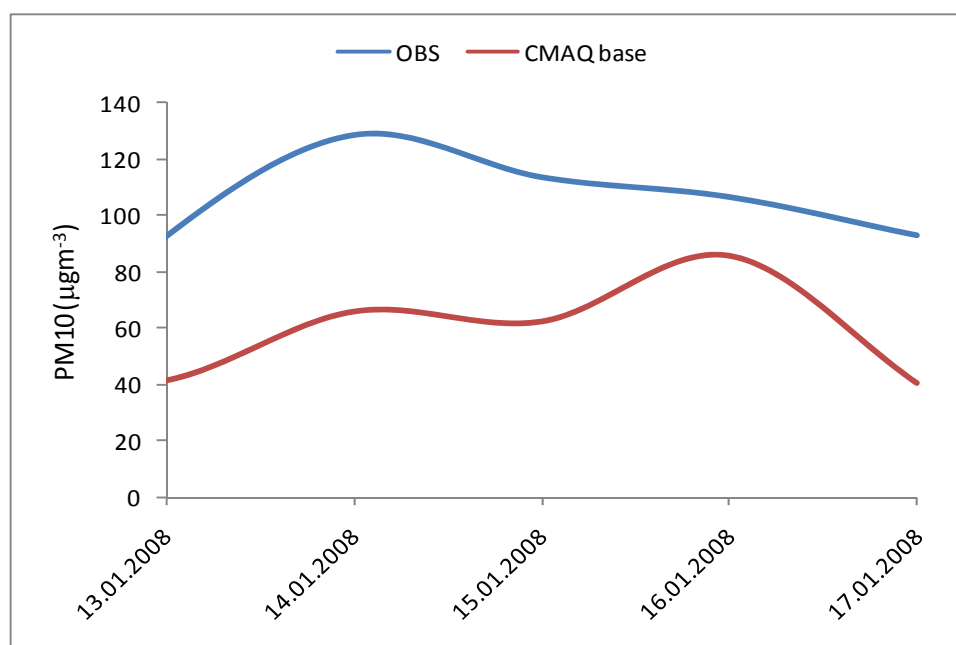


Figure 4.36. 24-hour average PM₁₀ concentrations for a) 13th, b) 14th, c) 15th, d) 16th and e) 17th of January, 2008 for the İstanbul domain.

Table 4.4. Per cent contributions of aerosol species to PM₁₀ levels.

Aerosol Species	Contribution (%)
Primary Anthropogenic Organic Aerosols	36.67
Elemental Carbon	21.40
Primary PM _{2.5}	18.15
Sulfate Aerosols	13.86
Ammonium Aerosols	4.02
Nitrate Aerosols	3.33
Soil – derived Aerosols	1.39
Chloride	0.45
Sodium	0.39
Coarse – mode Aerosols	0.05
Anthropogenic Organic Aerosols	0.28
Biogenic Organic Aerosols	0.02

Figure 4.37. Model results and observation for PM₁₀ at Boğaziçi University from 13 to 17 January, 2008.

In Figure 4.38, the 24-hour averaged sulfate aerosol levels (SO_4^{2-}) calculated by the MM5/CMAQ modeling system are compared with the observations. The same second peak is also valid for the sulfate part of the samples. However, there is also a slight peak in the observed values of sulfate aerosol. Although this peak represents the highest sulfate level in the period, the trend in the increase is not as sharp as the model simulated. The correlation coefficient calculated for the period is 0.87, which shows that the trend is well captured. On the other hand, the model underestimated the observation between January 13 to 15, whereas it overestimated for January 16 and 17, 2008. It is known that sulfate aerosol production in gas phase occurs at a slow rate whereas very rapid sulfate formation occurs in aqueous phase (Seinfeld and Pandis, 1998; Redington et al., 2002). Sulfate aerosols are generated by reaction of dissolved SO_2 with either ozone or hydrogen peroxide. The ozone pathway is limited by the cloud pH, however hydrogen peroxide can be rapidly used up in aerosol production. Thus, it is possible that the MM5 model produced overestimated clouds, increasing the amount of sulfate generated through aqueous phase.

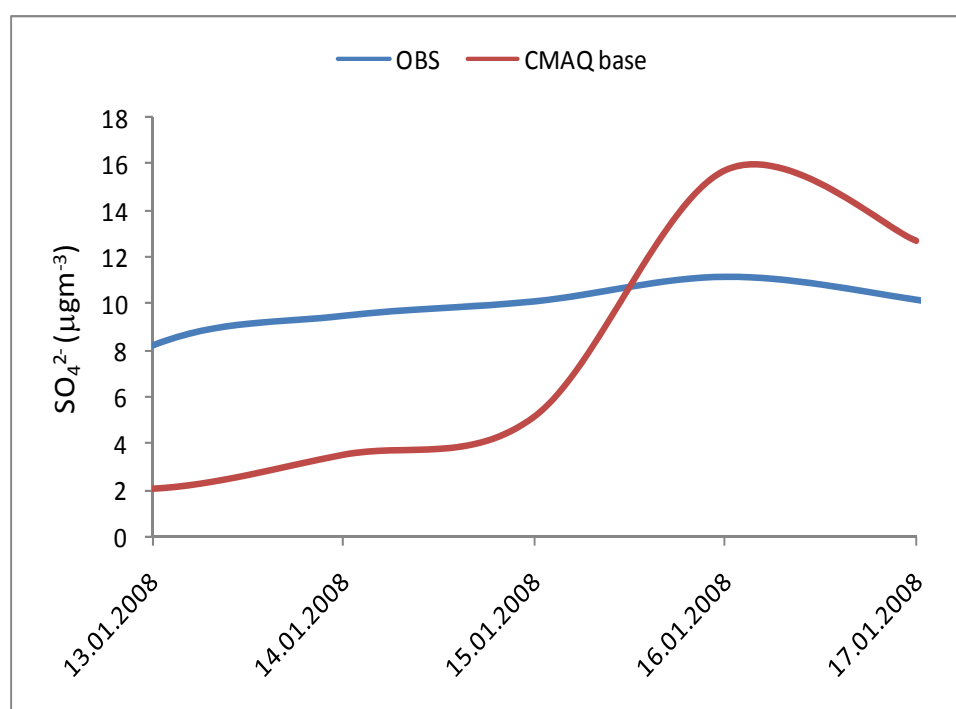


Figure 4.38. Model results and observation of SO_4^{2-} aerosols at Boğaziçi University from 13 to 17 January, 2008.

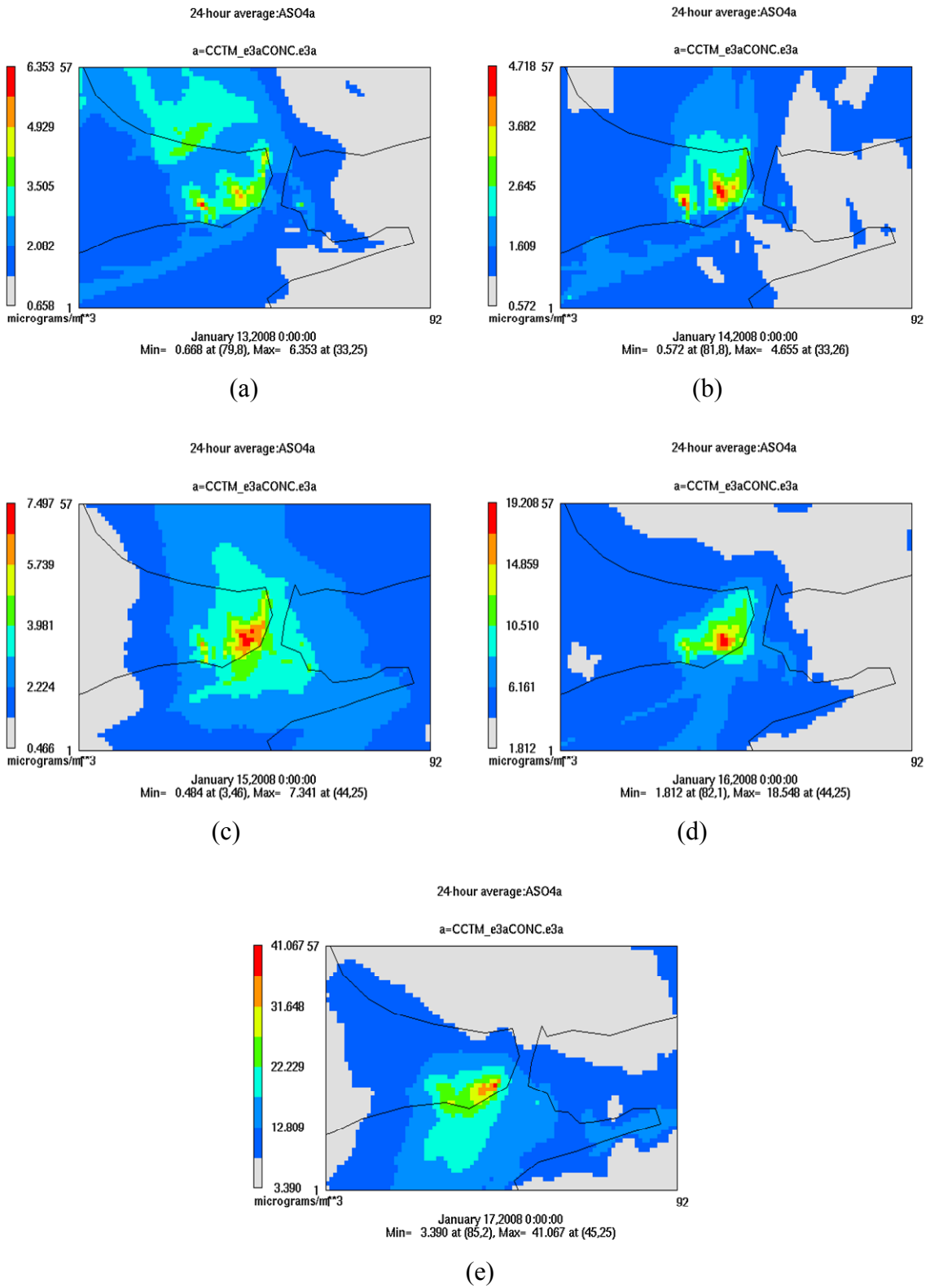


Figure 4.39. 24-hour average sulfate (SO_4^{2-}) concentrations for a) 13th, b) 14th, c) 15th, d) 16th and e) 17th of January, 2008 for the İstanbul domain.

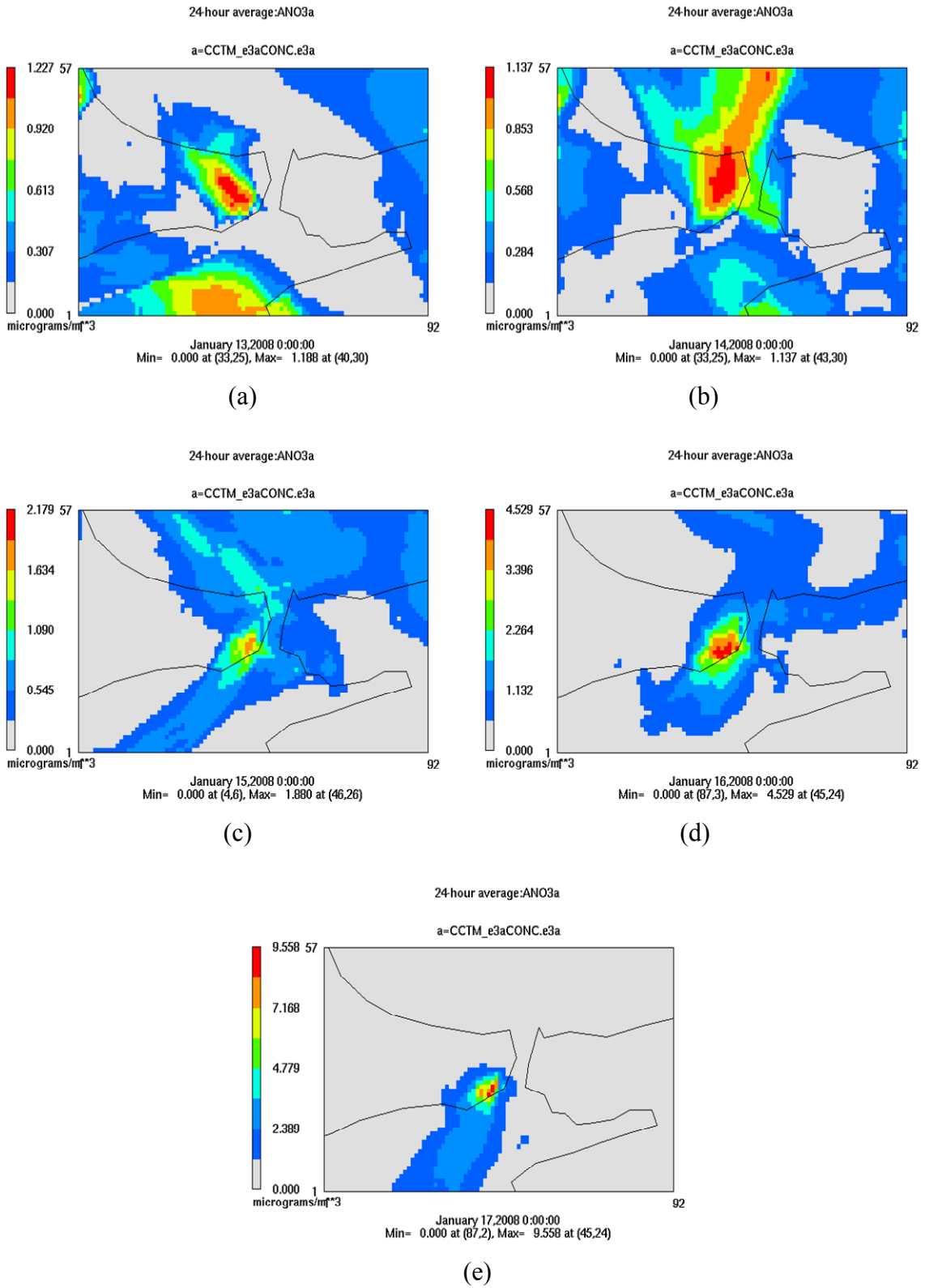


Figure 4.40. 24-hour average nitrate (NO_3^-) concentrations for a) 13th, b) 14th, c) 15th, d) 16th and e) 17th of January, 2008 for the İstanbul domain.

Figure 4.39 shows the spatial distribution of sulfate aerosols for the period between January 13 and 18, 2008. The figures show hot spots around Alibeyköy and İkitelli. This also shows that industrial combustion, which has the second largest share in elemental carbon leads to the increased concentrations in this regions. The southerly transport of aerosols on 13th, 14th and 15th of January, and northerly transport on 17th of January are clear in the figure. However, on 16th of January, the dispersion is not as large as of the other days. These poor dispersion conditions lead to the formation of highest concentrations that are produced by the model. Similar daily spatial distributions are also calculated by model for nitrate aerosols, showing maximum concentrations around Alibeyköy region (Figure 4.40).

In Figure 4.41, the daily variation of nitrate aerosol levels calculated by the modeling system is compared with the observations between 13 and 17 January, 2008. The peak concentrations observed on January 16th, and the trend is well reproduced by the model, however it is under estimated. On the other hand, the increase on 14th of January is not correctly simulated by the model. The correlation coefficient calculated for the period is 0.77, which shows good agreement between model and observations. The spatial distribution of nitrate aerosols for the same period is presented in Figure 4.40.

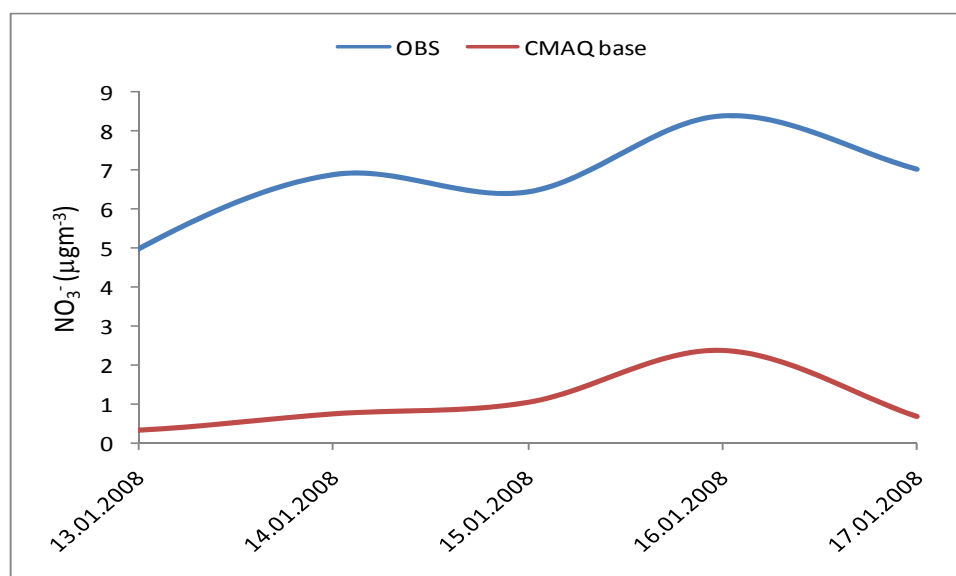


Figure 4.41. Model results and observation of NO_3^{2-} aerosols at Boğaziçi University from 13 to 17 January, 2008.

Finally in Figure 4.42, the daily variation of ammonium aerosol levels (NH_4^+) calculated by the MM5/CMAQ modeling system are compared with the observations for the same period. The correlation coefficient calculated for the period is 0.68, which points moderate agreement between model calculations and observations. On the other hand, the model also under estimated the observations. In Figure 4.43, the spatial distribution of 24-hour averaged ammonium aerosol levels are presented. As discussed before, ammonia is mainly emitted from solvent use so that the highest concentrations also occur in central parts of the city area. The temporal distribution of aerosol species points out that the second peak of PM_{10} concentrations (Figure 4.37) comes mainly from the sulfate estimation of the model (Figure 4.38). Particularly nitrate concentrations produced by the model match well with the observations regarding the timing of the maximum concentrations (Figure 4.41).

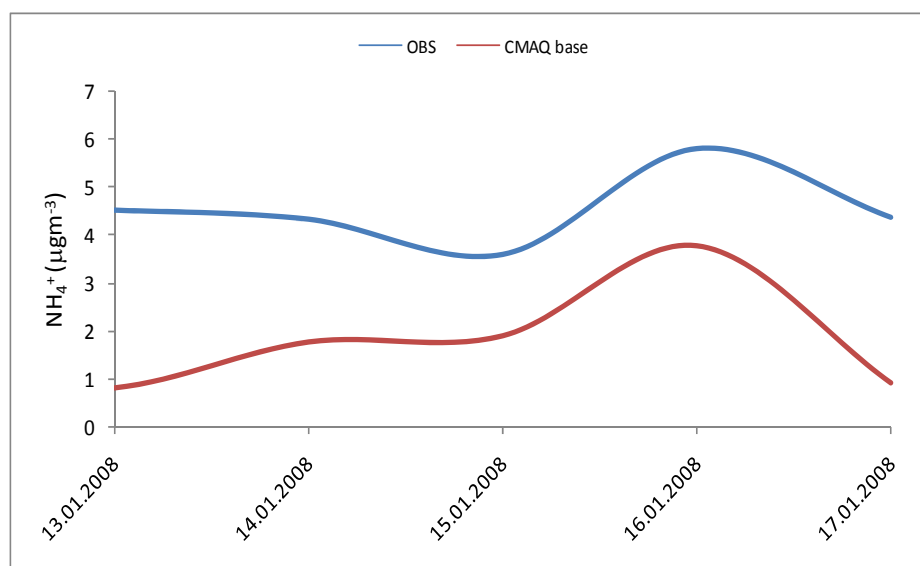


Figure 4.42. Model results and observation of NH_4^+ aerosols at Boğaziçi University from 13 to 17 January, 2008.

The comparison between 24-hour averaged CMAQ results and observations from the Boğaziçi University sampling station is presented in Table 4.5. The results show reasonable agreement between model and observations. The correlation factors are particularly high for sulfate and nitrate species (0.85 and 0.86, respectively). On the other hand, the model results are negatively biased for all aerosol species. The underestimations

of the observations are clear from the mean and standard deviation ratios as well as the BIAS values calculated. The IOA values indicate moderate agreement between the model results and observations. The results overall show that although there are differences that was discussed above, the model captures the trends and magnitudes. On the other hand, particularly the hourly profiles compared poorly with the observations, possibly resulting from the temporal profiles used in the emission processing kernel.

Table 4.5. Statistical results for comparison of CMAQ results with observation for Boğaziçi University station.

Measures	PM ₁₀	SO ₄ ²⁻	NO ₃ ⁻	NH ₄ ⁺
Correlation	0.62	0.85	0.86	0.68
Observed Mean	107.1	9.8	6.8	4.5
Model Mean/Obs. Mean	0.55	0.80	0.12	0.41
Observed STDEV	15.14	1.08	1.22	0.80
Model STDEV/Obs. STDEV	1.42	5.04	0.58	1.50
BIAS	-46.68	-1.98	-5.93	-2.69
ABSE	46.68	4.29	5.93	2.69
RMSE	50.69	4.54	5.96	2.80
R1	-1.00	-0.41	-1.00	-1.00
R2	0.96	0.95	0.99	0.96
IOA	0.38	0.43	0.24	0.27

4.3.3. Sensitivity Analyses

Various scenarios are simulated in order to understand the response of aerosol levels to changes in emissions of different chemical species. These scenarios can give ideas on how the PM₁₀ levels may response to emission changes in control strategy point of view. In Figure 4.44, the spatial distribution of percentage changes of PM₁₀ levels in response to 10 per cent increase of all emissions is presented. As expected, in response to increase in emissions, PM₁₀ level also increased ranging from -1.395 to 11.302 $\mu\text{g m}^{-3}$ (Table 4.6).

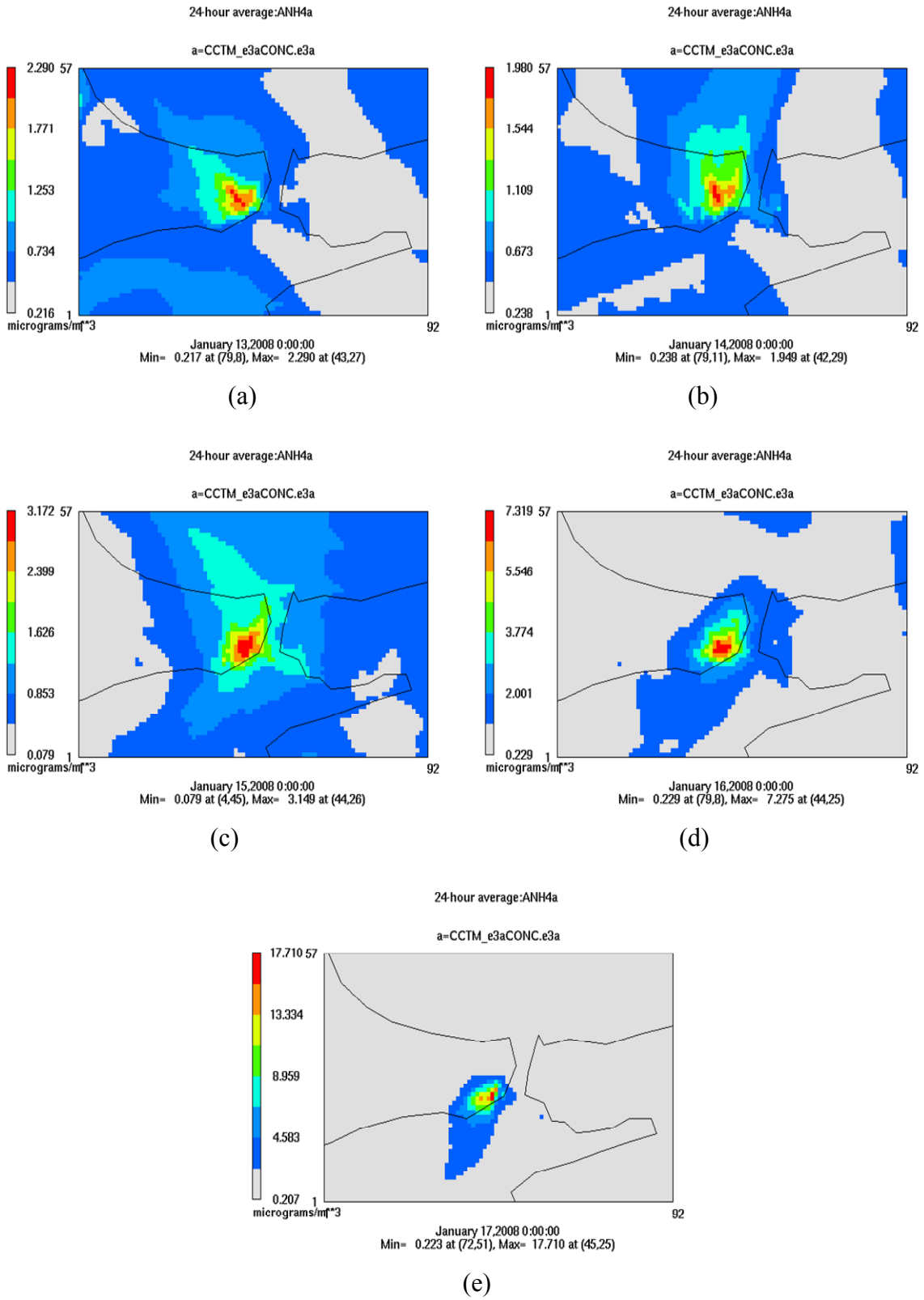


Figure 4.43. 24-hour average ammonium (NH_4^+) concentrations for a) 13th, b) 14th, c) 15th, d) 16th and e) 17th of January, 2008 for the İstanbul domain.

The highest increase occurs in the city centers around the coastal area where most of the population is located. In Figure 4.45, the change of PM₁₀ concentrations in response to a 10 per cent decrease reduction in all emissions is presented. The results are similar with the 10 per cent increase scenario, with highest decrease in concentration occurring in the city centers.

The spatial response of 24-hour averaged PM₁₀ concentrations to 10 per cent increased and reduced emissions of all pollutants, SO₂ alone, NO_x alone, NH₃ alone and finally VOCs alone, for the whole domain are presented in Figures 4.44 to 4.53. Figure 4.44 shows that the PM concentrations responded highest to the changes in all emissions (Figure 4.44a). The changes occurred in the same direction as the direction of change in the emissions. This result is expected due to the fact that the changes in the emissions are only on magnitudes of the emitted species. However, due to the complex chemistry, the rate of response to these changes also varies with time, as also seen in Table 4.6. The table shows that the highest increase of PM₁₀ concentrations of 8.53 per cent occurred due to the 10 per cent change in all emissions. Similarly, the highest reduction of -8.52 per cent occurred with the reduction of all emissions. The second highest change in PM₁₀ concentrations occurred in the case of SO₂ increase, with a per cent change of 3.28. The increase of SO₂ concentrations most effectively increases the sulfate aerosol concentrations by 11.11 per cent (Table 4.6). On the other hand, this increase leads to a very high reduction of nitrate aerosols, by 27.74 per cent. This results from the complex chemistry between nitrogen (N) and sulfur (S) species (Smyth et al., 2006; Phillips and Finkelstein, 2006). Sulfate and nitrate are converted from gas to aerosol phase by reacting with ammonium to produce ammonium sulfate (NH₄SO₄) and ammonium nitrate (NH₄NO₃) aerosols. On the other hand, ammonium reacts with sulfate at the first place. By increasing SO₂ emissions, the complex chemistry is fed by more S species, leading to production of NH₄SO₄ aerosols and thus, a decrease in gas-to-particle conversion of nitrate, reducing the nitrate (NH₄NO₃) aerosols. Similarly, decreasing the SO₂ emissions leads to a 17.36 per cent of nitrate aerosols. Similar research was done by Kindap et al. (2006) through increasing and reducing anthropogenic emissions by 50 per cent on regional scale covering Bulgaria, Romania, Poland, Ukraine, Russia, Hungary, Slovakia, Moldova, Belarus, Lithuania, Latvia and Estonia. The results showed an average increase 12 per cent response to increasing of emissions and 9 per cent to the reduction of emissions. The study

demonstrated clearly that the transport from Eastern Europe may significantly affect the PM₁₀ levels in İstanbul.

A very remarkable change occurs by the decrease of nitrate aerosols by -30.20 per cent because of a 10 per cent decrease in all emissions. This results from a reduction of availability of ammonium, nitrate and sulfate species, leading to the limitation of gas-to-particle conversion. A similar change occurs in the NH₃ change scenario. A 10 per cent increase of NH₃ emissions leads to a 46.92 per cent increase of nitrate aerosols whereas the same amount of decrease reduces nitrate aerosols by 38.87 per cent (Table 4.6). These changes also make ammonium aerosols increase and decrease around 6.80 per cent, which is expected because of the ammonia to ammonium conversion in the atmosphere. This shows that the nitrate levels are very sensitive in changes of S and particularly N emissions in the area.

The figures clearly demonstrate that the most visible changes occur with the change of all emissions (Figure 4.44a). Changes in SO₂ emissions also affected the PM₁₀ levels (Figure 4.44b). The figure also shows that changes in anthropogenic VOCs do not affect PM₁₀ concentrations. However, it should be noted that biogenic VOCs may have significant affect to PM levels through formation of secondary aerosols (Kulmala et al., 1998, Griffin et al., 1999).

The highest change in sulfate aerosol concentration (11.11 per cent) occurs due to an increase of SO₂ emissions (Table 4.6). Increasing all emissions leads to an increase of sulfate aerosols by 4.97 per cent, NO_x by 5.51 per cent, NH₃ by 2.79 per cent and anthropogenic VOCs by 0.17 per cent. The nitrate aerosol concentrations respond in a wide range and high variations (Table 4.6). The highest changes occur due to the changes in emissions of all pollutants (31.92 per cent), and NH₃ emissions (46.92 per cent). Additionally, the only significant response due to the changing of anthropogenic VOCs occurs for nitrate aerosols (5.95 per cent). Finally, the response of ammonium aerosols to the emission scenarios shows similar results with nitrate responses. The highest change occurs with the increasing of all emissions (by 7.99 per cent) and NH₃ emissions, as expected (6.79 per cent). The changes due to changing of SO₂ emissions and NO_x are calculated to be 3.77 and 2.85 per cent, respectively.

Reducing ammonia emissions reduces nitrate, sulfate and ammonium at both the upwind and downwind sites as seen in Table 4.6 (Morris et al, 2003). The table shows that both nitrate and sulfate concentrations decreased with decreasing ammonia emissions. Nitrate is reduced because there is less ammonia to combine with nitrate acid so less ammonium nitrate forms. Sulfate is reduced because there are more acidic water droplets due to less buffering by ammonia that inhibit aqueous sulfate production. Ammonium reductions are associated with both the nitrate and sulfate reductions. Reducing VOC emissions reduces organic matter, which also includes secondary organic aerosols, at both the upwind and downwind sites, leading to decreases in sulfate and nitrate concentrations as seen in Table 6. At the downwind site, reducing VOC emissions also reduces ammonium nitrate due to the reduced photochemical activity that lowers the production of nitric acid from NO_x .

Reducing NO_x emissions increases ammonium nitrate at the upwind site and decreases ammonium nitrate at the downwind site, as seen in Figure 4.49. Figure 4.49e shows that with the southerly winds, PM_{10} concentrations increase on downwind direction (northern parts of İstanbul) and decrease on upwind direction. This demonstrates that fundamental differences can exist between the NO_x –nitrate relationships at different sites, similar to well-known differences in ozone– NO_x relationships. The upwind increase in ammonium nitrate is explained by more rapid nitric acid production when NO_x emissions are reduced, i.e., nitric acid production is NO_x inhibited at the upwind site in the base case. The downwind decrease in ammonium nitrate is explained by lower nitric acid production when NO_x emissions are reduced, i.e., nitric acid is NO_x –limited at the downwind site in the base case. Reducing NO_x emissions increases organic matter (that includes secondary organic aerosols) at the upwind and downwind sites. This is due to acceleration in the oxidation of VOCs to secondary organic aerosols when NO_x emissions are reduced. The concentration responses to reductions in combinations of precursor emissions are generally consistent with the points listed above, but do not necessarily reflect linear combinations of effects.

These results show that the aerosol chemistry is very sensitive to any changes of emissions and flow in a particular area. Thus, in order to understand the background of chemistry in a region, more sensitivity test should be conducted with a range of different

increases and reductions of emissions, especially NO_x , VOCs and NH_3 . Additionally, different meteorological conditions should also be tested, especially wind characteristics, which determine the flow that carries the pollutants from upwind to downwind, and solar radiation that triggers the photochemical activity that is responsible of oxidation of VOCs to secondary organic aerosols, especially in presence of decreased NO_x emissions.

Table 4.6. Response (per cent) of aerosol levels to the emission scenarios for the whole domain and whole simulation period.

Species	Increase (All)			Decrease (All)		
	Min	Max	Ave	Min	Max	Ave
PM ₁₀	2.31	8.53	5.42	-8.52	-2.32	-5.42
SO4 Aerosol	0.27	4.97	2.62	-4.90	-0.28	-2.59
NO3 Aerosol	-1.77	31.92	15.07	-30.20	2.30	-13.95
NH4 Aerosol	0.80	7.99	4.40	-7.91	-0.80	-4.36
	Increase (SO ₂)			Decrease (SO ₂)		
	Min	Max	Ave	Min	Max	Ave
PM ₁₀	-2.88	3.28	0.20	-1.82	0.05	-0.89
SO4 Aerosol	-1.14	11.11	4.99	-3.93	0.00	-1.96
NO3 Aerosol	-27.74	4.66	-11.54	-5.30	17.36	6.03
NH4 Aerosol	-0.34	3.77	1.71	-0.23	3.69	1.73
	Increase (NO _x)			Decrease (NO _x)		
	Min	Max	Ave	Min	Max	Ave
PM ₁₀	-0.23	1.64	0.71	-0.23	0.36	0.07
SO4 Aerosol	-0.05	5.51	2.73	-0.05	0.81	0.38
NO3 Aerosol	-7.07	14.23	3.58	-7.62	14.23	3.30
NH4 Aerosol	-1.11	2.85	0.87	-1.11	0.75	-0.18
	Increase (NH ₃)			Decrease (NH ₃)		
	Min	Max	Ave	Min	Max	Ave
PM ₁₀	-7.75	0.87	-3.44	-0.92	-0.03	-0.48
SO4 Aerosol	0.00	2.79	1.40	-2.71	0.00	-1.35
NO3 Aerosol	-0.10	46.92	23.41	-38.87	0.20	-19.33
NH4 Aerosol	0.35	6.79	3.57	-6.80	-0.38	-3.59
	Increase (VOC)			Decrease (VOC)		
	Min	Max	Ave	Min	Max	Ave
PM ₁₀	-0.01	0.30	0.14	-0.31	0.01	-0.15
SO4 Aerosol	-0.03	0.17	0.07	-0.15	0.04	-0.06
NO3 Aerosol	-0.78	5.95	2.59	-6.44	0.48	-2.98
NH4 Aerosol	-0.06	0.12	0.03	-0.12	0.07	-0.03

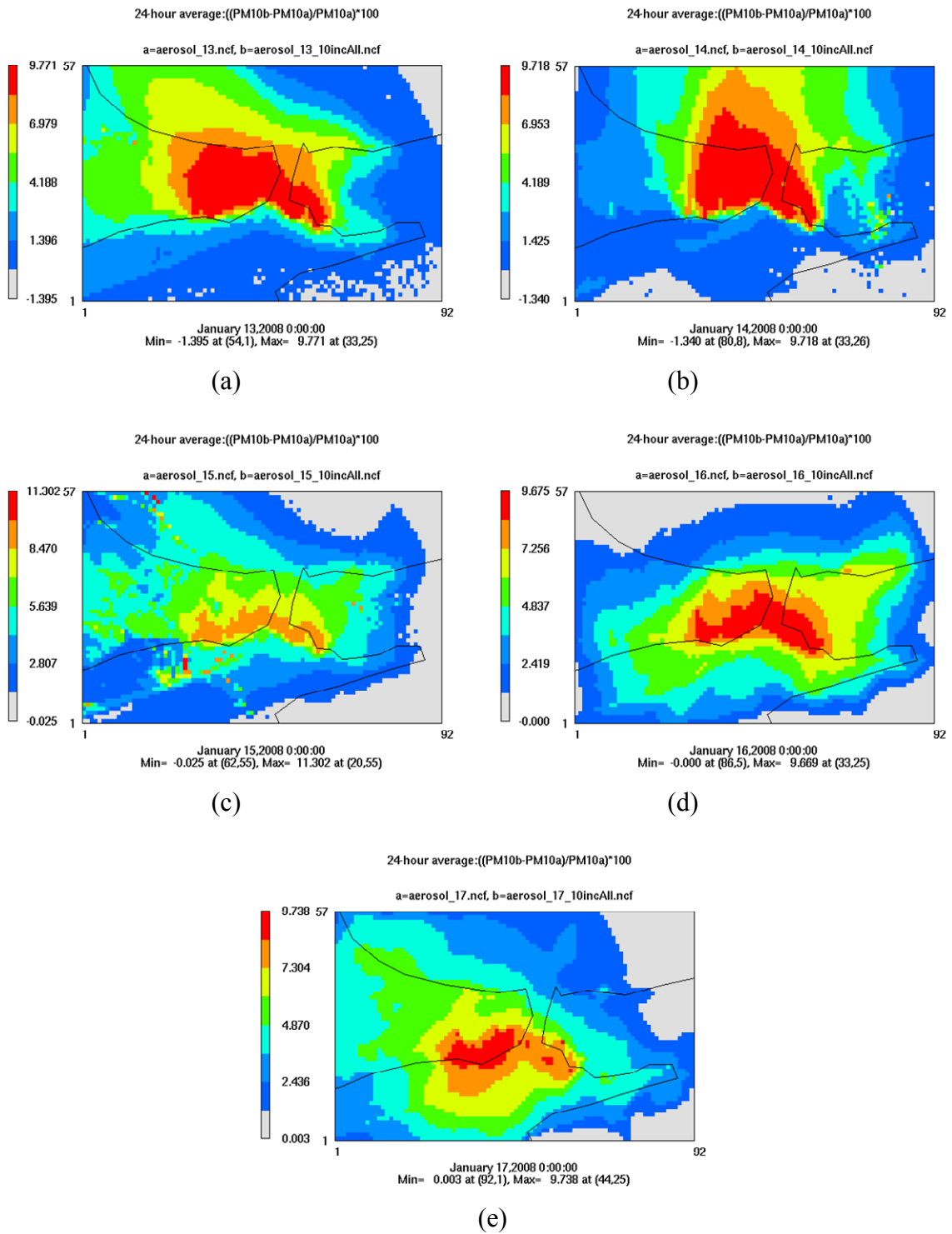


Figure 4.44. 24-hour average PM_{10} changes in response to 10 per cent increase of all emissions for a) 13th, b) 14th, c) 15th, d) 16th and e) 17th of January, 2008 for the İstanbul domain.

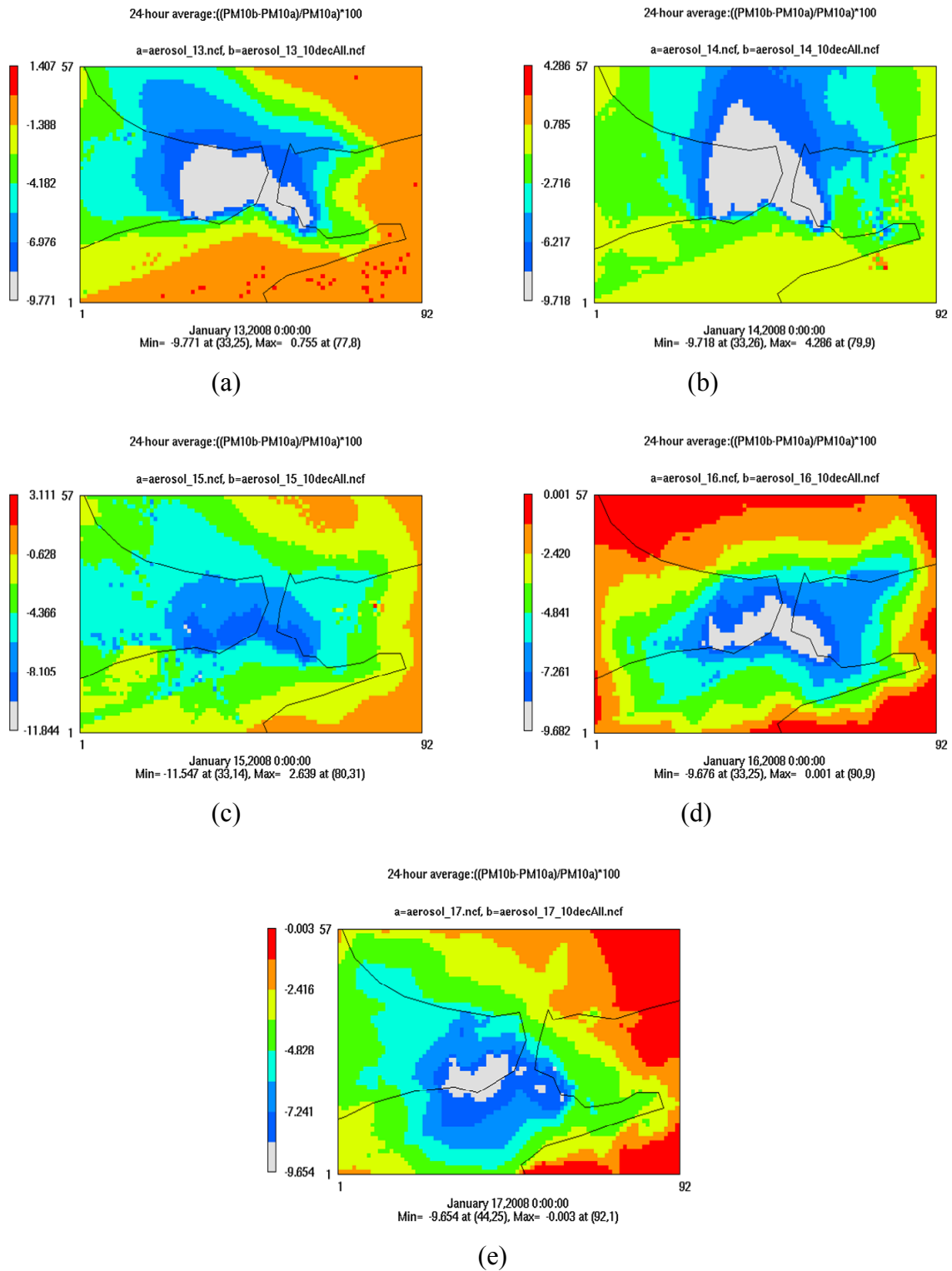


Figure 4.45. 24-hour average PM₁₀ changes in response to 10 per cent reduction of all emissions for a) 13th, b) 14th, c) 15th, d) 16th and e) 17th of January, 2008 for the İstanbul domain.

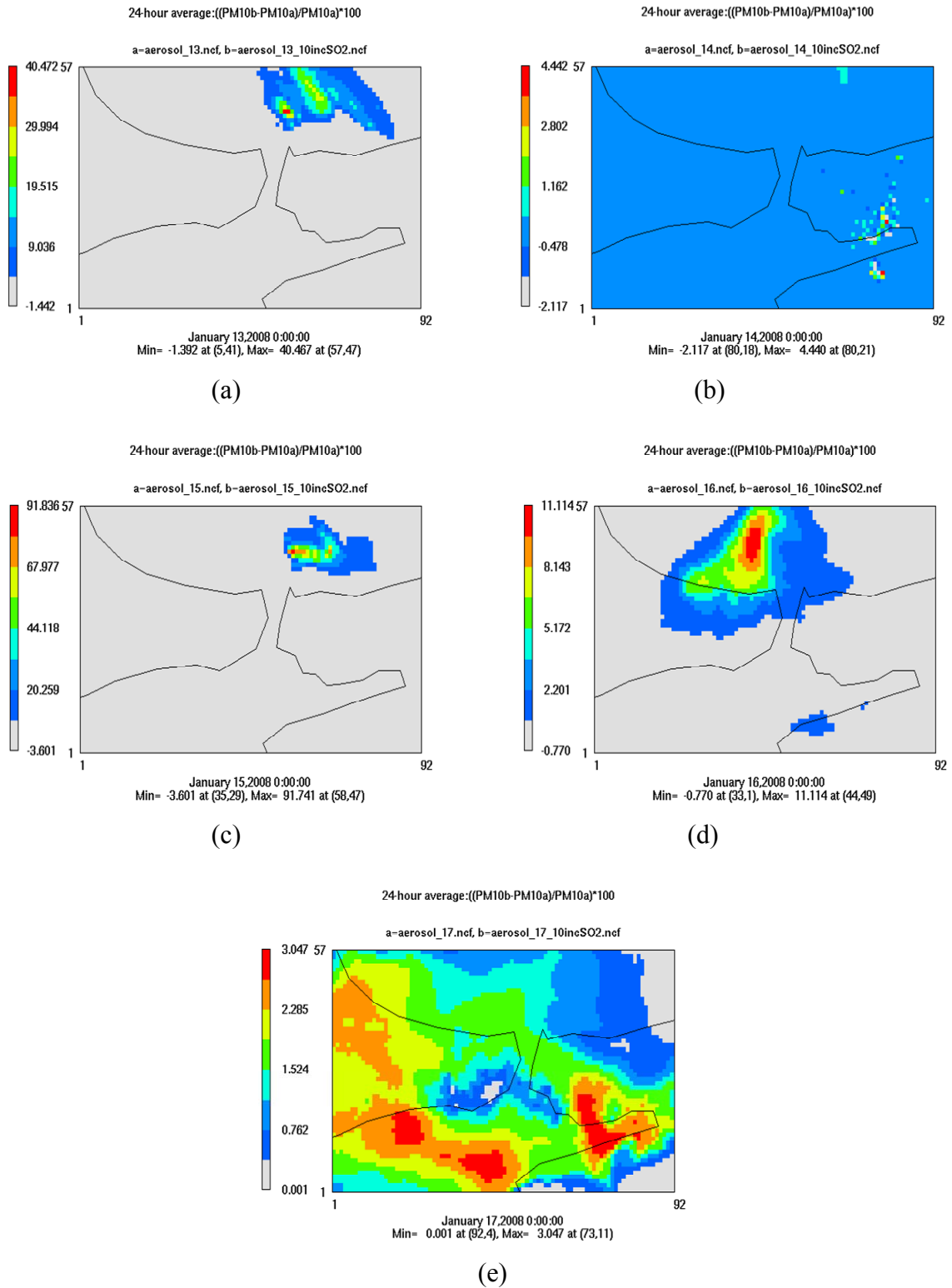


Figure 4.46. 24-hour average PM_{10} changes in response to 10 per cent increase of SO_2 emissions for a) 13th, b) 14th, c) 15th, d) 16th and e) 17th of January, 2008 for the İstanbul domain.

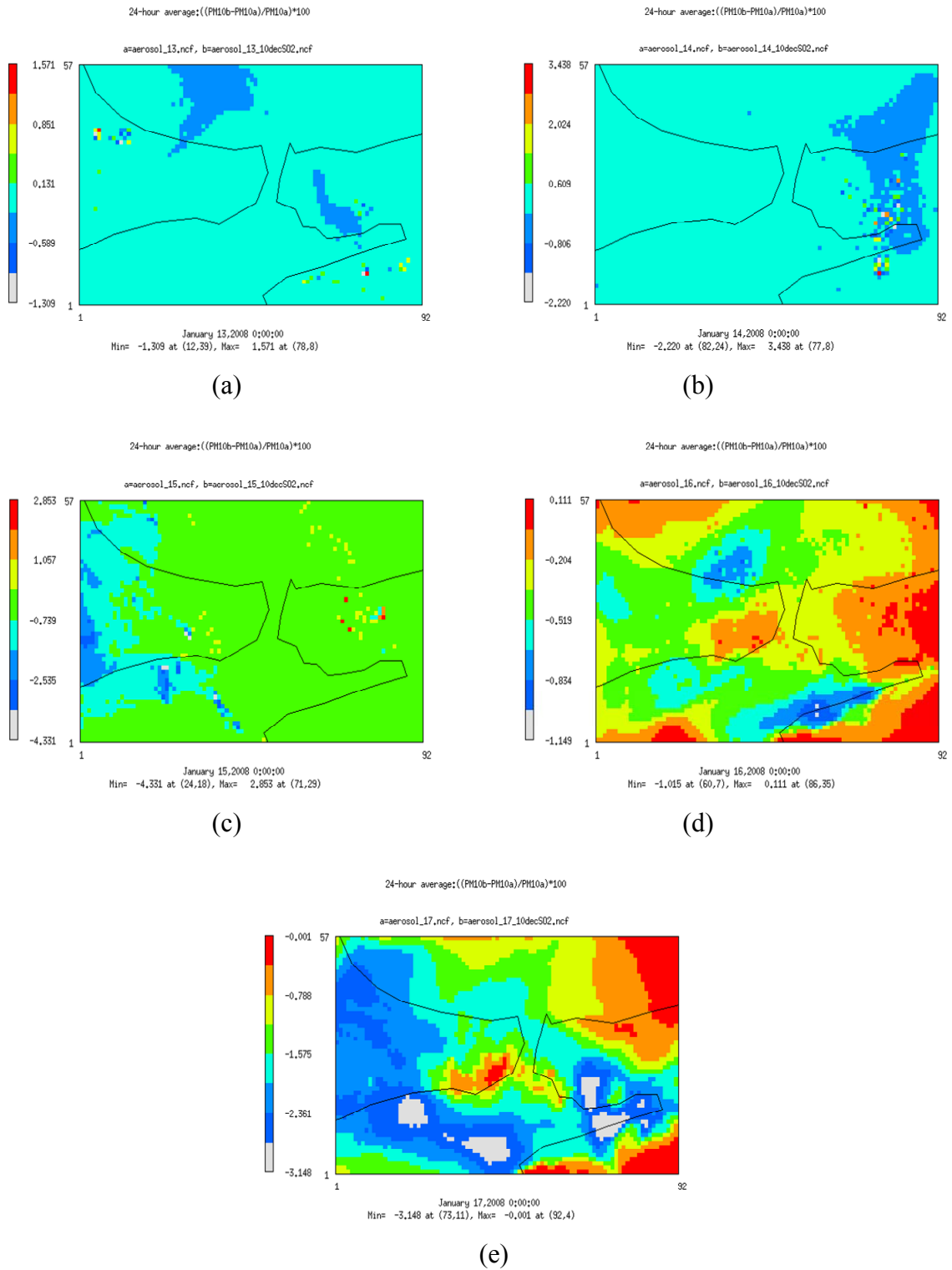


Figure 4.47. 24-hour average PM₁₀ changes in response to 10 per cent reduction of SO₂ emissions for a) 13th, b) 14th, c) 15th, d) 16th and e) 17th of January, 2008 for the İstanbul domain.

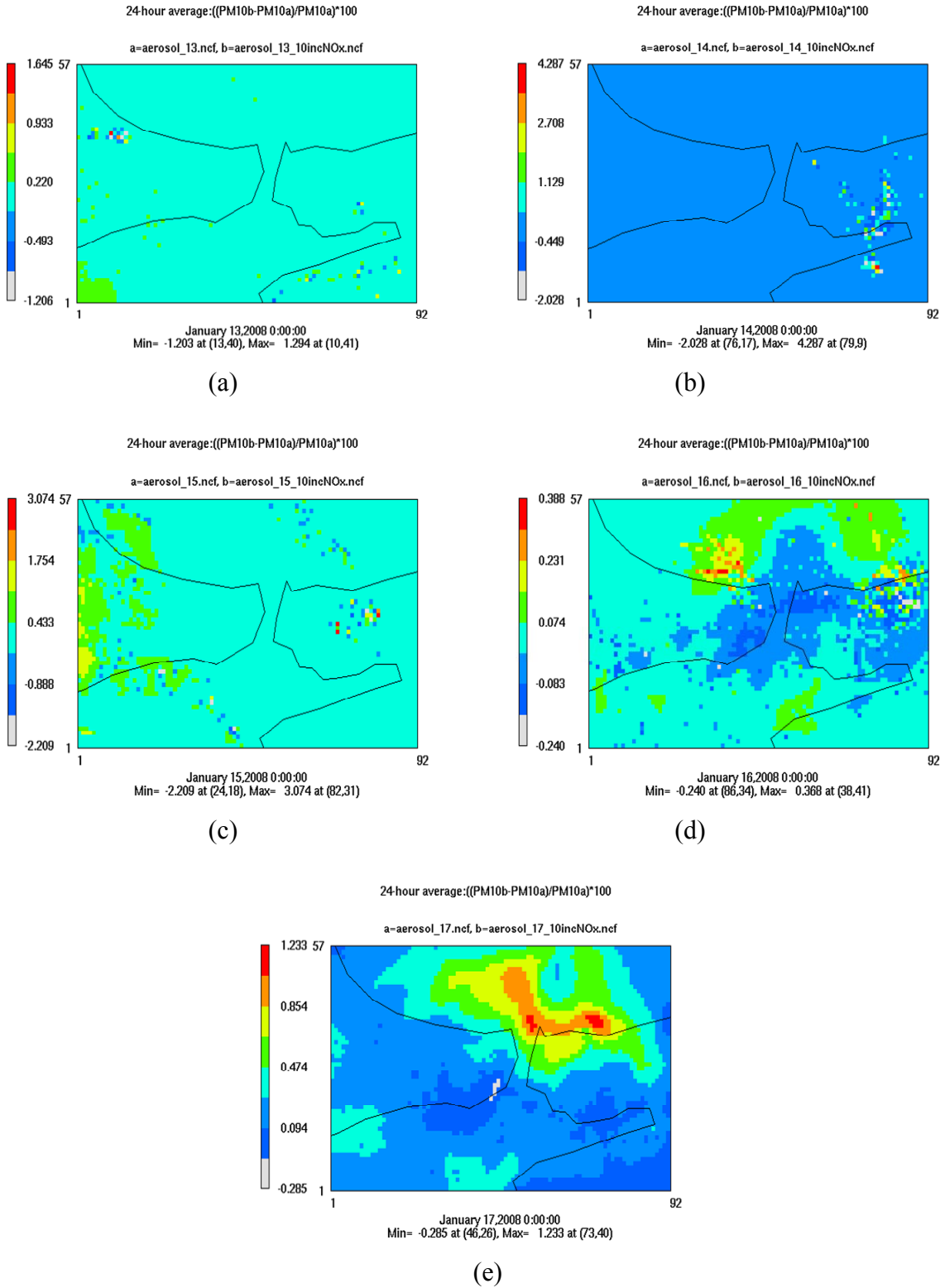


Figure 4.48. 24-hour average PM₁₀ changes in response to 10 per cent increase of NO_x emissions for a) 13th, b) 14th, c) 15th, d) 16th and e) 17th of January, 2008 for the İstanbul domain.

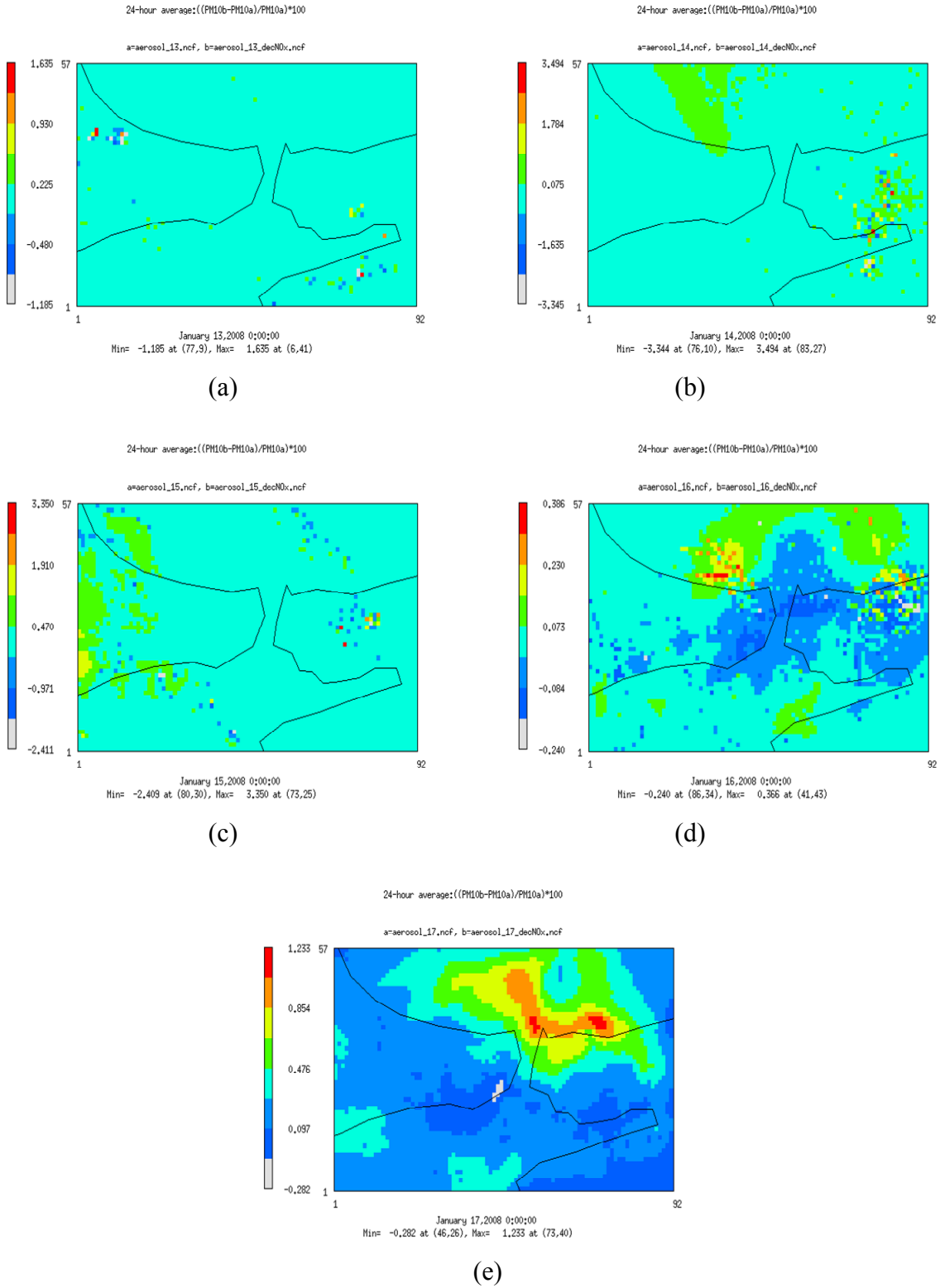


Figure 4.49. 24-hour average PM₁₀ changes in response to 10 per cent reduction of NO_x emissions for a) 13th, b) 14th, c) 15th, d) 16th and e) 17th of January, 2008 for the İstanbul domain.

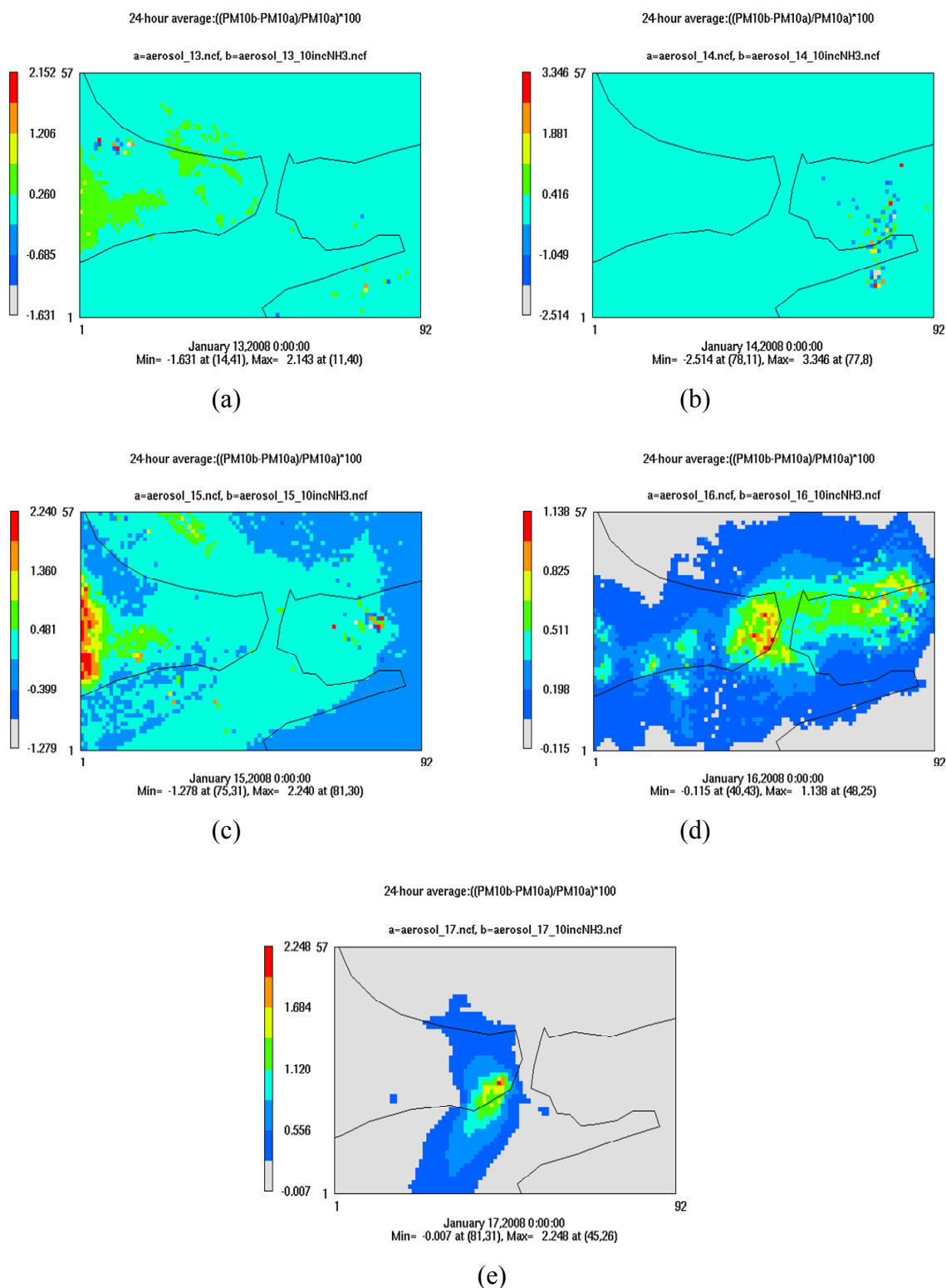


Figure 4.50. 24-hour average PM_{10} changes in response to 10 per cent increase of NH_3 emissions for a) 13th, b) 14th, c) 15th, d) 16th and e) 17th of January, 2008 for the İstanbul domain.

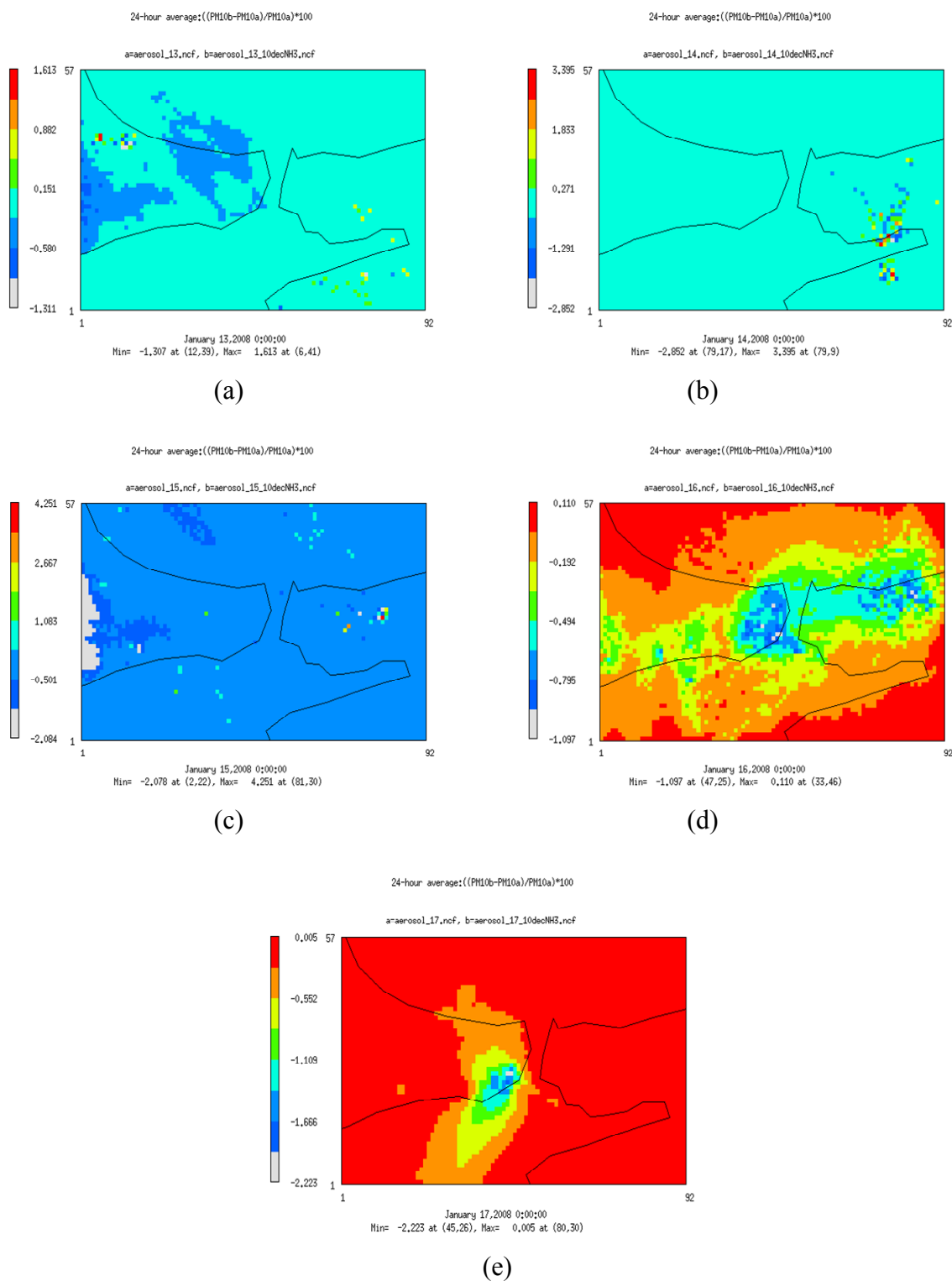


Figure 4.51. 24 – hour average PM₁₀ changes in response to 10 per cent reduction of NH₃ emissions for a) 13th, b) 14th, c) 15th, d) 16th and e) 17th of January, 2008 for the İstanbul domain.

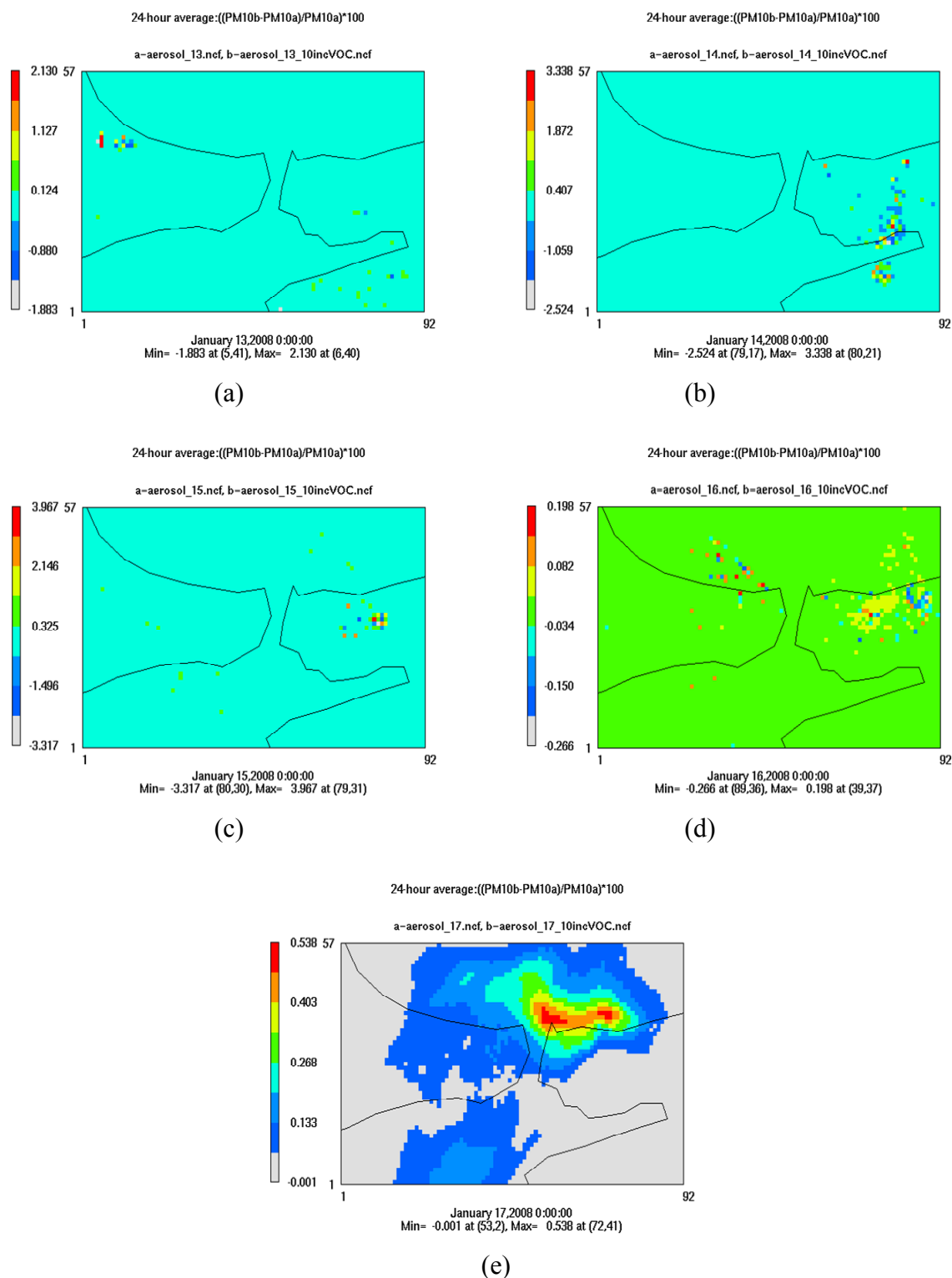


Figure 4.52. 24 – hour average PM_{10} changes in response to 10 per cent increase of VOC emissions for a) 13th, b) 14th, c) 15th, d) 16th and e) 17th of January, 2008 for the İstanbul domain.

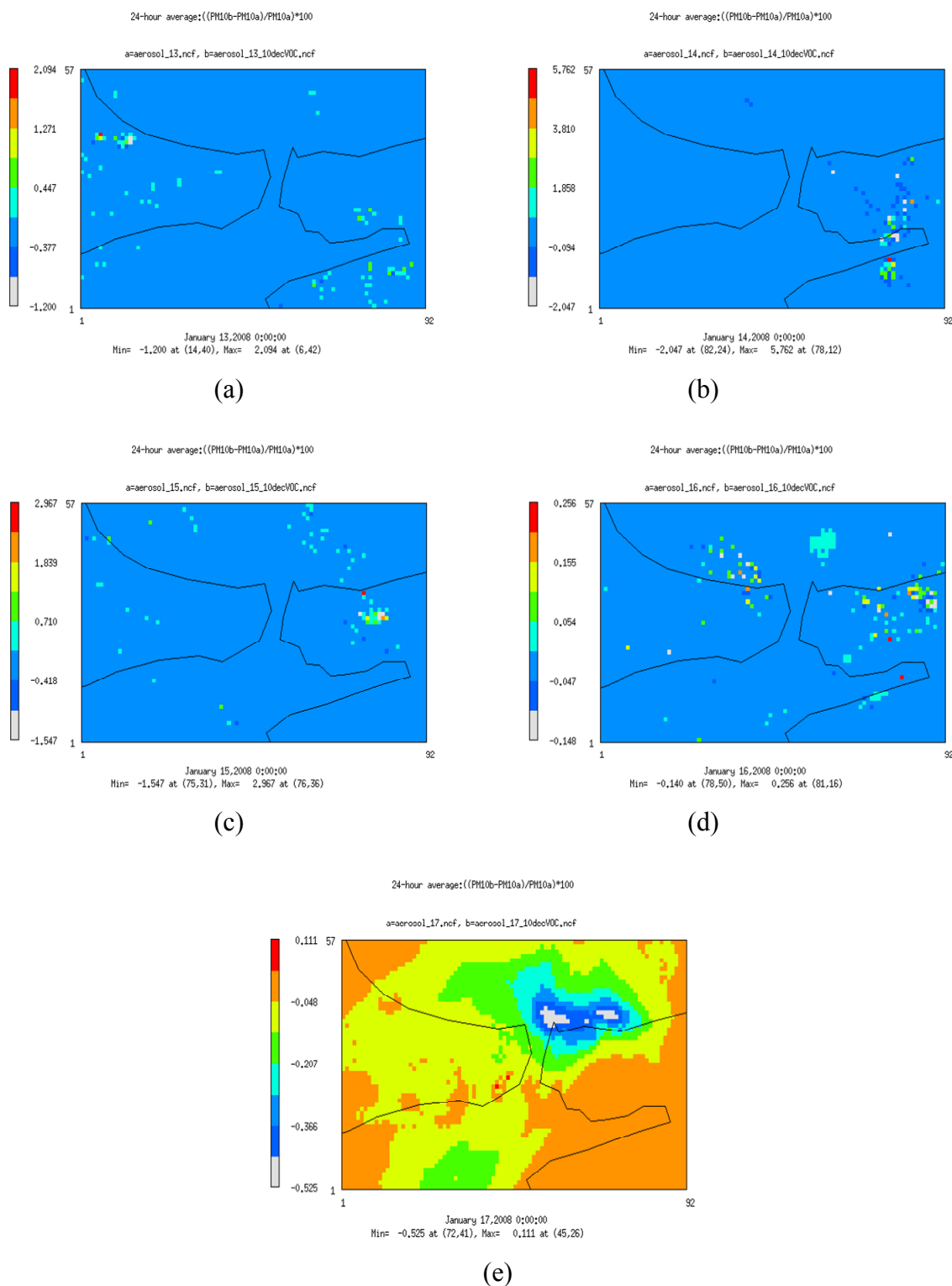


Figure 4.53. 24 – hour average PM₁₀ changes in response to 10 per cent reduction of VOC emissions for a) 13th, b) 14th, c) 15th, d) 16th and e) 17th of January, 2008 for the İstanbul domain.

5. CONCLUSIONS

The aerosol levels in İstanbul during high levels of PM_{10} are investigated using a mesoscale air quality modeling system, consisting of MM5 meteorological model and CMAQ chemistry and transport model. A model ready, high temporal (hourly), spatial (2 km resolution) and chemical emission inventory for the Greater İstanbul Area is developed in order to make high resolution simulations. It should be noted that a study having this detail has not been carried out before for İstanbul. Additionally, besides the total PM_{10} levels, concentrations of sulfate, nitrate and ammonium aerosols are also investigated within a modeling study for the first time in Turkey. For this purpose, 24-hour sampling campaigns at Boğaziçi University, Institute of Environmental Sciences, that were further analyzed at University of Crete, Environmental Chemistry Process Laboratory.

The results from emission modeling system shows that road transport is a significant source category for most of the pollutants. Regarding the emissions of particulate matter, traffic and industrial combustion are main contributing source categories. Particularly, the organic and elemental portion of both PM_{10} and $PM_{2.5}$ originate from traffic based emissions. 60 per cent of PM_{10} and 70 per cent of $PM_{2.5}$ are originated from road transport. Majority of the pollutants are originated from the two coastal sides of the Bosphorus strait, where most of the population resides. The old centers of the city at the European side and Kadıköy region on the Asian side are where the main and the oldest residential areas are located and experience high traffic loads. Industrial regions also contribute significantly to emissions, particularly the İkitelli organized industrial region. SO_2 emissions from industrial combustion are calculated to be 10 orders of magnitude higher than residential SO_2 emissions whereas PM emissions are more than one order of magnitude higher than those from residential heating. VOCs and ammonia are calculated to be emitted significantly from solvent use. The monthly, weekly and daily variations of pollutants from each sector are also calculated. The lack of national and local temporal profiles lead to inconsistencies in the modeling framework due to the fact that they are derived from European studies, particularly from TNO, 2007. Finally, the emission factors may not represent the conditions in İstanbul and may introduce large uncertainties in terms of amounts of emissions estimated and used in modeling.

The results from the MM5 simulation are compared with observations from Kandilli and Finokalia (Crete) meteorological stations. Statistical measures show that the model captured the surface temperature and wind profiles successfully. On the other hand, better agreement can be achieved by optimization studies that will focus on the physics option used for the parameterizations. The comparisons between the model and the observations clearly show that the model underestimated the measurements for most cases. It is concluded that the different biases calculated may arise from the estimation of the high resolution emissions developed. The highly uncertain PM emissions from the road traffic might be a reason for the over estimations of aerosol levels. The results showed that around 90 per cent of PM₁₀ concentrations were of PM_{2.5} origin, which indicates that the over estimations are most probably due to traffic emissions. In order to compare between simulations and observations for the speciated aerosol levels, 24-hour averages were calculated from the model results for the above hour intervals for PM₁₀, SO₄²⁻, NO₃⁻ and NH₄⁺. It is important to note that statistical measures for such a short period and number of data may not represent the overall performance of a model.

The statistical evaluations show very poor correlations factors on hourly basis, indicating that the trends in variations of PM₁₀ concentrations do not agree well with observations. This inconsistency may occur due to the temporal profiles that are used in the emission model. The results confirm that the model over estimated for Alibeyköy and under estimated for Beşiktaş air quality station, both around 40 µgm⁻³. The IOA values are around 25 per cent, indicating a poor agreement. However, the mean and standard deviation ratios between the model results and the observations show that in terms of magnitude, the model successfully simulated the observations.

Primary anthropogenic organic carbon constitutes almost 40 per cent of the PM₁₀ concentrations simulated by the model. Elemental carbon is the second main contributor with more than 20 per cent. Primary PM_{2.5} and sulfate aerosols are the third main contributors with 15 per cent each. The largest source for the primary anthropogenic organic aerosols and elemental carbon is calculated to be road traffic, which confirms that the concentration contributions are traffic induced concentrations. Industrial combustion is also an important contributor of elemental carbon, which has the second largest share in model calculated aerosol concentrations. The correlation coefficient calculated for sulfate,

nitrate and ammonium aerosols show that the trends are well captured. The calculated 24-hour averaged sulfate, nitrate and ammonium aerosol concentrations underestimated the observations for most of the simulation period. The spatial distribution of aerosol species shows hot spots around Alibeyköy and İkitelli. High correlation factors are calculated especially for sulfate and nitrate aerosols and moderate for PM₁₀ and ammonium aerosol. The underestimations of the observations are clear from the mean and standard deviation ratios as well as the BIAS values calculated. The IOA values indicate moderate agreement between the model results and observations. The temporal variation of aerosol species shows that the second peak of PM₁₀ concentrations comes mainly from the sulfate estimation of the model. The results overall show that the model successfully captures the magnitudes. On the other hand, particularly the hourly profiles compared poorly with the observations.

The Brute force sensitivity simulations showed the highest increase in PM₁₀ concentrations occurs in the city centers around the coastal area where most of the population is located. PM₁₀ concentrations respond highest to the changes in all emissions. Because of the complex chemistry, the rate of response to these changes also varies with time. A change of availability of ammonium, nitrate and sulfate species by emission controls, leads to the perturbation of gas-to-particle conversion. This shows that the nitrate levels are very sensitive in changes of sulfur and particularly nitrogen emissions in the area. The concentration responses to reductions in combinations of precursor emissions are generally consistent with the chemistry mechanisms discussed, but do not necessarily reflect linear combinations of effects.

There are numerous sources of uncertainties and discrepancies between model results and observations that need further studies. First of all, it is important to note that the emissions included in this work only include anthropogenic emissions. This study presents the first results from the validation of the high resolution emission inventory. Thus, the inventory also needs to be further developed and tested. As discussed before, being the most important source category, traffic emissions introduces high uncertainties, particularly for PM emissions. However, we believe that the inventory provides satisfactory results. Biogenic emissions are needed to be calculated for the area in order to take into account the formation of secondary aerosols. Although, in this particular study,

due to the fact that the episodic period took place in winter time, it is assumed that formation of secondary aerosols from biogenic origin might be negligible. Sensitivity studies are needed to be conducted to test the response of aerosol levels to variations in biogenic emissions. Another important source of error comes from lacking of the natural sources, most importantly, resuspension of dust. It should also be noted that dynamic boundary conditions should be implemented to the system in order to better represent the particular domain. An important factor in model simulations is the representativeness of the observation locations for the comparison purposes. Urban stations are not preferable in model evaluation studies, due to the fact that the geography and the land use is perturbed by urbanization effects. Unfortunately, the available air quality stations in the Greater İstanbul Area are characterized as urban stations. This points to the need of suburban and rural stations in the region in order to understand the background levels of pollutants as well to better evaluate the performance of the model systems. Last but not least, meteorology also introduces uncertainties to the modeling system.

Overall, it is concluded that the first results of the validation of the MM5/CMAQ modeling system present satisfactory results for the İstanbul domain. However, it should be noted that this is an ongoing research, focusing on different aspects of the system. The physical schemes for different meteorological parameters should be optimized for the region because of the large uncertainties the meteorology may introduce. There should be further developments to the emission inventory by including biogenic and natural sources and providing better activity data for the anthropogenic emissions. Static boundary conditions may introduce high uncertainties, thus, coupling of global chemistry models may be implemented in order to get more realistic and domain-specific boundary conditions. Additionally, the model evaluation should be done for longer periods and for the whole domain, meaning that incorporation of more observations should be conducted. The system can be used for development of emission control and air quality strategies.

REFERENCES

- Ackermann, I.J., Hass, H., Memmesheimer, M., Ebel, A., Binkowski, F.B., Shankar, U., 1998. Modal Aerosol dynamics model for Europe: Development and first applications. *Atmospheric Environment*, 32, 2891-2999.
- Al-Momani, F. I., Güllü, G., Ölmez, I., Eler, Ü., Örtel, E., Şirin, G., Tuncel, G., 1997. Chemical composition of eastern Mediterranean aerosol and precipitation: Indications of long-range transport. *Pure and Applied Chemistry*, 69, 1, 41-46.
- Al-Wali, K. I., Samson, P.J., 1996. Preliminary sensitivity analysis of urban airshed model simulations to temporal and spatial availability of boundary layer wind measurements, *Atmospheric Environment*, 30, 12, 2027-2042.
- Alapaty, K., Olerud Jr., D. T., Schere, K. L., Hanna, A. F., 1995. Sensitivity of regional oxidant model predictions to prognostic and diagnostic meteorological fields. *Journal of Applied Meteorology*, 34, 1787-1801.
- Alpert, D.J., Hopke, P.K., 1981. A determination of the sources of airborne particles collected during the regional air pollution study. *Atmospheric Environment*, 15, 675-687.
- Amundsen, C.E., Hanssen, J.E., Semb, A., Steinnes, E., 1992. Long-range atmospheric transport of trace elements to southern Norway. *Atmospheric Environment*, 26A, 1309-1324.
- Anantharaman, C., Philbrick, C. R., Clark, R., Doddridge, B., Georgopoulos, P., 2003. Evaluating the performance of a computationally efficient MM5/CALMET system for developing wind field inputs to air quality models. *Atmospheric Environment*, 37, 3267-3276.

Andreae, M.O., Browell, E.V., Garstang, M., Gregory, G.L., Harriss, R.C., Hill, G.F., Jacob, D.J., Pereira, M.C., Sachse, G.W., Setzer, A.W., Silva Dias, P.L., Talbot, R.W., Torres, A.L., Wofsy, S.C., 1988. Biomass-burning emissions and associated haze layers over Amazonia, *Journal of Geophysical Research.*, 93, D2, 1509-1527.

Andreae, M. O., 1991. Biomass burning. Its history, use, and distribution and its impact on environmental quality and global climate. In J.S. Levine (ed.), *Global Biomass Burning: Atmospheric, Climatic, and Biospheric Implications*. MIT Press, Cambridge, Massachusetts, 3-21.

Andreae, M. O., Crutzen, P.J., 1997. Atmospheric aerosols: biogeochemical sources and role in atmospheric chemistry, *Science*, 276, 1052-1058.

Andreani-Aksoyoglu, S., Prevot, A. S. H., Baltensperger, U., Keller, J., Dommen, J., 2004. Modeling of formation and distribution of secondary aerosols in the Milan area (Italy). *Journal of Geophysical Research*, 109, D05306.

Anteplioglu U., 2000. Modeling of surface ozone with UAM: a case study for İstanbul. Ph.D. Thesis, Istanbul Technical University.

Arellano J. Vila-Guerau de, Vellinga, O., Holtslag, A. A. M., 2001. Wageningen University, Bosveld F. C.(KNMI), Duivendaal. Observational evaluation of PBL parameterizations modelled by MM5 Workshop Program for the Eleventh PSU/NCAR MM5 Users' Workshop Foothills Laboratory NCAR June 25- 27 2001.

Asman A.H.W., Münier B., Andersen J.A., 1999. Spatially Detailed Ammonia Emission/Deposition Calculations for Denmark. Eurotrac-2 (A Eureka Environmental Project) GENEMIS-Generation and Evaluation of Emission Data Annual Report.

Baldasano M. J., Soriano C., Toll I., 1999. Development of an Upgrade Urban Source Emission Model for Atmospheric Pollutants. Eurotrac-2 (A Eureka Environmental Project) GENEMIS-Generation and Evaluation of Emission Data Annual Report.

Ballard, S.P., Golding, B.W. Smith, R. N., 1991. Mesoscale model experimental Forecasts of the Haar of Northeast Scotland. *Monthly Weather Review*, 119, 2107-2123.

Baltensperger, U., 1999. Aerosol Measurements Within the WMO Global Atmosphere Watch Programme: Providing Data Related to Climate Forcing and Air Quality. EMEP/WMO Workshop on Fine Particles, Interlaken, November 22-25.

Barna, M., Lamb, B., O'Neill, S., Westberg, H., Figueroa-Kaminsky, C., Otterson, S., Bowman, C., DeMay, J., 2000. Modeling ozone formation and transport in the Cascadia region of the Pacific Northwest. *Journal of Applied Meteorology*, 39, 349-366.

Barna, M., Lamb, B., 2000. Improving ozone modeling in regions of complex terrain using observational nudging in a prognostic meteorological model. *Atmospheric Environment*, 34, 4889-4906.

Barna, M.G., Gebhart, K.A., Schichtel, B.A., Malm, W.C., 2006. Modeling regional sulfate during the BRAVO study: Part 1. Base emissions simulation and performance evaluation. *Atmospheric Environment*, 40, 2439-2448.

Batchvarova, E., Gryning, S.-E., 1998. Wind climatology, atmospheric turbulence and internal boundary-layer development in Athens during the MEDCAPHOT-TRACE experiment. *Atmospheric Environment*, 32, 12, 2055-2069.

Bell, M., Ellis, H., 2004. Sensitivity analysis of tropospheric ozone to modified biogenic emissions for the Mid-Atlantic region. *Atmospheric Environment*, 38, 1879-1889.

Berge, E., Laupsa, H., Ødegaard, M., Sorteberg, A., Tønnesen, D., Eastwood, S., Walker, S.E. and Ødegård, R., 2000. Development, testing and implementation of a prognosis models for meteorology and air pollution in Trondheim. The Norwegian Meteorological Institute Research Report No. 107. ISSN 0332-9879 (in Norwegian).

Berge, E., Huang, H.-C., Chang, J., Liu, T.-H., 2001. A study of the importance of initial conditions for photochemical oxidant modeling. *Journal of Geophysical Research*, 106, D1, 1347-1363.

Berkowitz, C. M., Fast, J.D., 1996. The influence of regional-scale atmospheric circulations on chemical mixing over the western north Atlantic. In *Proceedings of American Meteorological Society's Ninth Joint Conference on Applications of Air Pollution Meteorology with the AWMA*, January 28-February 2, 1996, Atlanta, Georgia.

Bessagnet, B., Hodzic, A., Vautard, R., Beekmann, M., Cheinet, S., Honore, C., Liousse, C., Rouil, L., 2004. Aerosol modeling with CHIMERE-preliminary evaluation at the continental scale. *Atmospheric Environment*, 38, 2803-2817.

Betts, A. K., 1986. A new convective adjustment scheme. Part I: Observational and theoretical basis. *Quarterly Journal of Royal Meteorological Society*, 112, 677-692.

Betts, A. K., Miller, M. J., 1986. A new convective adjustment scheme. Part II: Single column tests using GATE wave, BOMEX, ATEX and Arctic air – mass data sets. *Quarterly Journal of Royal Meteorological Society*, 112, 693-709.

Betts, A. K., Miller, M. J., 1993. The Betts-Miller scheme. The representation of cumulus convection in numerical models. Emanuel, K. A. and Raymond, D. J. (Eds.), *American Meteorological Society*.

Binkowski, F.S., U. Shankar, 1995. The regional particulate matter model, 1, Model description and preliminary results, *Journal of Geophysical Research*, 100, 1729-1736.

Binkowski, F.S., 1999. Aerosols in MODELS-3 CMAQ, in *Science Algorithms of the EPA Models-3 Community Multiscale Air Quality (CMAQ) Modelling System*, EPA 600/R-99-030, EPA.

Borge R., Lumbreras J., Rodríguez M.E., 2002. Departamento de Ingeniería Química Industrial y del Medio Ambiente, Universidad Politécnica de Madrid (UPM). C/ José Gutiérrez Abascal, 2. 28006- Madrid, Spain.

Bozo, L., Pinto, J., Gyovai, A., Kiss, I., Kelecsenyi, S., 2002. Source Origin and Spatial Distribution of Aerosol Particles in Budapest. A contribution to subproject SATURN.

Brulfert, G., Galvez, O., Yang, F., Sloan, J. J., 2007. A regional modeling study of the high ozone episode of June 2001 in southern Ontario. *Atmospheric Environment*, 41, 3777-3788.

Brücher, W., Kessler, C., Kerschings, M.J., Ebel, A., 2000. Simulation of traffic-induced air pollution on regional to local scales. *Atmospheric Environment*, 34, 4675-4681.

Burk, S. D., Thompson, W. T., 1989. A vertically nested regional numerical prediction model with second – order closure physics. *Monthly Weather Review*, 117, 2305-2324.

Byun, D.W., Ching, J. K. S. (Eds.), 1999. Science algorithms of the EPA Models-3 Community Multi-scale Air Quality (CMAQ) modeling system. US EPA Report No. EPA/600/R – 99/030., Office of Research and Development, Washington, DC.

Byun, D. W., Kim, S.T., Kim, S.B., 2007. Evaluation of air quality models for the simulation of a high ozone episode in the Houston metropolitan area. *Atmospheric Environment*, 41, 837-853.

CARB, 2007. Speciation Profiles Used in ARB Modeling. California Air Resources Board, Sacramento, California.

Carpenter, L. J., Clemitshaw, K. C., Burgess, R. A., Penkett, S. A., Cape, J. N., McFadyen, 1998. Investigation and evaluation of the NO_x/O₃ photochemical steady state. *Atmospheric Environment*, 32, 19, 3353-3365.

Carter, W. P. L., 1996. A detailed mechanism for the gas-phase atmospheric reactions of organic compounds. *Atmospheric Environment*, 24A, 481-518.

Carter, W. P. L., 2000. Implementation of the SAPRC-99 chemical mechanism into the Models-3 Framework. Report to the U.S. Environmental Protection Agency.

Chan, L.Y., Kwok, W.S., 2000. Vertical dispersion of suspended particulates in urban area of Hong Kong. *Atmospheric Environment*, 34, 4403-4412.

Chang, J. S., Brost, R. A., Isaksen, I. S. A., Madronich, S., Middleton, P., Stockwell, W. R., Walcek, C. J., 1987. A three-dimensional acid deposition model: physical concepts and formulation. *Journal of Geophysical Research*, 92, 14681-14700.

Chang, M.E., Cardelino, C., 2000. Application of the Urban Airshed Model to Forecasting Next-Day Peak Ozone Concentrations in Atlanta, Georgia. *Journal of the Air & Waste Management Association*, 50, 2010-2024.

Chatfield, R., Crutzen, P.J., 1984. Sulfur dioxide in remote oceanic air: Cloud transport of reactive precursors. *Journal of Geophysical Research*. 89, D5, 7111-7132.

Ching, J.K.S., Alkezweeny, A.J., 1986. Tracer study of vertical exchange by cumulus clouds. *Journal of Climatology and Applied Meteorology*. 25, 1702-1711.

Ching, J.K.S., Shipley, S.T., Browell, E.V., 1988. Evidence for cloud venting of named layer ozone and aerosols. *Atmospheric Environment*, 22, 225-242.

Choi, Y.J., Fernando, H.J.S., 2008. Implementation of a windblown dust parameterization into MODELS-3/CMAQ: Application to episodic PM events in the US/Mexico border. *Atmospheric Environment*, 42, 6039-6046.

Christakos G., Vyas, V. M., 1998. A composite space/time approach to studying ozone distribution over eastern United States. *Atmospheric Environment*, 32, 16, 2845-2857.

Christensen, J. H., Brandt, J., Frohn, L., Geels, C. and Hansen, K. M., 2003. The parameterisation of heterogeneous chemistry and wet and dry deposition of eutrophying and acidifying compounds in the DEHM model. National Environmental Research Institute Department of Atmospheric Environment Denmark. EMEP-TFMM_review2003.

Civerelo, K., Hogrefe, C., Lynn, B., Rosenthal, J., Ku, J.Y., Solecki, W., Cox, J., Small, C., Rosenzweig, C., Goldberg, R., Knowlton, K., Kinney, P., 2007. Estimating the effects of increased urbanization on surface meteorology and ozone concentrations in the New York City metropolitan region. *Atmospheric Environment*, 41, 1803-1818.

Cohan, D. S., Hu, Y., Russel, A. G., 2006. Dependence of ozone sensitivity analysis on grid resolution. *Atmospheric Environment*, 40, 126-135.

Colella, P., Woodward, P. L., 1984. The piecewise parabolic method (PPM) for gas-dynamical simulations. *Journal of Computational Physics*, 54, 174-201.

Cooper, D.A, Gustafsson, T., 2004. Methodology for calculating emissions from ships: 1. Update of emission factors. Report series SMED and SMED & SLU 4.

Cowling, E.B., Chameides, W.L., Kang, C.S., Fehsenfeld, F.C., Meagher, J.F., 1998. Introduction to special section: Southern Oxidants Study Nashville/Middle Tennessee Ozone Study. *Journal of Geophysical Research*, 103, 22209-22212.

Çetin, S., Karademir, A., Pekey, B., Ayberk, S., 2007. Inventory of emissions of primary air pollutants in the city of Kocaeli. *Environment Monitoring Assessment*, 128, 165-175.

Dabdub, D., DeHaan, L. L., Seinfeld, J. H., 1999. Analysis of ozone in the San Joaquin Valley of California. *Atmospheric Environment*, 33, 2501-2514.

Dailey, P. S., Keller, J., 2002. (AIR Worldwide Corp.) Modeling of Extreme Wind Events Using MM5. Approach and Verification. Papers Presented at the Twelfth PSU/NCAR Mesoscale Model Users' Workshop NCAR June 24-25.

Davis, J. M., Speckman, P., 1999. A model for predicting maximum and 8 h average ozone in Houston. *Atmospheric Environment*, 33, 2487-2500.

Deniz C, Durmuşoğlu Y., 2008. Estimating shipping emissions in the region of the Sea of Marmara, Turkey. *Science of the Total Environment*. 390, 255-261.

Dennis, R.L., McHenry, J.N., Barchet, W.R., Binkowski, F.S., Byun, D., 1993. Correcting RADM's sulfate underprediction: discovery and correction of model errors and testing the corrections through comparisons against field data. *Atmospheric Environment*, 27A, 975-997.

Derwent, R. G., Simmonds, P. G., Seuring, S., Dimmer, C., 1997. Observation and interpretation of the seasonal cycles in the surface concentrations of ozone and carbon monoxide at Mace Head, Ireland. *Atmospheric Environment*, 32, 2, 145-157.

Diem, J. E., Comrie, A. C., 2001. Allocating anthropogenic pollutant emissions over space: application to ozone pollution management. *Journal of Environmental Management*, 63, 425-447.

Dimitroulopoulou, C., Marsh, A. R. W., 1997. Modelling studies of NO₃ nighttime chemistry and its effects on subsequent ozone formation. *Atmospheric Environment*, 31, 18, 3041-3057.

Dodge, M. C., 1989. A comparison of photochemical oxidant mechanisms. *Journal of Geophysical Research*. 94, 5121-5136.

Dudhia, J., 1996. A multi-layer soil temperature model for MM5. Preprints, The Sixth PSU/NCAR Mesoscale Model Users' Workshop, 22-24 July 1996, Boulder, Colorado, 49-50.

Ebel A, H. Elbern, H. Feldmann, H.J. Jakobs, C. Kessler, M. Memmesheimer, 1997. A. Oberreuter, and G. Piekorz, Air pollution studies with the EURAD Model System(3):

EURAD-European air pollution dispersion model System. Mitteilungen aus dem Institut für Geophysik und Meteorologie der Universität Köln, 120, pp 172.

EEA Topic Report, 2003. Air pollution by ozone in Europe in summer 2003: Overview of exceedances of EC ozone threshold values during the summer season April-August 2003 and comparisons with previous years. No. 3.

EEA Technical Report, 2005. Air pollution by ozone in Europe in summer 2004: Overview of exceedances of EC ozone threshold values during April–September 2004. No. 3.

EMBARQ, 2008. İstanbul'da Tekerlekli Araçlardan Kaynaklanan Emisyon Envateri Çalışması, İstanbul Büyükşehir Belediyesi için hazırlanan teknik rapor (English: Inventory for vehicle emissions in İstanbul: Technical report for the Greater Municipality of İstanbul).

Elbir, T., Muezzinoglu A., 2004. Estimation of emission strengths of primary air pollutants in the city of Izmir, Turkey. *Atmospheric Environment*, 38, 1851-1857.

EMEP-EEA, 2001. CORINAIR emission inventory guidebook, third edition. EEA Technical Report no. 30

Entwistle, J., Weston, K., Singles, R., Burgess, R., 1997. The magnitude and extent of elevated ozone concentrations around the coasts of British Isles. *Atmospheric Environment*, 31, 13, 1925-1932.

Environ International Corporation, 2002. Environ User's Guide: Comprehensive Air Quality Model with Extensions (CAMx), version 3.10, Novato, California.

EPA, 1996a. Air quality criteria for particulate matter. North Carolina, U.S. Environmental Protection Agency (EPA/600/P-95/001).

Erturk, F., 1986. Investigation of strategies for the control of air pollution in the Golden Horn region, Istanbul, using a simple dispersion model. *Environmental Pollution Series B, Chemical and Physical*, 11, 3, 161-168.

Feng, Y., Wang, A., Wu, D., Xu, X., 2007. The influence of tropical cyclone Melor on PM₁₀ concentrations during an aerosol episode over the Pearl River Delta region of China: Numerical modeling versus observational analysis. *Atmospheric Environment*, 41, 4349-4365.

Finlayson-Pitts, B.J. and Pitts, J.N., 1986. *Atmospheric Chemistry: fundamentals and experimental techniques*. New York, Wiley.

Friedrich R., Wickert B., Schwarz U. and Reis S., 1999. Improvement and Application of Methodology and Models to Calculate Multiscale High Resolution Emission Data for Gego, E., Porter, P.S., Hogrefe, C., Irwin, J.S., 2006. An objective comparison of CMAQ and REMSAD performances. *Atmospheric Environment*, 40, 4920-4934.

Friedrich R., 1997. GENEMIS: Assessment, improvement, temporal and spatial disaggregation of European emission data. *Tropospheric Modelling and Emission Estimation, (PART 2)*. Ebel, A., Friedrich, R., Rhode, H., (Eds.). Springer, New York.

Fritsch, J. M., Chappell, C. F., 1980. Numerical prediction of convectively driven mesoscale pressure systems. Part I: Convective parameterization. *Journal of Atmospheric Science*, 37, 1722-1733.

Fuentes, J.D., Lerdau, M., Atkinson, R., Baldocchi, D., Bottenheim, J.W., Ciccioli, P., Lamb, B., Geron, C., Gu, L., Guenther, A., Sharkey, T.D., Stockwell, W., 2000. Biogenic hydrocarbons in the atmospheric boundary layer: A review, *Bulletin of American Meteorological Society*, 81, 1537-1575.

Gaza, R. S., 1998. Mesoscale meteorology and high ozone in the Northeast United States. *Journal of Applied Meteorology*, September 1998, 961-977.

Gego, E., Porter, P.S., Hogrefe, C., Swall, J., Gilliland, A., Irwin, J.S., Rao, S.T., 2006. Objective comparison of CMAQ and REMSAD performances. *Atmospheric Environment*, 40, 26, 4920-4934.

Gery, M. W., Crouse, R. R., 1989. User's guide for executing OZIPR. Atmospheric Research and Exposure Research Laboratory, US Environmental Protection Agency, Research Triangle Park, North Carolina.

Gery, M. W., Whitten G. Z., Killus, J. P., Dodge, M. C., 1989. A photochemical kinetics mechanism for urban and regional scale computer modeling. *Journal of Geophysical Research*, 94, 12925-12956.

Gidel, L.T., 1983. Cumulus cloud transport of transient tracers. *Journal of Geophysical Research*, 88C, 6587-6599.

Graedel T.E., Mandich, M. L., Weschler, C. J., 1986. Kinetic model studies of atmospheric droplet chemistry, 2. Homogeneous transition metal chemistry in raindrops. *Journal of Geophysical Research*, 91(D4), 5225-5221.

Grant, R. H., Wong, K., 1999. Ozone profiles over a suburban neighborhood. *Atmospheric Environment*, 33, 51-63.

Grell, G. A., Dudhia, J., Stauffer, D. R., 1994. A description of the fifth-generation Penn State/NCAR mesoscale model (MM5). NCAR Technical Note, NCAR/TN-398+STR.

Greenhut, G.K., 1986. Transport of ozone between boundary layer and cloud layer by cumulus clouds. *Journal of Geophysical Research*, 91D, 8613-8622.

Greenhut, G.K., Ching, J.K.S., Pierson, R., Jr., Repoff, T.P., 1984. Transport of ozone by turbulence and clouds in an urban boundary layer. *Journal of Geophysical Research*, 89D, 4757-4766.

Griffin, R.J., D.R. Cocker III, R.C. Flagan, and J.H. Seinfeld, 1999. Organic aerosol formation from the oxidation of biogenic hydrocarbons. *Journal of Geophysical Research*, 104, 3555-3567.

Guo, Y.R., Chen, S., 1994. Terrain and land use for the fifth-generation Penn State/NCAR mesoscale modeling system (MM5). NCAR Technical Note, NCAR/TN-397+IA, 114 pp.

Güsten, H., Heinrich, G., Monnich, E., Weppner, J., Cvitas, T., Klasinc, L., Varotsos, C. A., Asimakopoulos, N., 1996. Thessaloniki '91 field measurement campaign – II, ozone formation in the Greater Thessaloniki Area. *Atmospheric Environment*, 37, 8, 1115-1126.

Hacisalihoglu, G., Eliyakut, F., Olmez, I., Balkas, T. I., Tuncel, G., 1992. Chemical composition of particles in the Black Sea atmosphere. *Atmospheric Environment*, 26A, 3207.

Heintzenberg, J., 1994. The life cycle of the atmospheric aerosol. European Research Course on Atmospheres, Vol. 1: Topics in Atmospheric and Interstellar Physics and Chemistry. Eds. Claude F. Boutron. 251-267.

Hoek, G., Forsberg, B., Borowska, M., Hlawczka, S., Vaskovi, E., Welinder, H., Branis, M., Benes, N., Kotesovec, F., Hagen, L. O., Cyrus, J., Jantunen, M., Roemer, W. and Brunekreef, B., 1997. Wintertime PM₁₀ and Black Smoke Concentrations Across Europe: Results From The Peace Study. *Atmospheric Environment*, 31, No. 21, pp. 3609-3622.

Hogrefe, C., Rao, S. T., Kasibhatla, P., Hao, W., Sistla, G., Mathus, R., McHenry, J., 2001. Evaluating the performance of regional – scale photochemical modeling systems: Part II- ozone predictions. *Atmospheric Environment*, 35, 4175-4188.

Hogrefe, C., Rao, S. T., Kasibhatla, P., Kallos, G., Tremback, C. J., Hao, W., Olerud, D., Xiu, A., McHenry, J., Alapaty, K., 2001. Evaluating the performance of regional – scale photochemical modeling systems: Part I -meteorological predictions. *Atmospheric Environment*, 35, 4159-4174.

Hogrefe, C., Porter, P. S., Gego, E., Gilliland, A., Gilliam, A., Swall, J., Irwin, J., Rao, S. T., 2006. Temporal features in observed and simulated meteorology and air quality over the Eastern United States. *Atmospheric Environment*, 40, 5041-5055.

Hong, S.Y., Pan, H.-L., 1996. Nonlocal boundary layer vertical diffusion in a medium-range forecast model. *Monthly Weather Review*, 124, 2322-2339.

Houthuijs, D., Breugelmans, O., Hoek, G., Vaskövi, E., Mihalikova, E., Pastuszka, J. S., Jirik, V., Sachelarescu, S., Lolova, D., Meliefste, K., Uzunova, E., Marinescu, C., Volf, J., Frank de Leeuw, Henk van de Wiel, Fletcher, T., Lebret, E., Brunekreef, E., 2001. PM₁₀ and PM_{2.5} concentrations in Central and Eastern Europe: results from the Cesar study. *Atmospheric Environment*, 35, 2757-2771.

Hollingsworth, A., Engelen, R.J., Textor, C., Benedetti, A., Boucher, O., Chevallier, F., Dethof, A., Elbern, H., Eskes, H., Flemming, J., Granier, C., Kaiser, J.W., Morcrette, J-J., Rayner, P., Peuch, V.-H., Rouil, L., Schultz, M.G., Simmons, A.J., 2008., Toward a monitoring and forecasting system for atmospheric composition: The GEMS project. *Bulletin of the American Meteorological Society*, 89, 8, 1147-1164.

Hong, S.-Y., Pan, H.-L., 1996. Nonlocal boundary layer vertical diffusion in a medium-range forecast model. *Monthly Weather Review*, 124, 2322-2339.

Hovland M., Judd A.G., Burke R.A., 1993. The global flux of methane from shallow submarine sediments, *Chemosphere*, 26, 559-578.

IPCC, 1999. Aviation and the global atmosphere: Summary for the policymakers

İm, U., Tayanc, M., Yenigun, O., 2008. Interaction patterns of major photochemical pollutants in İstanbul, Turkey. *Atmospheric Research*, 89, 382-390.

İm, U., Tayanc, M., Yenigun, O., 2006. Analysis of major photochemical pollutants with meteorological factors for high ozone days in Istanbul, Turkey. *Water, Air & Soil Pollution*, 175, 335-359.

İm, U., Yenigün, O., 2005. An application of a puff dispersion model on power plant emissions in Yatağan region, Turkey. *International Journal of Environment and Pollution*, 23, 3, 314-324.

İncecik, S., 1996. Investigation of atmospheric conditions in Istanbul leading to air pollution episodes. *Atmospheric Environment*, 30, 15, 2739-2749.

Jackson, B., Chau, D., Gurer, K., Kaduwela, A., 2006. Comparison of ozone simulations using MM5 and CALMET/MM5 hybrid meteorological fields for the July/August 2000 CCOS episode. *Atmospheric Environment*, 40, 2812-2822.

Jakobs, H.J., Feldmann, H., Hass, H., Memmesheimer, M., 1995. The use of nested models for air pollution studies: An application of the EURAD model to a SANA episode. *Journal of Applied Meteorology*, 34, 1301-1319.

Jakobs, H.J., Tilmes, S., Heidegger, A., Nester, K., Smiatek, G., 2002a. Short-term ozone forecasting with a network model system during summer 1999. *Journal of Atmospheric Chemistry*, 42, 23-40.

Jakobs, H. J., Friese, E., Memmesheimer, M., Ebel, A., 2002b. A real-time forecast system for air pollution concentrations. Contribution to subproject GLOREAM. Rheinisches Institut für Umweltforschung, Projekt EURAD.

Janjic, Z.I., 1990. The step-mountain coordinate: Physical package. *Monthly Weather Review*, 118, 1429-1443.

Janjic, Z.I., 1994. The step-mountain eta coordinate model: Further development of the convection, viscous sublayer, and turbulent closure schemes. *Monthly Weather Review*, 122, 927-945.

Jiang, W., Singleton, D. L., Hedly, M. and McLaren, R., 1996. Sensitivity of ozone concentrations to VOC and NO_x emissions in the Canadian Lower Fraser Valley. *Atmospheric Environment*, 31, 4, 627-638.

Jimenez, P., Baldasano, J. M., 2004. Ozone response to precursor controls in very complex terrains: Use of photochemical indicators to assess O₃-NO_x-VOC sensitivity in the northeastern Iberian Peninsula. *Journal of Geophysical Research*. 109, D20309.

Jimenez, P., Jorba, O., Parra, R., Baldasano, J. M., 2006. Evaluation of MM5-EMICAT2000-CMAQ performance and sensitivity in complex terrain: High-resolution application to the northeastern Iberian Peninsula. *Atmospheric Environment*, 40, 5056-5072.

Jorquera, H., Perez, R., Cipriano, A., Espejo, A., Letelier, M. V., Acuna, G., 1998. Forecasting ozone daily maximum levels at Santiago, Chile. *Atmospheric Environment*, 32, 20, 3415-3424.

Kain, J. S., Fritsch, J. M., 1993. Convective parameterization for mesoscale models: The Kain-Fritsch scheme. The representation of cumulus convection in numerical models, K. A. Emanuel and D. J. Raymond (Eds.), American Meteorological Society.

Kain, J. S., 2002. The Kain-Fritsch convective parameterization: An update. *Journal of Applied Meteorology*, 43, 170-181.

Kalabokas, P. D., Bartzis, J. G., 1998. Photochemical air pollution characteristics at the station of the NCSR-Demokritos, during the MEDCAPHOT-TRACE campaign in Athens, Greece (20 August-20 September 1994). *Atmospheric Environment*, 32, 12, 2123-2139.

Karamachandani, P., Ventkaram, A., 1992. The role of non-precipitating clouds in producing ambient sulfate during summer: results from simulations with the Acid Deposition and Oxidant Model (ADOM). *Atmospheric Environment*, 26A, 1041-1052.

Kasting, J. F., Singh, H. B., 1986. Non-methane hydrocarbons in the troposphere: Impact on the odd hydrogen and odd nitrogen chemistry. *Journal of Geophysical Research*, 91, 13239-13256.

- Kesgin, U., 2006. Aircraft emissions at Turkish airports. *Energy*, 31, 372-384.
- Kesgin, U., Vardar, N., 2001. A study on exhaust gas emissions from ships in Turkish straits. *Atmospheric Environment*, 35, 1863-1870.
- Kessler, R.C., 1988. What Techniques are Available for Generating Wind-fields? Conference on Photochemical Modeling as a Tool for Decision Makers, State of California Air Resources Board, Pasadena, California.
- Kılıç A. Exhaust gas emissions from ships and dispersion modeling, İstanbul Technical University, MSc Thesis 2006, 129 pp.
- Kındap T., 2005. Long-range aerosol transport from Europe to İstanbul, Turkey. PhD Thesis, İstanbul Technical University, Eurasia Institute of Earth Sciences.
- Kındap, T., Unal, A., Chen, S.-H., Hu, Y., Odman, M. T., Karaca, M., 2006. Long-range aerosol transport from Europe to Istanbul, Turkey. *Atmospheric Environment*, 40, 3536-3547.
- Kındap, T., 2008. Identifying the trans-boundary transport of air pollutants to the city of Istanbul under specific weather conditions. *Water, Air & Soil Pollution*, 189, pp. 279-289.
- Kim, D., Stockwell, W. R., 2007. An online coupled meteorological and air quality modeling study of the effect of complex terrain on the regional transport and transformation of air pollutants over the Western United States. *Atmospheric Environment*, 41, 2319-2334.
- Klausmann A. M., Phadnis, M., Scire, J., 2003. The Application of MM5/WRF Models to Air Quality Assessments. Papers Presented at the Thirteenth PSU/NCAR Mesoscale Model, NCAR, Users' Workshop, June 10-11.

Klemm, O., Ziomas, I. C., Balis, D., Suppan, P., Slemr, J., Romero, R., Vyras, L. G., 1998. A summer air – pollution study in Athens, Greece. *Atmospheric Environment*, 32, 12, 2071-2087.

Klimont Z, Bertok I, Amann M, Cofala J, Heyes Ch, Gyarmas F., 2002. Modelling Particulate Emissions in Europe: A Framework to Estimate Reduction Potential and Control Costs. Interim Report IR-02-076, IIASA, Laxenburg, Austria, 169 p.

Kulmala, M., A. Toivonen, J.M. Mäkelä, 1998. Analysis of the growth of nucleation mode particles observed in Boreal forest, *Tellus*, 50B, 449-462.

Kumar, N., Armistead, G. R., 1996. Comparing prognostic and diagnostic meteorological fields and their impacts on photochemical air quality modeling. *Atmospheric Environment*, 30, 12, 1989-2010.

Kühlwein, J., Wickert, B., Trunkenmüller, A., Theloke, J., Friedrich, R., 2002. Emission-modeling in high spatial and temporal resolution and calculation of pollutant concentrations for comparisons with measured concentrations. *Atmospheric Environment*, 36, 1, S7-S18.

Langmann, B., Bauer, S.E. and Bey, I., 2003. The influence of the global photochemical composition of the troposphere on European summer smog, Part I: Application of a global to mesoscale model chain. *Journal of Geophysical Research*, 108, D4, 4146, doi:10.1029/2002JD002072.

Langner, J., Rodhe, H., 1991. A global three-dimensional model of the atmospheric sulfur cycle. *Journal of Atmospheric Chemistry*, 13, 225-263.

Lannefors, H.O., Hansson, H.C. and Granat, L., 1983. Background aerosol composition in southern Sweden-fourteen micro and macro constituents measured in seven particle size intervals at one site during one year. *Atmospheric Environment*, 17, 87-101.

Lazaridis, M., Semb, A. and Hov, Ø., 1999. EMEP/CCC-Report: Long-range transport of aerosol particles A literature review.

Lee, S.-H., Kim, Y.-K., Kim, H.-S., Lee, H.-W., 2007. Influence of dense surface meteorological data assimilation on the prediction accuracy of ozone pollution in the southeastern coastal area of the Korean Peninsula. *Atmospheric Environment*, 41, 4451-4465.

Lelieveld, J., Siegmund, P., 2002. Global air pollution crossroads over the Mediterranean. *Science*, 298, 794-799.

Liu, M., Carroll, J.J., 1996. A high resolution model suitable for air pollutant dispersion studies in complex terrain. *Monthly Weather Review*, 124, 10, 2396-2409.

Lu, W. Z., Wang, X. K., 2004. Interaction patterns of major air pollutants in Hong Kong territory. *Science of the Total Environment*, 324, 247-259.

Lloyd's Register, 1995. Marine Exhaust Emissions Research Programme. Lloyd's Register Engineering Services, London.

Lyons, W. A., Tremback, C. J., Pielke, R., 1995. Applications of the Regional Atmospheric Modeling System (RAMS) to provide input to photochemical grid models for the Lake Michigan Ozone Study (LMOS). *Journal of Applied Meteorology*, 34, 1762-1786.

Mao, Q., Gautney, L. L., Cook, T. M., Jacobs, M. E., Smith, S. N., Kelsoe, J. J., 2006. Numerical experiments on MM5-CMAQ sensitivity to various PBL schemes. *Atmospheric Environment*, 40, 3092-3110.

Marintek, 1990. Exhaust gas emissions from international marine transport. Norwegian Maritime Technology Research Institute, Trondheim.

Markakis, K., Im, U., Unal, A., Dimitros, M., Yenigün, O., Incecik, S., 2009. A computational approach for the compilation of a high spatially and temporally resolved emission inventory for the İstanbul Greater Area. 7th Int. Conference on Air Quality Science and Application 24-27 March 2009, İstanbul.

Mass, C. F., Kuo, Y.-H., 1998. Regional Real-Time Numerical Weather Prediction. Current Status and Future Potential. *Bulletin of American Meteorological Society*, 79, 253-263.

Mass, C., Ovens, D., Gritmit, E. and Albright, M., 2002. (Dept. of Atmospheric Sciences, University of Washington). Issues in Mesoscale Verification: Implications of the Verification of High Resolution MM5 Forecasts over the Northwest Pacific Papers Presented at the Twelfth PSU/NCAR Mesoscale Model Users' Workshop NCAR June 24-25.

McInnes G. EMEP/CORINAIR, 1996. Atmospheric Emission Inventory Guidebook. A joint EMEP/CORINAIR Production. Prepared by the EMEP Task Force on Emission Inventories. Edited by G. McInnes. European Environment Agency.

Melas, D., Ziomas I, Klemm, O., Zeferos, C. S., 1998. Anatomy of the sea-breeze circulation in Athens area under weak large scale ambient winds. *Atmospheric Environment*, 32, 12, 2223-2237.

Memmesheimer, M., Friese, E., Jakobs, H. J. , Feldmann, H., Ebel, A. , Kessler, C., 2004. From Europe to North-Rhine-Westphalia Long-Term Calculations of Air Pollutants With The Eurad Model. Rhenish Institute for Environmental Research (RIU), EURAD-Project, University of Cologne.

Milford, J. B., Gao, D., Sillman, S., Blossey, P., Russel, A. G., 1994. Total reactive nitrogen (NO_y) as an indicator of the sensitivity of ozone to reductions in hydrocarbon and NO_x emissions. *Journal of Geophysical Research*, 99, D2, 3533-3542.

Millan, M, Salvador, R., Mantilla, E., 1996. Meteorology and photochemical air pollution in southern Europe: experimental results from EC research projects. *Atmospheric Environment*, 30, 12, 1909-1924.

Mlawer, E. J., Taubman, S. J., Brown, P. D., Iacono, M. J., Clough, S. A., 1997. Radiative transfer for inhomogeneous atmosphere: RRTM, a validated correlated-K model for the longwave. *Journal of Geophysical Research*, 102 (D14), 16663-16682.

Monforti, F., Pederzoli, A., 2005. THOSCANE: a tool to detail CORINAIR emission inventories. *Environmental Modeling and Software*, 20, 505-508.

Monks, P. S., Carpenter, L. J., Penkett, S. A., Ayers, G. P., Gillett, R. W., Galbally, I. E. and Meyer, C. P., 1998. Fundamental ozone photochemistry in the remote marine boundary layer, the Soapex experiment, measurement and theory. *Atmospheric Environment*, 32, 21, 3647-3664.

Morris, R.E., Yardwood, G., Emery, C., Pandis, S., Lurmann, F., 2003. Implementation of State-of-science PM modules into the PMCAMx photochemical grid model. 96th Annual Conference and Exhibition of A&WMA, San Diego, California

Müezzinoğlu A., Elbir T., Dinçer F., 1999. Emission Inventory of Turkey. Eurotrac-2 (A Eureka Environmental Project) GENEMIS-Generation and Evaluation of Emission Data Annual Report.

Müller, J.F., 1992. Geographical distribution and seasonal variation of surface emissions and deposition velocities of atmospheric trace gases. *Journal of Geophysical Research*, 97, 3787-3804.

Nam, J., Kimura, Y., Vizuete, W., Murphy, C., Allen, D. T., 2006. Modeling the impacts of emission events on ozone formation in Houston, Texas. *Atmospheric Environment*, 40, 5329-5341.

NARSTO, 2004. Particulate Matter Assessment for Policy Makers: A NARSTO Assessment. P. McMurry, M. Shepherd, and J. Vickery, (Eds.), Cambridge University Press, Cambridge, England. ISBN 0 52 184287 5.

Nguyen, K. C., Noonan, J. A., Galbally, I. E., Physick, W. L., 1997. Prediction of plume dispersion in complex terrain: Eulerian versus Lagrangian models. *Atmospheric Environment*, 31, 7, 947-958.

Nielsen-Gammon, J. W., 2002. Evaluation and Comparison of Preliminary Meteorological Modeling for the August 2000 Houston-Galveston Ozone Episode. TNRCC Report, 83 pp.

Nolte, C.G., Bhave, P.V., Arnold, J.R., Dennis, R.L., Zhang, K.M., Wexler, A.S., 2008. Modeling urban and regional aerosols-Application of the CMAQ-UCD aerosol model to Tampa, a coastal urban site. *Atmospheric Environment*, 42, 3179-3191.

Olivier, J.G.J., Berdowski, J.J.M., Peters, J.A.H.W., Bakker, J., Visschedijk, A.J.H., Bloos, J.-P.J., 2001. Applications of EDGAR. Including a description of EDGAR 3.0: reference database with trend data for 1970-1995. RIVM, Bilthoven. RIVM report no. 773301 001/ NOP report no. 410200 051.

Pakkanen, T.A., Hillamo, R.E., Keronen, P., Maenhaut, W., Ducastel, G., Pacyna, J.M., 1996. Sources and physico-chemical characteristics of the atmospheric aerosol in southern Norway. *Atmospheric Environment*, 30, 1391-1405.

Palmer C, Tuncali E, Dennena K, Coburn T, Finkelman T., 2004. Characterization of Turkish coals: a nationwide perspective. *International Journal of Coal Geology*, 60, 85-115.

Pandis, S.N., Seinfeld, J.H., Pilinis, C., 1990. The smog-fog-smog cycle and acid deposition. *Journal of Geophysical Research*, 95, 18489-18500.

Pandis, S.N., Seinfeld, J.H., Pilinis, C., 1992. Heterogeneous sulfate production in an urban fog. *Atmospheric Environment*, 26A, 2509-2522.

Parra, R., Jimenez, P., Baldasano, J. M., 2005. Development of the high spatial resolution EMICAT2000 emission model for air pollutants from the north-eastern Iberian Peninsula (Catalonia, Spain). *Environmental Pollution*, 140, 2, 200-219.

Peleg, M., Luria, M., Sharf, G., Vanger, A., Kallos, G., Kotroni, V., Lagouvardos, K., Varinou, M., 1997. Observational evidence of an ozone episode over the Greater Athens Area. *Atmospheric Environment*, 31, 3969-3983.

Perez, C., Jimenez, P., Jorba, O., Sicard, M., Baldasano, J. M., 2006. Influence of the PBL scheme on high resolution photochemical simulations in an urban coastal area over the Western Mediterranean. *Atmospheric Environment*, 40, 5247-5297.

Piccot, S. D., J. J. Watson, Jones, J. W., 1992. A global inventory of volatile organic compound emissions from anthropogenic sources. *Journal of Geophysical Research*, 97, 9897-9912.

Pielke, R.A., 1984. *Mesoscale Meteorological Modeling*. Academic Press. 612 pp., New York.

Pielke, R. A., Uliasz, M., 1998. Use of meteorological models as input to regional and mesoscale air quality models-limitations and strengths. *Atmospheric Environment*, 32, 8, 1455-1466.

Pirovano, G., Coll, I., Bedogni, M., Alessandrini, S., Costa, M. P., Gabusi, V., Lasry, F., Menut, L., Vautrad, R., 2007. On the influence of meteorological input on photochemical modelling of severe episode over a coastal area, *Atmospheric Environment*, 41, 30, 6445-6464.

Pleim, J. E., Chang, J.S., 1992. A non-local closure model for vertical mixing in the convective boundary layer. *Atmospheric Environment*, 26A, 965-981.

Ponche J. P., Vinuesa J. F., François S., Mirabel P., 1999. High space and time resolution emission inventories and scenarios for the air quality modeling. Eurotrac-2 (A Eureka Environmental Project) GENEMIS-Generation and Evaluation of Emission Data Annual Report.

Poupkou, A., Symeonidis, P., Lisaridis, I., Melas, D., Ziomas, I., Yay, O.D., Balis, D., 2008. Effects of anthropogenic emission sources on maximum ozone concentrations over Greece. *Atmospheric Research*, 89, 4, 374-381.

PSU/NCAR, 2005. Mesoscale modeling system tutorial class notes and user's guide: MM5 modeling system version 3. Mesoscale and Microscale Meteorology Division, National Center for Atmospheric Research

Pryor, S. C., 1998. A case study of emission changes and ozone responses. *Atmospheric Environment*, 32, 2, 123-131.

Redington, A. L., Derwent, R. G., 2002. Calculation of sulphate and nitrate aerosol concentrations over Europe using a Lagrangian dispersion model. *Atmospheric Environment*, 36, 4425-4439.

Reisner, J., Rasmussen, R. J., Bruintjes, R. T., 1998. Explicit forecasting of supercooled liquid water in winter storms using the MM5 mesoscale model. *Quarterly Journal of Royal Meteorological Society*, 124B, 1071-1107.

Reynolds, A. W., Broderick, B. M., 2000. Development of an emission inventory model for mobile sources. *Transportation Research, Part D* 5, 77-101.

Riemer, N., Vogel, H., Vogel, B., Schell, B., Ackermann, I.J., Kessler, C., Hass, H., 2003. The impact of the heterogeneous hydrolysis of N_2O_5 on chemistry and nitrate aerosol formation in the lower troposphere under photochemical conditions. *Journal of Geophysical Research*, 108, D4, ACH 5-1, CiteID 4144, DOI 10.1029/2002JD002436.

San José R., Cámara D., Salas I., 1999. A Comparison between Different Emission Data Models (IER, Germany) and EMIMO (UPM, Spain) for Air Quality Objectives. Eurotrac-2 (A Eureka Environmental Project) GENEMIS-Generation and Evaluation of Emission Data Annual Report.

Salisbury, G., Williams, J., Holzinger, R., Gros, V., Mihalopoulos, N., Vrekoussis, M., Sarda-Esteve, R., Berresheim, H., von Kuhlmann, R., Lawrence, M. and Lelieveld, J., 2003. Ground-based PTR-MS measurements of reactive organic compounds during the MINOS campaign in Crete, July-August 2001. *Atmospheric Chemistry and Physics*, 3, 925-940.

Sanadze, G.A., Kalandadze, A.N., 1966. Light and temperature curves of the evolution of C5H8. *Soviet Plant Physiology*, 13, 411-413.

Say N.P., 2006. Lignite-fired thermal power plants and SO₂ pollution in Turkey. *Energy Policy*, 34, 2690-2701.

Scheffe, R. D., Morris, R. E., 1993. A review of the development and application of the urban airshed model. *Atmospheric Environment*, 27B, 23-39.

Schmidt, H., Derognat, C., Vautard, R. and Beekmann, M., 2001. A comparison of simulated and observed ozone mixing ratios for the summer of 1998 in Western Europe. *Atmospheric Environment*, 35, 6277-6297.

Schöpp, W., Amann, M., Cofala, J., Heyes, C., Klimont, Z., 1999. Integrated Assessment of European Air Pollution Emission Control Strategies. *Environmental Modeling and Software*, 14, 1.

Sciare, J., Bardouki, H., Moulin, C., Mihalopoulos, N., 2003. Aerosol sources and their contribution to the chemical composition of aerosols in the Eastern Mediterranean Sea during summertime. *Atmospheric Chemistry and Physics*, 3, 291-302.

Seaman, N.L., 2000. Meteorological Modeling for Air-Quality Assessments. *Atmospheric Environment*, 34 2231-2259.

Shafran, P. C., Seaman, N. L., Gayno, G. A., 2000. Evaluation of numerical predictions of boundary layer structure during the Lake-Michigan Ozone Study. *Journal of Applied Meteorology*, 39, 412-426.

Seaman, N. L., Stauffer, D. R., Lario-Gibbs, A. M., 1995. A multiscale Four-Dimensional Data Assimilation System applied in the San Joaquin Valley during SARMAP. Part I: Modeling design and basic performance characteristics. *Journal of Applied Meteorology*, August, 1739-1761.

Seinfeld, J.H., Pandis, S.N., 1998. *Atmospheric chemistry and physics: From air pollution to climate change*, John Wiley & Sons, Inc., New York.

Seufert, G., Bartzis, J., Bomboi, T., Ciccioli, P., Cieslik, S., Dlugi, R., Foster, P., Hewitt, C. N., Kesselmeier, J., Lenz, D., Kotzias R., Manes, F., Perez-Pastor, R., Steinbrecher, R., Torres, L., Valentini, R., Versino, B., 1997. The bema-project: and overview of the castelporziano experiments. *Atmospheric Environment*, 31, 5-18.

Sievering, H., Botman, J., Gorman, E., Kim, Y., Anderson, L., Ennis, G., Luria, M., Pandis, S.N., 1992. Removal of sulfur from the marine boundary layer by ozone oxidation in sea-salt. *Nature*, 360, 571-573.

Sillman, S., Logan, J.A., Wofsy, S.C., 1990. A regional scale model for ozone in the United States with subgrid representation of urban and power plant plumes. *Journal of Geophysical Research*, 95, 5731-5748.

Sillman, S., 1999. The relation between ozone, NO_x and hydrocarbons in urban and polluted rural environments. *Atmospheric Environment*, 33, 1821-1845.

Sillman S., Vauratd, R., Menut, L., Kley, D., 2003. O₃-NO_x-VOC sensitivity and NO_x-VOC indicators in Paris: Results from models and Atmospheric Over the Paris Area (ESQUIF) measurements. *Journal of Geophysical Research*, 108, D17, 8563.

Simpson, D., 1992. Long-period modeling of photochemical oxidants in Europe: Model calculations for July 1985. *Atmospheric Environment*, 26A, 9, 1609-1634.

Simpson, D., 1993. Photochemical model calculations over Europe for two extended summer periods: 1985 and 1989 -Model results and comparison with observations. *Atmospheric Environment*, 27A, 6, 921-943.

Simpson D., Winiwarter W., Borjesson B., Cinderby S., Ferreiro A., Guenther A., Hewitt C.N., Janson R., Khalil A.M.K., Owen S., Pierce T.E., Puxbaum H., Shearer M., Skiba U., Steinbrecher R., Tarraso'n L. and Oquist M.G., 1999. Inventorying emissions from nature in Europe, *Journal of Geophysical Research*, 104, D7, 8113-8152.

Singles R.J and Carruthers D.J., 1999. ADMS-Urban Air Quality Management System: Some Examples of Applications and Validation in the UK. *Proceedings of EUROTRAC Symposium 98*, 821, WIT Press Southampton.

Sistla G., N. Zhou, W. Hao, J.Y Ku, S.T. Rao, R. Bornstein, F. Freedman and P. Thunis., 1996. Effects of uncertainties in meteorological inputs on urban airshed model predictions and ozone control strategies. *Atmospheric Environment*, 30, 2011-2025.

Skov, H., Egelov, A. H., Granby, K., Nielsen, T., 1996. Relationships between ozone and other photochemical products at L1. Valby, Denmark. *Atmospheric Environment*, 31, 5, 685-691.

Smiatek G., 1999. Land-use Data for Modeling Anthropogenic and Biogenic Emissions. Eurotrac-2 (A Eureka Environmental Project) GENEMIS-Generation and Evaluation of Emission Data Annual Report.

Smyth, S.C., Jiang, W., Dazhong, Y., Helmut, R., Giroux, E., 2006. Evaluation of CMAQ O₃ and PM_{2.5} performance using Pacific 2001 measurement data. *Atmospheric Environment*, 40, 2735-2749.

Srinivas, C. V., Venkatesan, R., Singh, A. B., 2007. Sensitivity of mesoscale simulations of land-sea breeze to boundary layer turbulence parameterization. *Atmospheric Environment*, 41, 2534-2548.

Stockwell, W.R., F. Kirchner, M. Kuhn Seefeld, S., 1997. A new mechanism for regional atmospheric chemistry modeling. *Journal of Geophysical Research*, 102, 25847-25879.

Sturm, P. J., Sudy, Ch., Almbauer, R. A., Meinhart, J., 1999. Updated urban emission inventory with a high resolution in time and space for the city of Graz. *The Science of the Total Environment*, 235, 111-118.

Suppan, P., Fabian, P., Vyras, L., Gryning, S. E., 1998. The behavior of ozone and peroxyacetyl nitrate concentrations for different wind regimes during the MEDCAPHOT-TRACE CAMPAIGN in the Greater Area of Athens, Greece. *Atmospheric Environment*, 32, 12, 2089-2102.

Svensson G., 1996(a). A numerical model for chemical and meteorological processes in the atmospheric boundary layer-Part I. A model description and a one-dimensional parameter study. *Journal of Applied Meteorology*, 35, 955-973.

Svensson G., 1996(b). A numerical model for chemical and meteorological processes in the atmospheric boundary layer-Part II. A case study of the air quality in Athens, Greece. *Journal of Applied Meteorology*, 35, 955-973.

Svensson, G., 1998. Model simulations of the air quality in Athens, Greece, during the Medcaphot-Trace Campaign. *Atmospheric Environment*, 32, 12, 2239-2268.

Tayanç, M., 2000. An assessment of spatial and temporal variation of sulfur dioxide levels over Istanbul, Turkey. *Environmental Pollution*, 107, 61-69.

Tayanç, M., Berçin, A., 2007. SO₂ modeling in Izmit Gulf, Turkey during the winter of 1997: 3 cases. *Environmental Modeling & Assessment*, 12, 119-129.

Tesche, T.W. 1983. Photochemical dispersion modeling: Review of model concepts and applications studies. *Environment International*, 9, 465-490.

Tesche, T. W., Morris, R., Tonnesen, G., McNally, D., Boylan, J., Brewer, P., 2006. CMAQ/CAMx annual 2002 performance evaluation over the eastern US. *Atmospheric Environment*, 40, 4906-4919.

Theodisi, C., Im, U., Bougiatioti, A., Yenigün, O., Mihalopoulos, N., 2009. Chemical composition and sources of aerosols over İstanbul, Turkey. 7th International Conference on Air Quality Science and Application 24-27 March 2009, İstanbul, Turkey.

Thunis, P., 2001. The influence of scale on modelled ground level O₃ concentrations. Norwegian Meteorological Institute EMEP /MSC-W Note 2/01.

Titov, M., Sturman, A. P., Zawar-Reza, P., 2007. Application of MM5 and CAMx4 to local scale dispersion of particulate matter for the city of Christchurch, New Zealand. *Atmospheric Environment*, 41, 327-338.

TNO/CEPMEIP emission database. Available at
http://www.air.sk/tno/cepmeip/em_factors.php.

Topçu, S., İncecik, S., 2002. Surface ozone measurements and meteorological influences in the urban atmosphere of Istanbul. *International Journal of Environment and Pollution*, 17, 4, 390-404.

Topçu, S., Anteplioğlu, U., İncecik, S., 2003. Surface ozone concentrations and its relation to wind field in Istanbul. *Water, Air & Soil Pollution, Focus* 3, 53-64.

Trozzi C, Vaccaro R., 1998. Methodologies for estimating air pollutant emissions from ships. Technical report methodologies for estimating air pollutant emissions from transport, RF98.

TUIK (Turkish Statistical Institution), 2007. Addressed Based Population Registration System Population Census 2007.

UMA (Undersecretariat for Maritime Affairs), 2007. Available at <http://www.denizecilik.gov.tr/tr/istatistik/istatistik.asp>.

USEPA (U.S. Environmental Protection Agency), 1995. Compilation of Air Pollutant Emission Factors AP-42, Fifth Edition, Volume I: Stationary Point and Area Sources. U.S. Environmental Protection Agency, Research Triangle Park, NC, January 1995.

USEPA (U.S. Environmental Protection Agency), 1996. Air quality criteria for particulate matter. Vol. I. Office of Research and Development. EPA/600/P-95/001aF.

USEPA (U.S. Environmental Protection Agency), 2000. Analysis of Commercial Marine Vessels Emissions and Fuel Consumption Data. EPA420-R-00-002, February 2000.

USEPA (U.S. Environmental Protection Agency), 2002. SPECIATE database V3.2. Available at <http://www.epa.gov/ttn/chief/software/speciate>.

van den Dool, H.M., Saha, S., 1990. Frequency dependence in forecast skill. Monthly Weather Review, 118, 128-137.

van de Velde, R. J., Faber, W. S., van Katwijk, V. F., Kuylenstierna, J. C. I., Scholten, H. J., Thewessen, T. J. M., Verspuij, M., Zevenbergen, M., 1994. The Preparation of a European Land Use Data Base. Rivm Report, Number 712401001, Bilthoven, The Netherlands.

van der Zee, S.K., Hoek, G., Harssema, H., Brunekreef, B., 1998. Characterization of particulate air pollution in urban and non-urban areas in the Netherlands. *Atmospheric Environment*, 32, 3717-3729.

Vaughan, J., B. Lamb, C. Frei, R. Wilson, C. Bowman, C. Figueroa – Kaminsky, S. Otterson, M. Boyer, C. Mass, M. Albright, J. Koenig, A. Collingwood, M. Gilroy, N. Maykut, 2004. A Numerical Daily Air – Quality Forecast System for the Pacific Northwest, *The Bulletin of the American Meteorological Society*.

Versino, B., 1997. Introduction and objectives. *Atmospheric Environment*, 31, S1, BEMA special issue, 1-3.

Vestreng V, Rigler E, Adams M, Kindbom K, Pacyna JM, Denier van der Gon H, Reis S, Travnikov O., 2006. Inventory review 2006, Emission data reported to LRTAP and NEC Directive, Stage 1, 2 and 3 review and Evaluation of Inventories of HM and POPs. EMEP/MSC-W Technical Report 1/2006 ISSN 1504-6179.

Visschedijk AJH, Zandveld PYJ, Denier van der Gon H., 2007. High Resolution Gridded European Emission Database for the EU Integrate Project GEMS, TNO-report 2007-A-R0233/B.

Walcek, C.J., Stockwell, W.R., Chang, J.S., 1990. Theoretical estimates of dynamic, radiative and chemical effects of clouds on tropospheric gases. *Atmospheric Research*, 25, 53-69.

Wilson, W.E., Suh, H.H., 1997. Fine particles and coarse particles: concentration relationships relevant to epidemiologic studies. *Journal of the Air and Waste Management Association*, 47, 1238-1249.

Winner, D. A., Cass, G. R., 1999. Modeling the long term frequency distribution of regional ozone concentrations. *Atmospheric Environment*, 33, 431-451.

Wu, Y., Hao, J., Fu, L., Wang, Z., Tang, T., 2002. Vertical and horizontal profiles of airborne particulate matter near major roads in Macao, China. *Atmospheric Environment*, 36, 4907-4918.

Xiu, A., Pleim, J. E., 2000. Development of a land surface model part I: Application in a mesoscale meteorology model. *Journal of Applied Meteorology*, 40, 192-209.

Yamartino, R. J., Scire, J. S., Hanna, S. R., Carmichael, G. R., Chang, Y. S., 1992. The CALGRID mesoscale photochemical grid model-I. Model Formulation. *Atmospheric Environment*, 26A, 1493-1512.

Yarwood, G., Rao, S., Yocke, M., Whitten, G., 2005. Updates to the Carbon Bond chemical mechanism: CBV. Final Report to the U.S. EPA, RT-0400675.

Zannetti, P., 1990. *Air Pollution Modeling: Theories, Computational Methods and Available Software*, Computational Mechanics Publications, Southampton, Boston.

Zhang, M., Uno, I., Yoshida, Y., Xu, Y., Wang, Z., Akimoto, H., Bates, T., Quinn, T., Bandy, A., Blomquist, B., 2004. Transport and transformation of sulfur compounds over East Asia during the TRACE-P and ACE-Asia campaigns. *Atmospheric Environment*, 38, 6947-6958.

Ziomas, I. C., Tzoumaka, P., Balis, D., Melas, D., Zerefos, C. S., Klemm, O., 1998. Ozone episodes in Athens, Greece: A modeling approach using data from the Medcaphot-Trace. *Atmospheric Environment*, 32, 12, 2513-2321.

APPENDICES

Appendix A Chemical Mechanisms Included in the CMAQ System

Table A.1 CB4 Mechanism Species List

Table A.2 RADM2 Photolysis Reactions (Adapted from Stockwell et al., 1990)

Table A.3 CB4 Mechanism (CB4_AE_AQ Mechanism)

Appendix B CMAQ Predefined Vertical Profiles for Initial and Boundary Concentrations

Table B.1 CMAQ Predefined Vertical Profiles for Initial Concentrations

Table B.2 CMAQ Predefined Vertical Profiles for Boundary Conditions

Appendix C Aerosol

Table C.1 Aerosol Species Concentrations

Table C.2 Equilibrium Relations and Constants (Kim et al., 1993a)

Table C.3 Organic Aerosol Yields in Terms of Amount of Precursor Reacted
(From Pandis et al., 1992 and Bowman et al., 1995)

Appendix A Chemical Mechanisms Included in the CMAQ System

Table A.1 CB-IV Mechanism Species List

Nitrogen Species NO Nitric oxide NO2 Nitrogen dioxide HONO Nitrous acid NO3 Nitrogen trioxide N2O5 Nitrogen pentoxide HNO3 Nitric acid PNA Peroxynitric acid	Oxidants O3 Ozone H2O2 Hydrogen peroxide	Sulfur Species SO2 Sulfur dioxide SULF Sulfuric acid	Atomic Species O Oxygen atom (triplet) O1D Oxygen atom (singlet)
Carbon oxides CO Carbon monoxide	Hydrocarbons PAR Paraffin carbon bond (C-C) ETH Ethene (CH ₂ =CH ₂) OLE Olefinic carbon bond (C=C) TOL Toluene (C ₆ H ₄ -CH ₃) XYL Xylene (C ₆ H ₅ -(CH ₃) ₂) ISOP Isoprene	Carbonyls and phenols FORM Formaldehyde ALD2 Acetaldehyde and higher aldehydes MGLY Methyl glyoxal (CH ₃ C(O)C(O)H) CRES Cresol and higher molecular weight phenols	Organic nitrogen PAN Peroxyacyl nitrate (CH ₃ C(O)OONO ₂) NTR Organic nitrate
Organic Radicals C2O3 Peroxyacyl radical (CH ₃ C(O)OO·) ROR Secondary organic oxy radical CRO Methylphenoxy radical	Operators XO2 NO-to-NO2 Operation XO2N NO-to-nitrate operation	Products of organics TO2 Toluene-hydroxyl radical adduct OPEN High molecular weight aromatic oxidation ring fragment ISPD Products of isoprene reactions	Species added for aerosols SULAER Counter species for H ₂ SO ₄ production TOLAER Counter species for toluene reaction XYLAER Counter species for xylene reaction CSLAER Counter species for cresol reaction TERPAER Counter species for terpene reaction TERP Monoterpenes
Species added for aqueous chemistry FACD Formic acid AACD Acetic and higher acids PACD Peroxy acetic acid UMHP Upper limit of methylhydroperoxide			

Table A.2 RADM2 Photolysis Reactions (Adapted from Stockwell et al., 1990)

Reaction	Description
$O_3 + h\nu \rightarrow O_2 + O^1D$	Ozone Photolysis to O^1D
$O_3 + h\nu \rightarrow O_2 + O^3P$	Ozone Photolysis to O^3P
$NO_2 + h\nu \rightarrow NO + O^3P$	Nitrogen Dioxide Photolysis
$NO_3 + h\nu \rightarrow NO + O_2$	Nitrate Photolysis to NO
$NO_3 + h\nu \rightarrow NO_2 + O^3P$	Nitrate Photolysis to NO_2
$HONO + h\nu \rightarrow OH + NO$	Nitrous Acid Photolysis
$HNO_3 + h\nu \rightarrow OH + NO_2$	Nitric Acid Photolysis
$HNO_4 + h\nu \rightarrow HO_2 + NO_2$	Pernitric Acid Photolysis
$H_2O_2 + h\nu \rightarrow OH + OH$	Hydrogen Peroxide Photolysis
$HCHO + h\nu \rightarrow H + HCO$	Formaldehyde Photolysis to Radicals
$HCHO + h\nu \rightarrow H_2 + CO$	Formaldehyde Photolysis to Molecular Hydrogen
$CH_3CHO + h\nu (+2O_2) \rightarrow CH_3OO + HO_2 + CO$	Acetaldehyde Photolysis
$CH_3COCH_3 + h\nu \rightarrow CH_3 + CH_3CO$	Acetone Photolysis
$CH_3COC_2H_5 + h\nu \rightarrow ACO_3 + ETH$	Methyl Ethyl Ketone Photolysis
$HCOCHO + h\nu \rightarrow HCHO + CO$	Glyoxal Photolysis to Formaldehyde
$HCOCHO + h\nu \rightarrow 2CO + H_2$	Glyoxal Photolysis to Molecular Hydrogen
$CH_3COCHO + h\nu \rightarrow ACO_3 + HO_2 + CO$	Methyl Glyoxal Photolysis
$HCOCH=CHCHO + h\nu \rightarrow 0.98HO_2 + TCO_3 + 0.02ACO_3$	Unsaturated Dicarbonyl Photolysis
$CH_3OOH + h\nu \rightarrow CH_2O + OH + HO_2$	Methyl Hydrogen Peroxide Photolysis
$CH_3ONO_2 + h\nu \rightarrow 0.2ALD + 0.8KET + HO_2 + NO_2$	Organic Nitrate Photolysis
$C_3H_4O + h\nu \rightarrow \text{products}$	Acrolein Photolysis

Table A.3 CB4 Mechanism (CB4_AE_AQ Mechanism)

Reaction List

{1}	NO2	+	hv	-->	NO	+	O
{2}	O	+	[O2]	-->	O3		
{3}	O3	+	NO	-->	NO2		
{4}	O	+	NO2	-->	NO		
{5}	O	+	NO2	-->	NO3		
{6}	O	+	NO	-->	NO2		
{7}	O3	+	NO2	-->	NO3		
{8}	O3	+	hv	-->	O		
{9}	O3	+	hv	-->	O1D		
{10}	O1D	+	[N2]	-->	O		
{11}	O1D	+	[O2]	-->	O		
{12}	O1D	+	[H2O]	-->	2.000*OH		
{13}	O3	+	OH	-->	HO2		
{14}	O3	+	HO2	-->	OH		
{15}	NO3	+	hv	-->	0.890*NO2 + 0.890*O + 0.110*NO		
{16}	NO3	+	NO	-->	2.000*NO2		
{17}	NO3	+	NO2	-->	NO + NO2		
{18}	NO3	+	NO2	-->	N2O5		
{19}	N2O5	+	[H2O]	-->	2.000*HNO3		
{20}	N2O5			-->	NO3 + NO2		
{21}	NO	+	NO + [O2]	-->	2.000*NO2		
{22}	NO	+	NO2 + [H2O]	-->	2.000*HONO		
{23}	OH	+	NO	-->	HONO		
{24}	HONO	+	hv	-->	OH + NO		
{25}	HONO	+	OH	-->	NO2		
{26}	HONO	+	HONO	-->	NO + NO2		
{27}	OH	+	NO2	-->	HNO3		
{28}	OH	+	HNO3	-->	NO3		
{29}	HO2	+	NO	-->	OH + NO2		
{30}	HO2	+	NO2	-->	PNA		
{31}	PNA			-->	HO2 + NO2		
{32}	PNA	+	OH	-->	NO2		
{33}	HO2	+	HO2	-->	H2O2		
{34}	HO2 + HO2 + [H2O]			-->	H2O2		
{35}	H2O2	+	hv	-->	2.000*OH		
{36}	H2O2	+	OH	-->	HO2		

Table A.3 (continued)

{37}	CO	+	OH	-->	HO2
{38}	FORM	+	OH	-->	HO2 + CO
{39}	FORM	+	hv	-->	2.000*HO2 + CO
{40}	FORM	+	hv	-->	CO
{41}	FORM	+	O	-->	OH + HO2 + CO
{42}	FORM	+	NO3	-->	HNO3 + HO2 + CO
{43}	ALD2	+	O	-->	C2O3 + OH
{44}	ALD2	+	OH	-->	C2O3
{45}	ALD2	+	NO3	-->	C2O3 + HNO3
{46}	ALD2	+	hv	-->	XO2 + 2.000*HO2 + CO + FORM
{47}	C2O3	+	NO -	->	NO2 + XO2 + FORM + HO2
{48}	C2O3	+	NO2	-->	PAN
{49}	PAN			-->	C2O3 + NO2
{50}	C2O3 + C2O3			-->	2.000*XO2 + 2.000*FORM + 2.000*HO2
{51}	C2O3 + HO2			-->	0.790*FORM+0.790*XO2+0.790*HO2+ 0.790*OH
{52}	OH			-->	XO2 + FORM + HO2
{53}	PAR	+	OH	-->	0.870*XO2+0.130*XO2N+0.110*HO2+ 0.110*ALD2 + 0.760*ROR - 0.110*PAR
{54}	ROR			-->	1.100*ALD2 + 0.960*XO2 + 0.940*HO2 - 2.100*PAR + 0.040*XO2N + 0.020*ROR
{55}	ROR			-->	HO2
{56}	ROR	+	NO2	-->	NTR
{57}	OLE	+	O	-->	0.630*ALD2 + 0.380*HO2 + 0.280*XO2 + 0.300*CO + 0.200*FORM + 0.020*XO2N+ 0.220*PAR + 0.200*OH
{58}	OLE	+	OH	-->	FORM + ALD2 + XO2 + HO2 - PAR
{59}	OLE	+	O3	-->	0.500*ALD2 + 0.740*FORM + 0.330*CO + 0.440*HO2 + 0.220*XO2 + 0.100*OH - PAR
{60}	OLE	+	NO3	-->	0.910*XO2 + 0.090*XO2N + FORM + ALD2 - PAR + NO2
{61}	ETH	+	O	-->	FORM+0.700*XO2+ CO+ 1.700*HO2 + 0.300*OH
{62}	ETH	+	OH	-->	XO2 + 1.560*FORM + HO2+ 0.220*ALD2
{63}	ETH	+	O3	-->	FORM + 0.420*CO + 0.120*HO2
{64}	TOL	+	OH	-->	0.080*XO2+0.360*CRES+0.440*HO2+ 0.560*TO2
{65}	TO2	+	NO	-->	0.900*NO2+0.900*HO2+0.900*OPEN+ 0.100*NTR
{66}	TO2			-->	CRES + HO2
{67}	CRES	+	OH -	->	0.400*CRO+0.600*XO2+0.600*HO2+ .300*OPEN
{68}	CRES	+	NO3	-->	CRO + HNO3+CSLAER

Table A.3 (continued)

{69}	CRO	+	NO2	-->	NTR
{70}	XYL	+	OH	-->	0.700*HO2 + 0.500*XO2 + 0.200*CRES +0.800*MGLY+1.100*PAR+0.300*TO2+XYLAER
{71}	OPEN	+	OH	-->	XO2 + 2.000*CO + 2.000*HO2+ C2O3 + FORM
{72}	OPEN	+	hv	-->	C2O3 + HO2 + CO
{73}	OPEN	+	O3	-->	0.030*ALD2 + 0.620*C2O3 + 0.700*FORM + 0.030*XO2 + 0.690*CO + 0.080*OH+ 0.760*HO2 + 0.200*MGLY
{74}	MGLY	+	OH	-->	XO2 + C2O3
{75}	MGLY	+	hv	-->	C2O3 + HO2 + CO
{76}	ISOP	+	O	-->	0.750*ISPD + 0.500*FORM + 0.250*XO2 + 0.250*HO2 + 0.250*C2O3 + 0.250*PAR
{77}	ISOP	+	OH	-->	0.912*ISPD + 0.629*FORM + 0.991*XO2 + 0.912*HO2 + 0.088*XO2N
{78}	ISOP	+	O3	-->	0.650*ISPD + 0.600*FORM + 0.200*XO2 + 0.066*HO2 + 0.266*OH + 0.200*C2O3+ 0.150*ALD2 + 0.350*PAR + 0.066*CO
{79}	ISOP	+	NO3	-->	0.200*ISPD + 0.800*NTR + XO2 + 0.800*HO2 + 0.200*NO2 + 0.800*ALD2+ 2.400*PAR
{80}	XO2	+	NO	-->	NO2
{81}	XO2	+	XO2	-->	
{82}	XO2N	+	NO	-->	NTR
{83}	SO2	+	OH	-->	SULF + HO2+SULAER
{84}	SO2			-->	SULF+SULAER
{85}	XO2	+	HO2	-->	UMHP
{86}	XO2N	+	HO2	-->	
{87}	XO2N	+	XO2N	-->	
{88}	XO2N	+	XO2	-->	
{89}	ISPD	+	OH	-->	1.565*PAR + 0.167*FORM + 0.713*XO2 + 0.503*HO2 + 0.334*CO + 0.168*MGLY+ 0.273*ALD2 + 0.498*C2O3
{90}	ISPD	+	O3	-->	0.114*C2O3 + 0.150*FORM + 0.850*MGLY + 0.154*HO2 + 0.268*OH + 0.064*XO2+ 0.020*ALD2 + 0.360*PAR + 0.225*CO
{91}	ISPD	+	NO3	-->	0.357*ALD2 + 0.282*FORM + 1.282*PAR + 0.925*HO2 + 0.643*CO + 0.850*NTR+ 0.075*C2O3 + 0.075*XO2 + 0.075*HNO3
{92}	ISPD	+	hv	-->	0.333*CO + 0.067*ALD2 + 0.900*FORM + 0.832*PAR + 1.033*HO2 + 0.700*XO2+ 0.967*C2O3
{93}	ISOP	+	NO2	-->	0.200*ISPD + 0.800*NTR + XO2 + 0.800*HO2 + 0.200*NO + 0.800*ALD2+ 2.400*PAR

Table A.3 (continued)

{94}	TERP	+	OH	-->	TERPAER + OH
{95}	TERP	+	NO3	-->	TERPAER + NO3
{96}	TERP	+	O3	-->	TERPAER + O3

Rate Expression	Rate Constant
k(1) uses photo table NO2_CBIV88, scaled by 1.00000E+00	{0.00000E+00}
k(2) is a falloff expression using:	{1.37387E-14}
$k_0 = 6.0000E-34 * (T/300)**(-2.30)$	
$k_{inf} = 2.8000E-12 * (T/300)**(0.00)$	
F = 0.60, n = 1.00	
k(3) = $1.8000E-12 * \exp(-1370.0/T)$	{1.81419E-14}
k(4) = $9.3000E-12$	{9.30000E-12}
k(5) is a falloff expression using:	{1.57527E-12}
$k_0 = 9.0000E-32 * (T/300)**(-2.00)$	
$k_{inf} = 2.2000E-11 * (T/300)**(0.00)$	
F = 0.60, n = 1.00	
k(6) is a falloff expression using:	{1.66375E-12}
$k_0 = 9.0000E-32 * (T/300)**(-1.50)$	
$k_{inf} = 3.0000E-11 * (T/300)**(0.00)$	
F = 0.60, n = 1.00	
k(7) = $1.2000E-13 * \exp(-2450.0/T)$	{3.22581E-17}
k(8) uses photo table NO2_CBIV88, scaled by 5.30000E-02	{0.00000E+00}
k(9) uses photo table O3O1D_CBIV88, scaled by 1.00000E+00	{0.00000E+00}
k(10) = $1.8000E-11 * \exp(107.0/T)$	{2.57757E-11}
k(11) = $3.2000E-11 * \exp(67.0/T)$	{4.00676E-11}
k(12) = $2.2000E-10$	{2.20000E-10}
k(13) = $1.6000E-12 * \exp(-940.0/T)$	{6.82650E-14}
k(14) = $1.4000E-14 * \exp(-580.0/T)$	{1.99920E-15}
k(15) uses photo table NO2_CBIV88, scaled by 3.39000E+01	{0.00000E+00}
k(16) = $1.3000E-11 * \exp(250.0/T)$	{3.00805E-11}
k(17) = $2.5000E-14 * \exp(-1230.0/T)$	{4.03072E-16}
k(18) is a falloff expression using:	{1.26440E-12}
$k_0 = 2.2000E-30 * (T/300)**(-4.30)$	
$k_{inf} = 1.5000E-12 * (T/300)**(-0.50)$	
F = 0.60, n = 1.00	

Table A.3 (continued)

k(19) = 1.3000E-21	{1.30000E-21}
k(20) = k(18) / Keq, where Keq = 2.700E-27 * exp(11000.0/T)	{4.36029E-02}
k(21) = 3.3000E-39 * exp(530.0/T)	{1.95397E-38}
k(22) = 4.4000E-40	{4.39999E-40}
k(23) is a falloff expression using:	{6.69701E-12}
k0 = 6.7000E-31 * (T/300)**(-3.30)	
kinf = 3.0000E-11 * (T/300)**(-1.00)	
F = 0.60, n = 1.00	
k(24) uses photo table NO2_CBIV88, scaled by 1.97500E-01	{0.00000E+00}
k(25) = 6.6000E-12	{6.60000E-12}
k(26) = 1.0000E-20	{1.00000E-20}
k(27) is a falloff expression using:	{1.14885E-11}
k0 = 2.6000E-30 * (T/300)**(-3.20)	
kinf = 2.4000E-11 * (T/300)**(-1.30)	
F = 0.60, n = 1.00	
k(28) is a special rate expression of the form:	{1.47236E-13}
k = k0 + {k3[M] / (1 + k3[M]/k2)}, where	
k0 = 7.2000E-15 * exp(785.0/T)	
k2 = 4.1000E-16 * exp(1440.0/T)	
k3 = 1.9000E-33 * exp(725.0/T)	
k(29) = 3.7000E-12 * exp(240.0/T)	{8.27883E-12}
k(30) is a falloff expression using:	{1.48014E-12}
k0 = 2.3000E-31 * (T/300)**(-4.60)	
kinf = 4.2000E-12 * (T/300)**(0.20)	
F = 0.60, n = 1.00	
k(31) = k(30) / Keq, where Keq = 2.100E-27 * exp(10900.0/T)	{9.17943E-02}
k(32) = 1.3000E-12 * exp(380.0/T)	{4.65309E-12}
k(33) = 5.9000E-14 * exp(1150.0/T)	{2.79783E-12}
k(34) = 2.2000E-38 * exp(5800.0/T)	{6.23927E-30}
k(35) uses photo table HCHOmole_CBIV88, scaled by 2.55000E-01	{0.00000E+00}
k(36) = 3.1000E-12 * exp(-187.0/T)	{1.65514E-12}
k(37) = 1.5000E-13 * (1.0 + 0.6*Pressure)	{2.40000E-13}
k(38) = 1.0000E-11	{1.00000E-11}
k(39) uses photo table HCHOrad_CBIV88, scaled by 1.00000E+00	{0.00000E+00}
k(40) uses photo table HCHOmole_CBIV88, scaled by 1.00000E+00	{0.00000E+00}
k(41) = 3.0000E-11 * exp(-1550.0/T)	{1.65275E-13}
k(42) = 6.3000E-16	{6.30000E-16}

Table A.3 (continued)

$k(43) = 1.2000E-11 * \exp(-986.0/T)$	{4.38753E-13}
$k(44) = 7.0000E-12 * \exp(250.0/T)$	{1.61972E-11}
$k(45) = 2.5000E-15$	{2.50000E-15}
$k(46)$ uses photo table ALD_CBIV88, scaled by 1.00000E+00	{0.00000E+00}
$k(47) = 3.4900E-11 * \exp(-180.0/T)$	{1.90766E-11}
$k(48) = 2.6300E-12 * \exp(380.0/T)$	{9.41356E-12}
$k(49) = 2.0000E+16 * \exp(-13500.0/T)$	{4.23268E-04}
$k(50) = 2.5000E-12$	{2.50000E-12}
$k(51) = 6.5000E-12$	{6.50000E-12}
$k(52) = 1.1000E+02 * \exp(-1710.0/T)$	{3.54242E-01}
$k(53) = 8.1000E-13$	{8.10000E-13}
$k(54) = 1.0000E+15 * \exp(-8000.0/T)$	{2.19325E+03}
$k(55) = 1.6000E+03$	{1.60000E+03}
$k(56) = 1.5000E-11$	{1.50000E+11}
$k(57) = 1.2000E-11 * \exp(-324.0/T)$	{4.04572E-12}
$k(58) = 5.2000E-12 * \exp(504.0/T)$	{2.82173E-11}
$k(59) = 1.4000E-14 * \exp(-2105.0/T)$	{1.19778E-17}
$k(60) = 7.7000E-15$	{7.70000E-15}
$k(61) = 1.0000E-11 * \exp(-792.0/T)$	{7.01080E-13}
$k(62) = 2.0000E-12 * \exp(411.0/T)$	{7.94340E-12}
$k(63) = 1.3000E-14 * \exp(-2633.0/T)$	{1.89105E-18}
$k(64) = 2.1000E-12 * \exp(322.0/T)$	{6.18715E-12}
$k(65) = 8.1000E-12$	{8.10000E-12}
$k(66) = 4.2000E+00$	{4.20000E+00}
$k(67) = 4.1000E-11$	{4.10000E-11}
$k(68) = 2.2000E-11$	{2.20000E-11}
$k(69) = 1.4000E-11$	{1.40000E-11}
$k(70) = 1.7000E-11 * \exp(116.0/T)$	{2.50901E-11}
$k(71) = 3.0000E-11$	{3.00000E-11}
$k(72)$ uses photo table HCHOrad_CBIV88, scaled by 9.04000E+00	{0.00000E+00}
$k(73) = 5.4000E-17 * \exp(-500.0/T)$	{1.00858E-17}
$k(74) = 1.7000E-11$	{1.70000E-11}
$k(75)$ uses photo table HCHOrad_CBIV88, scaled by 9.64000E+00	{0.00000E+00}
$k(76) = 3.6000E-11$	{3.60000E-11}
$k(77) = 2.5400E-11 * \exp(407.6/T)$	{9.97368E-11}
$k(78) = 7.8600E-15 * \exp(-1912.0/T)$	{1.28512E-17}
$k(79) = 3.0300E-12 * \exp(-448.0/T)$	{6.73819E-13}

Table A.3 (continued)

$k(80) = 8.1000\text{E-}12$	{8.10000E-12}
$k(81) = 1.7000\text{E-}14 * \exp(1300.0/T)$	{1.33359E-12}
$k(82) = 8.1000\text{E-}12$	{8.10000E-12}
$k(83) = 4.3900\text{E-}13 * \exp(160.0/T)$	{7.51005E-13}
$k(84) = 1.3600\text{E-}06$	{1.36000E-06}
$k(85) = 7.6700\text{E-}14 * \exp(1300.0/T)$	{6.01684E-12}
$k(86) = 7.6700\text{E-}14 * \exp(1300.0/T)$	{6.01684E-12}
$k(87) = 1.7300\text{E-}14 * \exp(1300.0/T)$	{1.35712E-12}
$k(88) = 3.4500\text{E-}14 * \exp(1300.0/T)$	{2.70640E-12}
$k(89) = 3.3600\text{E-}11$	{3.36000E-11}
$k(90) = 7.1100\text{E-}18$	{7.11000E-18}
$k(91) = 1.0000\text{E-}15$	{1.00000E-15}
$k(92)$ uses photo table ACROLEIN, scaled by $3.60000\text{E-}03$	{0.00000E+00}
$k(93) = 1.4900\text{E-}19$	{1.49000E-19}
$k(94) = 1.0700\text{E-}11 * \exp(549.0/T)$	{6.75269E-11}
$k(95) = 3.2300\text{E-}11 * \exp(-975.0/T)$	{1.22539E-12}
$k(96) = 7.2900\text{E-}15 * \exp(-1136.0/T)$	{1.61125E-16}

Table B.1 (continued)

35	TPAN	0.100E-07	0.100E-07	0.100E-07	0.100E-07	0.100E-07	0.100E-07	0.100E-07
36	HONO	0.100E-08	0.100E-08	0.100E-08	0.100E-08	0.100E-08	0.100E-08	0.100E-08
37	HNO4	0.200E-08	0.200E-08	0.200E-08	0.200E-08	0.200E-08	0.200E-08	0.200E-08
38	KET	0.300E-04	0.350E-04	0.300E-04	0.200E-04	0.200E-04	0.100E-04	
39	GLY	0.250E-06	0.250E-06	0.250E-06	0.200E-06	0.100E-06	0.500E-07	
40	MGLY	0.250E-06	0.250E-06	0.250E-06	0.200E-06	0.100E-06	0.500E-07	
41	DCB	0.250E-06	0.250E-06	0.250E-06	0.200E-06	0.100E-06	0.500E-07	
42	ONIT	0.200E-04	0.200E-04	0.160E-04	0.600E-05	0.200E-05	0.000E+00	
43	CSL	0.100E-08	0.100E-08	0.100E-08	0.100E-08	0.100E-08	0.100E-08	
44	ISO	0.250E-05	0.250E-05	0.250E-05	0.250E-05	0.250E-05	0.250E-05	
45	HO	0.000E+00	0.000E+00	0.000E+00	0.000E+00	0.000E+00	0.000E+00	
46	HO2	0.000E+00	0.000E+00	0.000E+00	0.000E+00	0.000E+00	0.000E+00	
47	ASO4I	4.810E-02	3.207E-02	1.603E-02	1.603E-02	3.207E-03	1.603E-03	
48	ASO4J	1.154E+00	7.696E-01	3.848E-01	3.848E-01	7.696E-02	3.848E-02	
49	NUMATKN	1.437E+10	9.583E+09	4.791E+09	4.791E+09	9.583E+08	4.791E+08	
50	NUMACC	4.110E+08	2.740E+08	1.370E+08	1.370E+08	2.740E+07	1.370E+07	
51	ASOIL	1.000E+00	8.000E-01	4.000E-01	4.000E-01	8.000E-02	4.000E-02	
52	NUMCOR	1.740E+04	1.392E+04	6.960E+03	6.960E+03	1.392E+03	6.960E+02	

Table B.2 CMAQ Predefined Vertical Profiles for Boundary Conditions

1	Optional boundary condition: The vertical coordinate of the model to
2	generate these b.c. is the terrain-following sigma coordinate. The number of
3	sigma layers and defined sigma levels are listed below.
4	6 47 1.00 0.98 0.93 0.84 0.60 0.30 0.00 4
5	
6	North
7	
8	SO2 0.300E-03 0.200E-03 0.100E-03 0.100E-03 0.200E-04 0.100E-04
9	SULF 0.150E-03 0.150E-03 0.100E-03 0.100E-03 0.200E-04 0.100E-04
10	NO2 0.200E-04 0.200E-04 0.100E-04 0.000E+00 0.000E+00 0.000E+00
11	NO 0.200E-04 0.200E-04 0.100E-04 0.000E+00 0.000E+00 0.000E+00
12	O3 0.350E-01 0.350E-01 0.400E-01 0.500E-01 0.600E-01 0.700E-01
13	HNO3 0.500E-04 0.500E-04 0.500E-04 0.500E-04 0.700E-04 0.100E-03
14	H2O2 0.100E-02 0.100E-02 0.150E-02 0.100E-02 0.800E-03 0.200E-03
15	ALD 0.300E-04 0.350E-04 0.300E-04 0.200E-04 0.200E-04 0.100E-04
16	HCHO 0.250E-03 0.250E-03 0.250E-03 0.200E-03 0.100E-03 0.500E-04
17	OP1 0.250E-06 0.250E-06 0.250E-06 0.200E-06 0.100E-06 0.500E-07
18	OP2 0.300E-07 0.350E-07 0.300E-07 0.200E-07 0.200E-07 0.100E-07
19	PAA 0.300E-04 0.300E-04 0.300E-04 0.250E-04 0.200E-04 0.150E-04
20	ORA1 0.100E-05 0.100E-05 0.500E-06 0.500E-06 0.500E-06 0.000E+00
21	ORA2 0.100E-05 0.100E-05 0.500E-06 0.500E-06 0.500E-06 0.000E+00
22	NH3 0.100E-03 0.100E-03 0.300E-04 0.200E-04 0.200E-04 0.100E-04
23	N2O5 0.000E+00 0.000E+00 0.000E+00 0.000E+00 0.000E+00 0.000E+00
24	NO3 0.000E+00 0.000E+00 0.000E+00 0.000E+00 0.000E+00 0.000E+00
25	PAN 0.200E-04 0.200E-04 0.100E-04 0.100E-04 0.100E-04 0.000E+00
26	HC3 0.400E-04 0.400E-04 0.320E-04 0.120E-04 0.400E-05 0.000E+00
27	HC5 0.400E-04 0.400E-04 0.320E-04 0.120E-04 0.400E-05 0.000E+00
28	HC8 0.200E-04 0.200E-04 0.160E-04 0.600E-05 0.200E-05 0.000E+00
29	ETH 0.000E+00 0.000E+00 0.000E+00 0.000E+00 0.000E+00 0.000E+00
30	CO 0.800E-01 0.800E-01 0.800E-01 0.700E-01 0.650E-01 0.500E-01
31	OL2 0.500E-05 0.300E-05 0.200E-05 0.100E-05 0.100E-05 0.000E+00
32	OLT 0.200E-06 0.200E-06 0.100E-06 0.000E+00 0.000E+00 0.000E+00
33	OLI 0.100E-06 0.100E-06 0.000E+00 0.000E+00 0.000E+00 0.000E+00
34	TOL 0.100E-05 0.100E-05 0.100E-05 0.100E-05 0.000E+00 0.000E+00
35	XYL 0.200E-06 0.200E-06 0.100E-06 0.000E+00 0.000E+00 0.000E+00
36	ACO3 0.100E-08 0.100E-08 0.100E-08 0.100E-08 0.100E-08 0.100E-08
37	TPAN 0.100E-07 0.100E-07 0.100E-07 0.100E-07 0.100E-07 0.100E-07

Table B.2 (continued)

38	HONO	0.100E-08	0.100E-08	0.100E-08	0.100E-08	0.100E-08	0.100E-08
39	HNO4	0.200E-08	0.200E-08	0.200E-08	0.200E-08	0.200E-08	0.200E-08
40	KET	0.300E-04	0.350E-04	0.300E-04	0.200E-04	0.200E-04	0.100E-04
41	GLY	0.250E-06	0.250E-06	0.250E-06	0.200E-06	0.100E-06	0.500E-07
42	MGLY	0.250E-06	0.250E-06	0.250E-06	0.200E-06	0.100E-06	0.500E-07
43	DCB	0.250E-06	0.250E-06	0.250E-06	0.200E-06	0.100E-06	0.500E-07
44	ONIT	0.200E-04	0.200E-04	0.160E-04	0.600E-05	0.200E-05	0.000E+00
45	CSL	0.100E-08	0.100E-08	0.100E-08	0.100E-08	0.100E-08	0.100E-08
46	ISO	0.250E-05	0.250E-05	0.250E-05	0.250E-05	0.250E-05	0.250E-05
47	HO	0.000E+00	0.000E+00	0.000E+00	0.000E+00	0.000E+00	0.000E+00
48	HO2	0.000E+00	0.000E+00	0.000E+00	0.000E+00	0.000E+00	0.000E+00
49	ASO4I	2.405E-02	2.405E-02	1.603E-02	1.603E-02	3.207E-03	1.603E-03
50	ASO4J	5.772E-01	5.772E-01	3.848E-01	3.848E-01	7.696E-02	3.848E-02
51	NUMATKN	7.187E+09	7.187E+09	4.791E+09	4.791E+09	9.583E+08	4.791E+08
52	NUMACC	2.055E+08	2.055E+08	1.370E+08	1.370E+08	2.740E+07	1.370E+07
53	ASOIL	5.000E-01	5.000E-01	4.000E-01	4.000E-01	8.000E-01	3.000E-01
54	NUMCOR	8.750E+03	8.750E+03	7.000E+03	7.000E+03	1.400E+03	5.250E+02
55	East						
56							
57	SO2	0.000E+00	0.000E+00	0.000E+00	0.000E+00	0.000E+00	0.000E+00
58	SULF	0.200E-03	0.200E-03	0.200E-03	0.200E-03	0.200E-04	0.100E-04
59	NO2	0.100E-04	0.100E-04	0.000E+00	0.000E+00	0.000E+00	0.000E+00
60	NO	0.000E+00	0.000E+00	0.000E+00	0.000E+00	0.000E+00	0.000E+00
61	O3	0.300E-01	0.350E-01	0.400E-01	0.500E-01	0.600E-01	0.700E-01
62	HNO3	0.500E-04	0.500E-04	0.500E-04	0.500E-04	0.500E-04	0.150E-03
63	H2O2	0.200E-02	0.200E-02	0.200E-02	0.200E-02	0.150E-02	0.150E-02
64	ALD	0.400E-04	0.400E-04	0.400E-04	0.400E-04	0.400E-04	0.400E-04
65	HCHO	0.250E-03	0.250E-03	0.250E-03	0.200E-03	0.150E-03	0.100E-03
66	OP1	0.250E-06	0.250E-06	0.250E-06	0.200E-06	0.150E-06	0.100E-06
67	OP2	0.400E-07	0.400E-07	0.400E-07	0.400E-07	0.400E-07	0.400E-07
68	PAA	0.500E-04	0.500E-04	0.500E-04	0.500E-04	0.500E-04	0.500E-04
69	ORA1	0.150E-05	0.500E-06	0.500E-06	0.500E-06	0.500E-06	0.500E-06
70	ORA2	0.150E-05	0.500E-06	0.500E-06	0.500E-06	0.500E-06	0.500E-06
71	NH3	0.500E-04	0.500E-04	0.500E-04	0.200E-04	0.200E-04	0.200E-04
72	N2O5	0.000E+00	0.000E+00	0.000E+00	0.000E+00	0.000E+00	0.000E+00
73	NO3	0.000E+00	0.000E+00	0.000E+00	0.000E+00	0.000E+00	0.000E+00
74	PAN	0.100E-04	0.100E-04	0.100E-04	0.100E-04	0.100E-04	0.100E-04

Table B.2 (continued)

75	HC3	0.120E-04	0.120E-04	0.120E-04	0.800E-05	0.400E-05	0.400E-05
76	HC5	0.120E-04	0.120E-04	0.120E-04	0.800E-05	0.400E-05	0.400E-05
77	HC8	0.600E-05	0.600E-05	0.600E-05	0.400E-05	0.200E-05	0.200E-05
78	ETH	0.000E+00	0.000E+00	0.000E+00	0.000E+00	0.000E+00	0.000E+00
79	CO	0.800E-01	0.800E-01	0.800E-01	0.750E-01	0.700E-01	0.650E-01
80	OL2	0.000E+00	0.000E+00	0.000E+00	0.000E+00	0.000E+00	0.000E+00
81	OLT	0.000E+00	0.000E+00	0.000E+00	0.000E+00	0.000E+00	0.000E+00
82	OLI	0.000E+00	0.000E+00	0.000E+00	0.000E+00	0.000E+00	0.000E+00
83	TOL	0.000E+00	0.000E+00	0.000E+00	0.000E+00	0.000E+00	0.000E+00
84	XYL	0.000E+00	0.000E+00	0.000E+00	0.000E+00	0.000E+00	0.000E+00
85	ACO3	0.100E-08	0.100E-08	0.100E-08	0.100E-08	0.100E-08	0.100E-08
86	TPAN	0.100E-07	0.100E-07	0.100E-07	0.100E-07	0.100E-07	0.100E-07
87	HONO	0.100E-08	0.100E-08	0.100E-08	0.100E-08	0.100E-08	0.100E-08
88	HNO4	0.200E-08	0.200E-08	0.200E-08	0.200E-08	0.200E-08	0.200E-08
89	KET	0.400E-04	0.400E-04	0.400E-04	0.400E-04	0.400E-04	0.400E-04
90	GLY	0.250E-06	0.250E-06	0.250E-06	0.200E-06	0.150E-06	0.100E-06
91	MGLY	0.250E-06	0.250E-06	0.250E-06	0.200E-06	0.150E-06	0.100E-06
92	DCB	0.250E-06	0.250E-06	0.250E-06	0.200E-06	0.150E-06	0.100E-06
93	ONIT	0.600E-05	0.600E-05	0.600E-05	0.400E-05	0.200E-05	0.200E-05
94	CSL	0.100E-08	0.100E-08	0.100E-08	0.100E-08	0.100E-08	0.100E-08
95	ISO	0.250E-05	0.250E-05	0.250E-05	0.250E-05	0.250E-05	0.250E-05
96	HO	0.000E+00	0.000E+00	0.000E+00	0.000E+00	0.000E+00	0.000E+00
97	HO2	0.000E+00	0.000E+00	0.000E+00	0.000E+00	0.000E+00	0.000E+00
98	ASO4I	3.207E-02	3.207E-02	3.207E-02	3.207E-02	3.207E-03	1.603E-03
99	ASO4J	7.696E-01	7.696E-01	7.696E-01	7.696E-01	7.696E-02	3.848E-02
100	NUMATKN	9.583E+09	9.583E+09	9.583E+09	9.583E+09	9.583E+08	4.791E+08
101	NUMACC	2.740E+08	2.740E+08	2.740E+08	2.740E+08	2.740E+07	1.370E+07
102	ASOIL	8.000E-01	8.000E-01	8.000E-01	8.000E-01	8.000E-02	4.000E-02
103	NUMCOR	1.392E+04	1.392E+04	1.392E+04	1.392E+04	1.392E+03	6.960E+02
104	South						
105							
106	SO2	0.000E+00	0.000E+00	0.000E+00	0.000E+00	0.000E+00	0.000E+00
107	SULF	0.200E-03	0.200E-03	0.200E-03	0.100E-03	0.500E-04	0.200E-04
108	NO2	0.100E-04	0.100E-04	0.000E+00	0.000E+00	0.000E+00	0.000E+00
109	NO	0.100E-04	0.100E-04	0.000E+00	0.000E+00	0.000E+00	0.000E+00
110	O3	0.300E-01	0.350E-01	0.400E-01	0.500E-01	0.600E-01	0.700E-01
111	HNO3	0.500E-04	0.500E-04	0.500E-04	0.500E-04	0.500E-04	0.150E-03

Table B.2 (continued)

112	H2O2	0.200E-02	0.200E-02	0.200E-02	0.200E-02	0.150E-02	0.100E-02
113	ALD	0.400E-04	0.400E-04	0.400E-04	0.400E-04	0.400E-04	0.500E-05
114	HCHO	0.250E-03	0.250E-03	0.250E-03	0.200E-03	0.150E-03	0.100E-03
115	OP1	0.250E-06	0.250E-06	0.250E-06	0.200E-06	0.150E-06	0.100E-06
116	OP2	0.400E-07	0.400E-07	0.400E-07	0.400E-07	0.400E-07	0.500E-08
117	PAA	0.100E-03	0.100E-03	0.100E-03	0.100E-03	0.500E-04	0.500E-04
118	ORA1	0.150E-05	0.500E-06	0.500E-06	0.500E-06	0.500E-06	0.500E-06
119	ORA2	0.150E-05	0.500E-06	0.500E-06	0.500E-06	0.500E-06	0.500E-06
120	NH3	0.500E-04	0.500E-04	0.500E-04	0.300E-04	0.200E-04	0.200E-04
121	N2O5	0.000E+00	0.000E+00	0.000E+00	0.000E+00	0.000E+00	0.000E+00
122	NO3	0.000E+00	0.000E+00	0.000E+00	0.000E+00	0.000E+00	0.000E+00
123	PAN	0.100E-04	0.100E-04	0.100E-04	0.100E-04	0.100E-04	0.100E-04
124	HC3	0.120E-04	0.120E-04	0.120E-04	0.400E-05	0.400E-05	0.400E-05
125	HC5	0.120E-04	0.120E-04	0.120E-04	0.400E-05	0.400E-05	0.400E-05
126	HC8	0.600E-05	0.600E-05	0.600E-05	0.200E-05	0.200E-05	0.200E-05
127	ETH	0.000E+00	0.000E+00	0.000E+00	0.000E+00	0.000E+00	0.000E+00
128	CO	0.700E-01	0.700E-01	0.700E-01	0.700E-01	0.650E-01	0.550E-01
129	OL2	0.000E+00	0.000E+00	0.000E+00	0.000E+00	0.000E+00	0.000E+00
130	OLT	0.000E+00	0.000E+00	0.000E+00	0.000E+00	0.000E+00	0.000E+00
131	OLI	0.000E+00	0.000E+00	0.000E+00	0.000E+00	0.000E+00	0.000E+00
132	TOL	0.000E+00	0.000E+00	0.000E+00	0.000E+00	0.000E+00	0.000E+00
133	XYL	0.000E+00	0.000E+00	0.000E+00	0.000E+00	0.000E+00	0.000E+00
134	ACO3	0.100E-08	0.100E-08	0.100E-08	0.100E-08	0.100E-08	0.100E-08
135	TPAN	0.100E-07	0.100E-07	0.100E-07	0.100E-07	0.100E-07	0.100E-07
136	HONO	0.100E-08	0.100E-08	0.100E-08	0.100E-08	0.100E-08	0.100E-08
137	HNO4	0.200E-08	0.200E-08	0.200E-08	0.200E-08	0.200E-08	0.200E-08
138	KET	0.400E-04	0.400E-04	0.400E-04	0.400E-04	0.400E-04	0.500E-05
139	GLY	0.250E-06	0.250E-06	0.250E-06	0.200E-06	0.150E-06	0.100E-06
140	MGLY	0.250E-06	0.250E-06	0.250E-06	0.200E-06	0.150E-06	0.100E-06
141	DCB	0.250E-06	0.250E-06	0.250E-06	0.200E-06	0.150E-06	0.100E-06
142	ONIT	0.600E-05	0.600E-05	0.600E-05	0.200E-05	0.200E-05	0.200E-05
143	CSL	0.100E-08	0.100E-08	0.100E-08	0.100E-08	0.100E-08	0.100E-08
144	ISO	0.250E-05	0.250E-05	0.250E-05	0.250E-05	0.250E-05	0.250E-05
145	HO	0.000E+00	0.000E+00	0.000E+00	0.000E+00	0.000E+00	0.000E+00
146	HO2	0.000E+00	0.000E+00	0.000E+00	0.000E+00	0.000E+00	0.000E+00
147	ASO4I	3.207E-02	3.207E-02	3.207E-02	1.603E-02	3.207E-03	1.603E-03
148	ASO4J	7.696E-01	7.696E-01	7.696E-01	3.848E-01	7.696E-02	3.848E-02

Table B.2 (continued)

149	NUMATKN	9.583E+09	9.583E+09	9.583E+09	4.791E+09	9.583E+08	4.791E+08
150	NUMACC	2.740E+08	2.740E+08	2.740E+08	1.370E+08	2.740E+07	1.370E+07
151	ASOIL	8.000E-01	8.000E-01	8.000E-01	4.000E-01	8.000E-02	4.000E-02
152	NUMCOR	1.400E+04	1.400E+04	1.400E+04	7.000E+03	1.400E+03	7.000E+02
153	West						
154							
155	SO2	0.300E-03	0.200E-03	0.200E-03	0.100E-03	0.000E+00	0.000E+00
156	SULF	0.300E-03	0.200E-03	0.200E-03	0.100E-03	0.000E+00	0.000E+00
157	NO2	0.100E-03	0.100E-03	0.100E-03	0.500E-04	0.000E+00	0.000E+00
158	NO	0.500E-04	0.500E-04	0.500E-04	0.200E-04	0.000E+00	0.000E+00
159	O3	0.350E-01	0.400E-01	0.450E-01	0.500E-01	0.600E-01	0.700E-01
160	HNO3	0.500E-03	0.500E-03	0.500E-03	0.500E-03	0.200E-03	0.100E-03
161	H2O2	0.200E-02	0.200E-02	0.200E-02	0.200E-02	0.800E-03	0.200E-03
162	ALD	0.400E-04	0.400E-04	0.400E-04	0.400E-04	0.400E-04	0.500E-05
163	HCHO	0.400E-03	0.400E-03	0.400E-03	0.400E-03	0.100E-03	0.500E-04
164	OP1	0.400E-06	0.400E-06	0.400E-06	0.400E-06	0.100E-06	0.500E-07
165	OP2	0.400E-07	0.400E-07	0.400E-07	0.400E-07	0.400E-07	0.500E-08
166	PAA	0.250E-04	0.250E-04	0.250E-04	0.250E-04	0.200E-04	0.100E-04
167	ORA1	0.250E-05	0.250E-05	0.250E-05	0.250E-05	0.500E-06	0.500E-06
168	ORA2	0.250E-05	0.250E-05	0.250E-05	0.250E-05	0.500E-06	0.500E-06
169	NH3	0.300E-03	0.300E-03	0.300E-03	0.200E-03	0.100E-03	0.500E-04
170	N2O5	0.000E+00	0.000E+00	0.000E+00	0.000E+00	0.000E+00	0.000E+00
171	NO3	0.000E+00	0.000E+00	0.000E+00	0.000E+00	0.000E+00	0.000E+00
172	PAN	0.100E-03	0.100E-03	0.100E-03	0.500E-04	0.100E-04	0.100E-04
173	HC3	0.800E-04	0.800E-04	0.800E-04	0.600E-04	0.800E-05	0.400E-05
174	HC5	0.800E-04	0.800E-04	0.800E-04	0.600E-04	0.800E-05	0.400E-05
175	HC8	0.400E-04	0.400E-04	0.400E-04	0.300E-04	0.400E-05	0.200E-05
176	ETH	0.000E+00	0.000E+00	0.000E+00	0.000E+00	0.000E+00	0.000E+00
177	CO	0.800E-01	0.800E-01	0.800E-01	0.800E-01	0.650E-01	0.500E-01
178	OL2	0.100E-04	0.100E-04	0.500E-05	0.500E-05	0.100E-05	0.000E+00
179	OLT	0.200E-05	0.100E-05	0.500E-06	0.300E-06	0.000E+00	0.000E+00
180	OLI	0.100E-05	0.200E-06	0.100E-06	0.000E+00	0.000E+00	0.000E+00
181	TOL	0.100E-04	0.500E-05	0.500E-05	0.300E-05	0.000E+00	0.000E+00
182	XYL	0.300E-05	0.200E-05	0.400E-06	0.400E-06	0.000E+00	0.000E+00
183	ACO3	0.100E-08	0.100E-08	0.100E-08	0.100E-08	0.100E-08	0.100E-08
184	TPAN	0.100E-07	0.100E-07	0.100E-07	0.100E-07	0.100E-07	0.100E-07
185	HONO	0.100E-08	0.100E-08	0.100E-08	0.100E-08	0.100E-08	0.100E-08

Table B.2 (continued)

186	HNO4	0.200E-08	0.200E-08	0.200E-08	0.200E-08	0.200E-08	0.200E-08
187	KET	0.400E-04	0.400E-04	0.400E-04	0.400E-04	0.400E-04	0.500E-05
188	GLY	0.400E-06	0.400E-06	0.400E-06	0.400E-06	0.100E-06	0.500E-07
189	MGLY	0.400E-06	0.400E-06	0.400E-06	0.400E-06	0.100E-06	0.500E-07
190	DCB	0.400E-06	0.400E-06	0.400E-06	0.400E-06	0.100E-06	0.500E-07
191	ONIT	0.400E-04	0.400E-04	0.400E-04	0.300E-04	0.400E-05	0.200E-05
192	CSL	0.100E-08	0.100E-08	0.100E-08	0.100E-08	0.100E-08	0.100E-08
193	ISO	0.250E-05	0.250E-05	0.250E-05	0.250E-05	0.250E-05	0.250E-05
194	HO	0.000E+00	0.000E+00	0.000E+00	0.000E+00	0.000E+00	0.000E+00
195	HO2	0.000E+00	0.000E+00	0.000E+00	0.000E+00	0.000E+00	0.000E+00
196	ASO4I	4.810E-02	3.207E-02	3.207E-02	1.603E-02	3.207E-03	1.603E-03
197	ASO4J	1.154E+00	7.696E-01	7.696E-01	3.848E-01	7.696E-02	3.848E-02
198	NUMATKN	1.437E+10	9.583E+09	9.583E+09	4.791E+09	9.583E+08	4.791E+08
199	NUMACC	4.110E+08	2.740E+08	2.740E+08	1.370E+08	2.740E+07	1.370E+07
200	ASOIL	1.000E+00	8.000E-01	8.000E-01	4.000E-01	8.000E-02	4.000E-02
201	NUMCOR	1.750E+04	1.400E+04	1.400E+04	7.000E+03	1.400E+03	7.000E+02

Appendix C Aerosols

Table C.1 Aerosol Species Concentrations

Units: mass [$\mu\text{g m}^{-3}$], number [$\# \text{m}^{-3}$]

{ a1 }	ASO4 J	Accumulation mode sulfate mass
{ a2 }	ASO4I	Aitken mode sulfate mass
{ a3 }	ANH4J	Accumulation mode ammonium mass
{ a4 }	ANH4I	Aitken mode ammonium mass
{ a5 }	ANO3J	Accumulation mode nitrate mass
{ a6 }	ANO3I	Aitken mode aerosol nitrate mass
{ a7 }	AORGAJ	Accumulation mode anthropogenic secondary organic mass
{ a8 }	AORGAI	Aitken mode anthropogenic secondary organic mass
{ a9 }	AORGAJ	Accumulation mode primary organic mass
{ a10 }	AORGAJ	Aitken mode mode primary organic mass
{ a11 }	AORGBJ	Accumulation mode secondary biogenic organic mass
{ a12 }	AORGBI	Aitken mode biogenic secondary biogenic organic mass
{ a13 }	AECJ	Accumulation mode elemental carbon mass
{ a14 }	AECI	Aitken mode elemental carbon mass
{ a15 }	A25J	Accumulation mode unspecified anthropogenic mass
{ a16 }	A25I	Aitken mode unspecified anthropogenic mass
{ a17 }	ACORS	Coarse mode unspecified anthropogenic mass
{ a18 }	ASEAS	Coarse mode marine mass
{ a19 }	ASOIL	Coarse mode soil-derived mass
{ a20 }	NUMATKN	Aitken mode number
{ a21 }	NUMACC	Accumulation mode number
{ a22 }	NUMCOR	Coarse mode number
{ a23 }	SRFATKN	Aitken mode surface area
{ a24 }	SRFACC	Accumulation mode surface area
{ a25 }	AH2OJ	Accumulation mode water mass
{ a26 }	AH2OI	Aitken mode water mass